Application of integrated geophysicaI techniques for characterizing subsurface structures at different scales for environmental management in the northern part of the Voltaian sedimentary basin, Ghana

Richard Adams Mejida

COLLEGE SCIENCES
DOCTORAL DE LA MER
BRETAGNE ET DU LITTORAL

Université de Bretagne Occidentale

THESE DE DOCTORAT DE

L'UNIVERSITE
DE BRETAGNE OCCIDENTALE

ECOLE DOCTORALE N° 598
Sciences de la Mer et du Littoral
Spécialité : *Marine Geoscience*

Par

Richard Adams MEJIDA

Application of integrated geophysical techniques for characterizing subsurface structures at different Scales for environmental management in the northern part of the Voltaian sedimentary basin, Ghana.

Thèse présentée et soutenue à Brest le 06/02/2024
Unité de recherche : Geo-Ocean

Rapporteurs avant soutenance :

Yves GERAUD : Professeur Ecole Nationale Supérieure de Géologie/ Université de Lorraine
Giulio VIGNOLI: Professeur, Dept. Of Civil, Environmental Engineering and Architecture/Universita degli studi di Cagliari

Composition du Jury :

Président : Yves GERAUD Professeur Ecole Nationale Supérieure de Géologie/ Université de Lorraine
Examinateurs: Julie ALBARIC, Université Bourgogne Franche-Comte, UFR ST UMR 6249 Chrono-environment
Daniel ASLANIAN IFREMER – Centre de Brest – REM/GEO-OCEAN/GIPS
Giulio VIGNOLI: Professeur, Dept. Of Civil, Environmental Engineering and Architecture/ Universita degli studi di Cagliari

Dir. de thèse : Pascal TARITS Professeur IUEM/ Université de Bretagne Occidentale
Co-dir. de thèse : Mark S.M. YIDANA Professeur University of Ghana, Accra Ghana

Invité(s)
Sophie HAUTOT Docteur, Gérante IMAGIR Sarl. Invitée
Thomas E.K. ARMAH Docteur, University of Ghana Co-encadrant

ACKNOWLEDGEMENT

First and foremost, I would like to thank God for blessing me with good health and strength to be able to successfully finish this thesis.

I would like to acknowledge the French government through the French embassy in Ghana, the Nyasapong Project, and the Ghana government through the Ghana Scholarship Secretariat for their financial support. Also, I want to thank laboratory Geo-Ocean of UBO for the financial assistance for my fieldwork as well as conferences and training programs. It has been an honor to be a recipient of the inaugural joint scholarship award and I am indebted to the donors for providing me with the financial assistance to pursue my academic dreams.

My immense thank you goes to my Ph.D. supervisors: Prof. Pascal Tarits, Dr. Sophie Hautot, Prof. S.M Yidana, and Dr. T.E.K Armah for their support, constructive criticisms, and guidance throughout this research. Your contributions have been invaluable. Pascal in particular has been an exemplary mentor and a great supervisor always available to listen and provide suggestions, all I can say is thank you. A big thank you to all the academic staff especially, Margot, Elizabeth, and Aurelie for always being available to assist when needed.

Also, I want to thank my CSI committee members Prof. Roger Guerin and Dr. Julie Albaric for their constructive criticisms, suggestions, and advice which have guided me all through my study, to them, I say I am utterly grateful. Thank you to Geosoft Inc. for extending the Oasis Montaj package to allow me to finish processing my data.

It has been an amazing experience working with my PhD colleagues in this research group. Thank you to everyone from the Geo-Ocean laboratory who has helped me in one way or the other. I want to thank Dr. E. A. Dzikunoo, Christophe Martin, Simon Vedrine, and Rachid Robleh for all the discussions and contributions to this work. I am grateful to everyone that I have collaborated with externally and internally. My appreciation goes to my wonderful friends both here and abroad for their support and encouragement.

Last but not the least, I want to thank my wonderful family and sweetheart for their support, encouragement, advice, and prayers. I love you all and may God richly bless everyone who has contributed in diverse ways to this thesis.

Table des matières

List of Tables

List of Figures

CHAPTER ONE

SCIENTIFIC CONTEXT AND BACKGROUND OF STUDY

1.0 INTRODUCTION

Geophysical methods are non-invasive tools that provide the means to measure material properties which help assess potential subsurface conditions. Geophysics as a discipline has grown substantially over the past decades earning the reputation as a cost-effective and non-destructive tool that supplements the traditional subsurface exploration techniques to provide valuable information. Originally, these techniques were developed for oil/gas and mineral exploration then and academic research (Knight, 2000; Rubin & Hubbard, 2005) but have recently emerged as useful tools for investigating the subsurface as well as monitoring the dynamic hydrogeological and anthropogenic processes that ensue below the surface. In subsurface investigation, different techniques measure different physical parameters. For instance, in environmental investigations, parameters such as electrical resistivity are of interest since readings of these parameters can be influenced by the presence of subsurface fluids such as groundwater or leachate in pores and fractures. Geophysical methods offer the advantage of spatial continuity of information (especially when the data is densely collected) making them suited for characterizing spatial structures at varying scales (Day-Lewis et al., 2017).

1.1 APPLICATION OF GEOPHYSICAL TECHNIQUES IN SUBSURFACE INVESTIGATION (CHARACTERIZATION)

Geophysical techniques have played a major role in subsurface investigations. These techniques have been used widely in environmental management such as pollution studies and groundwater exploration. The recent increase in the preferred use of these methods is due to the cost-effectiveness and the increasing sensitivity of the geophysical methods in defining environmental targets (Balwant et al., 2022; Wiederhold et al., 2021). Furthermore, their application can be quick in providing information useful in determining subsurface conditions at a given site. These conditions may include; the location of voids, faults, or fractures, depth to bedrock, hydro stratigraphic framework, , the presence of buried materials, such as steel drums or tanks and extent of concentrated groundwater contaminant plumes (Yusuf, 2016). Different geophysical techniques provide different subsurface information therefore choosing a technique is significantly influenced by the objective of interest though other factors may play a role. The ability of these techniques to continuously scan the subsurface enhances their suitability and application in environmental management (Kenworthy, 2016).

1.2 ENVIRONMENTAL MANAGEMENT

Any practice that ensures the protection and preservation of natural resources that are essential to the existence of living organisms in the environment is termed as environmental management. The need to properly manage the environment keep increasing by the day. This is because today's modern society is faced with many environmental issues including rapid population growth and environmental pollution which significantly diminish the quality of life on Earth. Increase in human population and its accompanied anthropogenic activities continuously threaten the availability and quality of both surface and groundwater sources (Egbueri et al., 2023). The trend is even more precarious in developing countries where continuous supply of potable water remains a challenge (Edokpayi et al., 2018). Similarly, the effects of environmental pollution is warming the earth's environment. This warming of the earth is seen in the global annual average temperature analysis which clearly indicate rise in temperature over the past 80 years (Fig. 1.1) (Kabir, 2023). The effect of these high temperatures is more pronounced in tropical regions such as Ghana where extreme temperatures and high evapotranspiration have resulted in depletion of surface water bodies. The interplay of these factors underscores the important of proper environmental management in order not to exacerbate the already calamitous environmental issues.

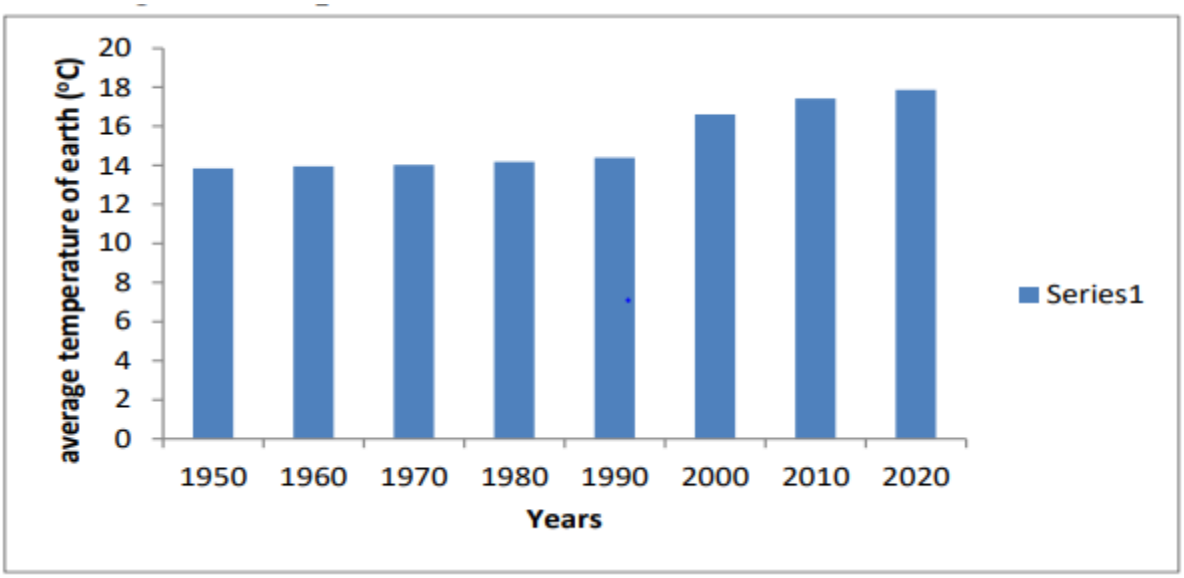

Figure 1. 1: Global annual average temperature of the Earth recorded for different years (Kabir, 2023).

1.2.1 Environmental Management Challenges Associated with Anthropogenic Activities

1.2.1.1 Municipal Solid Waste Disposal

The lack of proper management of waste observed in many communities is a worrying concern likely to derail efforts in groundwater development in Africa. According to Asuma, (2013), African countries generate thousands of tons of solid waste every day and less than half of this solid waste is collected while over 90 percent of the uncollected quantity is indiscriminately discarded at various dumping sites mostly at the outskirts of municipalities. The generation of solids waste is mostly influenced by population growth, industrialization, urbanization, and the constant change in the living standards of people (Tripathi & Dwivedi, 2021). The tremendous increase in solid waste generation is a serious issue at the local, regional, and global levels. This problem is more intense in developing countries than in the developed country (Manfredi et al., 2010). In developing countries, open dumping is seen as the most convenient and cheapest way of solid waste disposal with no recourse to the adverse effect it poses to the environment. Open dumping of municipal solid waste is a common practice in Ghana, and the problem of solid waste disposal is one of the major problem facing communities and municipalities in the country (Lissah et al., 2021). Apart from openly dumping of rubbish occupying land space, it produces toxin, bad odour, and attract pest and micro-organisms which breed various diseases. When waste is dumped into non-engineered landfills (open dump sites), it undergoes physical, chemical and microbiological changes resulting in leachate production (Singh et al., 2019). The leachate from such dump sites are a threat to groundwater development (Rathod et al., 2013) as they could migrate into the subsurface if pore spaces exist.

1.2.1.2 Impact of Anthropogenic Activities on the Environment and Geologic Systems

Accessibility of water resources by rural People in African countries such as Ghana is through boreholes, wells, water vendors, small town piped water systems and springs. Most of these boreholes and wells tap into the shallow aquifer system which derive their recharge from the surface through weathered zones and fractures after a downpour. This phenomenon increases the chances of leachate from open non-engineered dump sites infiltrating into the shallow aquifer systems and consequently causing pollution to groundwater. While this phenomenon could likely

affect shallow aquifers, deep aquifers are somewhat safe from leachate contamination except in peculiar situations where deep vertical fracture may exist to serve as conduit.

Although deep aquifers are not completely immune to surface leachate contamination, they are less vulnerable than shallow aquifers. In contrast to surface water and shallow aquifers, deep aquifer contamination is greatly decreased due to the slow movement of contaminants in the subsurface, as contaminants maybe filtered by natural processes while passing through the soil layers (Buddies, 2016). Deep aquifers have longer flowed path and less contact time with surface materials making them less prone to pollution via surface contaminant plumes (Geris et al., 2022). It has often been argued that water that comes from deep aquifers is considered better than water from shallow unconfined aquifers (St. Johns River Water Management District, 2023; Thaw et al., 2022; Barberio et al., 2021) because of the depths at which they are located. Ferguson et al., (2018) observed that, the diminishing water table and shallow surface pollution are pushing many water users in the United States to resort to construction of deep groundwater wells. Also, deep aquifers are used in the metropolitan area of Guadalajara to recover overexploited aquifers while removing surface runoff that could otherwise cause flooding. This technology is emerging as an effective flood-mitigating measure and could be used to address the negative environmental impact caused by flooding (Vanegas-Espinosa et al., 2022). Flooding is frequently caused by the waterproof nature of urban surfaces. Furthermore, the over-reliance on shallow aquifers in the face of looming contamination from indiscriminate solid waste dumping should be a major concern, providing even another incentive to search for deeper aquifers. Concerns over solid waste disposal in Ghana is growing, particularly in densely populated communities in the already challenged Voltaian sedimentary basin in terms of groundwater. According to Acheampong and Hess (1998), the shallow aquifers of the Voltaian are vulnerable to contamination due to permeable and fractured soil cover within the thin overlaying vadose zone and as a result, the development of groundwater suffers even more. Groundwater development in the Voltaian sedimentary basin has been disappointing (Agyekum & Asare, 2016b; Banoeng-Yakubo et al., 2011; Dapaah-Siakwa & Gyau-Boakye, 2000), yet the few successes achieved within the shallow subsurface face contamination threats from indiscriminately dumping of solid waste. The lack of research to determine the likely impact of this practice could be dire in the near future as most of the rural communities rely on the shallow unconfined aquifer system for their water needs. Such issues maybe overcome by exploring for deep aquifers as alternative to the basin's shallow low productive aquifers. The vast

water stored in deep aquifers is less affected by abrupt changes in regional hydrological (rainfall/climate) cycle (Salameh, 2021). The U.S. National Groundwater Association estimate that there are 22.6 million cubic kilometers of groundwater in the upper two kilometers of the earth crust, adding that the resource is enough to supply water to Earth for about six thousand years at the current global consumption rate (Aquaterrex, 2023). They further argued that, deep aquifers are not only safe from pollution or contamination via surface infiltration, but they also allow shallow aquifers to recharge and restore the surface environment which can improve the water quality and quantity as well as ecological security. Despite the numerous advantages of deep aquifers, little has been done to thoroughly investigate them in Ghana.

1.3 GEOPHYSICAL METHODS IN ENVIRONMENTAL MANAGEMENT

1.3.1 Near-Surface Applications

Geophysical methods have emerged as the most effective tool for monitoring, evaluating, and managing environmental issues (Day-Lewis et al., 2017). The increasing use of the techniques in environmental research is attributable to improved sensitivity and resolution of geophysical tools in investigating environmental targets such as mapping contaminated objects in the soil matrix (Balwant et al., 2022). This has paved the way for many researches centred on the mapping of contaminant plumes in many places in the world (e.g. Bugan et al., 2018; Shao et al., 2019; Srena et al., 2011; Vaudelet et al., 2011). The significant contrast that exist between the anomaly of interest and the host soil matrix or rock enable the deployment of techniques like the electrical resistivity tomography (ERT), and electromagnetic (EM) in environmental investigations (Castillo-Widener, 2013). ERT and EM methods measure physical parameters like resistivity which is key parameters in understanding hydrogeological conditions and contaminant plume migrations within the subsurface.

In most environmental investigations, the incorporation of different geophysical methods allows for the best and most effective results in terms of resolution, coverage, investigation depth, and speed (Martorana et al., 2023), even though some of the techniques have indicated good outcomes when used independently (Aristodemou & Thomas-Betts, 2000). The key as to whether or not to integrate various geophysical techniques depends mostly on the objective of the investigation and the choice of physical parameter that demonstrate the biggest contrast with respect to the ground (Martorana et al., 2023). The integration of techniques reduces the uncertainties and enhance

confidence in the results. The available techniques are distinguished by diverse penetration depth and resolution capabilities ranging from few centimetres to hundreds of kilometres. As a result, there seem to be an interest in the scientific community to integrate geophysical methods so as to detect and characterize the subsurface from the analysis of different physical parameters (Tinivella et al., 2013). For example, a leachate contamination plume caused by indiscriminate discharge of effluents from a cassava processing factory was investigated by Osinowo et al., (2020) using the integration of ERT and frequency domain EM. They successfully characterized the lateral and vertical resistivity patterns likely induced by the contaminant and highlighted the potential contaminated areas. Similarly, contaminated areas along the Almisk lake in Jeddash was investigated using integrated techniques of ERT and ground based magnetic. The models generated by the techniques were validated with results of chemical analysis which showed good agreement with high resistivity areas corresponding to areas with high total dissolve solutes (TDS) (Rehman et al., 2021). Greenfield and Stoyer, (1976) used the ERT and EM methods to undertake environmental pollution monitoring in Kylertown to determine the extent and impact of acid mine water on the groundwater system. Their research identified fracture traces as the primary conduits for the propagation of the acid mine water.

Characterization of leachate from municipal solid waste dumps is another environmental concern that has seen an increase in the use of geophysical techniques. In particular, the ERT method has commonly been used due to the high concentration of ion in the leachate from solid waste. It is the most ideal technique for investigating waste dumps as it can effectively define contaminated zones of groundwater due to the conductive nature of most contaminants (Ganiyu et al., 2015). Appiah et al., (2018) used the ERT methods to delineate the physical boundary and aerial extent of a municipal solid waste dump at Sunyani, Ghana. Their efforts were successful in delineating contamination zones and the preferential pathways of the leachate beneath the waste site. Ganiyu et al., (2015) employed the ERT method to investigate an open dumpsite in the southern part of Nigeria to determine the horizontal and vertical extent of the leachate plume and its impact on the shallow groundwater system. Again, using the 2D resistivity tomography, Okpoli, (2013) noted possible groundwater contamination caused by leachate from solid waste dump that has migrated through fracture zones into the aquifer system below. All the examples clearly suggest an imminent danger of the shallow groundwater system considering the fact that municipal solid waste management is daunting task for many cities in most developing countries. Municipal solid waste

management have been identified as a major environmental problem that has the potential to pollute both surface and groundwater sources (Hepburn et al., 2019).

Globally, various techniques and methodologies exist for the exploration and development of groundwater resources. Notable among these are surface geophysical methods. Surface geophysical methods can provide both qualitative and quantitative subsurface information about groundwater in a given terrain when used appropriately (Guireli Netto et al., 2020; Martinho & Dionísio, 2014). Over the last decade, surface geophysical methods have become increasingly popular in groundwater research (Ramalho et al., 2023). Depending on the scale (targeted depth to be investigated), the complexity and the level of details required, the methods could range from simple to more sophisticated methods (Aliou et al., 2022). The majority of hydrogeological investigation combine geophysics and geology to provide thorough information useful in adequately delineating the anomaly of interest. The exploration for groundwater aquifers, should focus on the identification of the main geologic, tectonic and sedimentological structures similar to oil and gas exploration (Baumle & Himmelsbach, 2018). Such explorations can be accomplished with the use of the right geophysical techniques. The techniques provide the tools for characterizing the physical properties to infer information about the subsurface in order to understand the regional hydrogeological conditions of the various lithologic strata (Vignoli et al., 2012). Understanding the hydrogeological processes of the subsoil is crucial for the calibration of geophysical models to properly describe and predict groundwater potential zones (Mockler et al., 2016).

Geophysical model interpretation can be unclear at times; in that several different models can explain same dataset to an agreeable fit. As a result, a combination of methodologies may be required to improve the accuracy and precise interpretation and decision making. For example, Azaiez et al., (2021) demonstrated the used of seismic reflection and gravity data along with geology to characterize the hydrogeological potential of the Ain El Beidha plain in Tunisia. A 3D model from their investigation revealed a deep tertiary aquifer in the arid region. Demirci et al. (2020) integrated seismic refraction technique to resolve high ambiguity prevalent in electric and electromagnetic data collected over the Bafra plain in Turkey. The introduction of the seismic geophysical method reduced the uncertainty in the resistivity response observed in the geologic formation. The seismic refraction method is sensitive to several physical characteristics of which helped to lessen the uncertainty in the interpretation that led to the discovery of the complex aquifer of Bafra plain. Also, the amalgamation of resistivity and seismic resulted in the detection of thrust

structure in the Varde area in Denmark and a channel structure in Hamburg-Sulldorf area in Germany both of which are regarded as potential aquifers (Wiederhold et al., 2021). The combine use of the magnetic resonance sounding (MRS) and vertical electric sounding (VES) enabled the detection and characterization of the Dhar Nema aquifer located in the south-eastern part of Mauritania. These techniques did not only revealed the presence of a water bearing layer, but also, the porosity and permeability as well as the extent of the aquifer layer in the area (Bernard et al., 2004). Clearly, the combination of geophysical methods have been critical in reducing uncertainties in geophysical data interpretation while helping to reveal subsurface properties to aid in groundwater exploration (e.g. Bradford, 2002; Bruno & Vesnaver, 2021; Feroci et al., 1986; Miller et al., 1986).

While the integration of geophysical methods is imperative in reducing uncertainties and increasing confidence in geophysical data interpretations, some geophysical methods still produce good results when used independently. The efficacy and accuracy of the interpretation however depend on the proper understanding of geology and hydrogeology. Yaramanci et al. (2002), for example tested and successfully demonstrated the use of surface nuclear magnetic resonance (SNMR) to detect aquifers, including their geometries and hydrological properties. Additionally, several groundwater potential zones and aquifers including their depths have been delineated using solely time domain electromagnetic (TDEM) geophysical technique (Alshehri & Abdelrahman, 2022; Al-Amoush et al., 2015; Jørgensen et al., 2003). The TDEM technique was initially designed for mineral survey but it was later shown to be capable of detecting and recording minor changes in conductivity induced by the presence of high-quality groundwater (Farag et al., 2019). The system has been used to locate geological structures such as fractures zones, favourable for hosting groundwater (Alshehri & Abdelrahman, 2022; McNeill & Snelgrove, 1995). The ground penetrating radar is another geophysical technique that has been singularly used to map out groundwater bearing zones while clearly delimiting the stratigraphic layers of the subsurface strata (Bauer et al., 2006; Benson, 1995).

Despite the fact that several geophysical methods have been used for hydrogeological investigations, superior success have been demonstrated by the ERT and EM methods (Eke & Igboekwe, 2011). These methods can either be employed independently or in conjunction with other geophysical methods (Alshehri & Abdelrahman, 2022; Omosuyi et al., 2007). For several decades, both techniques have been extensively used in hydrogeological exploration including

aquifer characterization (Senos Matias et al., 1994). Geoelectrical resistivity surveys using vertical resistivity sounding (VES) with different arrays (Sharma, 1997; Telford et al., 1990) have proven to be unswerving and useful in identifying not only the structural entity of the aquifer (Hubbard et al., 1999) but also the petrophysical characteristics (Aizebeokhai et al., 2016), groundwater properties (Hubbard et al., 1999), hydraulic parameters (Niwas & Celik, 2012), and contamination assessment (Senos Matias et al., 1994). For instance, the Nubian aquifer and the fractured basement aquifer in the Wadi Morra region of southern Sinai in Egypt were discovered via the application of VES using the Schlumberger array (Zayed, 2021). The water-bearing zone within the karst-granite formation in Gannan region of China was delineated using the geoelectrical method (Lubang et al., 2023). The geometry of the Port de la Selva aquifer was characterized as uneven including the aquifer thickness following a strong correlation between ERT and borehole information over the area (Sendrós et al., 2021). Niwas and Celik, (2012) used VES to map the Ruthrtal aquifer in Western Germany and estimated the aquifer porosity and hydraulic conductivity using the Kozeny - Archie equation and ohm's – Darcy laws.

1.3.2 Geophysical Methods in Deep Subsurface Structural Investigations

In spite of the enormous success achieved with the use of geophysical techniques in hydrogeological researches, a significant number of the methods are limited in terms of deep (deep here represent depths >100m) aquifer study. The characterization of deep aquifers requires a robust approach to delineate subsurface structures using geophysical techniques with good spatial and depth coverage (Mohamed et al., 2022). Airborne techniques come across as the most appropriate techniques as they have proven effective in delineating structures and have an advantage owing to the speed of operation and the large aerial coverage. Airborne surveys cover a variety of geophysical techniques; however, aeromagnetic and airborne EM are the most used in groundwater prospecting. Their application in groundwater exploration have evolved in the last three decades (Siemon, 2009) which have seen the introduction of improved systems such as the SkyTEM and drones. More recently, the SkyTEM mounted on helicopter and airborne drones have been deployed in structural mapping and groundwater investigations especially in complex terrains where access for land survey is a challenge (Binley et al., 2015; Knight et al., 2018; Pirttijarvi et al., 2022; Shaji, 2021). Techniques like aeromagnetic are mostly used in groundwater survey for reconnaissance to delineate and define areas for land survey while aero-electromagnetic system such as the SKyTEM has been successful in discriminating potential aquifers (Paterson &

Bosschart, 1987; Shaji, 2021). These techniques have been used to provide information about aquifer thickness and location of major geologic structures such as faults (Dawoud, 2011). However, airborne methods like the EM only penetrate down to few hundreds of meters, hence, deep aquifer studies that involve characterizing thicker basins (sediment thickness exceeding 5km) down to basement, the airborne EM technique may fall short. Other geophysical methods which have been utilized in deep aquifer investigations include; seismic, long offset CSEM, and magnetotelluric (MT) (e.g. Attias et al., 2020; Bertoni et al., 2020; Giroux et al., 1997; Ishizu & Ogawa, 2021). The seismic method offer good resolution in deep aquifer investigations (Bellali et al., 2018; Bertoni et al., 2020) but it is expensive. Long offset CSEM also give good resolution but the technique is more sensitive to resistive bodies (Boerner, 1992). Passive MT on the other hand utilizes natural sources and could be affected due to weak source signals. However, it give good resolution with good source signals and is highly sensitive to conductive bodies in the subsurface which may be caused by presence fluids in hard rock terrains (Malleswari et al., 2019). MT has been used along with airborne techniques to delineate deep seated subsurface structures that have the potential to produce groundwater in commercial quantities (e.g. Aboud et al., 2014; Chandrasekhar et al., 2009; Meju et al., 1999). There have been an increased in the application of airborne techniques in regional hydrogeological investigations (e.g. Al-Garni, 2009; Joel et al., 2016) whereas MT has been successfully used to characterized water-bearing zones in geological complex terrains (e.g. Bai et al., 2019; Yadav et al., 2020).

In hard rock terrains such as the Voltaian Sedimentary Basin (VSB) where groundwater is said to be controlled by geologic structures (Acheampong & Hess, 1998; Aliou et al., 2022; Carrier et al., 2008), the integration of airborne techniques and MT could be useful in characterizing the structures at different spatial scales for groundwater production. The MT method can effectively detect subtle changes and delineate subsurface structures making its integration with airborne techniques suitable for deep aquifer investigations (Harinarayana, 2008). It is useful for detecting and recording resistivity variations induced by the presence of high-quality of groundwater (Farag et al., 2019; Manzella et al., 2004). The MT technique have been deployed to delineate structural entities such as faults and fracture zones favourable for groundwater (Bourgeois et al., 1994; Giroux et al., 1997; Sumanovac, 2012). The interpretation of MT results relies on the fact that the technique is sensitive to conductive geologic features such as fractures which can serve as water-bearing zones when considered together with the geology and hydrogeological factors of an area

(Alshehri & Abdelrahman, 2022). Improved understanding of the limitation of the MT method has seen more combination of the technique with other geophysical methods. It has become a more acceptable tool in the arsenal for exploring the subsurface for natural resources such as groundwater (Vozoff, 1990). The combination of airborne techniques and MT could prove crucial at unravelling the groundwater potential of the VSB as previous studies have largely concentrated on the shallow surface (< 100 m) which has not yielded the much-needed results.

1.4 OVERVIEW OF GEOPHYSICAL METHODS FOR GROUNDWATER EXPLORATION IN THE VOLTAIAN SEDIMENTARY BASIN

Over the last few years most geophysical explorations carried out in the Voltaian Sedimentary Basin have been for the drilling of boreholes for groundwater production for communities. As a result, several projects initiated by both successive governments and non-governmental organizations have utilized geophysical methods to try and delineate potential zones suitable for borehole drilling. Among the geophysical methods adopted by most of these organizations are the electrical resistivity method and the electromagnetic method, specifically the Geonics EM-34. These two techniques have been used in the basin to characterize the physical properties of the near subsurface, primarily the weathered zone and discrete fractures in order to better understanding the regional and local hydrogeological conditions of the various lithologic formations of the Voltaian Supergroup (Akudago et al., 2009; Carrier et al., 2011). The thickness of the weathered zone of the basin has been reported to average about 11 m while the fractures are said to be discrete and erratic (Bannerman, 1990; Chegbeleh et al., 2009) due to possible diagenesis or low grade metamorphism which affected sediments (Kesse, 1985) in the basin. Most of these explorations initiatives however have been confronted with borehole siting challenges leading to very low success rate and yields below the minimum approved limit for well construction as advised by Community Water and Sanitation Agency (CWSA) in Ghana. Ewusi et al., (2020) noted that, the low success rate is as a result of the use of common geophysical methods such as the 4-electrode electrical resistivity and EM-34 methods. However, Aliou et al., (2022) deployed the more sophisticated 2-D ERT technique and the Geonics EM-34 systems in the basin but still reported drilling dry wells at certain locations in the basin. Mainoo et al., (2019) on the other hand utilized the 2-D ERT equipment with total current electrode spacing covering over 1 Km and was able to encounter very high yielding borehole at depths deeper than 150 m into the subsurface. This perhaps is an indication that groundwater fortunes of the basin could be improved if investigations were to target relative deeper

(<100 m) depths as opposed to the investigating the shallow (<100 m) subsurface. Agyekum and Asare, (2016) suggested that, the magnetotelluric technique should be deployed in the basin to effectively characterize the electrical resistivity structure to enhance proper understanding of the hydrogeological conditions of the basin. The techniques effectively discriminate the fractures as an EM method and at the same time provide good resolution with depth. A common consensus by all previous studies relating to groundwater occurrence in the basin is that, the groundwater is controlled by fractural entities such as faults, joints and folds as well as lithological contacts (Acheampong & Hess, 2000; Aliou et al., 2022; Carrier et al., 2008; Chegbeleh et al., 2009; Dapaah-Siakwa & Gyau-Boakye, 2000; Mainoo et al., 2019). The results of geophysical investigation should be interpreted more detailed fashion targeting lithological contacts and fractures zones for borehole siting in the basin (Aliou et al., 2022; Chegbeleh et al., 2009).

1.5 THE STUDY AREA

1.5.1 Location

The study area (Fig 1.2a) comprises of two sub-basins of the White Volta basin in the Northern part of Ghana. The terrain falls precisely between the latitudes 10° 28'N and 9° 29'N and longitudes 0° 30'E and 0° 45'E and covers part of the Northern and Northeast regions of Ghana. It spans an approximate total area of 9400 Km^2.

1.5.2 Climate and Vegetation

The usual vegetation in the area is mainly the savanna grassland with clusters of shrubs, and drought-resistant trees such as the shea, acacia, kapok and baobabs. Most of the grassland and trees have been destroyed by human's actions including annual bush-burning, farming and construction. The majority of the residents are subsistent and farmers, cultivating crops such as rice, sorghum, maize, yams, groundnuts, soya beans, beans and millets (Chegbeleh et al., 2009).

The climatic conditions found in the research area are characterized by the movement of inter-tropical convergence zone (ITCZ). Weather conditions varies annually in the area. The monthly average temperature ranges between 24°C to 32°C but can sometimes goes as high 40°C (Shahin, 2002). Two distinct seasons are found in the area the rainy season which start from May to early October each year. Followed by a prolonged dry season starting from October to April. The yearly rainfall average is around 1.1m (Chegbeleh et al., 2009; Gyau-Boakye & Dapaa-Siakwan, 1999). The atmosphere is usually dry with the coolest month been December and the warmest around

March each year. Annual humidity in area ranges between 20% in January to 80% in September (Adam & Appiah-Adjei, 2019).

1.5.3 Geology of the Study Area

The Neoproterozoic Voltaian sedimentary basin (VSB), which underlies the study area is among a series of smaller depositional basins located at the eastern margin of the Leo-man shield of the West African craton (Carney, et al., 2010). The Leo-Man shield consists of Achaean and Paleoproterozoic rocks estimated to be about 2.00 Ga and the forms the basement rocks of the Voltaian Supergroup. The Voltaian Supergroup comprises three main groups namely; Bombouaka, Oti-Pendjari and the Obosum Groups (Fig. 1.2) and underlies about two-thirds of the total landmass of Ghana (Carney et al., 2010; Kesse, 1985). Each of these groupings are separated by a tillite-marked unconformity. The groups are divided into formations comprising various lithological units. A recent lithostratigraphic classification of the Supergroup (Carney et al., 2010) indicates six rock formations with different lithologies within the study area. They include the Obosum Formation, Bimbilla Formation, Kodjari, Panabako Sandstones, Poubogou Formation and the Tossiegou shales and sandstones.

In the study area, the youngest of the Supergroup is referred to as the Obosum, occurring to the southern part (Fig 1.2a). It rests unconformably on the Bimbilla Formation of the Oti-Pendjari Group. This Group is made up of very distinctive lithic, feldspar-rich arenites and conglomerates that were deposited as terrestrial molasse at the latter stage of the Dahomeyide orogen uplift (Affaton et al., 1980; Carney et al., 2010; Kalsbeek et al., 2008). It also comprises of variegated siltstones and mudstone with some sturdy beds of sandstones mostly known as the Tamale sandstones.

The Bimbilla Formation has two sandstone members occurring at the base and the uppermost boundaries which are the major unifying features of the formation. The unit comprises of green to light brown, micaceous stratified siltstones, mudstones and flat, sharp-based sandstones. The mudstones often appear as reedy, flat beds with wind-rippled tops and low angle cross-bedding. The thin beds of the sandstones intercalates within the mudstones and siltstone units forming the Chereponi and Bunya end members (Jordan et al., 2009).

The basal member of the Oti-Pendjari Group is the Kodjari Formation and it comprises a distinctive triad of tuff, cap carbonate (Buipe limestone) and tillites which lie unconformably on the Panabako

sandstones (Carney et al., 2010). The Kodjar Formation also includes lithologies such as mudstones and shales, and lenses of different facies of sandstones, tuffs, silexites, greywackes, and limestones (Barfod et al. 2004).

The thickness of the Panabako sandstones in the research area ranges from 150-200 meters with an average of about 175 meters. It is made up of well-compacted, well-cemented, hard, well-sorted, medium-grained, quarzitic sandstones, that are mostly stiffened and seem crystalline in the northern part of the basin. Covering the Panabako sandstones is a characteristically lateritic layer, sometimes capped by thin iron oxide cement (Carney et al., 2010; Jordan et al., 2009).

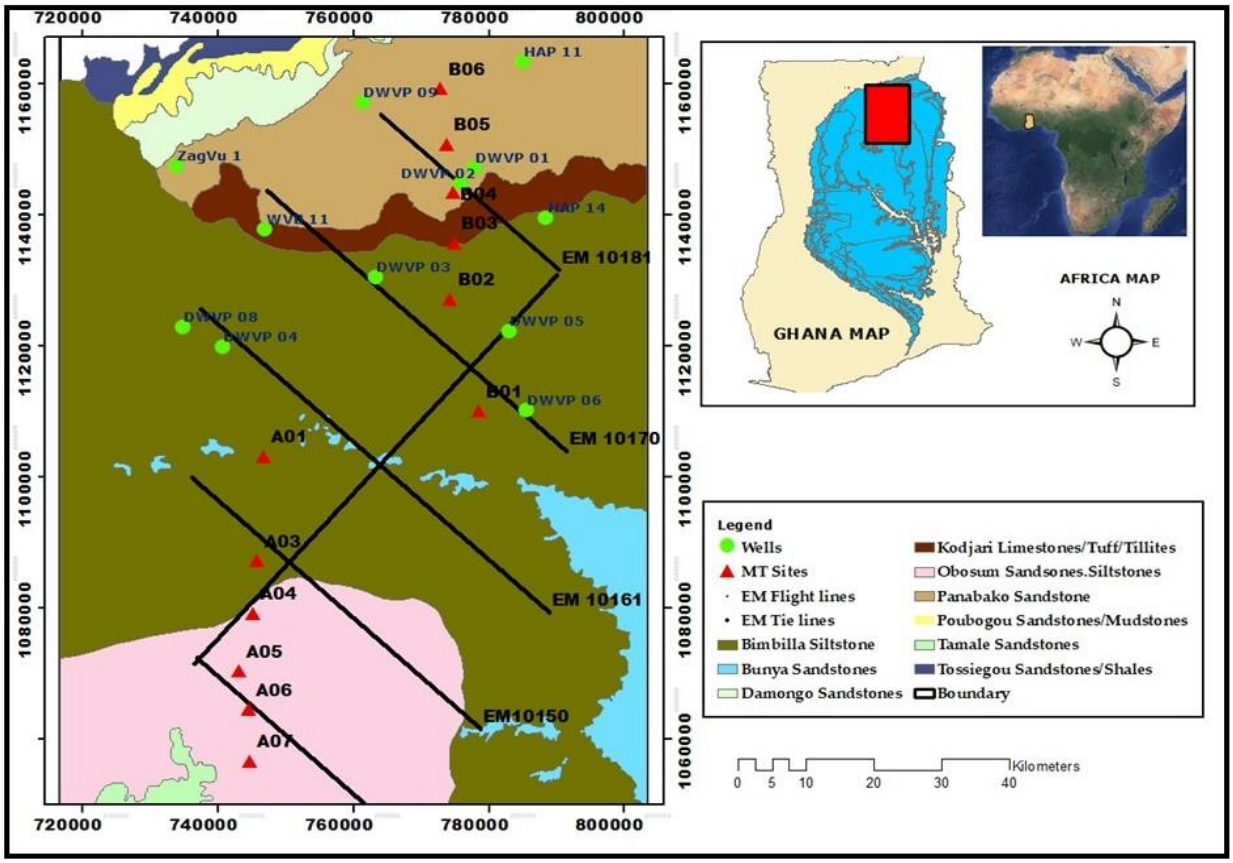

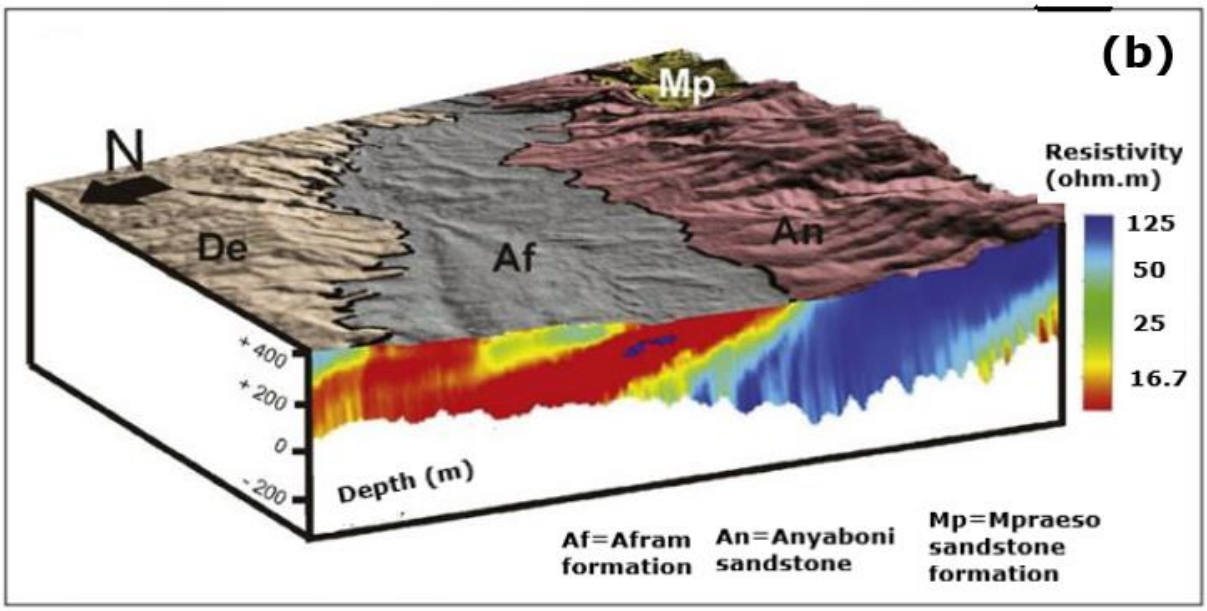

Figure 1. 2: (a) Geological map (modified after Carney et. al., 2010), showing AEM flight lines (black) and MT sites (Red triangles), with an inset, map of Ghana defining the study area in red rectangle (b) Stratigraphically succession of the different formation of the Voltaian Sedimentary Basin from satellite imagery overlain on AEM section (carney et al., 2010).

The Poubogou formation underlies the Panabako sandstones in the study area and it comprises shales and siltstones (mudstones), and outcrop to the north of the area along the Gambaga escarpment. This Formation thickness is estimated to be averaging around 170 meters. The Formation grades into the sandstone of the Panabako Formation overlying the Poubogou (Carney et al., 2010). Ayite et al (2008), noted that Poubogou Formation to be made up of micaceous siltstones (mudstones) which intercalates with thin beds of fine-grained sandstone mostly around the fringes of the basin.

1.5.4 Hydrogeology of the Area

In the Voltaian basin, the rocks are generally flat-lying and impervious except for some few locations (Amponsah et al., 2022). The rocks of the Supergroup have lost their primary porosities and permeabilities due to the Pan-African tectonic event which caused the sediments to be partially metamorphosed (Kesse, 1985). As a result, hydrogeological properties are based on the intensity of weathering and fractural entities such as faults, joints, fissure, bedding planes and lithological contacts (Acheampong & Hess, 2000; Aliou et al., 2022; Banoeng-Yakubo et al., 2011; Chegbeleh

et al., 2009; Gyau-Boakye & Dapaa-Siakwan, 1999). Well yields in the basin generally vary and decrease in the order of sandstones, limestones, siltstones/mudstones, and shales (Acheampong & Hess, 1998). Regional hydrogeological studies revealed that the fractures in the basin are erratic and in certain areas, they are dried and non-productive (Chegbeleh et al., 2009). The well output in the basin is between 5 to 1200 l/min, with water table fluctuation averaging about 4 meters while the static water levels (SWL) varies from 1 to 20 meters. Dapaah-Siakwa and Gyau-Boakye (2000) indicated that the success rates of well drilling is below sixty percent (60%) with discrete fractural entities which varies significantly in lateral extent controlling the movement and storage of groundwater in the basin.

The average well depth in the area is about 55 m with the most productive fractures observed between 13 m and 80 m (Bannerman, 1990). Aquifer yields are typically low to moderate with transmissivity spanning from 0.3 and 267 m^2 /day, with a mean value of 11.9 m^2 /day (Carrier, 2008; Banoeng-Yakubo et al., 2011). The majority of the aquifers in the basin are observed to be semi-confined (Chegbeleh et al., 2009). Groundwater recharge estimated for the area using chloride mass balance (CMB) method averages about 94 mm/year and ranges between 73 – 110 mm/year. Groundwater recharge occurs vertical through piston flow in the area (Addai et al., 2016).

The majority of the boreholes in the research area are completed with within the regolith consisting of saprolite and the saprock. The saprolite is made of sand, silt and clay size particles derived from the in-situ weathering and leaching of the bedrock. The composition of the Saprolite unit varies considerably ranging from highly clayey material to a mixture of clay and sand-size material (HAP, 2011). The upper part of the saprolite contains a lot of clay which in most places has transitioned into highly impermeable duricrust. The high clay material in the upper portions of the saprolite imposes confining to semi-confining conditions to the relatively permeable saprock and the topmost part of the fractured bedrock (Akudago et al., 2009). The variable nature of the saprolite unit suggest the possibility of perch aquifers in the area.

The saprock unit occurs between saprolite and the fresh bedrock at depth of about 20m in the basin (Carrier et al., 2011). In comparison to saprolite, the saprock is a zone with significantly high hydraulic conductivity. It is thinner compare to the saprolite and has been described as a zone where good yielding wells are found in the area (Carrier et al., 2011).

Because of the absence of primary porosity and permeability within the bedrock, hydrogeological conditions are determined by the existence and degree of interconnectivity of discrete fractures (faults and lithological contacts). The hydrogeologic conditions of the bedrock can be enhanced significantly depending on the degree of fracturing and the extent of interconnectivity of the fractures. The bedrock unit has been described as the zone where most prolific aquifers have been encountered and the yields of aquifers within this unit appeared to increased depths (HAP, 2011; Mainoo et al., 2019). Based on the analysis of borehole drilling data and geophysical log data, the thickness of productive structures in the bedrock unit usually exceed 20m (HAP, 2011). Available hydrogeological information for this unit indicates that, majority of high productive boreholes that have been drilled in Voltaian sedimentary basin tapped into a fracture aquifer at depth beyond 150m (Agyekum et al., 2006). The well yield versus depth trend analysis within the Voltaian basin by some groundwater experts (Agyekum & Asare, 2016b; Dapaah-Siakwa & Gyau-Boakye, 2000; Mainoo et al., 2019; Yidana et al., 2012) supports the assertion that, the yield of wells increases with increasing in most cases within the basin. It therefore suggests that, the groundwater fortunes of the basin could be improved if groundwater investigation efforts are channelled to characterized the basin subsurface at greater depths for possible productive structures.

1.5.5 Topography and Drainage

The topography of the area is mainly due to lithology or tectonic. Prolonged weathering and erosion are aided by some type of lithology. For instance, Banoeng-Yakubo et al., (2011) indicated that, areas underlain by arkosic sandstones is most likely to experience deep-seater weathering due of the rocks being rich in K-feldspar and low-temperature plagioclase. Such rocks weather faster compared to quartz rich lithologies. This differential weathering may influence topographical variations as well as water storing capacity and flow within the basin. In the area, higher elevations mostly occur at fringes while towards the centre of the basin is essential flat-lying.

The study area is principally drained by two main rivers which are tributaries of the White Volta. The rivers are the Nasia river occurring to the north and the Nabogo river found toward the south in the area (Fig 1.3). The Nasia and Nabogo rivers are sustained by network of streams within their catchments. Most of the catchment streams are ephemeral surviving only the rainy seasons except for a north-south stream to the northern. This stream defies the extreme temperatures and high evapotranspiration in the area flowing all year around and may probably sustained by groundwater.

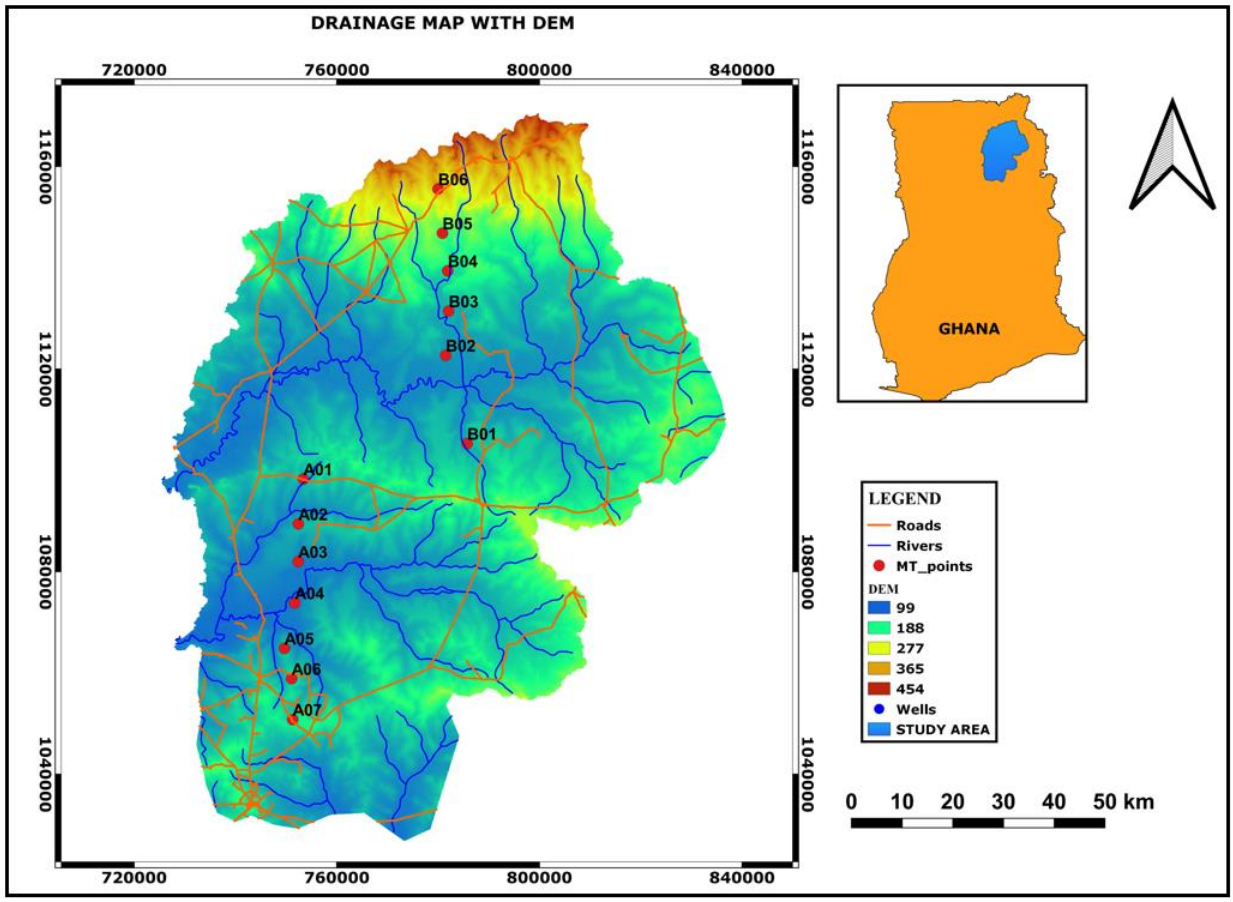

Figure 1. 3: Digital elevation model showing drainage patterns and MT stations (Red dots) in the area. The coordinates are in UTM as indicated in the map have been converted to geographic coordinates in the text for clarity. The shape of this map delimits the boundaries Nasia and Nabogu sub-basins of the white Volta basin and represent the study area.

CHAPTER TWO

OVERVIEW OF GEOPHYSICAL METHODS

2.0 GEOPHYSICAL METHODS USED IN THIS STUDY

Geophysics is the application of physics to geology to infer physical properties that maybe connected to geological processes. Geophysical methods enable the imaging of subsurface property distributions and the monitoring of spatiotemporal changes in a non-invasive manner (Wagner & Uhlemann, 2021). Different geophysical techniques measure different subsurface physical properties which are subsequently used for modeling. Understanding the basic principles of the techniques forms an important basis for their deployment in data acquisition and modeling. It is commonly acknowledged that geophysical models created by integrating data sources from different geophysical techniques minimize model uncertainty and enhance accuracy. The scientific principles of each method used in this study are presented in the sections that follows. Details of the basic principles are well established in many geophysical textbooks; hence a synopsis of each principle is shown.

2.1 ELECTRICAL RESISTIVITY METHOD

The electrical resistivity technique is among the commonly used geophysical methods for near surface investigations. This is because it is simple to use and the data inversion can be performed quickly to obtain results of resistivity for interpretation. It is robust and can be used within urban environment provided there is space to plant the electrodes. It has been used in many geological investigations due to the widespread of resistivity values exhibit by geologic materials. In a variety geologic settings, resistivities values can ranging from less than 1Ωm for ore deposits to above 10000 Ωm for Precambrian gneiss (Caselle et al., 2019; Hasan et al., 2018). Previously, the electrical resistivity procedure was thought to be extremely labour intensive. The introduction of the multi-electrode system has however, been able to lessen the laborious nature of the technique (Heather et al., 1999; Saad & Tonnizam, 2012).

2.1.1 Basic Principles

Electrical resistivity technique has been accepted as one of the effective subsurface exploration technique (Al-saadi et al., 2021). This is due to the fact that, resistivity of the subsurface materials is influenced by factors such as lithology, ionic content in pore fluids and metallic content. In a survey the ERT can be employed in a variety of configurations. The type of survey configuration used will be determined by factors including the survey objective, accessibility, the expected

electrical properties variability, availability of equipment and the data the processing capability (e.g. computers and softwares) (Binley & Kemna, 2005).

In subsurface characterization, the ERT can be used for 2-D, 3-D and multitemporal (e.g. Kamiński et al., 2023; Michot et al., 2003), depending on the depth of penetration and the resistivity differences between anomaly and the background values. The 2-D is the most commonly used and the 2-D traverse are executed by using multielectrode configuration which automatically measure the difference in potential across the electrodes. This allows to obtained resistivity values both in lateral and vertical orientations. The 3-D ERT has also proven effective at defining plumes or filtration path in the subsoil (Martorana et al., 2023). The multitemporal ERT approach has been useful in highlighting changes in groundwater content in the vadose (de Jong et al., 2020). The 2-D technique can sample down to depths of about 100m or even greater with wider electrode spacing.

2.1.2 Theory of the Electrical Resistivity method

Electrical resistivity technique is used for characterizing resistivity of the subsurface soil and structures (Reynolds, 2011). In resistivity measurement current is pushed into the ground using a pair of electrodes and the difference in potential is in turn recorded by another pair of electrodes planted into the ground. The external pair of electrodes represents the current electrodes (commonly denoted as C1 and C2 or A and B) for pushing electric current into the subsurface while the internal pair of electrodes (denotes potential electrodes P1 and P2 or M and N) connected to the voltmeter are used for measuring potential difference (Figure 2.1). A single reading yields the resistance R:

$$R = \frac{V}{I} \qquad (2.1)$$

Where V is the voltage and I is the current and R depends on the distribution of the subsurface resistivity and on the geometry (i.e. configuration) of the electrode array. The relation between the resistance and the sensor layout is represented by a geometry factor K which is dependent on the electrode array.

$$\rho = KR \qquad (2.2)$$

where K represents the geometry of the electrode array. In the Earth, for a homogeneous medium or resistivity rho, electrical current flow in all direction as shown in Figure 2.2 and the Voltage is represented by equation (2.3):

$$V = \frac{\rho I}{2\pi r} \qquad (2.3)$$

Where r is the distance between the current electrode and the point the voltage is measured. In a heterogeneous medium such as the ground, the distribution of resistivity yields the so-called apparent resistivity rhoa.

The resistivity in equation (2.2 and 2.3) becomes the apparent resistivity:

$$\rho = \rho_a \quad \text{e.i.}$$

$$\rho_a = 2\pi r \frac{V}{I} \qquad (2.4)$$

Current movement is concentrated in the more conductive volume. Potential difference pattern reveal information about the electrical properties of the subsurface inhomogeneities (Al-saadi et al., 2021; Samouëlian et al., 2005).

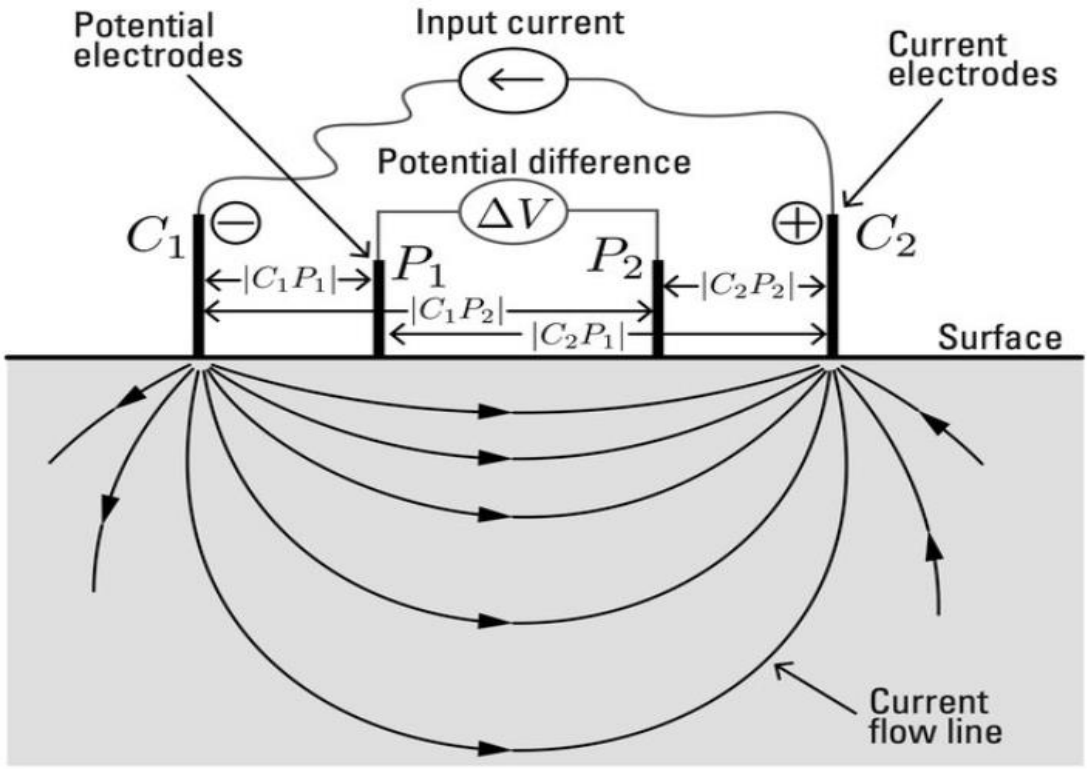

Figure 2. 1: Quadripolar configuration in a homogeneous half space showing current flow. C1, C2 represent electrodes pushing current into the subsurface and P1, P2 denote potential electrodes (Conti et al., 2021) for measuring potential difference.

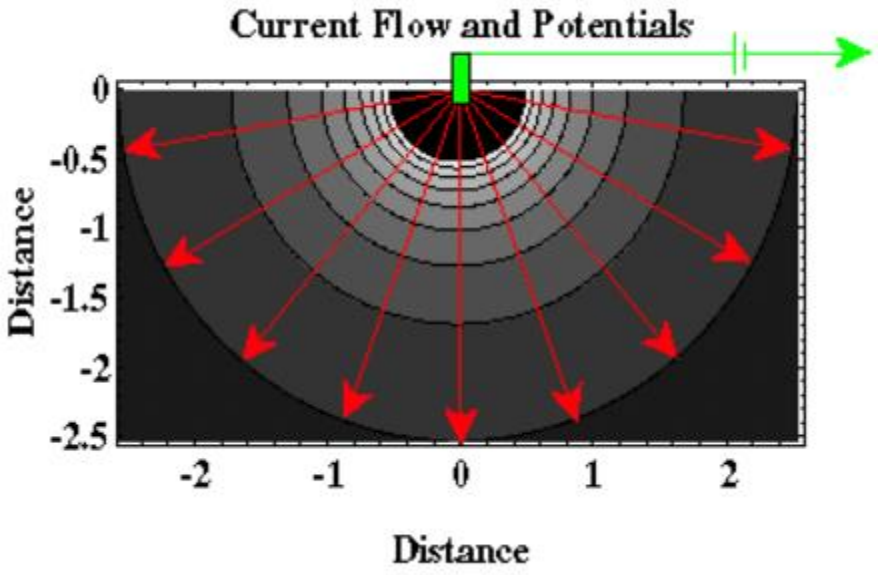

Figure 2.2: Electric current injected into the ground via an electrode (green square) and flowing (red arrows) through a three-dimensional earth (Boyd & Burnley, 2020).

For an electrode pair with current I at electrode C1 and -I at electrode C2 (Figure 2.1), the potential at a point is given by the algebraic sum of the individual contributions:

i.e. $V = V_{P1} + V_{P2}$

$$V_{P1} = \frac{\rho I}{2\pi}\left(\frac{1}{C1P1} - \frac{1}{C2P1}\right) \qquad (2.5)$$

$$V_{P2} = \frac{\rho I}{2\pi}\left(\frac{1}{C1P2} - \frac{1}{C2P2}\right) \qquad (2.6)$$

For two pairs of electrodes (Figure 2.1) used to measure the potential difference between the points P1 and P2.

The potential difference V may be measured as $\Delta V = V_{P2} - V_{P1}$

$$\Delta V = V_{P1} - V_{P2} = \frac{\rho I}{2\pi}\left(\frac{1}{C1P1} + \frac{1}{C2P1} + \frac{1}{C1P2} - \frac{1}{C1P2}\right) \qquad (2.7)$$

$V_{P1}\ and\ V_{P2}$ are potentials at P1 and P2. C1P1 is distance between C1 and P1, C1P2 is the distance between C1 and P2. Likewise, C2P1 is the distance between C2 and P1, C2P2 is the distance between C2 and P2. The distances are the actual distance between the respective electrodes, whether or not all electrodes lie on the same line.

2.1.3 Types of arrays

The ideal array to deploy for any field investigations hinges on the resistivity structure to be mapped, the sensitivity of the resistivity meter and the background noise level (Loke, 2001). The most commonly used array for resistivity survey measurements are;

a. Werner
b. Schlumberger
c. Dipole-dipole
d. Pole-pole
e. Pole-dipole

According to Loke (2001) some of the characteristics to consider when choosing an array for a resistivity survey include, the array's sensitivity to both the lateral and vertical variations in resistivity, the investigation depth, the lateral data coverage as well as the strength of the signal. The choice of electrode spacing is also significant as it influence the resolution of the data acquired and determine the depth of the investigation (Ewusi et al., 2020). The Werner and Schlumberger arrays were used in this current research to characterized waste dumpsites in some municipalities in the northern and northeast regions of Ghana. These two arrays are briefly presented below;

2.1.3.1 Werner Array

The Werner setup is utilized for both profiling and vertical sounding to detect resistivity variations in the subsurface (Faleiro et al., 2019; Loke, 2001). The Werner sounding technique setup spacing expands around the array centre while keeping an equal separation between each electrode (Figure 2.3). The Werner configuration has nearly horizontal contours underneath the centre of the setup hence making the Werner setup relatively sensitive to vertical variations in resistivity below the centre of the array and less sensitive to the lateral variations in ground resistivity (Loke, 2001). The advantages of this setup are that the apparent resistivity can easily be calculated and relatively small current magnitudes are needed to create measurable potential difference.

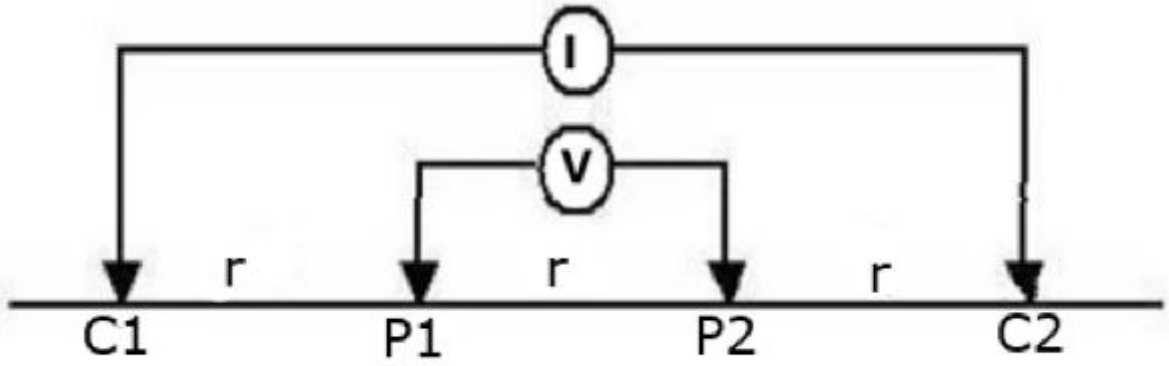

$$\rho_a = 2\pi r \frac{V}{I}$$

Figure 2. 3: Diagram showing four collinear equally spaced electrodes of Werner configuration (LANGEO, 2023).

2.1.3.2 Schlumberger Array

In the Schlumberger array, the spacing of two outer current electrodes is varied while the potential electrodes at the centre remain relatively constant (Figure 2.4). The position or spacing of the potential electrodes are only changed when the voltage becomes too small to be measure as a result of the wide spacing in current electrodes. The advantage of this array is that, it gives better resolution for greater depth sounding and consumed less-time during field deployment compare to Werner array.

$$\rho A = \frac{V}{I}\pi \frac{b\,(b+a)}{a} = \frac{V}{I}\pi \frac{b^2}{a} \quad \text{if a<<b}$$

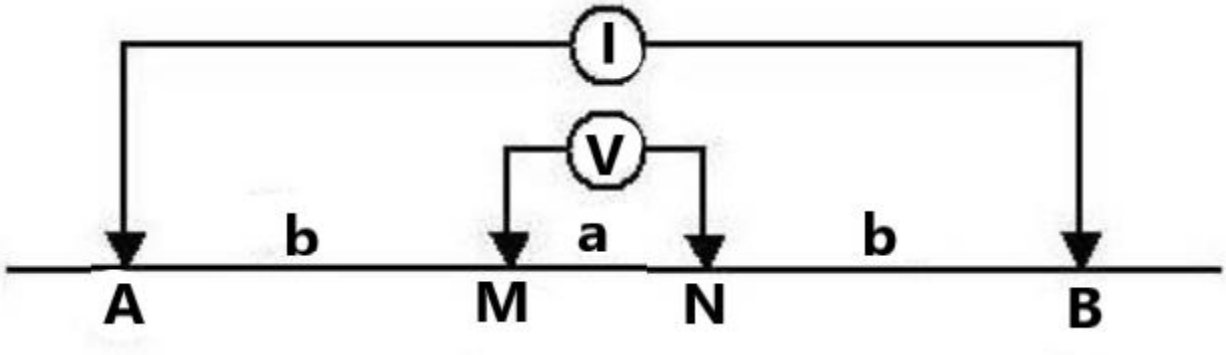

Figure 2. 4: Diagrammatic illustration of the Schlumberger configuration with four collinear electrodes (LANGEO, 2023).

2.1.4 2-D Electrical Imaging Survey (Multi-electrode Survey)

This system comprises of multielectrode for 2D and 3D resistivity survey used for delineating geological structures. Data is measured in series, recording both horizontal and vertical resistivity variations along traverse with electrode spacing increased at each successive measurement (Figure 2.5). As the electrode spacing is increased, the depth of penetration increases, and the recorded apparent resistivities can be utilized to create pseudo-sections that show variations in resistivity in both the lateral and vertical directions. On the field of measurements, the pair of potential and current electrodes are kept at a systematic fixed distance from each other and are gradually moved automatically along a line at the surface and measurements are made at each step. The spacing between electrodes is increased automatically by a factor of $n = 2$, then a second measurement is started. The process is repeated until the maximum spacing between electrodes is reached. The greater the n-values, the deeper the depth of investigation (Figure 2.5). The depth of investigation deduced is known as pseudo-depth since current also depend on the resistivity of the medium. The depth of investigation can also be calculated through the Jacobian, however, it only correlate to the maximum depth in the Pseudo-section to some extend (Vest Christiansen & Auken, 2012). The resolution of sections produced from the inversion of the apparent resistivity data depends on the electrode spacing. The smaller the spacing, the better the resolution and the lesser the penetration. Since its inception, 2-D electrical imaging technique has shown to be more potent and capable of measuring resistivity changes both in the horizontal and vertical orientations making it more accurate than the erstwhile 1-D measuring technique. The 2-D imaging technique usually involve about 100 to 1000 measurements to compare to about 10 to 20 sounding recorded in 1-D survey (Loke, 2001). The technology can deliver information on various subsurface boundaries and conditions, which can indicate soil or bedrock lithology variations (Crawford et al., 2018; Heather et al., 1999). This allows for the identification of weathered areas as well as subterranean fluid flow pathways. An example of the 2-D imaging system is the Lund resistivity imaging system which is an automatic electrical imaging suited for measuring resistivity and induce polarization (IP) (ABEM, 2010).

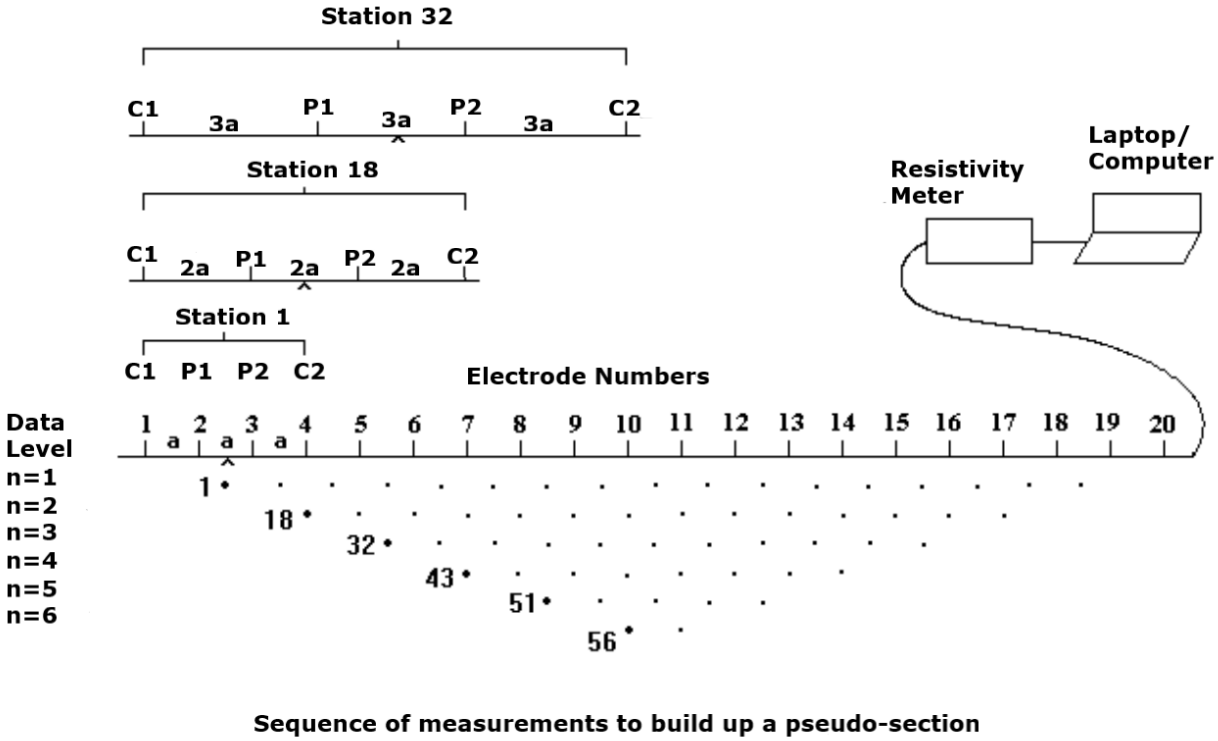

Figure 2. 5: Distributions of measured resistivity used for building up a pseudo-section in multi-electrode survey (Loke, 2001).

Figure 2. 6: Field setup using the ABEM LS Terrameter at Taha dumpsite located in the Tamale metropolitan district, northern Ghana.

2.1.5 RES2DINV Inversion

The RES2DINV inversion code described in Loke (2001) was used to invert the apparent resistivity data collected from the waste dumpsites. For start, the model used by the inversion software (RES2DINV) is divided into several blocks (Figure 2.7) of apparent resistivity values. The distribution of the blocks is linked to the arrangement of data points. The distribution and size of the of the blocks is automatically created by the application. The bottom row of the blocks is approximately set to be equal to the equivalent depth of investigation (Edwards, 1977) of the data points with the widest electrode separation. The apparent resistivity values are calculated using a forward modeling subroutine, and the inversion process is performed using a non-linear least-square optimization technique (Loke & Barker, 1996).

By adjusting the resistivity of the model blocks, the application tries to minimize the variations between the computed and measured apparent resistivity values. The model is deemed suitable

when the computed values and the observed data best fit and the root mean square (RMS) error indicate the measure of difference between the computed and the measured apparent resistivity. Iterations stop when the defined number of iterations is reached or the variations in values of RMS error is lower than a threshold value. At this point, extra iteration will not yield any significant improvement on the results. The model with the lowest probable RMS error can at times give large illogical changes in the model resistivity values and may not necessarily be the model from geology standpoint (Loke, 2001). In general, the best strategy is to select the model at the iteration after which the error does not vary significantly. This typically occurs between the third and fifth iterations (Loke, 2001).

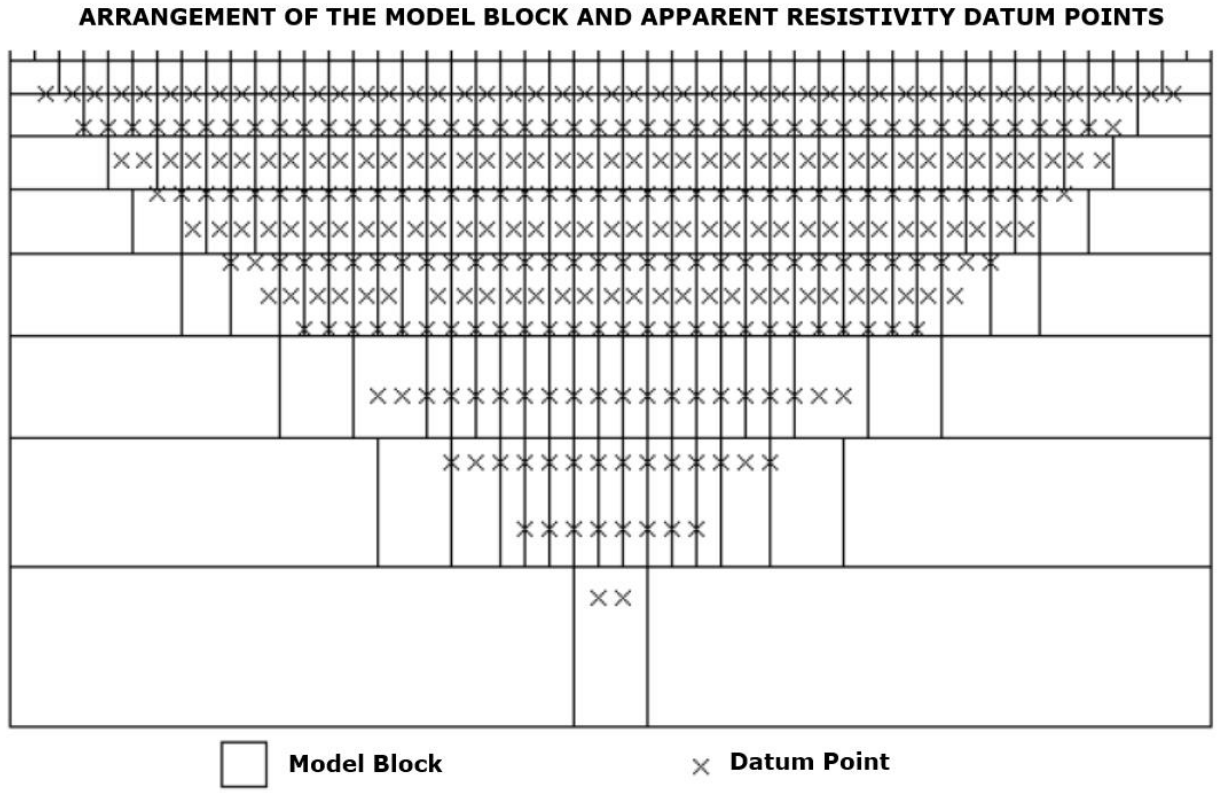

Figure 2. 7: The arrangement of the blocks with distribution of data points used by inversion program to create pseudo-section.

The conversional smoothness-constrained least square method (de Groot-Hedlin & Constable, 1990) tries to minimize the square of the differences in the model resistivity. The resistivity image that results is a model with smooth variation in the resistivity values that correspond to reality. This is the default method used by RES2DINV software. The smoothness-constrained method produces

images that are far from the real resistivity distribution in the presence of sharp boundaries with high resistivity contrast (Fiandaca et al., 2015; Loke & Barker, 1996). When the robust model constrains inversion, technique is used for the processing of the resistivity model, the inversion attempts to reduce the absolute variations in resistivity values. Figure 2.8 show the results from the inversion of a synthetic data set using the standard least-squares smoothness-constrain and the robust inversion model.

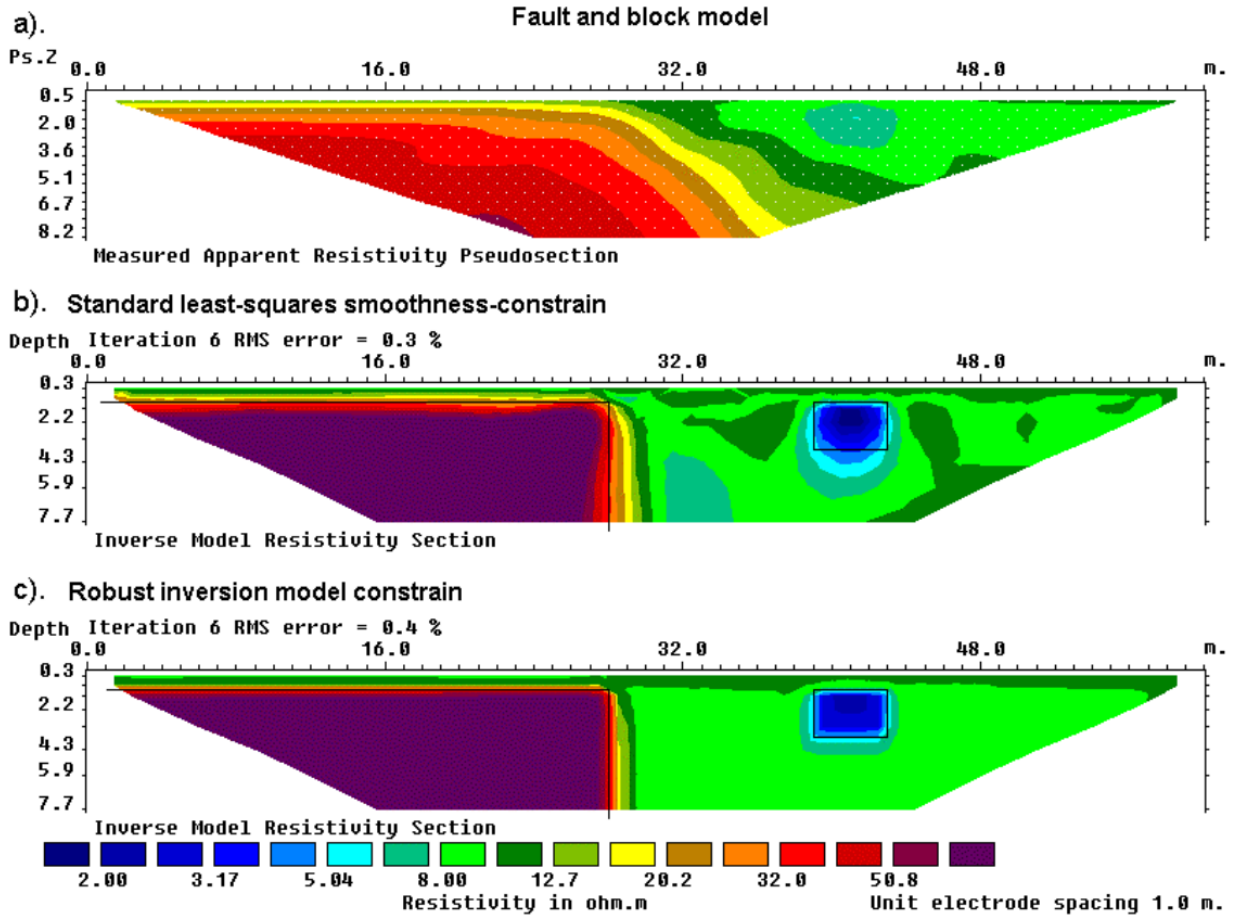

Figure 2. 8: A typical case of the inversion outcomes using the smoothness-constrain and robust inversion model constrains. (a) Apparent resistivity pseudo-section (Wenner array) for a synthetic test model with a faulted block (100 Ωm) in the bottom-left side and a small rectangular block (2 Ωm) on the right side with a surrounding medium of 10 Ωm. The inversion models produced by (b) the conventional least-squares smoothness-constrained method and (c) the robust inversion method.

The fundamental disadvantage of this inversion program is that a cell-based inversion model is normally applied to the model complex geological structures by making assumption such the variation of resistivity is smooth across the structure. The algorithm divides the subsurface into

several rectangular cells and then calculate the resistivities of each cell. These assumptions and divisions may not always result in optimal resistivities (Ewusi et al., 2020).

2.2 AIRBORNE GEOPHYSICAL SURVEY

Airborne geophysical survey techniques enable quick investigation of large areas without directly destroying the natural environment (Baranwal & Rønning, 2020). The techniques provide a means to map an otherwise inaccessible areas where ground-based geophysical techniques application may not be possible. When compared with ground-based methods, airborne techniques offer the advantage of rapid acquisition of data at scales that are suitable for many geophysical problems. Airborne surveys are useful for surveying places that are physically accessible but that have social, economic, or political barrier or environmentally hazardous (Roch, 2007). Airborne geophysical techniques have undergone continuous development including transition to digital technology and refinement of survey methods since their initiation. This improvement in the airborne technology has seen the introduction of systems such the EQUATOR, SkyTEM and airborne drones unmanned aerial systems). Due to the numerous advantages, the demand for the use of the airborne techniques have increased over the past decade. Airborne survey methods have been applied across many areas in the Earth sciences including, geology, hydrogeology, environmental, engineering, and hazards mapping (Siemon et al., 2020).

The methodology used in airborne geophysical surveys are similar to their ground-based counterpart. However, instruments used for airborne survey have to be more sensitive since the signal will be weaker due increased distance from the source (Nazari et al., 2023). The measurements are more complex due to external influences from electrical and magnetic disturbance from the aircraft (Roch, 2007). Elaborate instrumentation is also required for position location and data recording. There are basically four airborne geophysical survey procedures utilizing magnetic, electromagnetic, gravity and radiometric methods. These techniques were developed as powerful tools for mapping geological structures for minerals exploration. However, due to the improvement in the techniques resolution and the development of powerful data processing software, these techniques are now been applied across all sectors in geosciences. Three of the four airborne survey procedures are discussed in this current work as the fourth (radiometric data) was not used. The three include aeromagnetic, aerogravity and airborne electromagnetic (AEM). As of now, there are many different types of airborne survey systems and sensors used for

different surveys across the globe but in here, we describe only the airborne systems and sensors that were used to acquired data used in this study.

2.2.1. Airborne Magnetic (Aeromagnetic) Procedure

The magnetic method measures the spatial variation in Earth magnetic field. Magnetic measurements made from the air are known as aeromagnetic and have been used widely in regional survey for geological mapping and exploration. In terrains where outcrop exposures are limited, the aeromagnetic techniques become indispensable component of the exploration program (Dentith & Mudge, 2014). In aeromagnetic survey, the magnetic sensors are towed in a house called 'bird' designed to keep the instruments (e.g. magnetometers) way from the magnetic effect of the aircraft (e.g. helicopters and drones). Basically, there are two types of magnetometers used in magnetic survey; thus, the proton magnetometer and the optically pumped magnetometer. Other magnetometers such as the fluxgate magnetometer is also used in some surveys. For the data used in this study, the Scintrex CS-2 single cell optically pumped cesium vapor magnetometer sensor was used by Fugro Airborne Survey (FAS) for scalar measurements of the Earth's magnetic field. Three most important factors considered during airborne surveys are the flight height, the traverse line separation and the traverse direction (Figure 2.9). Position fixing used to be a problem in airborne survey but that has been solved with the availability of GPS. As stated earlier the concepts of airborne surveys are similar to their ground-based counter parts.

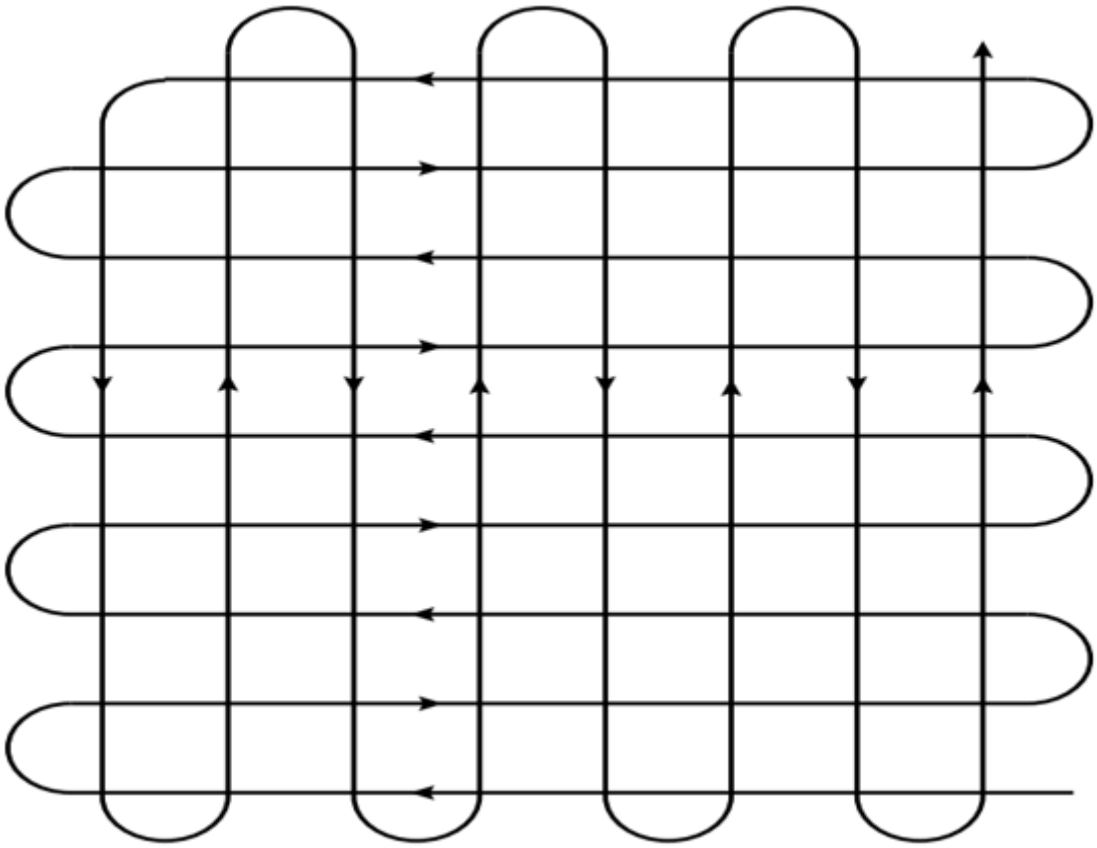

Figure 2. 9: Typical flight lines used in airborne survey (Reynolds, 2011).

2.2.1.1 Basic concept of the magnetic method

When a bar of magnet is present, a magnetic flux is formed and flow from one end of the magnet to the other establishing what is referred to as the magnetic poles (Figure 2.10). If this magnet is suspended in air, it naturally aligns itself to the flux of Earth magnetic field. The pole of the magnet which inclined to the direction of the Earth north pole is called the north-seeking pole or the positive pole, and this is balanced by a south-seeking pole at the other end (Kearey et al., 2002). The magnetic poles always exist in pairs forming a dipole and defined by the equation (2.8):

$$B = C_m \frac{m}{r^3}[3(\hat{m}\,.\,\hat{r})\hat{r} - \hat{m}] \qquad r \neq 0 \qquad (2.8)$$

The magnitude of B relates proportionally to the dipole moment (m) and inversely to the cube of the distance to dipole (r). The direction of B depends on the direction of both $\hat{r}$ *and* $\hat{m}$. All flux lines of B emanate from the positive end of m and ultimately return to the negative end. C_m is proportionality constant.

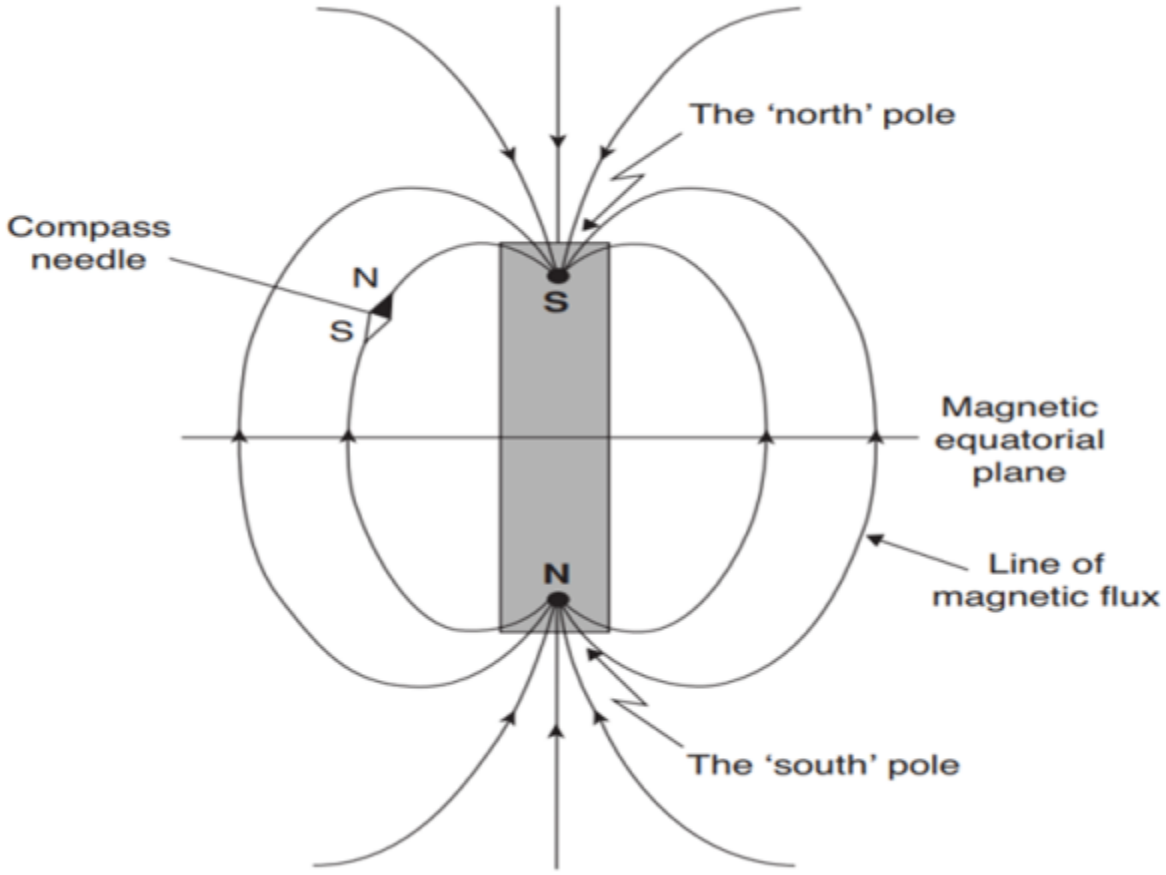

Figure 2. 10: A bar of magnet surrounded by magnetic flux (Reynolds, 2011).

The units of measurements are in Tesla (T). Since the magnitude of the Earth's magnetic field is only about $5 \times 10^{-5}T$, a more convenient unit of measurement used in geophysics is the nano Tesla $1nT = 10^{-9}T$. The magnetic moment of the magnetic dipole expressed in Am^2.

When a substance is exposed to a magnetic field, it may develop magnetization in the direction of the field. This phenomenon is called induced magnetization or magnetic polarization (Kearey et al., 2002) and it cause the elementary dipole of the substance to align in the direction of the field. The intensity of this magnetization on the substance J_i is defined as a dipole moment per unit volume of the substance:

$$J_i = \frac{m}{V} \qquad (2.9)$$

Where *m* is the magnetic moment of a sample of Volume *V*. By implication J_i is expressed in Am^{-1} which is also the unit of magnetizing force *H*.

The induced intensity of magnetization is proportional to the strength of the magnetizing force *H* and is defined as

$$J_i = kH \qquad (2.10)$$

Where k is the magnetic susceptibility of the substance. Since J_i *and* H are both measured in Am^{-1}, it implies susceptibility is dimensionless in the SI system.

The magnetic field *B* (also called magnetic induction) and the magnetizing force *H* are related in vacuum by:

$$B = \mu_0 H \qquad (2.11)$$

where $\mu_0$is the permeability of vacuum ($4\pi \times 10^{-7} Hm^{-1}$), hence the relationship (2.11) can be considered to represent the Earth magnetic field. The Earth's field induces magnetic anomalies in upper crustal rocks. The induce field is a dipolar and the amplitude of the anomaly is directly proportional to J_i in equation (2.10). Equation (2.10) shows that, in the presence of an inducing field a body with magnetic susceptibility (k) can be magnetized.

2.2.1.2 Types of Magnetism

At the atomic scale, every substance possesses magnetic property. Due to the orbital motion of electron around the nucleus and the spinning of the electrons, atoms have a magnetic moment. According quantum theory, two electrons can exist in the same electron shell (or state) as long as they spin in opposite directions (Reynolds, 2011). The spin of magnetic moment of such electrons cancels out and they are referred to as paired electrons.

In diamagnetic materials, all the electron shells are complete, without any unpaired electrons. When these materials encounter an external magnetic field, the orbits of the electron rotate so as to generate a magnetic field in opposition to the applied field. This results in a weak, negative susceptibility. Paramagnetic substances on the other hand have incomplete electron shells. An applied magnetic field causes the unpaired electron to produce an unbalanced spin of magnetic dipole moment in the same sense as the applied field resulting in a relatively weak positive susceptibility. Generally, paramagnetism is at least an order of magnitude stronger than diamagnetism (Reynolds, 2011). In ferromagnetic substance the dipoles are parallel (Figure 2.11), resulting in a very strong spontaneous magnetization that can even exist in the absence of external magnetic field. Ferromagnetic materials have a very high magnetic susceptibility. Examples of ferromagnetic materials include; iron, cobalt and nickel. The magnetic coupling within these materials can cause the magnetic moments to aligned either parallel or antiparallel as seen in

hematite. In antiferromagnetic materials (Figure 2.11) the magnetic field of the dipoles counterbalance each other, leading to no external magnetic effect. However, defects in the crystal structure of an antiferromagnetic material may give rise to small net of magnetization known as parasitic antiferromagnetism (Kearey et al., 2002).

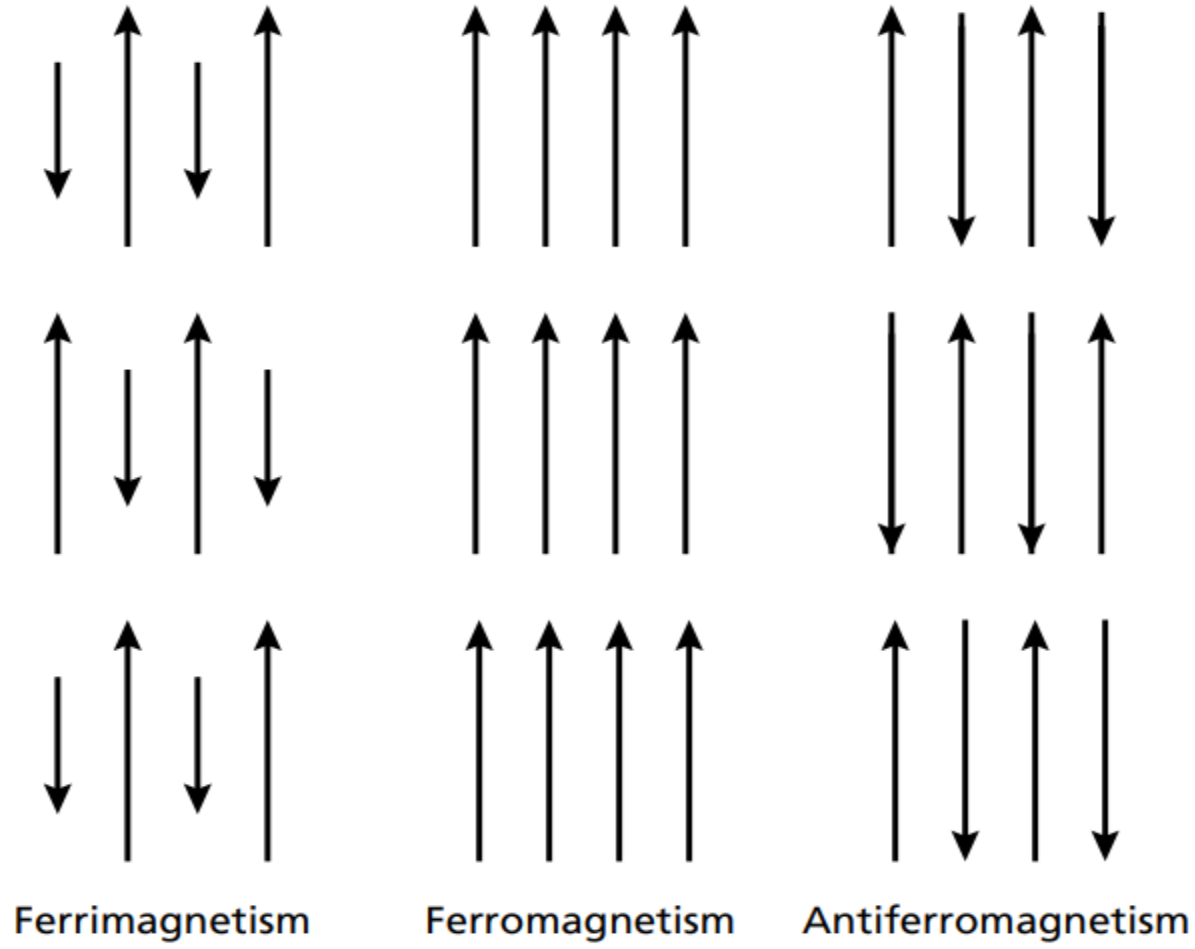

Figure 2. 11: Schematic representation of the strength and orientation of elementary dipoles within ferrimagnetic, ferromagnetic and antiferromagnetic domains (Kearey et al., 2002).

In ferrimagnetic material such as magnetite, one of the antiparallel magnetic moments is stronger than the other. As a result, ferrimagnetic materials can show strong spontaneous magnetization and high magnetic susceptibility. Almost all the minerals responsible for the magnetic properties of common rock types fall within this category (Dunlop & Ozdemir, 2007).

Both ferrimagnetic and ferromagnetic materials experience reduction in strength as temperature increase and disappear at the Curie temperature. Beyond the Curie temperature, the interatomic

distances increased, preventing electron coupling, and the material displays traits similar to those regular paramagnetic substance. The Curie temperature differs across various minerals and will be vary for whole rock depending on the magnetic minerals composition present (Kearey et al., 2002). The capability of a material or rock to acquire magnetism when exposed to an external field like the Earth's field is known as induced magnetization. Induced magnetization hinges on both magnetic susceptibility of the material (e.g. rock) and the external field strength. The magnetization left in a material after the external field is removed is called remanent or residual or permanent magnetization. This type of magnetism is permanently held by rocks after cooling below the Curie temperature at the time when the rock was formed. The induced and remanent magnetizations of rocks are as a result of a multifaceted interconnection among element like mineralogy, grain size, domain structure, temperature, time, and ambient geomagnetic field (Dunlop & Ozdemir, 2007).

2.2.1.3 Magnetic Anomalies

The geomagnetic field at or near the Earth's surface is mainly (98%) generated within the Earth's core (Reynolds, 2011). External current origins like the ionosphere and magnetosphere generate current within the Earth due to external field fluctuations in addition to the permanent and steady-state induced magnetization of crustal rocks all contribute to the overall geomagnetic field. The geomagnetic field associated with rocks, is measured during magnetic survey. The magnetic anomalies induced by rocks are superimposed on the geomagnetic field in a similar fashion like that gravity anomalies are superimposed on the Earth's gravitational field (Kearey et al., 2002). Modern instrument used in magnetic survey measures the total magnetic intensity (TMI) which is the modulus of the vector field. The magnetic scenario is more complicated, due to variations not just in the amplitude but also in the direction of the geomagnetic field. The TMI measured is subjected to data reduction techniques in order to obtain the magnetic anomalies associated with the source of the anomaly.

2.2.1.4 Acquisition, Processing and Reduction

After magnetic survey is carried out and measurements are made, data reduction is necessary to remove all factors contributing to the magnetic variations from the observations data leaving only magnetic effects arising from the subsurface. The airborne data used in this research was acquired from the Ghana Geological Survey Authority (GGSA) after all the data reduction procedures had been performed on the data by the data acquisition company, Fugro airborne survey limited (FAS).

The airborne survey was conducted between December 2005 and April 2008 by Fugro Airborne Survey (FAS) limited on behalf of the ministry of finance and economic planning Ghana, for the GGSA under the European sponsored mining sector support program (MSSP) (Fugro Airborne Surveys, 2009b). It was carried out for the purpose of mineral exploration. FAS limited using the Casa-212 aircraft, conducted an airborne survey over the Volta and Keta basins of Ghana. The airborne electromagnetic (AEM) data was recorded using the GEOTEM 20 channel multi-coil systems receivers with vertical loop (number of turns 6). The AEM data was flown at132° along 20 km line spacing with a flight height of 120m along and across the general geologic strike lines within the Volta and Keta basins. A much denser lines spacing of 200m within the 20 km spaced lines (Fugro Airborn Survey, 2009a) was also recorded as an additional AEM data over the area, however due to the revised data policy within GGSA, it was difficult to obtained that (200 m) data. The Scintrex CS-2 single-cell optically pumped cesium vapor magnetometer with a sensitivity of 0.01 nT was deployed to measure the total magnetic field component (Fugro Airborne Survey, 2009a) over the two basins in Ghana. The aeromagnetic data was acquired at a flight height of 75m with lines spacing of 500m along 135° direction. The aerogravity data was measured at a flight height of 859m along 5 km line spacing in NW-SE direction. Tie lines were flown at N042°E for AEM, and S225°W for aeromagnetic but no direction was recorded for the aerogravity data. The international geomagnetic reference field (IGRF) formular for 2005 was used to eliminate the geomagnetic gradient from the data. The data acquisition company also carried out other pre-processing operations such as micro-levelling, diurnal variations, deculturing, removal of effects from metallic features etc and subsequently stored in a geosoft database format consisting of different channels for different data parameters.

2.2.1.5 Processing and Interpretation of Aeromagnetic Data

A subset of the three sets of airborne data were obtained from GGSA for this study. The three data sets comprise aeromagnetic, aerogravity and AEM data. We processed the high resolution aeromagnetic data for interpretation using geophysical filters in Oasis Montaj version 2021.2 (Geosoft Inc., 2021). The choice of filters and processing techniques were informed by the objectives of the study. Filtering techniques such as the reduced to equator (RTE), first vertical derivative (FVD), total horizontal derivative (THD), and Euler deconvolution were applied on the residual TMI of the aeromagnetic data using Oasis Montaj.

The Oasis Montaj program is a software package produced by Geosoft and distributed by Seequent. It is equipped with several data processing capabilities and algorithms for processing and visualizing airborne data and other large data sets. It is flexible and user-friendly allowing for the integration of different geophysical data sets such seismic, resistivity and geological data sets. The program has an embedded automated and semi-automated algorithm for quick data processing and its used widely among the research community and industry.

2.2.1.5.1 Reduce to Equator (RTE)

The magnetic intensity anomaly was derived after subtracted the IGRF values to remove the regional effects of the earth's core magnetic field. The reduced to the magnetic equator (RTE) technique was applied to filter undesired distortions in shape and sizes, and locations of magnetic anomalies, potentially caused by the effect of the inclination and declination of the magnetic field. Thus, transformation using the RTE filters provides a more precise estimate of magnetic source positions, and thereby making the magnetic anomalies easier to interpret (Mohamed & Abu El Ella, 2021). The decision to apply RTE rather than RTP (reduce to magnetic pole) was determined by the location of the study area been closer to low magnetic latitudes. Reducing to pole at low magnetic latitudes poses challenges as certain bodies exhibit no detectable magnetic anomaly when the magnetic inclination is zero (Grauch et al., 2004). Also, the application of RTP on low magnetic latitude data can result in a north-south alignment of the magnetic anomalies hence making the data noisy (Hayatudeen et al., 2021; Osagie et al., 2021). The technique effectively improves the correlation of anomaly pattern to known geology by removing the influence of strong remnant component in the data.

2.2.1.5.2 Total Horizontal Derivative (THD)

This filtering technique measures the lateral rate of change of the potential field. Thus, the derivative is a vector filter which provides supplementary insights into the directional changes of the total field (Christensen & Dransfield, 2002; Salem et al., 2008) and is good for delineating linear features such as faults and dykes from magnetic data. THD technique is effective at highlighting edges and discontinuity patterns in potential field data (Osagie et al., 2021; Osinowo et al., 2019)**.** Even with a wider line spacing, the THD filter can deliver advance resolution and greater accuracy (Oni et al., 2020). It is modulus of the horizontal gradient dF. If F(x,y) is the TMI then the total horizontal derivative magnitude THD(x,y) is given by;

$$THD = \sqrt{(\partial F/\partial x)^2 + (\partial F/\partial y)^2} \quad (2.12)$$

The THD technique can be utilized to delineate edges of susceptibility difference (Saibi et al., 2021). The filter capitalizes on the details that the lateral gradients of the magnetic field caused by a planar body tend to have maximum values that exceed the boundaries of the anomalous body when the edges are vertical and well- separated from each other (Hayatudeen et al., 2021; Golshadi et al., 2016).

2.2.1.5.3 First Vertical Derivative

The first vertical derivative (FVD) computes the vertical rate of change of magnetic signal. The FVD is equivalent to an isotropic horizontal derivative. Its application to magnetic data helps to enhance the details of short wavelength signals and sharpens the geophysical anomalies for better interpretation as it remarkably enhances the resolution of closely spaced and superposed anomalies. It is a useful technique for identifying anomalies over different structures in potential field data and significantly represses the regional effects on the data (Mohamed & Abu El Ella, 2021; Blakely & Simpson, 1986). The FVD filter is more sensitive to local changes than to regional influence and is effective in highlighting high frequency features that might otherwise be overshadowed by large amplitude anomalies (Cheunteu Fantah et al., 2022).

2.2.1.5.4 Euler Deconvolution Technique

The 3D Euler method was applied to determine the source-depth and geometry of the linear structures revealed by the VD and THD techniques. The method operates on the principle that anomalous magnetic fields of localized structures are homogeneous functions of the source coordinates and hence satisfy the Euler homogeneity equation (Reid et al. 1990; Thompson 1982). The use of this method has emerged as a robust tool for determining the depth to source as well as the geometry of structures in magnetic data interpretation (e.g. Barbosa et al., 1999; Oni et al., 2020; Reid et al., 1990; Stavrev & Reid, 2007, 2007). In Euler deconvolution, a slide window operator is systematically moved across the entire dataset. The measured data inside the window are then solved using the Euler deconvolution homogeneity equation linearly to estimate the depth to source of the magnetic bodies. The homogeneity equation for magnetic data given by Blakely, (1996) can be written in the form:

$$(x - x_0)\frac{\partial F}{\partial x} + (y - y_0)\frac{\partial F}{\partial y} + (z - z_0)\frac{\partial F}{\partial z} = N(B - F) \quad (2.13)$$

Where (x_0, y_0, z_0) are the positions of the magnetic source whose total field (F) is detected at (x, y, and z). B is the regional magnetic field N is the measure of the fall-off rate of the magnetic field and may be interpreted as the structural index. The structural index (N) is a critical parameter in Euler deconvolution analysis and requires a good understanding since it characterizes the source geometry of the structures. In the magnetic case it varies from zero (0) (contact of infinite depth extent) to 3. Although no prior knowledge about the anomalous source of magnetization is required, the technique still has some setbacks. The Euler technique often generated large number of solutions with some invalid solutions caused by interference of adjacent field source (background field data) (Cooper, 2004). The interference caused by the background field data affects the accuracy of the technique leading to inconsistency in the source positioning (Liu et al., 2023).

2.2.1.5.5 Radial Average Spectrum Analysis of Aeromagnetic data

The radial average power spectrum has emerged as one of the modern automated methods for rapidly determining depth to source of magnetic anomalies. Over the last two decades, the spectral technique has been extensively applied to magnetic data infer the depth to source of certain geological features, such as the magnetic basement (e.g. Abdelaal et al., 2021; Al-Badani & Al-Wathaf, 2018; Bosum et al., 1989; Connard et al., 1983; Osinowo et al., 2019; Pedersen, 1991; Spector & Grant, 1970). One major advantage of the technique is its ability to filter the data while preserving the information in the data (Wahaab, et al., 2017). The radial average power spectrum technique depends on data analysis using Fourier Transform applied on magnetic data, which calculates the depth from the spectrum. Its application on potential field data was proposed by Spector and Grant, (1970). They studied the relationship between the power spectrum of aeromagnetic anomalies and the average depth of source bodies using some statistical assumptions. A potential field (e.g. aeromagnetic data) may be thought as representing a collection of interfering waves with different wavelength and direction. Regardless of the direction, a power spectrum can be generated by plotting each wave's log power against the radial wave number (Hayatudeen et al., 2021). Within a frequency domain, the distribution of the different wavelengths (short to long) can be analyse across all the measured frequency. The radial average power spectrum can then be divided into sequences of straight-line segments with each section representing a collective response of a group of sources at a given depth. The gradient of the line is directly related to the depth. The gradient or slope of each line segment gives an information about the depth to the top

of an ensemble of magnetic bodies (Kivior & Boyd, 1998). The general mathematical expression of radial average spectrum as stated by Spector and Grant, (1970) is given by;

$$h = \frac{M}{4\pi} \qquad (2.14)$$

Where M is the slope of the straight-line fitting semi log plot power versus wave number and h represent the depth of an ensemble in the spectrum. The drawback of this technique is that, it averages information over the spectrum window. The power spectrum is calculated automatically from the grid tapering outside the data to make the edges match hence introducing bias.

2.2.2 Airborne Gravity Data

The basis upon which gravity method derived is summarized in two laws derived by sir Isaac Newton. The first is the law of gravitation which states that the force of attraction (F) between two masses $m_1 and\ m_2$, whose dimensions are small with respect to the distance (r) between them, is given by:

$$F = \frac{Gm_1m_2}{r^2} \qquad (2.15)$$

Where G is the Gravitational constant $(6.67 \times 10^{-11} m^3 kg^{-1} S^{-2})$

Newton's law of motion states that a force (F) is equal to the mass (m) and times acceleration. If the acceleration is in the vertical direction then it is due to gravity (g);

$$F = mg \qquad (2.16)$$

Combining the two equations to obtain another simple relationship:

$$F = \frac{GMm}{r^2} = mg \qquad (2.17a)$$

$$g = \frac{GM}{r^2} \qquad (2.17b)$$

Theoretically, the Earth gravity is constant. However, the Earth's ellipsoidal shape, rotation, irregular surface topography and variable mass distribution cause gravity to differ from place to place. The gravitational field is defined in terms of the gravitational potential; thus, the potential field approach provides computing flexibility. (Kearey et al., 2002).

Aerogravity measures the relative lateral changes in gravity to establish subsurface distributions of densities. The resolution and accuracy of the data measured dependent on flying speed, line spacing and processing methodology (Thomas et al., 2007).

The aerogravity obtained was used for 2-D forward modelling in an attempt to define the interface between the sediment layer and the underlying basement rocks in the study area. The modelling

was performed using the 2-D GM-SYS tool embedded in Oasis Montaj software (Geosoft Inc., 2021). The program computes gravity and magnetic response from geologic models (Geosoft Inc., 2021) based on magnetic susceptibility (Morales-Ocaña et al., 2023) and densities of the rocks. GM-SYS offers a user-friendly interface for interactively building and manipulating models to match observed gravity and/or magnetic data. The technique involves creating a hypothetical geologic model and calculating the gravity and magnetic response based on Talwani & Hiertzler (1964) and Talwani et al. (1959), and applying the algorithms described in Won & Bevis (1987). The rapid calculation of the gravity and magnetic response from 2-D models speed the interpretation process of potential field data and allows for quick testing of alternative solution (NGA, 2004).

2.2.3 Airborne Electromagnetic (AEM) Data

The airborne electromagnetic (AEM) method is a widely used airborne survey technique because of its relatively, speed and large number of systems available. The technique was first designed to detect discrete isolated conductors such as massive sulphide orebodies in the subsurface. Like their ground-based counterpart, the AEM system measure secondary electromagnetic field from current induced in conducting bodies by either active primary sources wherein the primary field is generated by the system itself or passive source which use existing man made or natural source (e.g. thunderstorms) (Roch, 2007).

Electromagnetic (EM) methods make use of the response of the ground to the diffusion of EM field which are composed of an alternating electric intensity and magnetizing force. For the AEM data used in this study, FAS deployed a fixed-wing GEOTEM time-domain survey technique comprising of towed-bird. The survey method operates under the premise that variations in the primary EM field generated by the transmitting coil will result in eddy current being produced by any conductive bodies in the ground (Figure 2.12). The eddy current produce secondary EM field that may be detected in the receiver coil. Each primary pulse causes decaying eddy current in the ground to produce a secondary magnetic field. The secondary magnetic field in turn, induce a voltage in the receiver coil, which is the EM response. Good conductors decay slowly whereas poor conductors decay more rapidly. The primary EM pulses are created by a series of discontinuous sinusoidal current pulses fed into a six-turn transmitting loop surrounding the aircraft and fixed to the nose, tail and wing tips (Fugro Airborne Survey, 2009a).

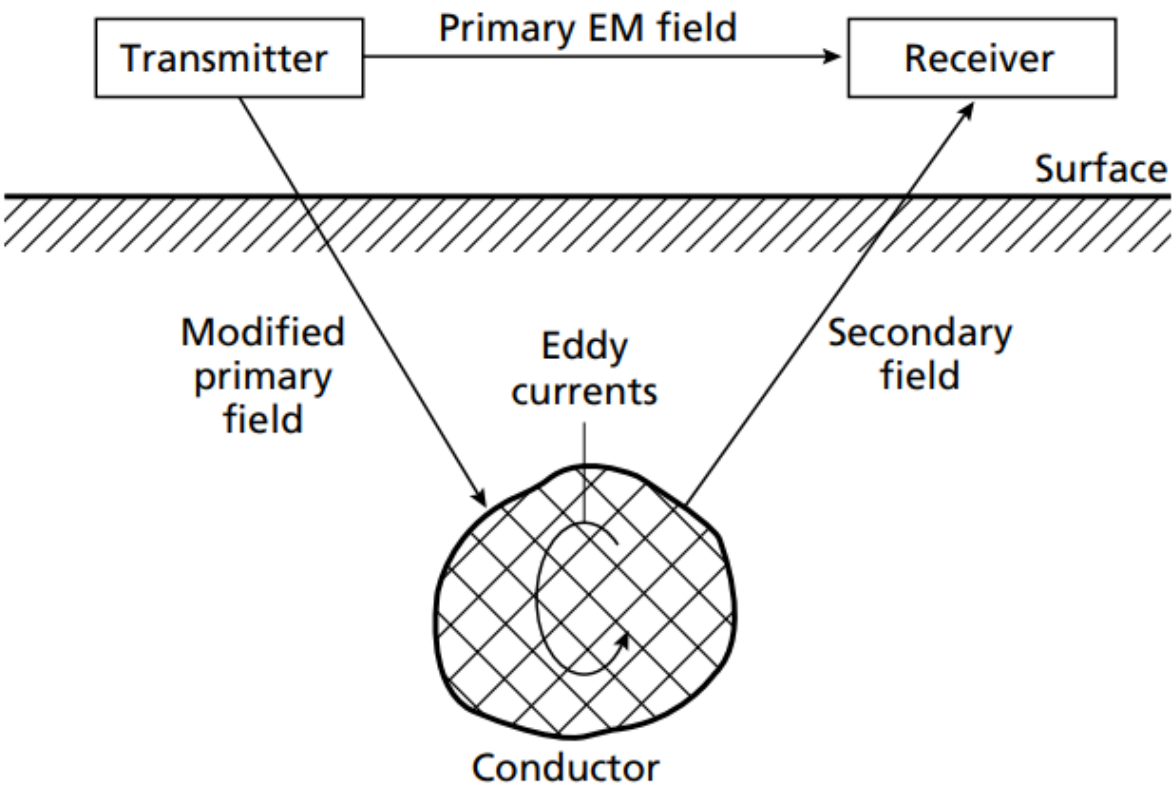

Figure 2. 12: Basic principle of electromagnetic survey (Kearey et al., 2002).

2.2.3.1 Penetration Depth of Electromagnetic Field.

The depth to which the electromagnetic field will penetrate depends both on the EM wave frequency and the electrical resistivity of the medium through which the field is propagated (Ciudad et al., 2010; Simpson & Bahr, 2005). As the EM fields propagates through the ground it attenuated resulting in the amplitude decreasing exponentially with depth.

2.2.3.2 Inversion Procedure Used by FAS for AEM Resistivity Depth Images

The receiver mounted on the aircraft measured three spatial components of the transmitter signals in x, y and z. This study however, used data processed from Bz-component (vertical) obtained from GGSA. Compared to the other components, the Bz-component data has higher signal to smaller percentage of sferic noise, hence it enhances the ability of the AEM system to resolve layered structures better (Rachie, 1998). The data acquisition company, FAS processed and transformed the Bz-coil data from GEOTEM system into resistivity depth images. The inversion of recorded signals to resistivities does not give a single, distinct output; the outcome is determined by the algorithm used (Rodriguez et al., 2001; Vignoli et al., 2015). All inversion algorithms are based on

the notion that the computed response from the Earth model must match the observed fields within a certain margin of error. The GEOTEM data were inverted using an application created in Australia for a group of organizations that included FAS. The application is referred to as AIRBEO (Rachie, 1998). The AIRBEO algorithm assumes a simple layered Earth resistivity structure and uses a single measurement point along the flight route. The resistivity model may be in any number of layers but the layer found at the bottom is an infinite half space. The program uses a 1-D singular value decomposition inversion. The inversion process, simply compared the observed data to the hypothetical electromagnetic fields from the layered earth model. This process is iterated until a good fit is attained, which is generally measured by the least square error of the fit between the observed and the computed. The application allows for some flexibility to control the inversion process to try to find a good match between the measured data and the computed data from the layered model. However, the inversion procedure is non-linear and can fit the data in a variety of plausible ways. The result is sensitive to the initial layer model used and the regularization term (Zaru et al., 2023). The final individual layered inversion results can then be plotted along the survey lines to create a 2-D map view representation of the subsurface resistivity and layer thickness variations over the area of study (Slattery & Andriashek, 2012). The individual lines can then be viewed in 3-D by stacking the 2-D images to form a 3-D image in Oasis Montaj. The resistivity depth images derived were stored in Geosoft database as an array data. The array consists of 114 levels of resistivity, from 0 to about 600m depth. The maximum depth varies along lines probably due to variations in ground resistivity and other objects that might be on the ground.

2.3 Magnetotelluric (MT)

Magnetotelluric (MT) technique is a passive electromagnetic (EM) technique that involves measuring fluctuations in the natural electric, E, and magnetic, B, fields in orthogonal directions at the surface of the Earth as a means of determining the resistivity structure of the Earth at depths ranging from a few meters to several hundreds of kilometers (Simpson & Bahr, 2005). The MT method operates under two main assumptions. The first assumption (also involved in any other EM technique except in geo-radar) is the quasi-static approximation which state that the electrical conduction current is always significantly greater than the electrical displacement current. This implies that the earth is a sufficiently good conductor, and as a result, the time-varying displacement currents are insignificant in comparison to the time-varying conduction currents. The

plane wave source is the second assumption and it states that, an incoming natural electromagnetic field propagates almost vertically into the Earth due to the significant resistivity contrast between the air-earth interface. This causes both fields transmitted into the earth to undergo vertical refraction (Vozoff, 1972). To cover frequencies from >10kHz to less than $10^{-5}s$, the MT technique uses a variety of sensors and data logger. In crustal investigations MT uses broad band electromagnetic field fluctuations with periods ranging from to $\sim 10^{-3}s\ to\ \sim 10^{3}s$.

2.3.1 MT Source Field

The main sources of MT signals are lightning at high frequencies and solar wind-earth magnetic field interaction at low frequencies (Figure 2.13). Electromagnetic (EM) waves with frequencies greater than 1 Hz which are typically used to probe the shallow part of the subsurface, are produced by meteorological events such as lightning discharges (Figure 2.13b). This high frequency signal propagates through the planet as guided waves between the earth and the ionosphere. A complex interaction between the charged solar wind particles, the earth magnetosphere and the ionosphere generate variations in the EM field with frequency lower than 1 Hz, called micro-pulsation. This field whose magnitude varies on daily, monthly and annually basis is utilized for deeper explorations that reaches down to the mantle. The solar wind is a continuous stream of plasma that carries a weak magnetic field. The pressure of the solar wind onto the magnetosphere causes compressions on the sun side and a tail on the night side (Figure 2.13a). The natural electromagnetic fluctuations have a low magnitude for frequencies between about 0.1 Hz to 10 Hz in the so-called dead band.

Figure 2. 13: Source of Electromagnetic field. (a) interaction of solar wind with magnetosphere (b) lightning discharges (Viljanen, 2012).

2.3.2 MT Transfer functions and Basic Principle

The MT transfer function also called the MT impedance tensor is a function which relates the registered electromagnetic field components at a given frequency. These functions depend only on the electrical properties of the material and frequency but not on the electromagnetic sources as long as the source field can be considered as a plane wave. Hence, they characterize the resistivity distribution of the underlying materials according to the frequency.

The basic theory of the MT method relies on the Maxwell's equations which are enshrined in several geophysical text books likewise the techniques presented above. Cagniard (1953) and Keller and Frischknecht (1966) provide an introduction to the theory of magnetotelluric field for a plane layered earth, where each layer is homogeneous and isotropic. In such a medium an electromagnetic wave propagates so that the electric and magnetic field vectors are orthogonal, and the ratio of electric to magnetic field (E_x/H_y) is a characteristic measure of the electromagnetic properties often called the characteristic impedance denoted by Z. The impedance tensor is defined in matrix form relating the electric and magnetic fields as:

$$\begin{pmatrix} E_x \\ E_y \end{pmatrix} = \begin{pmatrix} Z_{xx} & Z_{xy} \\ Z_{yx} & Z_{yy} \end{pmatrix} \begin{pmatrix} H_x \\ H_y \end{pmatrix} \qquad (2.19)$$

Where ($Z_{xy}\ and\ Z_{yx}$) are the principal impedance (off-diagonal components) and ($Z_{xx}\ and\ Z_{yy}$) are the supplementary impedance (diagonal components).

The impedance tensor (Z) contains information on the dimensionality and strike angle of the conductive structure.

For one-dimensional (1-D) earth, the conductivity distribution varies only with depth and as a result the MT transfer functions are independent of the orientation of the measured axes. The diagonal components of the impedance tensor ($Z_{xx}\ and\ Z_{yy}$) are zero and the off-diagonal components ($Z_{xy}\ and\ Z_{yx}$) are equal in magnitude but opposite in sign (see Equation 2.20). The impedance tensor in equation 2.19 becomes;

$$Z_{1D} = \begin{pmatrix} 0 & -Z \\ Z & 0 \end{pmatrix} \qquad (2.20)$$

And the corresponding apparent resistivity and phase can be defined as:

$$\rho_{ai} = \frac{1}{\mu_0 \omega} |Z_i|^2 \qquad (2.21)$$

$$\varphi = \tan^{-1}\left(\frac{Im\ Z}{Re\ Z}\right) \qquad (2.22)$$

For 2-D earth, the conductivity is constant along one horizontal direction but varies in the other horizontal direction and with depth. The diagonal components ($Z_{xx}\ and\ Z_{yy}$) of the tensor are now equal in magnitude but opposite in sign and exactly zero when x and y are aligned with the 2-D directions, while the off-diagonal components ($Z_{xy}\ and\ Z_{yx}$) differ i.e:

$$Z_{2D} = \begin{pmatrix} Z_{xx} = & -Z_{yy} \\ Z_{xy} \neq & -Z_{yx} \end{pmatrix} \qquad (2.23)$$

The direction along which the conductivity is constant is called the geoelectrical strike or the electromagnetic strike.

In the 2-D earth, measurements may not be performed in the strike direction because the geological strike might not be known. Consequently, the measuring axes generally don't coincide with the axes parallel or perpendicular to the geologic strike. However, it is possible to rotate the measuring axes mathematically by an angle (α) in the horizontal plane, so that the diagonal components of the impedance tensor become zero.

The most general type of geoelectric structure is the 3-D earth case. For the 3-D earth, the resistivity varies in all directions i.e. $\rho = (x, y\ and\ z)$. The MT transfer function takes the general form with all components being non-zero. Thus

$$Z_{3D} = \begin{pmatrix} Z_{xx} & Z_{xy} \\ Z_{yx} & Z_{yy} \end{pmatrix} \qquad (2.24)$$

2.3.3 Dimensionality of Magnetotelluric data

Dimensionality analysis of MT data is a common procedure for inferring the main properties of the geoelectric structure of the subsurface, such as the strike direction or the presence of superficial distorting bodies and enables the most appropriate inversion procedure to be determined (Martí et al., 2010). The analysis allows for the identification and quantification of distortion (Groom & Bailey, 1989). The dimensionality analysis technique search for particular relationships between

components of the MT impedance tensor to identify each dimensionality type (Kumar et al., 2021; Martí et al., 2010). There are a number of approaches to estimating the dimensionality of MT data. Three of these approaches used in this work include the Swift skew, Bahr skew and Phase tensor techniques.

2.3.3.1 Swift and Bahr Skew Approach

One of the ways of determining the dimensionality of MT data is through the estimation of skew. It is mostly the first parameter used to understand the dimensionality of the subsurface of MT data because it can be determined quickly. Skewness of MT data can be calculated using either the Swift or Bahr approach. The Swift skew (Swift, 1967) utilizes the amplitude response of the impedance tensor of MT to determine the skewness. It is defined as the ratio of the diagonal components (Z_{xx} and Z_{yy}) of MT data to the off diagonal components (Z_{xy} and Z_{yx}).

$$Swift\ skew = \frac{|Z_{xx} + Z_{xx}|}{|Z_{xy} - Z_{yx}|} \qquad (2.25)$$

Swift approach however had some drawbacks, in that it does not take into account the presence of distortions caused by coupling of regional one-dimension or two dimension inductive response due to localized small scale conductive anomalies (Simpson & Bahr, 2005). In order to deal with the drawback, Bahr introduced skew values that are depend on the phase of the impedance tensor which are not affected by amplitude distortion (Bahr, 1988). The Bahr skew also known as phase-sensitive or regional skew is defined mathematically as:

$$\text{Bahr skew} = \frac{\sqrt{|[D_1 S_2] - [S_1 D_2]|}}{|D_2|} \qquad (2.26)$$

Where

$$S_1 = Z_{xx} + Z_{yy};\ S_2 = Z_{xy} + Z_{yx}$$

$$D_1 = Z_{xx} - Z_{yy};\ D_2 = Z_{xy} - Z_{yx}$$

2.3.3.2 Phase Tensor Approach

According to Booker (2014) a phase tensor is a property of MT impedance that is resistant to common form of distortions caused by unresolved local structure. Phase tensor (Moorkamp, 2007; Caldwell et al., 2004) analysis remains one of the popular technique for determining the dimensionality of the subsurface structure and is unaffected by any galvanic distortions. It provides distortions-free phase information on the regional scale (Kumar et al., 2021). The phase tensor is defined by the equation:

$$\emptyset = X^{-1}Y \qquad (2.27)$$

Where X and Y are the real and imaginary parts of the impedance tensor (Z) of equation 2.20. The phase tensor can be represented graphically, as ellipse at each sample frequency, with a major and minor ellipse axes (Caldwell et al., 2004) denoting the maximum and minimum phase difference between the magnetic and electric fields (Stagpoole et al., 2009). The phase tensor response is sensitive to changes in both lateral and vertical conductivity and thus the tensor ellipse provides a direct indication of the structural features of the subsurface. It is independent of distortion caused by small-scale inhomogeneities and can be calculated without prior knowledge of the structure dimensionality. The phase tensors are typically drawn over study area maps to highlight the directionality of shallow or deep structures depending on the period of interest (Bravo-Osuna et al., 2021). Caldwell et al., (2004) introduced a parameter of skew angle which define the inherent dimensionality of the subsurface. For instance, in a 1-D case, the skew angle is almost equal to zero and the phase tensor ellipse is more or less equal to circle. In the case of 2-D regional resistivity structure, the phase tensor is characterized by an elliptical shape with a skew angle close or equal to zero (Saibi et al., 2021). In 3-D Earth, the phase tensors are non-symmetrical and the skew angles shows large values. Thus, the tensors will be represented as circles for 1-D and as ellipses for 2-D or 3-D subsurface resistivity. By evaluating the degree of asymmetry of the phase tensor, one can determine the dimensionality of subsurface structure.

2.3.4 Static Shift in Magnetotelluric Data

In MT measurements, small resistivity inhomogeneities can lead to distorted response of the MT sounding curves. Depending on the depth and size of the anomaly, the anomaly would has an inductive and /or galvanic effect which contributes to the MT response of the background resistivity. The distortion arises mainly from the telluric field, which is of galvanic or inductive nature as discussed in Berdichevskiy and Dmitriev (1976). These effects are normally of quasi-static character that causes vertical shifts in the MT apparent resistivity curves called static shift. The static shift does not have any effect on phase variation (Stephen et al., 2003). The distortion is caused by charges distribution accumulated on the surface of shallow bodies which produce anomalous electric field. The electric field can be of same order of magnitude as the field of interest and is frequency independent (Bahr, 1988; Stephen et al., 2003). This affect the entire sounding curve at all frequencies giving rise to static shift.

The effects of galvanic distortion introduce an unknown multiplicative factor, independent on the frequency in the apparent resistivity or a constant shift on log-scale (Pellerin & Hohmann, 1990). Some studies such as Park (1985) and Wannamaker et al (1984) showed the importance of static shift in 2-D and 3-D bodies. Different type of correction procedures have been proposed, such as transient EM method (Pellerin & Hohmann, 1990; Sternberg et al., 1988), laterally homogeneous layer constraints from MT data over a region (Jones, 1988), utilization of resistivity distribution chart over the region (Demidova et al., 1985), shallow resistivity sounding (Romo et al., 1997), etc. Among these possible treated procedures proposed for static shift, the transient EM and inverting the data in 3-D have been most common. Nowadays however with 3-D inversion, static shift corrections should be used only if 1-D or 2-D modeling is involved.

In this study, there was no static shift observed in the data probably due to the conductive sediments layer at near surface. The data was also inverted in 3-D which takes into accounts any static shift effect.

2.3.5 Inversion of MT Data

The MT data was inverted using an in-house codes known as MINIM3D (Hautot et al., 2007) and MINIM1D (Tarits, 1986). The full tensor 3-D inversion approach is based on the minimization of the misfit between the data and the model response using a non-linear steepest gradient method (Hautot et al., 2007). In this approach, the forward problem is solved at each iteration with a 3-D finite difference algorithm proposed by Mackie et al., (1993). The boundary condition at the base of the model is the impedance of homogeneous half-space. The model is parameterized into blocks in the x, y, and z directions. A starting model is defined to initiate the inversion and after a number of iterations the size of the blocks are adjusted and the inversion run again until a good agreement is obtained between the data and model response. The fit is shown by the reduction in root mean square value which decreases from an initial high value to low.

Because of small number of MT stations, the resistivity grid in 3-D is coarse. To improve the vertical resolution of the individual sites, a 1-D inversion was also performed. The 1-D inversion is based on the use of invariant determinant (Zdet) calculated from Berdichevsky averaging of the impedance (equation 2.29) and sum of squares of the impedance (equation 2.31) (Rung-Arunwan et al., 2016) for each site. Each determinant together with an initial half space model was used to run the inversion to infer the vertical resistivity variations of the Earth after a number of iterations.

$$Z_{det} = \sqrt{Z_{xx}Z_{yy} - Z_{xy}Z_{yx}} \quad (2.28)$$

$$SSQ = Z_{xx}^2 + Z_{xy}^2 + Z_{yx}^2 + Z_{yy}^2 \quad (2.29)$$

$$Z_{ssq} = \sqrt{\frac{SSQ}{2}} \quad (2.30)$$

1-D inversion using the determinant calculated from the SSQ was done on purposes for comparison, following the suggestion by Rung-Arunwan et al., (2016) that the SSQ is non-biased and is not affected by downwards distortion parameters such as shear and splitting in a heterogeneous geologic environment. However, there were no notable differences observed in the 1-D inversions results ran using the determinants calculated from the two approaches.

The number of layers defined for the 1-D starting homogeneous half space model were 50 with the thicknesses of the layers remaining fix while the resistivity varies at each run of the program. The number of iterations used for the inversion was set at a maximum of 1000. In 1-D inversion, the medium's geometry is reduced to a flat-parallel layer system, where the resistivity only changes with depth (Oryński et al., 2022). The inversion consists of multiple executions of a simple task, with new parameters introduced in each subsequent iteration until a model with minimum misfit error is obtained. The misfit function is the root-mean-square difference between measured and the computed values. The program offers the possibility to keep models smooth both with respect to resistivity variation between layers and layer thicknesses. After successful converging of iteration with best possible minimum error, the models with subsurface resistivity and phases were plotted using python 3 (Harris et al., 2020). A regularization term was introduced to add stability to the objective function for the inversion.

The inversion was performed for two different MT data sets (Chapter 4 and 5) obtained in two separate field campaigns. In the first field survey the MT soundings followed two parallel profiles with a total area coverage of about 96 Km while in the second campaign, the sites were designed in a 3-D array to suit 3-D inversion with a total spacing of about 1 Km between MT stations.

CHAPTER THREE

THE MINERALOGY OF ROCKS IN THE VOLTAIAN SEDIMENTARY BASIN AND THEIR IMPLICATIONS ON THE SEDIMENTS ELECTRICAL RESISTIVITY

2.0 INTRODUCTION

As presented in chapter one, the geology of the Voltaian sedimentary basin in the Ghana consist of several lithologies including different types of sandstones, mudstones, conglomerates, shales, tuffs, limestones and tillites. These lithologies belong to different formations which are group into three main rock groups based on ages of the rocks. The lithologies are described as hard and impervious at most places owing to sedimentary processes such as consolidation and some episodes of low-grade metamorphism that affected the sediments (Affaton et al., 1980; Carney et al., 2010; Kesse, 1985). The impervious and hard nature of these rocks have seen many researchers conclude that the rocks lack primary porosities (Chegbeleh et al., 2009; S. Yidana et al., 2011) and as a result, the rocks returns high resistivity readings (Aliou et al., 2022; Mainoo et al., 2019). The high resistivity readings could most likely be induced by the mineralogical composition. This is because mineralogical composition is one of the key factors that affect the flow of electrical current in the subsurface (Caselle et al., 2019; Ye et al., 2022) which in turn influence the resistivity readings. For instance, the presence of metallic minerals in a rock decreases the electrical resistivity of the rock as such metallic minerals enhance current flow. Similarly, the presence of minerals that weather and produce clay are likely to facilitate easy flow of current within the rock matrix. On the other hand, intrusive rocks such as granite has well-defined mineral grains resulting in very low porosities hence giving opposition to current flow and thereby increasing the resistivity readings (Fukushima et al., 2022). The resistivity of such rocks (e.g. granite) is driven largely by the composition (minerals) which are predominantly quartz and feldspar. Therefore, to understand the implications of the mineralogical composition on our resistivity data, the rock minerals of some rocks underlying the study areas (see sample location in Figure 3.1) were investigated using petrographic analysis and the scanning electron microscope (SEM). Several literatures are available that support the investigations of the influence of mineral composition of rocks on resistivities (e.g. Ersoy & Waller, 1995; Li et al., 2018; Park et al., 2016; Tuğrul & Zarif, 1999; Zhang et al., 2016). It is important therefore to evaluate the mineralogical composition and mineral content of the rocks in the basin which can serve as a guide for the interpretations of the resistivity patterns revealed by the geophysical models.

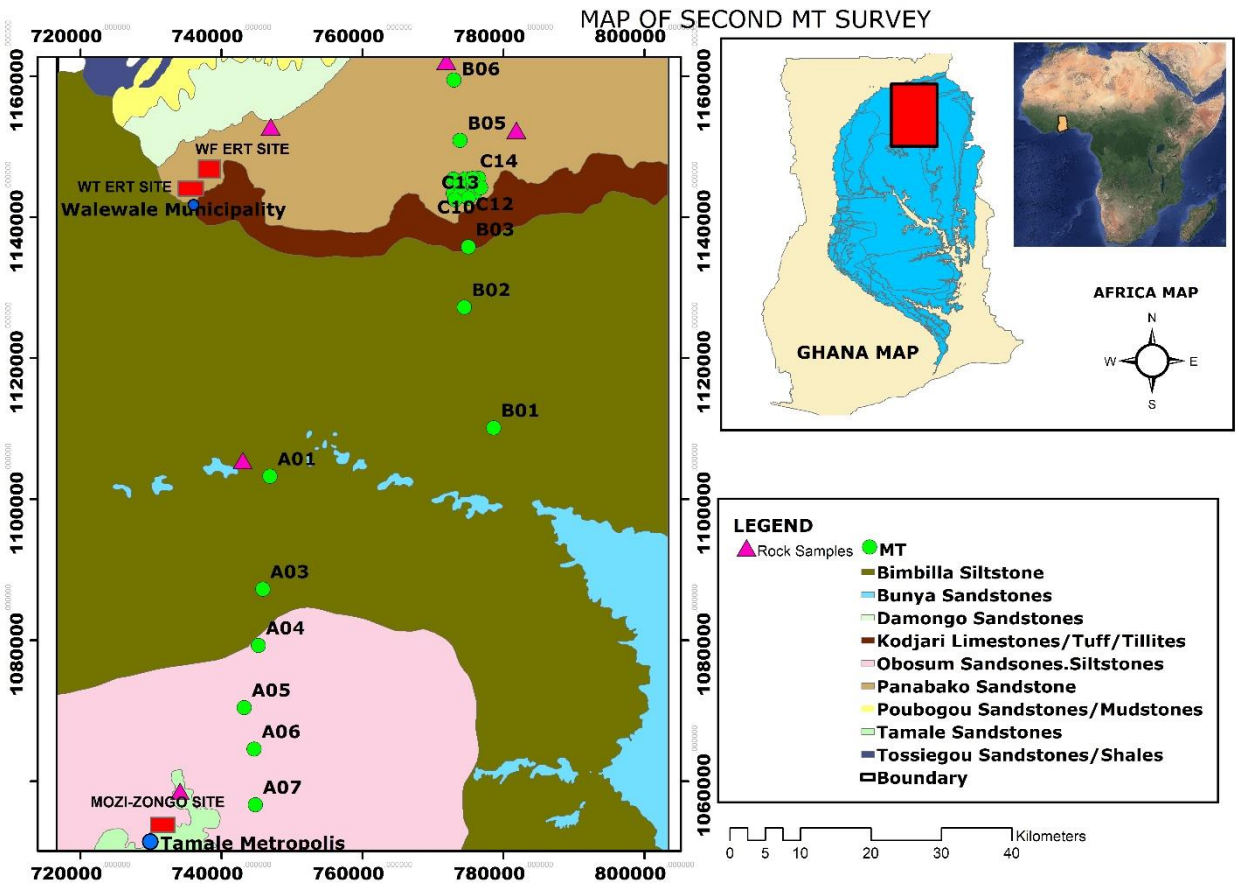

Figure 3. 1: Geological map of the study area-showing surface geology represented by different colours as seen in the legend along with an insert of map Africa and Ghana highlighting the study area in red. Rock sample locations are marked with pink triangles while red rectangles denote locations of dumpsites on the geological map.

3.1 Fields Sampling

Five rock samples were collected in the study area mostly along and near the survey profiles (Figure 3.1). The paucity of outcrops exposure in the basin resulted in the small number of samples nonetheless, the sampling was done ensuring fair representation of the different geological units in the study area. Three of the samples were collected around northern part of the area where there are well exposed outcrops, while the remaining two samples were collected at southern sector in the survey area. Samples were collected from in-situ rocks on the field using a geological hammer while ensuring samples picked were fresh with little or no alterations (Figure 3.2). The samples were assigned names based on sample locations and subsequently transported to the department of the Earth Science, University of Ghana for thin section and scanning electron microscopy (SEM) preparations and analysis (Figure 3.2).

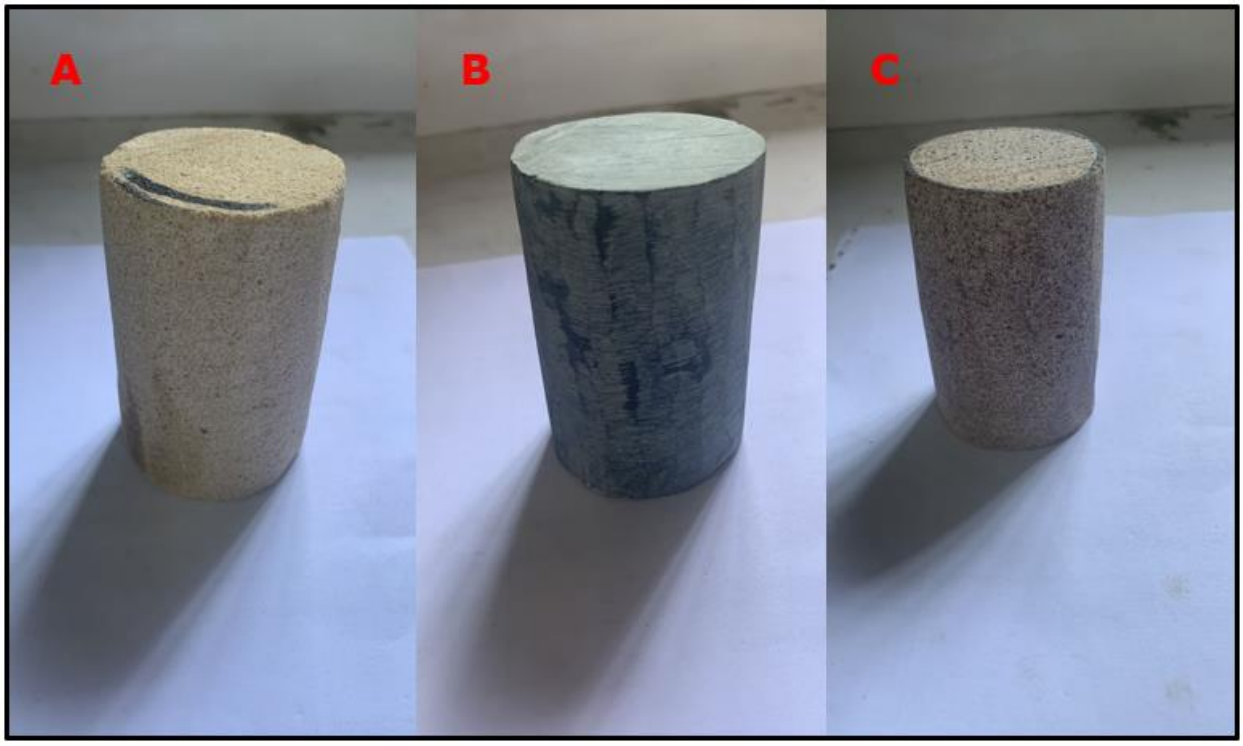

Figure 3. 2: Field samples being prepared for thin sections and SEM analysis; (a) Panabako sandstone north of profile B (b) Carbonate rock south of profile B and close to MT station A01 and (c) Tamale sandstone south of profile A.

3.1.1 Thin Section Preparation

The samples were cut and prepared at the petrographic laboratory at the University of Ghana's Department of Earth Science thin section laboratory. The analysis was carried out in the same Department using Leica DM 750P polarizing microscope equipped with AmScope camera to study the mineralogy, texture and possible micro structures of the rock in thin sections. The minerals present were identified using their optical properties both under plane polar (PPL) and cross polar (XPL). Quantitative measurements of 500point counts using the Pelcon point counter was used to determine the modal percentages of mineral composition. Rock names were assigned to the rock samples based on hand specimen description and laboratory analyses.

3.1.2 Scanning Electron Microscope (SEM)

The Scanning Electron Microscopy (SEM) with Energy Dispersive X-ray (EDX) is a semiautomated technique that has been used widely for rock mineral identification (Chen et al., 2023; Schulz et al., 2020; Yan et al., 2019; Webster et al., 2003). It operates on the principle where

a rock sample is bombarded with a beam of electrons produced from an electron source such as a heated tungsten filament. As the beam of accelerated electrons passes through series of electromagnetic lens and interacts with the rock sample, energies are emitted in the form of photons referred to as back scattering electrons. Most of the photons emitted falls within the energy range of X-rays. An EDX with silicon lithium crystal attached picks up the X-rays and within seconds produce a spectrum with intensity of the elements present (Severin, 2004).

The SEM-Image analysis was carried out using the Phenom World ProX desktop scanning electron microscopy at the Department of Earth Science, University of Ghana, Legon. Samples (Figure 3.3) were prepared to withstand vacuum conditions and high energy beam electrons (i.e. solid compact sample, dry and free from any form of dust particles). The samples were cut and trimmed to fit the specimen stage. The samples were then in turns mounted unto an aluminium stub with a pelco double sided carbon adhesive to keep the sample in place.

Figure 3. 3: Rock samples prepared for SEM-EDX Analysis. Each of the five samples analyzed are shown in the image.

An ultra-thin coating of gold was sputtered unto the samples with poor or no conductivity. Optical images were captured at the lowest magnification of 20x. Backscattered images were captured at different magnifications (minimum to maximum) using an image intensity and high-resolution voltage mode of 10 keV until best image focusing was obtained. The Phenom Pro-Suite software

(element identification) was utilized for EDX point analysis at 15 Kev, duration of 30 seconds and map analysis at 15 Kev duration of 4 minutes 26 seconds for the elemental identification, distribution and concentration respectively.

3.2 Petrographic Analysis

Three samples out of the five were taken at the northern part of the study area (Figure 3.1). These samples underlie the Walewale dumpsites (ERT profiles) and the MT profile B. The three rocks were sampled from the Panabako Sandstone formation (Carney et al., 2010) since it is the only member of the Bomboaka Group with exposures within the study area. The modal percentages by volume of minerals observed in the samples (rocks) under thin section are presented in table 3.1.

Table 3.1: Table showing the percentage by volume of the different minerals observed with thin sections under optical microscope.

Mineral in Thin Section	**Bongbini Sample**	**Gambaga Sample**	**Guabuligaliga Sample**	**Tamale Sample**	**Pigu Sample**
Quartz (Qz)	Qz (96.8%)	Qz (97.2%)	Qz (95.6%)	Qz (95.7%)	Qz (20%)
Plagioclase (PL)	Pl (0.4%)	Pl (0.1%)	-	-	Pl (0.5%)
Microcline (Mc)	Mc (0.2%)	Mc (0.2%)	-	-	-
Biotite (Bt)	Bt (0.2%)	-	Bt (1.2%)	-	-
Sericite (Ser)	-	Ser (0.4%)	Ser (1.8%)	-	-
Lithic (Lt)	Lt (2.4%)	Lt (2.1%)	Lt (1.4%)	Lt (3.4%)	Lt (0.5%)
Carbonate minerals (Micrite)	-	-	-	-	Micrite 50%
Clay Mineral	-	-	-		CL (19%)
Heavy Mineral (HM)	-	-	-	HM (0.6%)	-

The first rock sample collected to the north was assigned the name, Bongbini (name after the closest community). This sample was taken around MT station B06 (Figure 3.1). The rock in thin section shows a medium to coarse grained texture with a grain supported fabric. Mineralogically, it is composed of 96.8 % quartz, 0.4 % plagioclase feldspar, 0.2 % microcline feldspar, 0.2 % biotite and 2.4 % lithic fragments (Table 3.1). The quartz minerals are elongated with subangular to sub-rounded monocrystalline grain (Figure 3.4b). Some amount of alteration was observed in the biotite minerals changing their original brown colour to yellowish green colour (e.g. Figure 3.4a). The quartz crystals are crenulated and welded together as seen in figure 3.4. This sample was identified as quartz arenite sandstone based on the composition.

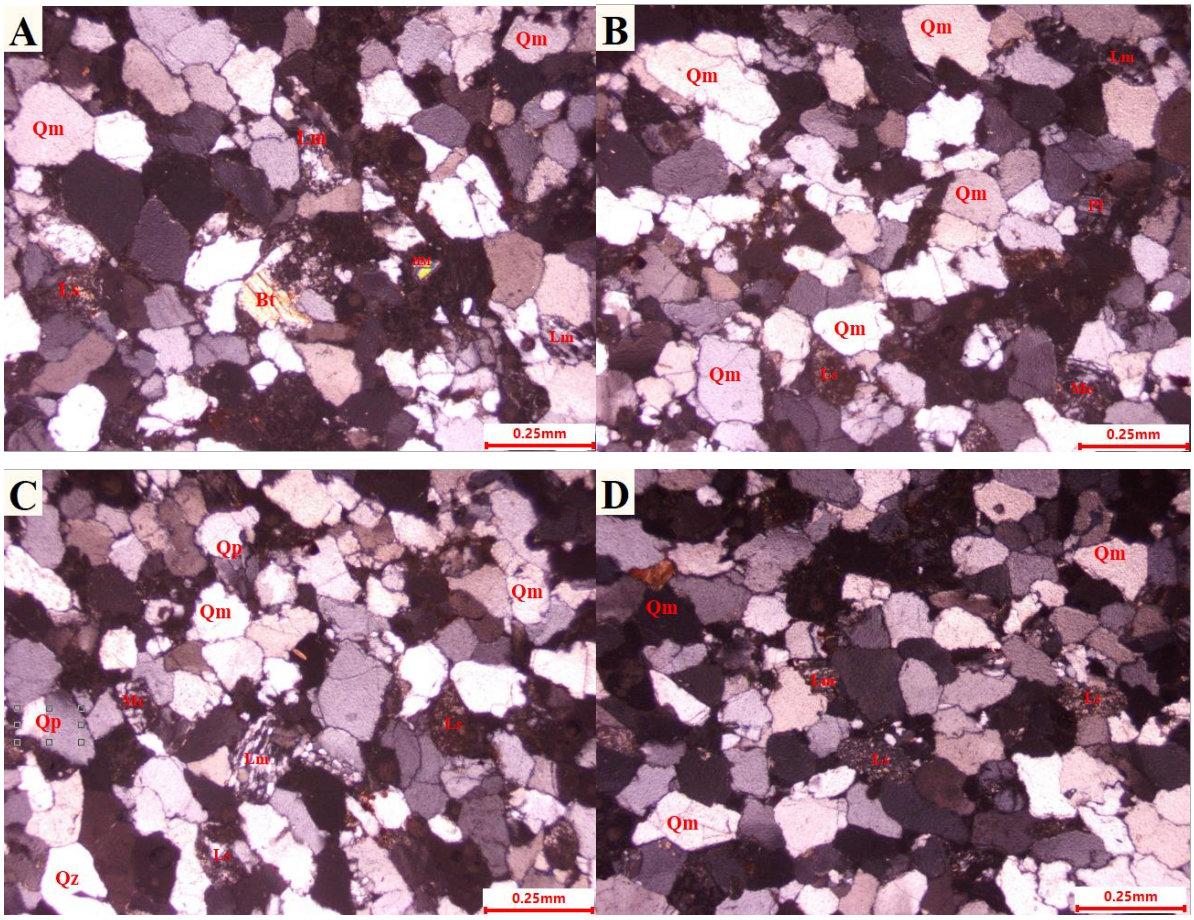

Figure 3. 4: Photomicrograhs of Bongbini sample north of Profile B: (a) Shows the medium to coarse grain texture and Biotite mineral alteration (b) Shows sub-rounded and monocrystalline quartz and subhedral feldspars (c) contains lithic materials of both sedimentary and metamorphic origin (d) Shows monocrystalline and few polycrystalline quartz.

The second rock sample herein referred to as the Gambaga sample was examined under the petrographic microscope. This rock under thin section composed of quartz (97.2%), microcline feldspar (0.2%), plagioclase feldspar (0.1%), sericite (0.4%) and some fragments (Table 3.1). Similar to the Bongbini sample, the quartz minerals (Figure 3.5a) in this sample show subangular and interlocking grains. Some of the feldspars appeared to have altered to form sericites (Figure 3.5a) which is observed as yellowish-brown grain matrix in thin section. Some lithic materials are present with numerous strain elongated quartz crystals (Figure 3.5). Texturally, the rock is medium to coarse grained that is mineralogically matured due to abundance of quartz minerals. The compositions suggest the rock is quartz arenite sandstone.

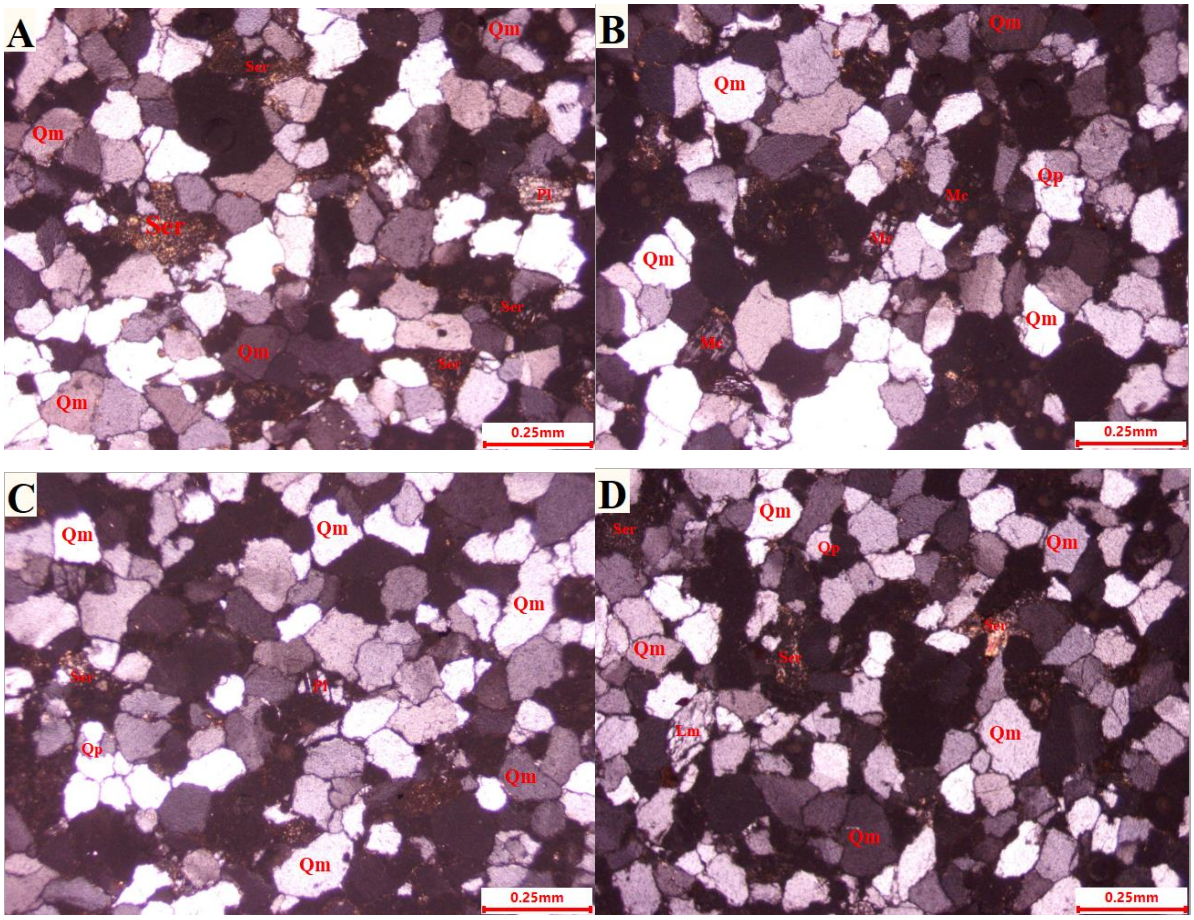

Figure 3. 5: Photomicrographs of Gambaga sample showing: (a) medium to coarse grain texture in matrix supported fabric and Sericite minerals (b) subhedral microcline feldspar minerals (c) plagioclase feldspar minerals (d) presence of distinct sub-rounded quartz and lithic in the rock.

The third rock sampled at the north of study area and close the Walewale dumpsites was the Guabuliga sample. This rock microscopically in thin section shows a medium to coarse grained texture with a matrix supported fabric. Mineralogically, it is composed of 95.6 % quartz, 1.2 % biotite mica,1.8 % sericite and 1.4 % lithics (Table 3.1). The biotite present in the rock were observed to be altered forming sericite which appeared as brownish fine-grained matrix (Figure 3.6c) in the rock. The quartz minerals are subangular to sub-rounded with monocrystalline and polycrystalline grain in thin section (Figure 3.6a). Some lithic fragments were also observed under the microscope in thin section. The rock is mineralogically matured due the high-volume percentage (95.6%) of quartz minerals. The sample was identified as a quartz arenite sandstone based on the percentages of mineralogical compositions as seen in Table 3.1.

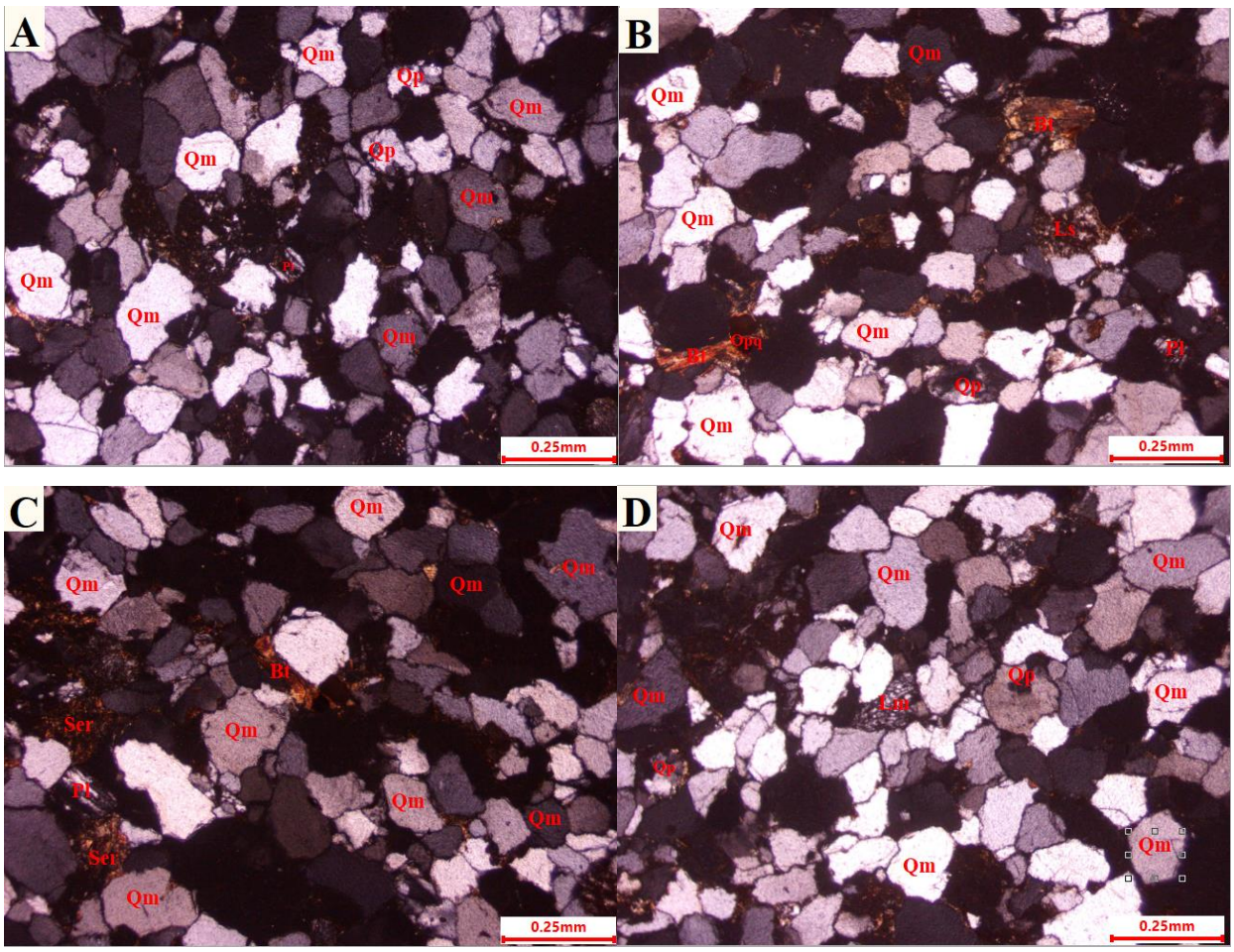

Figure 3. 6: Photomicrographs of Guabuliga sample showing: (a) medium to coarse grain texture with monocrystalline and polycrystalline quartz minerals, Sericites, plagioclase feldspar in matric supported fabric, (b) altered biotite minerals (c) Sericite fine grain matrix, (d) distinct sub-rounded lithic fragment present in the rock.

The Tamale Sandstone sample was collected at the southern part of the study area (Figure 3.1). It shows medium to coarse grain texture with matrix supported fabric under microscopic view (Figure 3.7a). Mineralogically, the rock is consisting of quartz, lithics and heavy minerals (Table 3.1). The quartz minerals are generally large subangular to sub-rounded monocrystalline and a few polycrystalline grains. Also, the quartz minerals appear stretched and elongated suggesting some amount of deformation (Figure 3.7). The modal composition of the rock results from mineral point counting are shown in table 3.1. The sample was identified as quartz arenite sandstone.

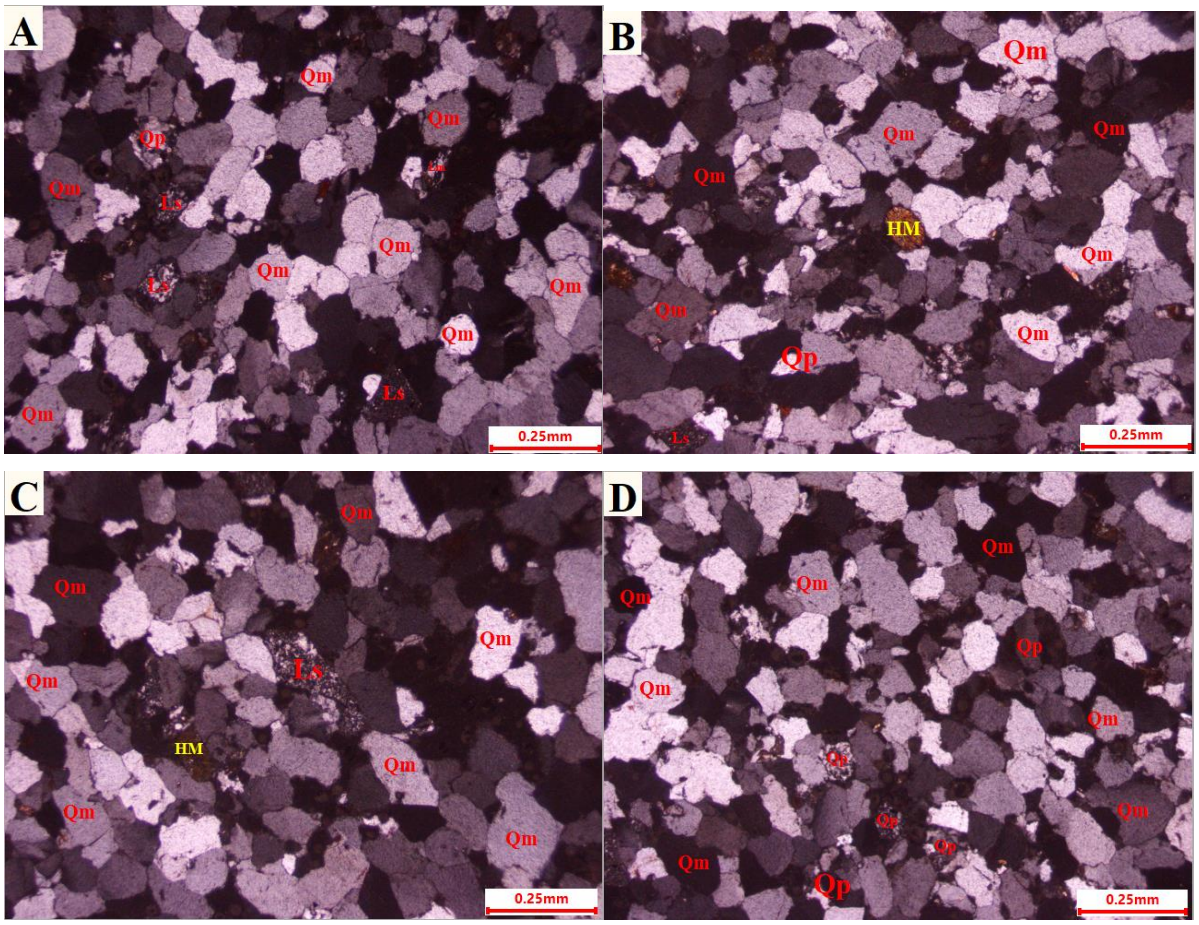

Figure 3. 7: Photomicrographs of Tamale sandstone sample shows: (a) medium to coarse grain texture monocrystalline, polycrystalline quartz minerals and lithic in grain supported rock fabric, (b) presence of some rounded brown heavy minerals, (c) elongated sub-rounded lithic and brown heavy minerals, (d) stretched and monocrystalline suggesting episode of deformation.

The Pigu sample microscopically showed mostly fine-grain mud calcite micrite. Other minerals observed include; quartz, plagioclase feldspar and fragments (Figure 3.8). The calcite micrite appears as light brown fine-grained matrix embedded with quartz grains. The plagioclase feldspars are tiny euhedral grains and exhibited polysynthetic twinning under thin section. Quartz occurs as tiny monocrystalline grains with first order grey interference exhibiting undulose extinction. The clay minerals appeared as fine dark brownish stretch like anhedral grains. These minerals were difficult to identify under the microscope hence we to performed an x-ray diffraction (XRD) on the sample which confirmed them as illite and dickite minerals (clay minerals) (see appendix 6). The lithics materials show fragments of quartz grains, clay minerals and some micas. The modal compositions of the minerals in the rock after point counting are presented in table 3.1. This sample was identified as dolomite limestone under thin section observation and in hand specimen using hydrochloric acid (HCl).

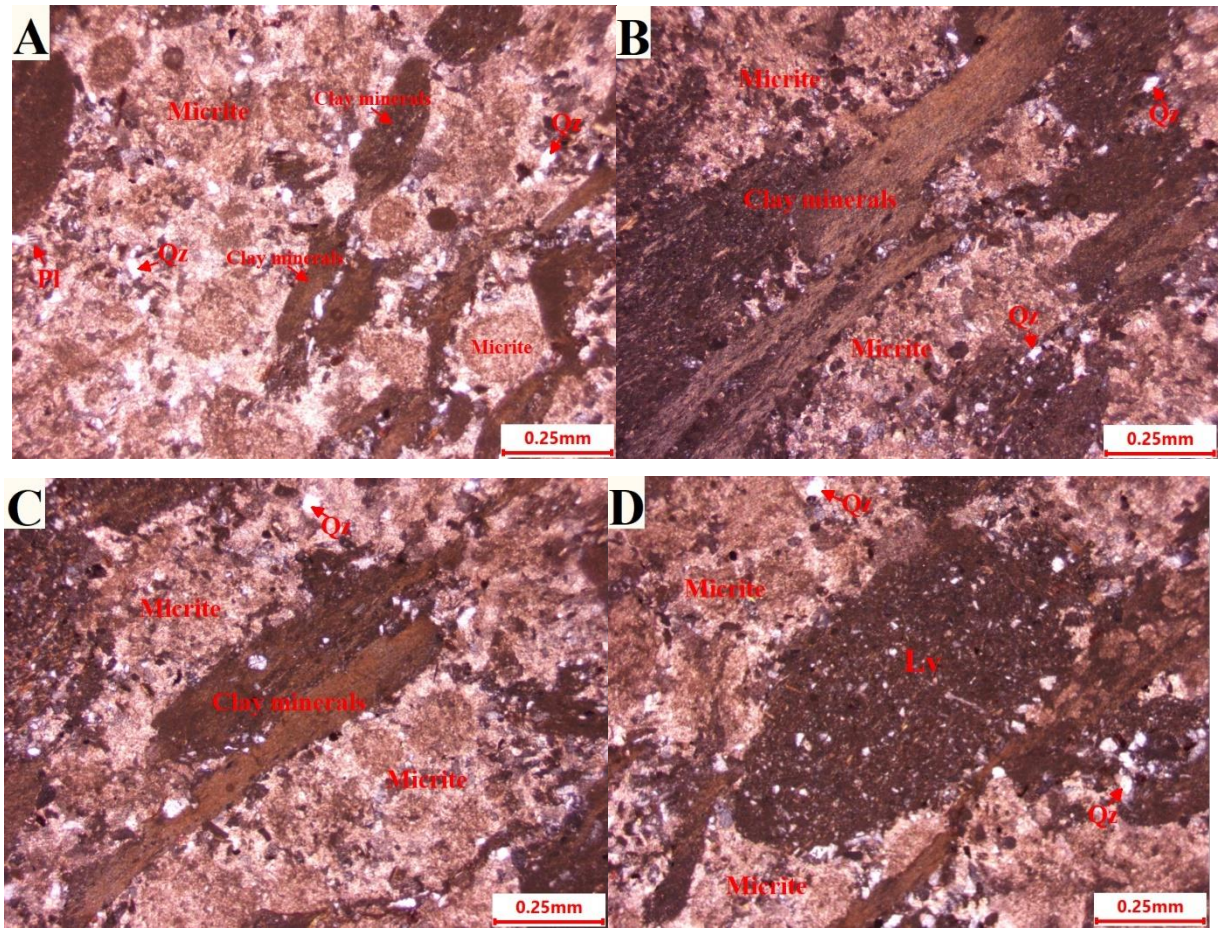

Figure 3. 8: Photomicrographs of Pigu sample: (a) fine grain texture with micrite and clay minerals, (b) and (c) dark brown stretched clay minerals, (d) presence of large rounded volcanic lithic.

The presence strain elongated and polycrystalline quartz minerals observed in some of the samples studied under the microscope suggest some form of metamorphism in the rock samples in the area. This observation agrees with low grade metamorphism of the sediments reported by Kesse (1985) for basin. Metamorphism result in the transformation of rocks causing both physical and chemical changes in the rock and has been noted as the one of the contributing factors leading to the loss of primary porosity and permeability in the sediments (Chegbeleh et al., 2009; Kesse, 1985). As metamorphism increases, hydrous minerals lose water and become less hydrous and the micro porosity and permeability of the rocks decreases leading to increase in resistivity of the rocks. In addition, quartz accounted for over 90% of the mineral composition (Table 3.1) in four out of the five samples. Quartz minerals are described as good electrical insulators (George et al., 1947; Han & Clark, 2021). The dominance of the quartz minerals in the rock samples as observed in thin sections could result in relatively high electrical resistivity readings across areas where these rock units underlies. Hence possible resistive regions in the geophysical models that coincide with the sample locations could be attributed to the quartz composition of the underlying rock. The ERT profiles, the north of MT profile B, south of profile A and the whole of profile C should expectantly return relatively high resistivity readings since the areas mentioned overlies the quartz dominated rocks. If the opposite is true, (thus the areas mentioned returns low resistivity readings) then it could be due to the presence of fractures such as lithological contacts (boundary) or faults or clay induced from weathering of the rocks. Also, leachate infiltration from the dumpsites could cause the resistivities values to be low. Similarly, the less resistive regions could be due to the biotite and feldspar minerals weathering in the samples. This is because the alteration of biotite and feldspar produces clay which could be conductive in the presence of water. Episodes of deformation were observed in the thin sections as the quartz mineral appeared stretched. Deformations could leads to development of secondary structures (Waldron & Snyder, 2020) which are of paramount interest in this investigation.

The fifth sample (Pigu Sample) was identified under thin section as dolomite limestone. Limestones show high resistivity up to 4000 Ωm when dry (Garcia et al., 2015). Therefore, the geophysical models should exhibit relatively high resistivity readings where this rock unit underlies. However, low resistivity signatures can be encountered and could be caused by other factors such as clay or fractures resulting from weathering either than the mineralogy of the rock. The limestone is the base member of the triad of the Kodjari formation of the Oti-Pendjari Group

and extend northeast resting unconformably on the Panabako Sandstone Formation (Carney et al., 2010) observed along profile B at the contact around MT station B01 (See figure 3.1). This unit should perhaps induce resistive areas close to B01 as seen in the MT models at near surface.

3.3 Scanning Electron Microscope Analysis

The Scanning Electron Microscope (SEM) with Energy Dispersive X-rays (EDX) was used to analyze all five samples already examined under the optical microscope. SEM is a semiautomated technique used to understand the elemental composition of rocks. The deployment of the technique helped to compared and corroborate observations made under the optical microscope. By using SEM-EDX, the size of minerals and morphology can be measured as well as the chemical composition (Nurit, 2022). At least five regions consisting an average of six spots were analyzed in each sample in SEM-EDX. Comparison of the elemental compositions of the different regions within same sampled all looked similar hence only a spot each from each of the five samples are presented and discussed with the remaining shown in Appendix 4.

The SEM-EDX analysis of all three samples collected at the north of the survey area showed elemental dominance of Silicon and Oxygen (i.e. SiO_2 is Quartz) as shown in table 3.2a to d. The X-ray intensity (intensity of the spectrum peak) which is directly proportional to the concentration of the elements in the sample equally showed high peaks (Figure 3.10) for Silicon and oxygen for all three rocks sampled at north of the area. The abundance of quartz in each of the three samples indicates the rocks are sandstones, which is consistent with the observations made under the optical microscope. Quartz is resistive and therefore will increase the resistivity of the host or parent rock. The three rocks sampled to the north are within the Panabako Sandstone Formation which has been described as resistive (Aliou et al., 2022; Dzikunoo et al., 2020; Jordan et al., 2009). The formation's resistive nature has attributed to the prevalence of the quartz minerals and therefore will elucidate the resistive zones (patterns) observed in the geophysical models. Images from the SEM analysis showed the morphology of the various mineral grains present in the samples but could not clearly distinguish them due the grey hue of the images (Figure 3.9).

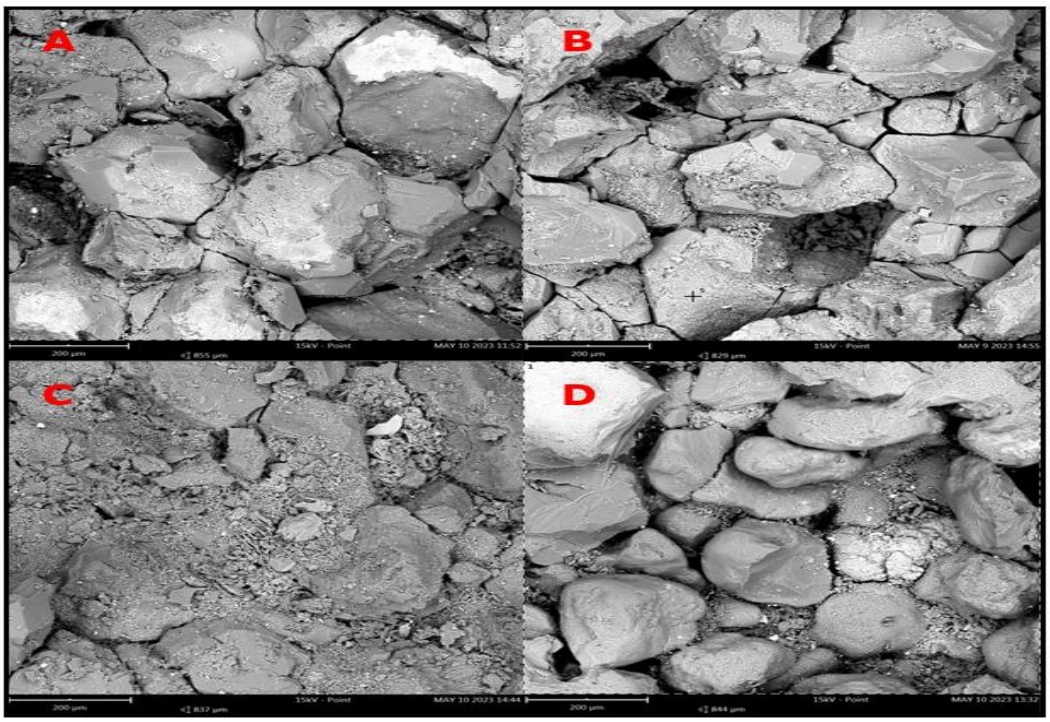

Figure 3. 9: SEM images of the different sandstone samples showing the morphology minerals grains of the rocks. (a) sample taken at Bongbi, close MT sounding station B06 (b) Gambaga sample (c) Guabuliga sample (d) Tamale sample. The pores and/or micro-fractures seen in these images are possibly induced during sample preparation via cutting of the rocks. It could also be due high magnification hence SEM images look different from the images obtained via the optical microscope.

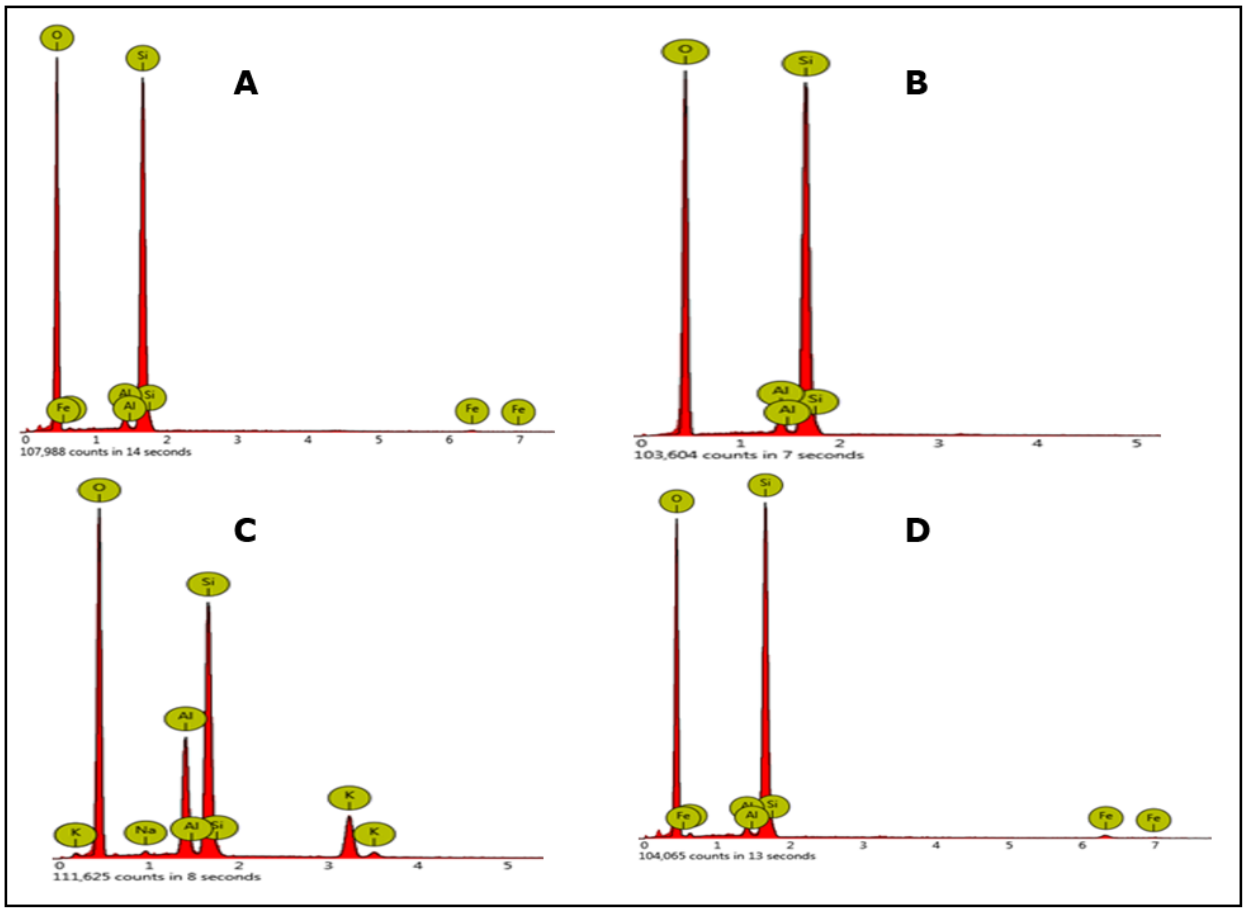

Figure 3. 10: SEM-EDX spectra images of the samples showing intensity of elements present in each sample.

The samples collected to south of the study area consist of the Tamale Sandstone and the Limestone as identified in thin section. SEM-EDX examination of the samples (Figure 3.9d) showed results which are similar to the observations made under optical microscope. The spectrum for the Tamale Sandstone (Figure 3.10d) indicates Silicon and Oxygen as the elements with high intensity. The high intensity of Silicon and Oxygen suggest substantial volume of quartz minerals in the sample indicating it is a Sandstone. The high percentage volume of quartz consequently makes the Tamale sandstone resistive and could probably reflect in the geophysical models sited in close proximity (e.g. A07). The fifth sample analysed in SEM-EDX was identified as a dolomite Limestone based on thin section observation (Figure 3.8). SEM-EDX analysis showed high intensity peaks of Calcium and some low peaks for magnesium, supported by high volume percentages seen in table 3.2. These elemental compositions indicate that the rock is dolomite although it is impure due the presence of intensity peaks and volume percentage of Silicon and Oxygen at some spots (Appendix

5). Limestones are resistant in the absence of water and therefore will increase the resistivity of their host rock.

Table 3. 2: SEM-EDX Elemental compositions of the rock samples near MT stations

A

Element Symbol	Atomic Conc.	Weight Conc.	Oxide Symbol	Stoich. wt Conc.
O	74.41	62.07		
Si	24.22	35.47	SiO_2	94.79
Al	1.02	1.43	Al_2O_3	3.38
Fe	0.35	1.03	Fe_2O_3	1.83

B

Element Symbol	Atomic Conc.	Weight Conc.	Oxide Symbol	Stoich. wt Conc.
O	74.06	61.98		
Si	24.36	35.78	SiO_2	94.75
Al	1.59	2.24	Al_2O_3	5.25

C

Element Symbol	Atomic Conc.	Weight Conc.	Oxide Symbol	Stoich. wt Conc.
O	71.62	58.02		
Si	16.35	23.25	SiO_2	62.45
Al	7.76	10.60	Al_2O_3	25.17
K	3.88	7.68	K_2O	11.61
Na	0.39	0.45	Na_2O	0.77

D

Element Symbol	Atomic Conc.	Weight Conc.	Oxide Symbol	Stoich. wt Conc.
O	72.54	59.33		
Si	25.66	36.84	SiO_2	92.89
Fe	0.91	2.59	Fe_2O_3	4.37
Al	0.89	1.23	Al_2O_3	2.74

E

Element Symbol	Atomic Conc.	Weight Conc.	Oxide Symbol	Stoich. wt Conc.
O	67.77	48.75		
Ca	19.39	34.94	CaO	58.93
P	8.98	12.51	P_2O_5	34.55
F	2.34	2.00		
Si	0.72	0.92	SiO_2	2.36
Al	0.34	0.41	Al_2O_3	0.94
Na	0.34	0.35	Na_2O	0.57
Mg	0.11	0.12	MgO	0.24

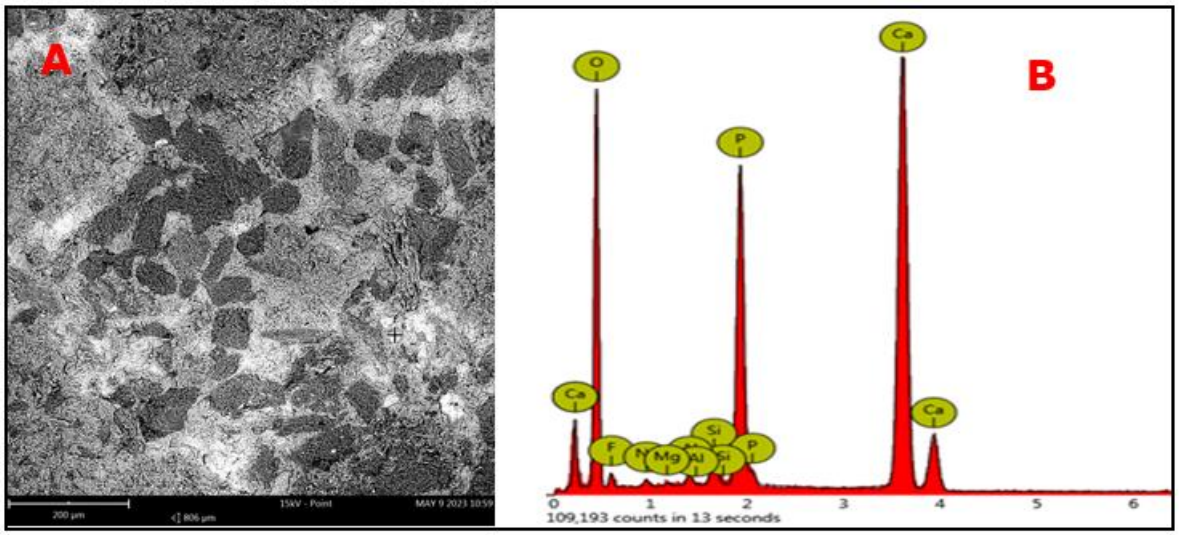

Figure 3. 11: SEM-EDX image of Pigu sample near Profile A: (a) SEM image showing mineral grains and morphology of the limestone, (b) EDX spectrum showing elemental peaks of various elements present in the rock sample.

3.4 CONCLUSION

The combination of petrographic analysis and SEM-EDX have been used to investigate the mineralogy composition of rock sampled collected from the study area. The analysis identified minerals including quartz, feldspars, plagioclase, biotite, sericites and some lithic fragments. The presence of lithic fragments and the stretched/strain nature of most of the quartz minerals observed indicate possible episodes of deformation in the rocks. The spectra energies peaks and the volume percentages found Silicon and Oxygen to be high indicating the abundance of quartz in the sandstone samples underlying the area. This analysis will form an important basis to understand and interpret resistivity patterns in the geophysical models.

CHAPTER FOUR

INVESTIGATING DUMPSITE LEACHATE AS AN EMERGING CHALLENGE TO GROUNDWATER DEVELOPMENT IN THE NORTHERN PART OF THE VOLTAIAN SEDIMENTARY BASIN, GHANA.

4.0 INTRODUCTION

Delineating groundwater productive zones in the near-surface of the Voltaian sedimentary basin (VSB) remains a challenge, yet the few successful wells completed appear to be under threat of contamination due to the practice of uncontrolled waste disposal known as dumpsites. Open dumpsites in the basin are growing rapidly due to increasing economic activities resulting in increased waste generation. This system of waste disposal has been used commonly in developing countries because it is considered the cheapest and fastest way of waste disposal (Siddiqua et al., 2022). However, the negative impact caused by this system of waste disposal on the environment is dire as toxic chemical substances gradually get released into both air and the ground. This undoubtedly has the greatest tendency of causing groundwater contamination and jeopardizing public health (Appiah et al., 2018). One of the leading causes of groundwater pollution is contamination by leachates emanating from solid waste dumpsites (Aboyeji & Eigbokhan, 2016). A large number of organic, inorganic, and microbiological pollutants in groundwater have been reported in several research in different parts of the world (e.g. Christensen et al., 2001; Han et al., 2014; Liu et al., 2010; Rapti-Caputo & Vaccaro, 2006) and much resources have been committed to efforts to remediate the problems. According to Akankpo and Igboekwe, (2011), poor solid waste management has had a wide range of negative consequences, including aesthetics, environmental dangers, and contamination. Organic kitchen waste, insecticides, pesticides, batteries, fecal waste, electronics waste, painting waste, hydrocarbon-containing materials, textiles, plastics, nylon, detergents, and other materials are commonly disposed of at open dumpsites. These can increase trace metals and nonmetals, chemicals, biochemical and pathogens, and other contaminants in dumpsites, which can pollute groundwater (Igboekwe et al., 2021). Areas near dumpsites have a greater possibility of groundwater contamination because of the potential pollution source of leachate originating from the nearby dumping site. Such contamination of groundwater results in a substantial risk to local groundwater resource users and to the natural environment (Nagarajan et al., 2012). In the VSB in particular where residents depend solely on groundwater as a result of the non-availability of surface water sources caused by extreme temperatures and high evapotranspiration (S. Yidana et al., 2011), it is important to investigate and understand the likely impact that the possible migration of leachates from the dumpsites could have on the development of the already scarce groundwater resources in the area. Although there is no documented evidence of leachate directly contaminating groundwater resources in the area, the alarming nature by which the open dumpsites are springing up should be a cause for worry.

Arhin et al., (2020) stated that the increasing amount of heavy metals and trace elements concentrations in the soil in some communities in northern Ghana is posing a threat to groundwater development as they could eventually find their way into the shallow aquifers in the area. Also, an unpublished report of field activities under the DANIDA White Volta project (DWVP) managed by the University of Ghana, indicated the presence of maggots in a borehole located close to a solid waste dumpsite at a community known as Tinguli. Acheampong and Hess, (1998) noted that the shallow aquifers which are particularly important in terms of water supply in VSB are vulnerable to contamination due to the permeable and fractured soil layer within the thin overlying vadose zone. The precariousness of the situation therefore shows the need to assess the risk pose by the dumpsites in the basin and findings of which could support the call on local authorities for the development and implementation of properly engineered landfills in the area.

The usefulness of surface geophysical methods in tackling a variety of challenges in dumpsite studies has continued to receive considerable attention. The non-invasive methods such as electrical resistivity tomography (ERT) has been identified as effective technique for properly characterization of dumpsites because it provide better, faster, and more cost-effective means of obtaining sporadically distributed information (Kearey & Brooks, 1991) about pollution levels in the immediate surroundings as well as groundwater systems. The ERT techniques has been extensively used in groundwater contamination studies to identify leachate plume (e.g. Iwmi et al., 2013). Leachate plume generated at a waste disposal site contains high ion concentrations and thus have low resistivity values. This makes an electrical imaging technique a reliable tool for mapping contamination plumes generated from solid waste dumpsites. Amongst other geophysical techniques, the electrical method is the most preferred for dumpsite investigation as it can delineate contaminated zones of groundwater effectively due to the conductive nature of most contaminants (Ganiyu et al., 2015).

The 2D electrical resistivity methods and physiochemical analysis of groundwater samples were used in this study to characterize and highlight the possible imminent danger facing the development of groundwater in the near surface (<100m) of the VSB. This would be necessary to help reduce losses related to the continuous investment on the near surface of the basin while emphasizing the need for alternative deeper sub-surface investigation as has been envisaged (Mainoo et al., 2019; Agyekum & Asare, 2016; Carrier et al., 2008) to hold the solution to the address the continuous water scarcity in the basin.

4.1 DUMPSITES LOCATIONS

The three dumpsites used in this study are located in the Walewale municipality and Tamale metropolitan districts in Ghana. The Walewale township, situated to the north in the study area (Figure 4.1) is located at latitude 10° 21' N and longitude 0° 48' W in the North east region of Ghana. The two-dumpsite investigated in Walewale are said to be among the oldest dumpsites in the municipality and have served as active sites till date. Although efforts are being made by local authorities to decommission them due to the stench emanating from sites, residents still dispose domestic waste at the sites due to lack of alternative refuse disposal sites. The third and the largest dumpsite is located in a city known as Tamale.

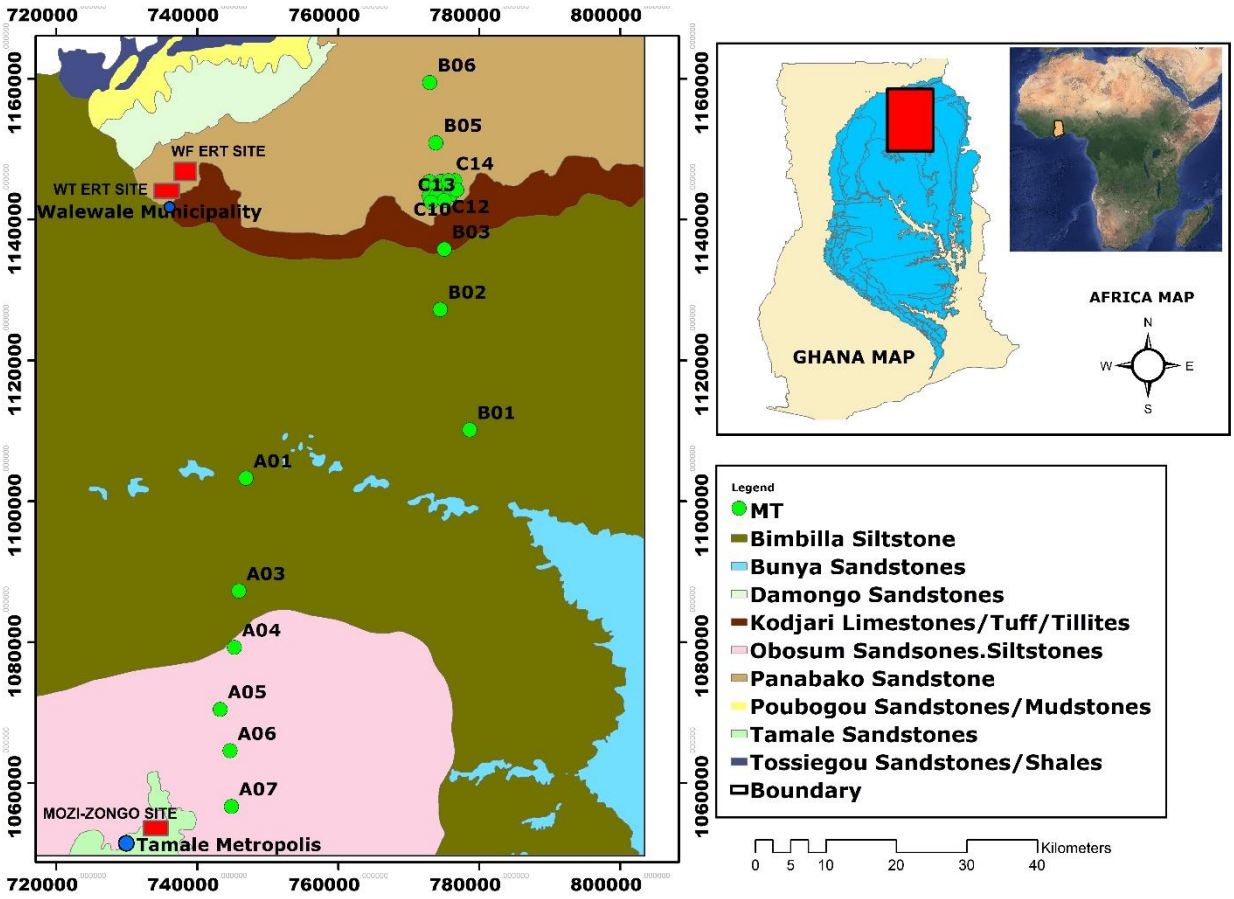

Figure 4. 1: Geological map of the study area showing ERT dumpsites (red rectangles) and MT locations (green dots) with inset map of Africa and Ghana showing the study area (red).

Tamale metropolis is the business and administrative capital of the northern region of Ghana. Within the scope of this study, the Tamale metropolis is located to the south within the coordinates 9° 32'N and 0° 49' W. The city cover a total landmass of 750 km^2 (Local Gov. Minstry, 2023). According to Puopiel and Owusu-Ansah, (2014), the daily waste generation in the Tamale metropolis is about 810 tons out of which only 216 tons are hauled daily. The backlog of about 594 tons subsequently end up in open dumpsites such as the Mosi-Zongo dumpiste which was investigated. This uncontrolled nature of solid waste disposal is becoming a concern and should be investigated to ascertain their likely impact these could on the development of groundwater resources which is already shrouded in difficulties in the area. The dumpsites are non-engineered and open. They are located within residential areas (Figure 4.2) and consist of heterogeneous wastes including domestic, medical, municipal, industrial and other forms of hazardous wastes.

Figure 4. 2: (A & D) Some selected non-engineered open dumpsites (B & C) leachate collected in a trench at a dumpsite (E) some open hand-dug wells where groundwater samples were taken for analysis. At the background of the hand-dug wells are residential buildings and the open hand-dug wells where the samples were collected are approximately 20-250m radius away from the dumpsites.

4.1.1 Data Acquisition

The 2-D electrical resistivity tomography (ERT) geophysical technique was employed along selected traverses at the dumpsites in the study area. Electrodes were arranged with constant separation of 5 m between adjacent electrodes spreading for a distance of 400 m. The subsurface 2D resistivity tomography data were acquired using ABEM Terrameter LS, a cutting-edge data acquisition system for spontaneous potential (SP), apparent resistivity and time-domain induced polarization (IP) (ABEM, 2010). To ensure reliability and consistency of the apparent resistivity values of the substrata, the conventional Wenner and Schlumberger configurations were used to conduct the apparent resistivity surveys. The 2-D ERT survey was intended to conduct continuous vertical electrical sounding along a traverse at selected dumpsites in order to generate 2-D resistivity pseudo-sections of the subsurface to analyze and characterize the probability of leachate migration. Apparent resistivity data were automatically measured by the resistivity equipment and stored in the Terrameter LS equipment. The multi-protocol approach was used principally as a quality-assurance tool to validate the results, and to establish the consistency and reliability of the data sets. The ABEM Terrameter LS Resistivity equipment was paired with two (2) electrical cables, each with a length of 200 m, for the study. Depending on the available lateral space, all traverse lines were given a profile length of 400 m.

4.1.2 Data Processing and Inversion

The RES2DINVx64 (Geotomo-Software, 2002) was used for the processing and inversion (see Chapter 2 section 2.1.5) of the resistivity data. After the data was imported into the RES2DINV platform, the edit tool was used to remove bad datum points from the data set (Figure 4.3). The main purpose is to remove data points that have apparent resistivity values that are obviously too large or too small compared to the neighboring data points (Mainoo et al., 2019). Bad data points were either negative data points or spikes. Spikes are positive data points with spurious values (Raji & Adeoye, 2017). The bad data points (negative) could be due to the failure of the relays at one of the electrodes, poor electrode ground contact due to dry soil, or shorting across the cables due to very wet ground conditions. The initial value of the damping factor used for the inversion was set at 0.1. However, in two cases where data were noisy, a damping factor of 0.3 was used as the initial inversion damping factor. The RES2DINV automatically determine the two-dimensional (2-D) resistivity model for the subsurface for the data obtained from electrical imaging surveys (Dahlin, 1996; Griffiths & Barker, 1993).

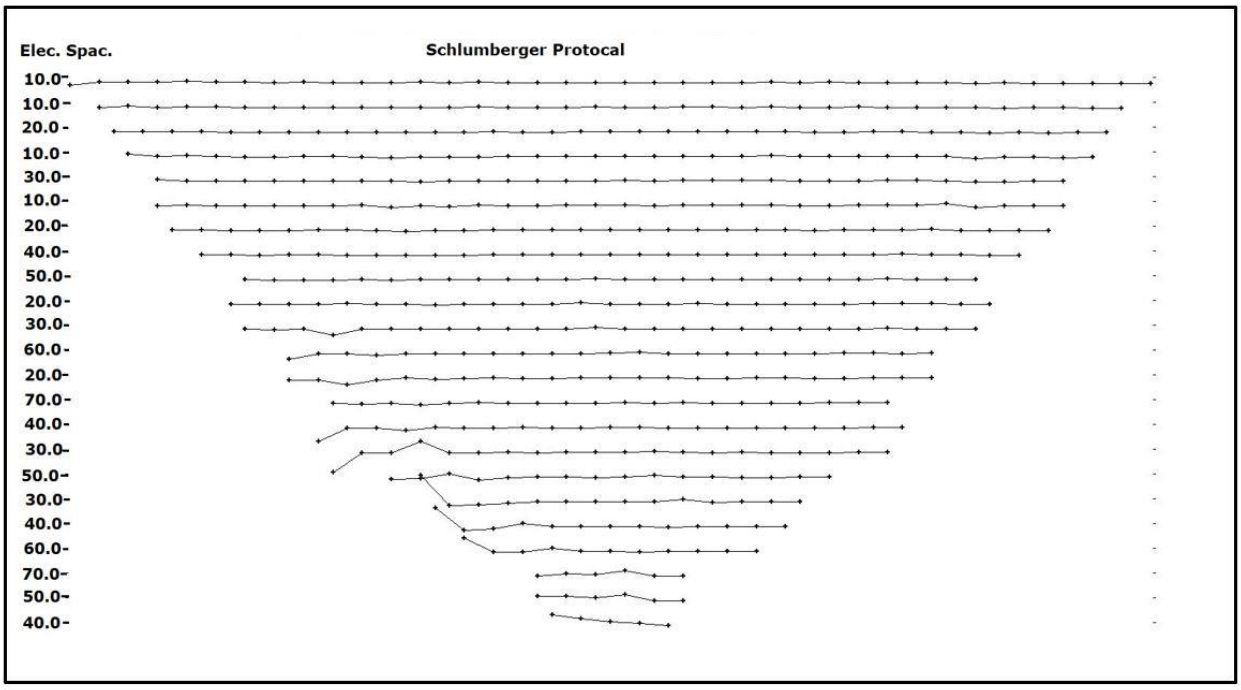

Figure 4. 3: A typical example of the arrangement of data points in pseudo-section with the Schlumberger protocol.

A finite-difference modeling subroutine was used to calculate the apparent resistivity values, and a non-linear smoothness-constrained least-squares optimization technique used to calculate the resistivity of the model blocks. To achieve good resolution, the cell width of the inversion routine was set to half the electrode spacing. This made the number of computation grid points in the tomographic inversion to be twice the number of electrodes used.

4.2 RESULTS AND DISCUSSION

The quality and authenticity of the ERT data used for the inversion were ensure through monitoring and recording parameters during the data collection, and inspecting and analysing the data after the acquisition. Also, appropriate electrode configuration and arrangement that suit the target and measurement objective was ensured for good data quality. The results of the inverted ERT data are presented in the following sections.

4.2.1 Walewale Fogni Dumpsite (WFD)

The figure 4.2 displays resistivity distribution of the formation underneath Fogni dumpsite (WFD) close to old market in the Walewale municipality. Ordinarily, profiles around the periphery of the dumpsites should not be characterized by any significant decrease in resistivity values unless the soils have been infiltrated with pollution plume (Appiah et al., 2018). In Figure 4.4a, a very low resistivity anomaly is observed at a depth of about 10 m and connect to the

surface at horizontal distances of 90 – 130m, 320m and 380m. This anomaly has resistivity value less than 20 Ωm suggesting a possible formation of leachate plume (Ganiyu et al., 2015) or a thin layer of clay within the overburden. However, the horizontal location (90-130m) of this low resistive anomaly correspond with a leachate pool (Figure 4.2b) accumulated from slowly emanating effluent from the pile of heterogeneous waste materials heaped on the surface of the resistive duricrust (Carney et al., 2010; Ewusi et al., 2020) in the area. The duricrust underneath the profile is reported to have resistivity values exceeding 1000 Ωm (Aliou et al., 2022) but the resistivity values observed close to the surface are rather low and could be attributed to the effect of the infiltrating leachate into the subsoil. The leachate appears to spread steadily within the overburden throughout the traverse. The low resistivity layer is identified as a possible contaminant plume (with values less than 20 Ωm) could migrate vertically with time when sub-vertical fractures are encountered.

The second profile line (Figure 4.4b), which was ran across the waste dump to the south (Figure 4.1), also revealed a low resistivity formation at horizontal distances of 110 m and from 320 - 380 m. This low resistivity formation occurring at an average depth of 15 m extend across the entire profile, in a similar fashion to the low resistivity layer observed in the first traverse. It however appears to have infiltrated a little deeper in the second profile than in the first profile for the same waste dump. The low resistivity layer could be associated with buried waste materials or possible leachate migrating from the dumpsite as the plume positions coincide with surface location of heap of waste materials. A formation with similar resistivity values is seen at around 60 m depth and could be hydrologically connected to the leachate plume above via infiltration through a sub-vertical fracture (black arrows). Several migration pathways were observed, suggesting the shallow (<100 m) groundwater table in the region could be prone to contamination if already not present.

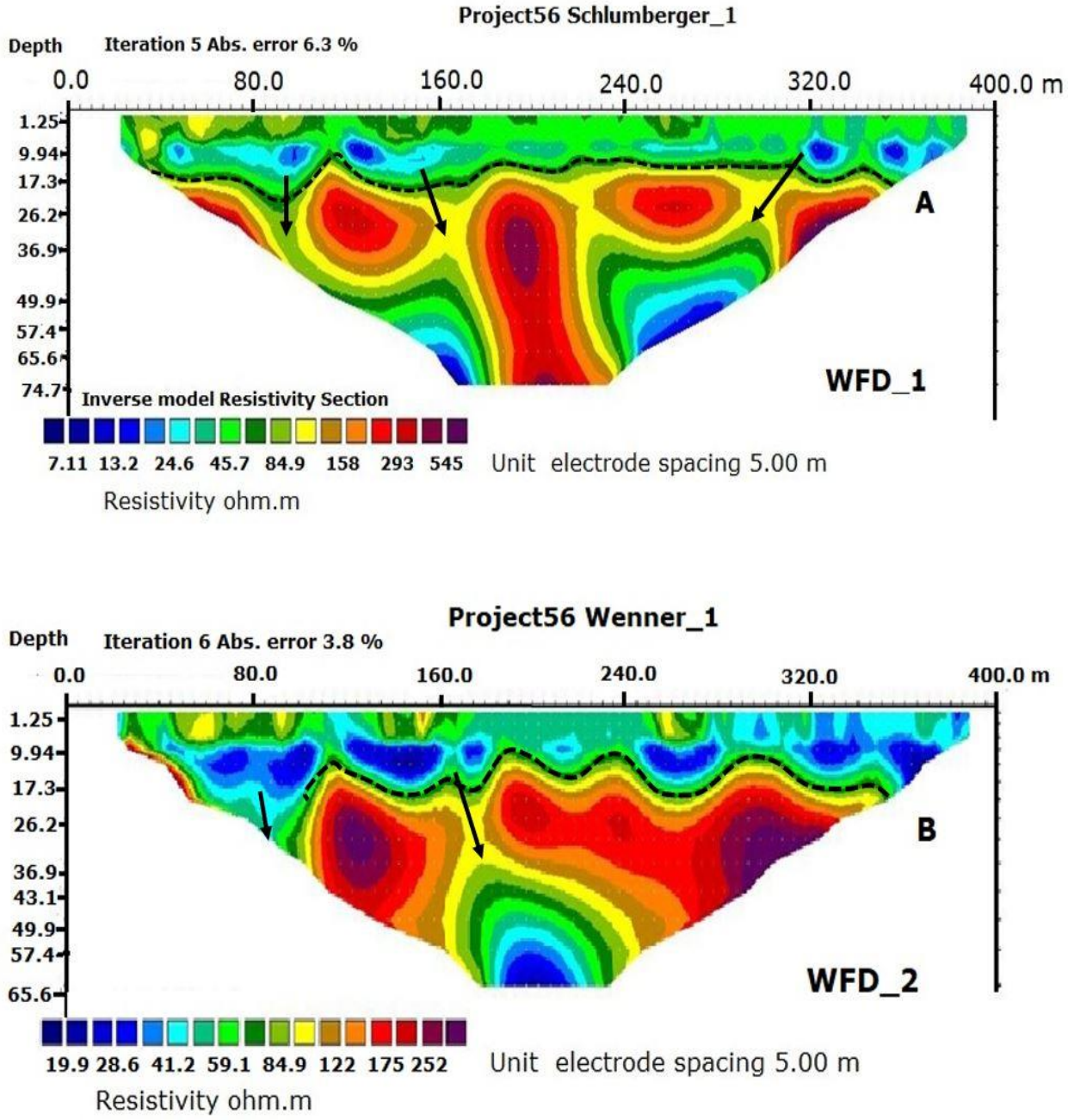

Figure 4. 4: 2-D electrical resistivity pseudo-section showing variations in formation resistivity of Fogni dumpsite in Walewale. Black arrow indication a possible sub-vertical fracture that could facilitate the transportation of possible pollutants into deeper depth. The dash line defines the regolith boundary underneath the profile.

4.2.2 Walewale Tugbini Dumpsite (WTD)

The second dumpsite that was investigated is located in a suburb of Walewale known as Tugbini (Tugbini dumpsite). Two profiles (WTD1 and WTD2) were laid in a north-south and east-west orientation respectively using the Wenner configuration. The pseudo-sections obtained after the

inverse modeling of the profiles are presented in figure 4.5. The topsoil beneath both traverse shows essentially very low resistivity anomaly (values < 20 Ωm) along the entire profile lines in a similar fashion. These low resistivities could be attributed to leachate permeating from the heterogeneous waste materials deposited directly on the loose soil cover. Leachate from dumpsite is a highly polluted liquid containing ionic constituents thereby making it very conductive (Nagarajan et al., 2012; Wijekoon et al., 2022). The decomposition of waste and formation of leachate is primarily influenced by factors such as high temperatures, humidity and age of waste materials (Bernardo et al., 2022). Apart of humidity which varies significantly throughout the year in the area, temperatures remain high and thereby favoring the decomposition and formation of leachate from the waste dumps. The low resistivity anomaly forms a bowl shape structure at a horizontal distance between 80 m to 150 m and was observed to seep deeper to depths arounds 20 m (Figure 4.5a). The structure is interpreted as leachate plume which has infiltrated from the surface beneath the waste dump. The continuous infiltration of the leachate plume was probably curtailed by a resistive body occurring just below the migrating fluid and perhaps resulting in the accumulation of the leachate in the form of a bowl shape structure as observed. At the center of the waste body, both traverses revealed a deep lying low resistivity anomaly with similar resistivity values (<20 Ωm) as those observed within the overburden. The deep lying anomaly could be a possible contaminant plume conceivably connected to leachate observed in the topsoil via infiltrating, as its position coincide with what seems to be a fracture (black arrow) formed by the displacement in the resistive body (Figure 4.5). Due to space constraints, control traverse to investigate how far the leachate from the dumpsites could have plausibly migrated was not carried out. The dumpsites in the municipality are located right within populated areas surrounded by many infrastructures (Figure 4.2a &f). The sites are conveniently created by locals and are unregulated, hence making it difficult to finding spaces wide enough to ran control profiles in the area.

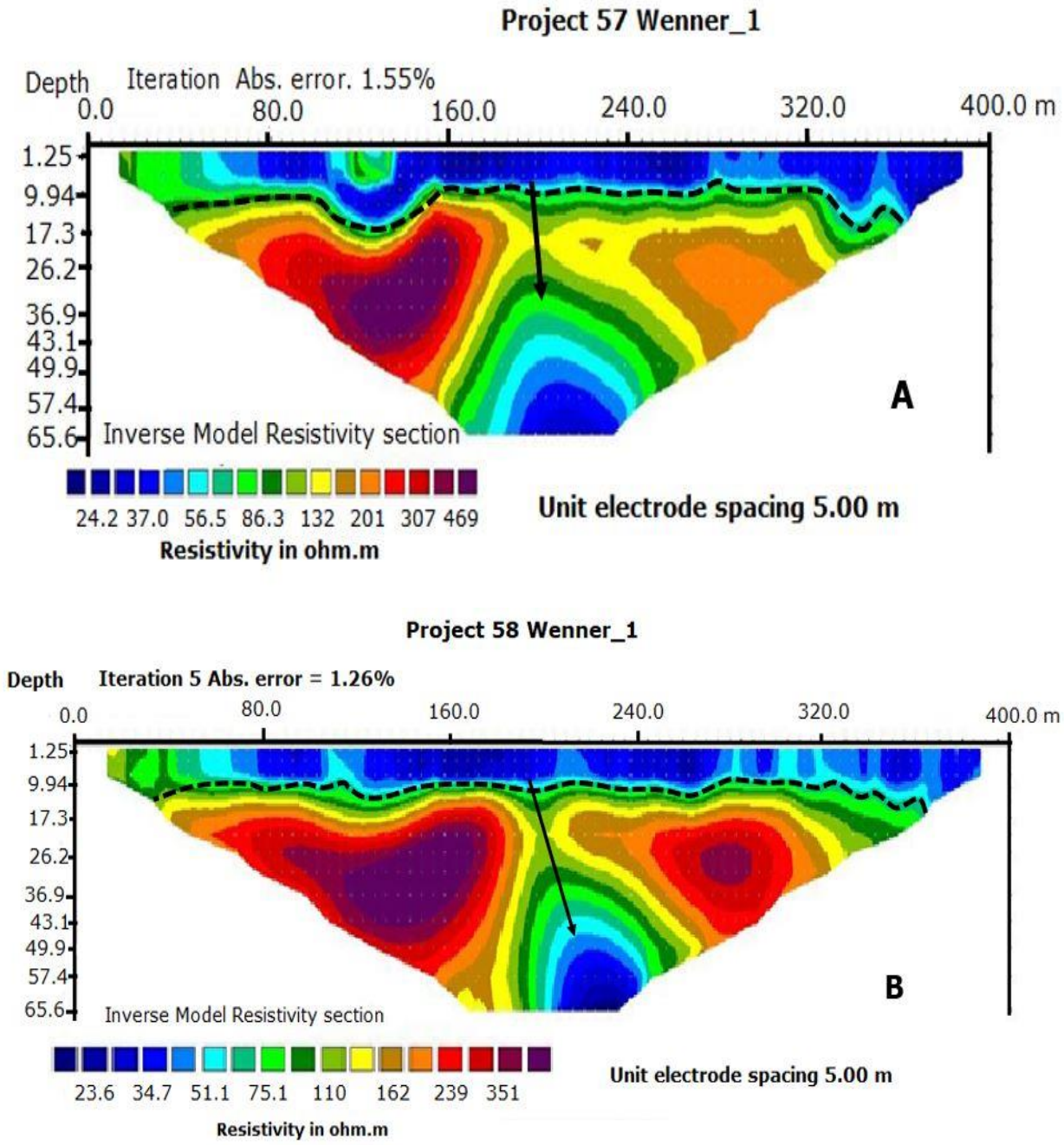

Figure 4. 5: 2-D electrical resistivity pseudo-section showing variation in formation resistivity at the Tugbini dumpsite in Walewale community. Black arrow indication a possible sub-vertical fracture that could facilitate the transportation of possible pollutants into deeper depth. The dash line defines the regolith boundary underneath the profile.

In the Walewale municipality, the low resistivity formations possibly induced by the infiltration of leachate into the weathered zone was used as basis to estimate the regolith thickness for the area. The regolith thickness estimated ranges between 4 to 15 m and averages approximately around 10 m. This assessment is in line with Carrier et al., (2008) regolith thickness estimation

of 6- 11 m for the VSB. The weathered surfaces are clearly distinguished from the resistive bedrock along all profiles at the vicinity of the waste dump in the Walewale area making it possible to delineate the regolith thickness (curvy dash line). The base of the regolith in particular, is described as an important source of groundwater in the area (Chegbeleh et al., 2009; HAP, 2011). Most of the hand-dug wells which are predominantly used for domestic water supply in the area are completed within this regolith units making them prone to possible contamination as the leachate within this unit could slowly migrate over time due to abstraction of groundwater resources.

4.2.3 Tamale Dumpsites

The third dumpsite investigated is located at the Mosi-Zongo community behind the mechanic shop in the Tamale central business district. The inverse resistivity model of the site showed variations in resistivity ranging from 4 – 225 Ωm (Figure 4.6). At a lateral distance from 145 to 180 m along the profile, a low resistivity anomaly with values less than 15 Ωm and at depth of about 6m is observed. This low resistivity anomaly at the central part of the waste dump could be associated with leachate gradually infiltrating into the top soil underneath the dumpsite. Several low resistivity patches gradually extend along the traverse except for some few places where relatively high resistivity areas are observed.

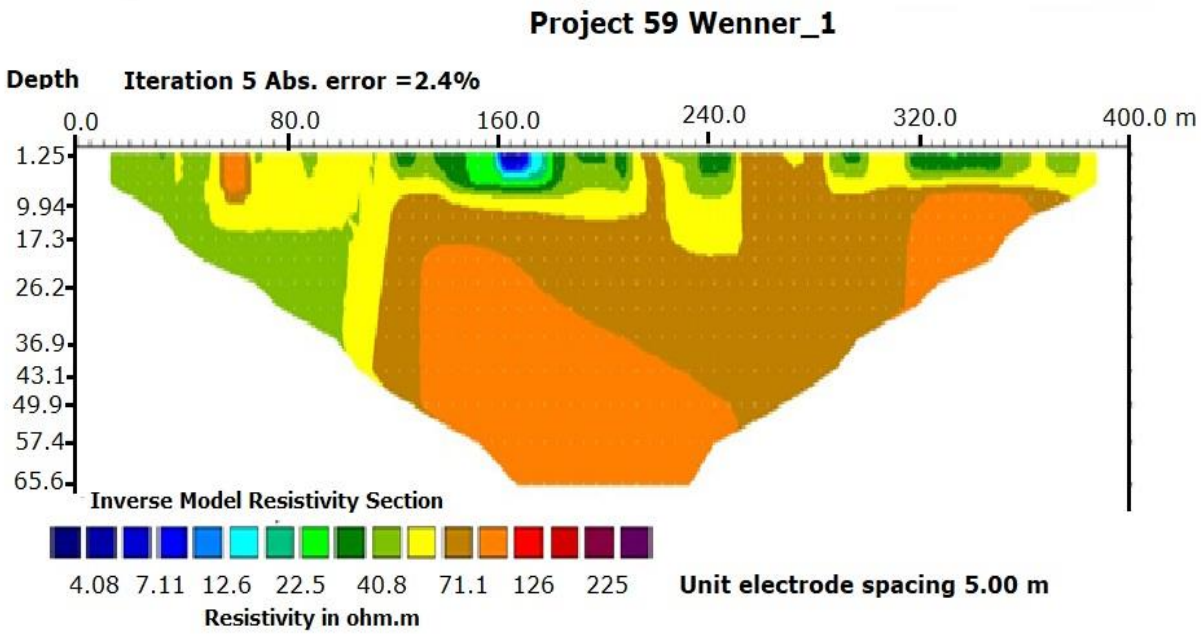

Figure 4. 6: 2-D electrical resistivity tomography results of a dumpsite in the Mosi-Zongo community in Tamale.

The resistive areas near the surface at the waste dump is interpreted to represent compact debris consisting of non-biodegradable materials possibly buried at shallow depth. The range of resistivity value distribution of the profile is low compared to the resistivity of the profiles around the Walewale area. The relatively low resistivities are reflective of the geology of mudstones and siltstones underneath the profile. The mudstones and siltstones forms part of the Obosum group of the Voltaian supergroup and have been described by Mainoo et al., (2019) and Carney et al., (2010) to have relatively low resistivity. Mudstones contains over 50% of clay materials (Aplin et al., 1999) which has the ability to limit fluids flow in the subsurface and that perhaps explains the restricted spread of the leachate pool (blue) beneath the waste body. The mudstones and siltstones however intercalate with thin beds of sandstones locally referred as the Tamale sandstones at some locations in the area.

It has previously been reported that certain heavy metal concentration found in vegetables cultivated in the Tamale metropolis surpass WHO permissible limits (Ametepey et al., 2018), albeit the report did not directly linked their finds to leachates from dumpsites. The trends as revealed by the resistivity sections clearly indicate the gradual migration of the leachates from the dumpsites suggest an imminent risk as many rural communities' sources water from locally hand-dug wells and boreholes most of which produces marginal yield. As the waste dump ages and produces more leachate and the abstraction and withdrawal of groundwater continues, the potential likelihood of groundwater contamination within the shallow sub-surface is heighten as leachate migration will increase due to suction pressure. With developmental quest high on government agenda, couple with increasing economic activity, solid waste generation will only increase and thereby making the situation more precarious. Where possible, groundwater quality assessment around these waste dumps should be perform to gauge any likely movement of the pollutants away from the dumpsites.

4.3 Groundwater Sampling

Groundwater sampling was carried out around two out of the three dumpsites after the ERT sounding. A total of fourteen (14) groundwater samples were collected consisting of 10 open hand-dug wells and 4 boreholes. The samples were taken within the ambient of the dumpsites on a radius of about 20-250m for the analysis of some heavy metals and total dissolve solids (TDS) in the laboratory. The purpose of the analysis was to check the possible presence of the heavy metals and to trace the extent of migration of these metals away from the dumpsites. Heavy metals are among the most important contaminants found in leachate from waste dumps (Beinabaj et al., 2023; Carvajal-Flórez & Cardona-Gallo, 2019). Analysis of the heavy metals

were done using the atomic absorption spectrometry (AAS) technique at the Ecological laboratory (ECOLAB) at the Geography Department of the University of Ghana. The AAS technique is based on the principle that free atoms in the grounds state can absorb light of certain wavelength which is specific to only that element (Filho et al., 2012). It is a single-element method used for analysis of trace elements and heavy metals across several fields including geoscience, biological, metallurgical, pharmaceuticals etc.

Table 4. 1: Physico-chemical and heavy mental concentration in groundwater samples compared with GEPA (Armah et al., 2010) and WHO (2022).

Sample	**App. Distance**	**TDS (mg/L)**	**Fe (mg/L)**	**Pb (mg/L)**	**Zn (mg/)**	**Cd (mg/L)**	**Cu (mg/L)**	**Cr (mg/L)**	**Cl^- (mg/L)**
WF 01	21m	288	0.283	0.002	0.001	0.009	0.002	0.001	75.331
WF 02	250m	279	0.001	0.002	0.006	0.002	0.003	0.001	53.175
WF 03	42m	268	0.004	0.001	0.001	0.003	0.001	0.001	39.881
WF 04	85m	156	0.002	0.002	0.001	0.002	0.002	0.006	26.588
WF 05	50m	169	0.223	0.002	0.001	0.002	0.001	0.001	44.313
GB 01		393	0.001	0.004	0.001	0.002	0.001	0.001	66.469
GB 02	25m	84	1.054	0.002	0.006	0.038	0.004	0.001	13.294
GB 03	211m	470	0.001	0.002	0.004	0.002	0.002	0.001	16.839
GB 04		508	0.001	0.004	0.002	0.001	0.002	0.001	17.725
GB 05	64m	179	0.41	0.002	0.001	0.002	0.001	0.001	53.175
NY 01	20m	281	0.002	0.001	0.001	0.111	0.001	0.001	44.313
KB 01	35m	53	1.15	0.002	0.001	0.034	0.001	0.001	31.019
GBN 1	112m	165	0.007	0.002	0.001	0.004	0.001	0.002	35.450
TG 1	80m	313	0.069	0.002	0.001	0.001	0.001	0.002	62.038
GEPA		1000	-	0.1	10	-	-	-	-
WHO		500	0.3	0.01	5	0.003	2	0.05	250

Table 4.1 shows the AAS analysis results of the 14 groundwater samples. The concentrations of the each of the heavy metals along with TDS and chloride in each of the samples were compared with the recommended drinking water standards from the world health organization (WHO) and Ghana environmental protection agency (GEPA). TDS values obtained from the analysis of the samples ranges from 53 mg/L to 508 mg/L. The TDS concentrations in all the sample are lower when compared with safety standard values given by GEPA and WHO (WHO, 2022). The sample GB 04 however, showed TDS value slightly higher than the WHO

value. Likewise, the concentration of Chloride in all the samples were below the recommended threshold limits (250 mg/L) suggested by both GEPA and WHO for potable groundwater. It is known that chloride can be used as an indicator of anthropogenic contamination in groundwater (Castaneda et al., 2012; Grisey & Aleya, 2016) but was not the case in the present study which showed low values (Table 4.1). It therefore suggests that the water is health risk free and could be safe for consumption based on the TDS and chloride assessment. For the heavy metals, the concentrations of Pb, Zn, Cu, Cr, in all the samples fall within the permissible limits stated by both GEPA and WHO (Figure 3.7a). However, the concentrations of Cd in sample WF 01, GB 02, NY 01 and KB 01(Figure 4.7a) and Fe in sample GB 02, KB 01 and GB 05 (Figure 3.4c) all exceeded the recommended threshold values advised by WHO for potable groundwater for domestic purpose.

Though the source of these heavy can be geogenic, there is the possibility that the high concentrations levels of Cd and Fe in some of the samples mentioned could be anthropogenic due to their nearness to the waste dump. Leachate from dumpsites contains several heavy metals including cadmium (Cd) and iron (Fe) which when infiltrate into the groundwater system, could increase their concentrations. According to WHO, (2022) report, the main source of cadmium (Cd) in drinking water is via wastewater (e.g. leachate) released into the environment. Cd is widely used in the steel industry and in plastics (Luparello et al., 2011). Plastics constitute large proportion of the materials in the waste dumps (Figure 4.2), hence forming a significant source of the metal (Cd) in the area. The high concentrations of Cd observed in some of the samples therefore could be due to gradual leaching and infiltration of the metal into the shallow groundwater table. The consumption Cd through food, water and air over time slowly build up Cd in the kidneys and cause kidney disease and fragile bones (Genchi et al., 2020). Iron (Fe) is one of the most abundant metal in Earth's crust and as a result it is found naturally in freshwater systems. However, it is also a major constitute in leachate from waste materials. The concentration of Fe was observed to be within the permissible limit given by WHO except for 3. The relative distances of the wells from which the 3 samples with high Fe concentration were taken are closer to the dumpsites hence the high concentrations could be due to contribution of Fe from leachate from the waste dumps. High concentration of Fe in water leads to overload which can cause diabetes, hemochromatosis, stomach problems and nausea (Hossain et al., 2023).

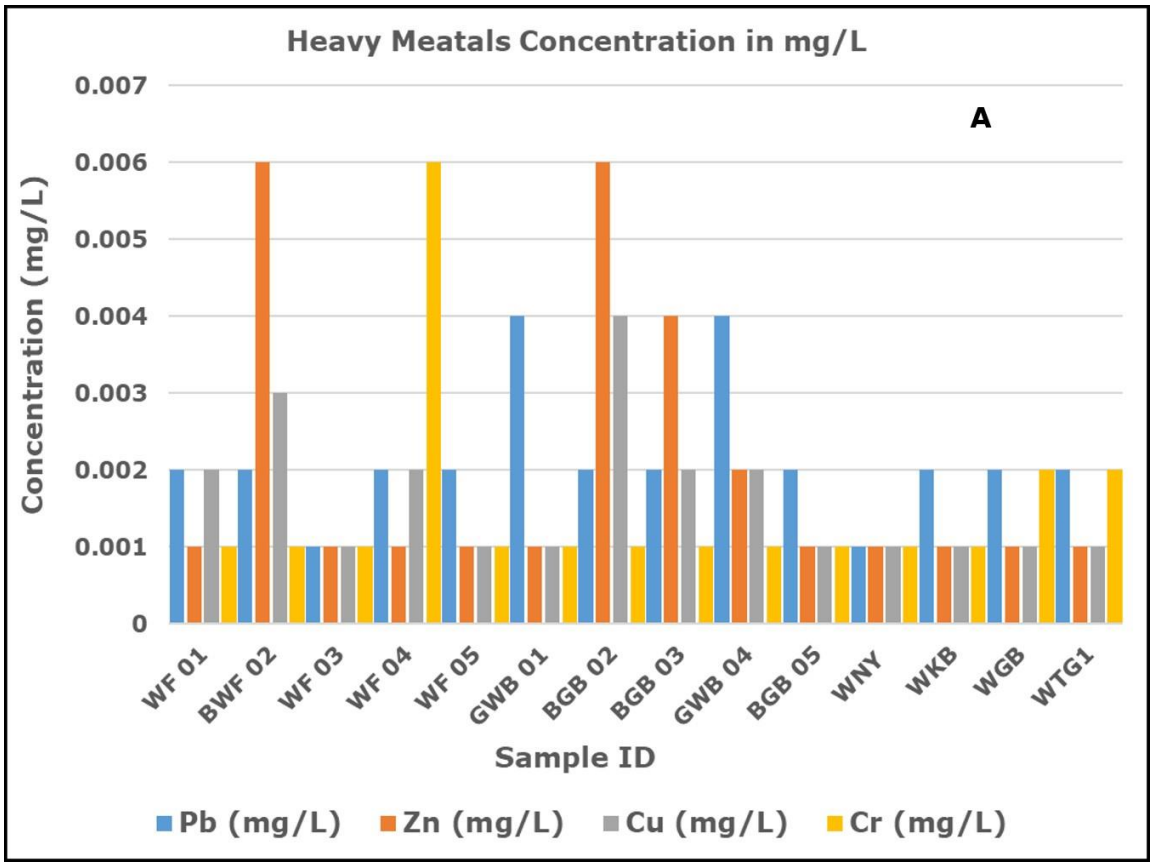
Heavy Meatals Concentration in mg/L
A
Concentration (mg/L)
0.007
0.006
0.005
0.004
0.003
0.002
0.001
0
WF 01
BWF 02
WF 03
WF 04
WF 05
GWB 01
BGB 02
BGB 03
GWB 04
BGB 05
WNY
WKB
WGB
WTG1
Sample ID
Pb (mg/L)
Zn (mg/L)
Cu (mg/L)
Cr (mg/L)

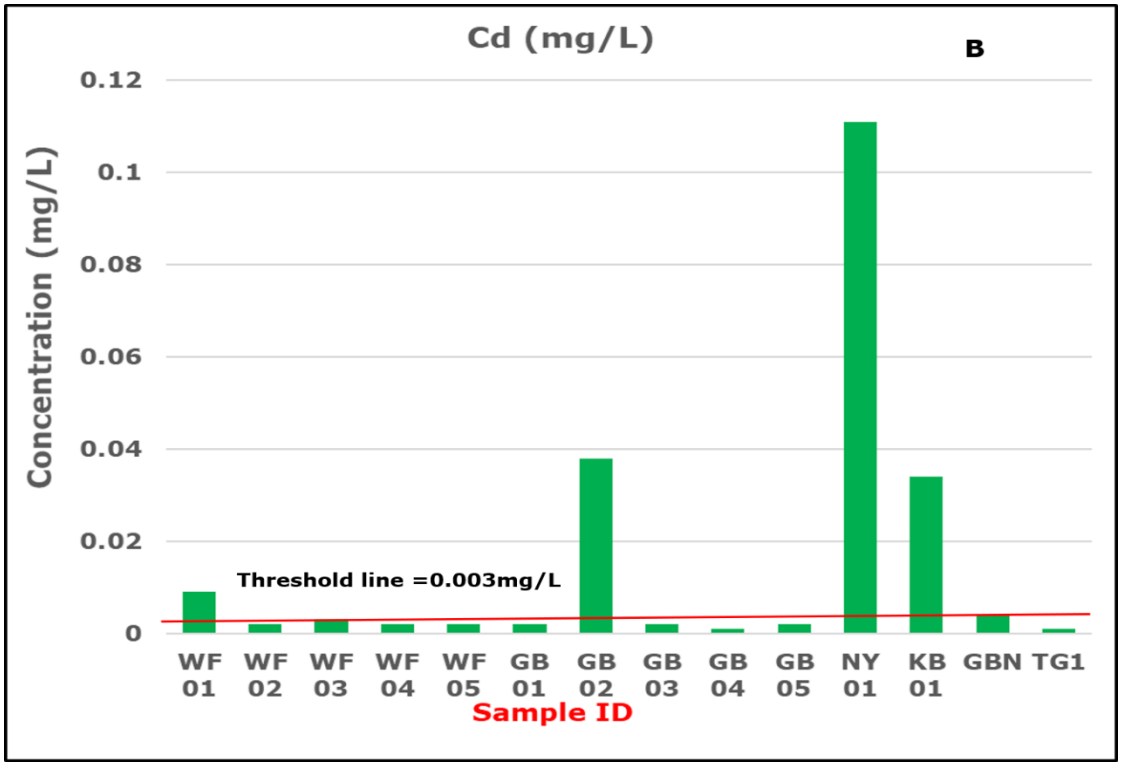
Cd (mg/L)
B
Concentration (mg/L)
0.12
0.1
0.08
0.06
0.04
0.02
0
Threshold line =0.003mg/L
WF 01
WF 02
WF 03
WF 04
WF 05
GB 01
GB 02
GB 03
GB 04
GB 05
NY 01
KB 01
GBN
TG1
Sample ID

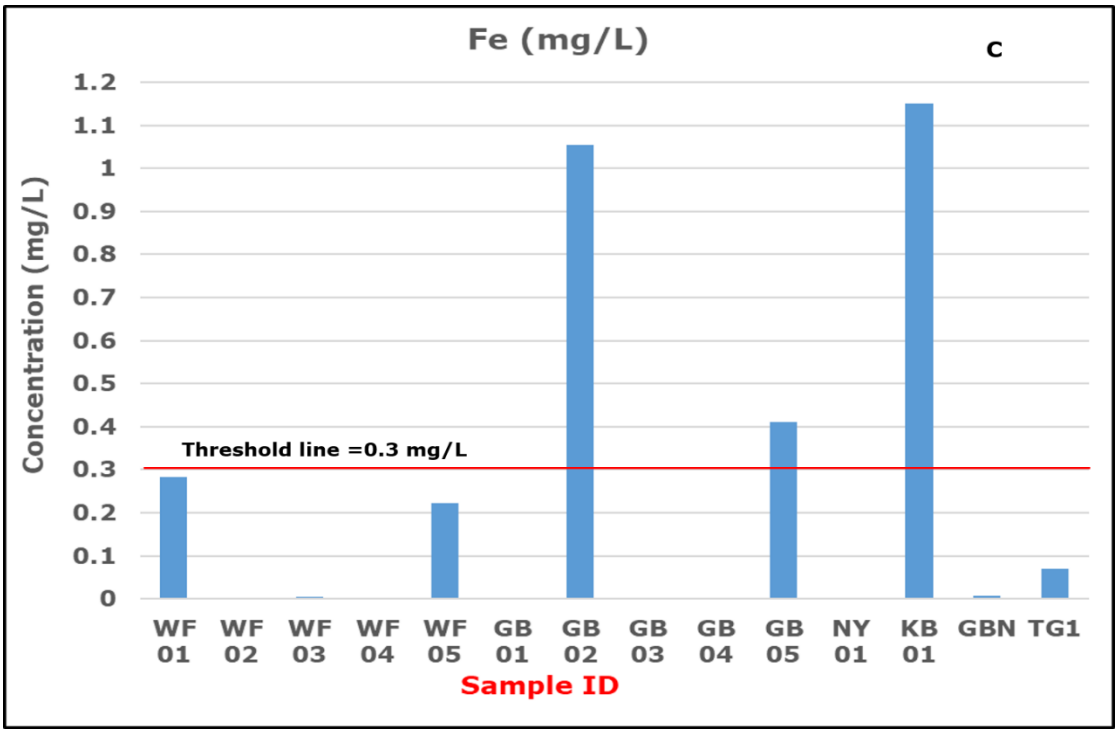

Figure 4. 7: Plots of heavy metals concentration verse sample ID showing which metal in which sample exceeds the recommended threshold values as suggested by GEPA and WHO. (a) is plot for Pb, Zn, Cr, Cu (b) is a plot Cd and (b) is a plot of Fe concentrations.

4.4 CONCLUSION

The application of the ERT technique aided the acquisition of data from some selected dumpsites which have been useful in deriving depth and lateral information about the waste bodies. The determination of the extent of incursions of contamination plumes and the delineation of preferential migration pathways of leachates have been investigated for the purposes of remediation and regulation. The delineated conductive fluids identified as leachate steadily spread across the loose overburden within the vicinity of the waste dump. Analyses of the profiles beneath the dumpsites in the Walewale municipality revealed the possible migration leachate plumes to depths beyond the weathered zone. The results of the ERT clearly defined the regolith thickness along the traverse of the survey area which agrees with what has been suggested by earlier researchers in the basin. The existence of subvertical fractures in the weathered zone will only aid the migration of the leachate from these hybrid waste dump over time putting the already scarce shallow groundwater table in danger of being contaminated.

The physico-chemical analysis carried out indicated high concentration of cadmium and iron in groundwater in the area. The high concentrations of these heavy metals could possibly be due to the gradual movement of leachates from the dumpsites into the shallow water below.

Although these observations were made in smaller number of the samples and more evidence maybe needed to reach a definite conclusion, it is still a wakeup call for well-meaning authorities to act in order to avert any future problems.

It will therefore be impractical to continue investigating the shallow part of the basin in the face of an imminent threat along with the low success rate for siting productive wells. Rather than committing resources to continue investigating the shallow subsurface (<100 m) which has been established by many to have low potential, effort could instead be channel for the deeper subsurface investigation suggested to be more likely to produce high yielding wells in the area.

CHAPTER FIVE

DELINEATING SURFACE STRUCTURES FOR DEEP AQUIFER STUDY USING MAGNETOTELLURICS AND AIRBORNE GEOPHYSICS IN THE NORTHERN PART OF THE VOLTAIAN SEDIMENTARY BASIN, GHANA, WEST AFRICA.

Delineating subsurface structures for deep aquifer study using MT, and airborne geophysics. Case study of the Voltaian sedimentary basin, Ghana West Africa.

R.A. Mejida[1,2], P. Tarits[1], T.E. Armah[2], S. Hautot[3] and S.M. Yidana [2], E.A. Dzikunoo[2]

[1] IUEM, Geo-Ocean, rmejida@ug.edu.gh, tarits@univ-brest.fr

[2] University of Ghana, tekarmah@ug.edu.gh, smyidana@ug.edu.gh

[3] IMAGIR, sophie.hautot@imagir.eu

ABSTRACT

A comprehensive study was conducted using airborne geophysics and magnetotelluric to reveal the complex nature of the subsurface geology and structures to delineate possible productive groundwater zones below the near-surface regolith in the Voltaian Sedimentary basin in Ghana. Resistivity maps derived from both 3-D and 1-D inversion of the magnetotelluric profile defined a deep zone of low resistivity formation indicating a probable groundwater-bearing zone. The resistivity signature of the structure is comparable to that of a unit in which a 132l/min-yielding research borehole in close proximity is completed. This promising conductive layer is approximately 30 m thick at 250 m below ground level and is about 45 km in length. This has presented new insights into the stratigraphic thickness of the two regionally significant geological formations: the Panabako and Poubogou Formations. The new data suggest thicker units than are currently known in the current literature. This finding is significant and will affect the current understanding of the geology and resource productivity of the Voltaian Basin.

5.0 INTRODUCTION

Access to sustainable groundwater is an important strategy towards enhancing the resilience of vulnerable communities to the impact of climate change. This is particularly significant in most communities in Sub-Saharan Africa where high intensity short duration of rainfall patterns (Coulibaly et al., 2018; Mensah et al., 2022) have affected rain-fed agricultural practice and the general standard of living. In the region, the short duration high intensity rainfall patterns are succeeded by the prolonged periods of drought with excruciatingly high temperatures and unremitting high potential evapotranspiration rates. These conditions in addition to high siltation rates do not bode well for investing in surface water-based systems for irrigation and domestic water supply under climate change conditions as most of such interventions have failed on the accounts of evaporation. The development and sustainable management of groundwater resources have the potential to enhance the ability of vulnerable communities

which have traditionally depended on rain-fed agricultural activities for their sustenance throughout the year. However, effective groundwater resource development requires adequate understanding of the hydrogeological conditions of the terrain. This requires extensive field investigations employing conventional strategies to unravel the parameters which contribute towards determining the depth, thickness, lateral extent, and the overall potential of groundwater bearing zones. In addition to being the largest usable freshwater reservoir (Fetter, 2002), groundwater resources exhibit characteristics which render it more likely to serve the purpose of building resilience to climate change and related stresses.

Several conventional strategies have been discussed in literature for regional hydrogeological studies. The application of various geophysical methodologies has proven useful in unravelling the subsurface characteristics and facilitating the determination of groundwater storage. Geophysical methods have been copiously used in hydrogeological investigations and have significantly been improved in terms of their capacity to provide useful data to assist in delineating prolific units (Binley et al., 2015; Wiederhold et al., 2021). Diverse geophysical methods have been tested and used to reveal different characteristics of the subsurface for hydrogeological purposes. However, the electrical resistivity methods are the commonest methods used in groundwater exploration (e.g. Abdel Moneim 2005; Khalil 2014; Mohamaden and Ehab 2017; Shawky et al. 2012; Soussa et al. 2012; Yousef et al. 2009). They have been perfected over the years in their capacity to provide useful information for decision making on the 2D and 3D architecture of the near subsurface. Electromagnetic methods have often been used conjunctively with electrical resistivity methods in most groundwater and hydrogeological studies. The electromagnetic methods have an advantage of providing resistivity maps over a wider area than ERT (Electrical Resistivity Tomography) methods. Airborne electromagnetic survey is particularly useful since they provide data to lead to the modelling of the 3D distribution of the electrical resistivity (Siemon et al. 2009), which are both important parameters in hydrogeological investigations and characterization of aquifers (Günther & Müller-Petke, 2012; Viezzoli et al., 2010). Airborne survey techniques such as magnetic and electromagnetic provide opportunity to cover wide areas of the surface, and when combine with other methods such as the magnetotelluric method can significantly enhance confidence in the characterization of the deeper subsurface lithological and structural variations and will prove useful in delineating prolific water-saturated zones.

In the Voltaian sedimentary basin (VSB) in Ghana, ERT and the EM-34 have been used extensively for groundwater prospecting but with limited success (Banoeng-Yakubo & Armah,

2001). The standard ERT gives effective results where a good contrast exists between the weathered zone and the bedrock down to depths of 100m (Porsani et al. 2004; Hazell et al. 1988) or may exceed depending on the current electrode spacing while the EM-34 is good for detecting fractured zones in the subsurface (Chegbeleh et al., 2009) at depths less than 40m. The ERT and EM-34 have been applied widely in Ghana and parts of the West African sub-region and have yielded varying levels of successes. Due to their limitations in terms of the depth of penetration and uniqueness of the results, successes in the Voltaian Sedimentary Basin have been relatively low. A more robust and integrated approach is required in such highly consolidated and partially metamorphosed terrains, to improve upon the characterization of the subsurface to aid detailed regional hydrogeological studies. The consolidation and partially metamorphism reduced porosity and permeability of the basin's sediments. As a results groundwater occurrence in the area is reported to be controlled by discrete fractures such as faults, joints and fissures (Acheampong and Hess 2000; Aliou et al. 2022; HAP 2011).

The main objective of this research is to demonstrate the application of an integrated geophysics (airborne and magnetotellurics-MT) methodology to characterize deep subsurface structures in the bedrock at different scales to enhance and improve groundwater development in the northern part of the VSB in Ghana. The application of airborne electromagnetic and aeromagnetic data in regional subsurface studies such as regional groundwater investigation (Chandra et al., 2016; Joel et al., 2016; Mokgatle & Fourie, 2017) and the application of magnetotellurics (MT) for subsurface structural mapping and aquifer delineation (Aboud et al. 2014; Chandrasekhar et al. 2009; Giroux et al. 1997; Sumanovac 2012) are well documented in literature. However, the use of these methods in an integrated fashion for hydrogeological purpose, especially in the West African sub-region is limited.

5.1 STUDY AREA

The study area (Fig. 5.1) underlies many rural communities where access to potable water has been a challenge over the years. Having access to quality groundwater plays a significant role in enhancing food security, especially in rural areas where smallholder farmers require an adequate supply of water for irrigation as a buffer against erratic and often insufficient rain during the rainy season (Atitsogbey et al., 2018). In spite of its crucial role, groundwater development in the northern part of the VSB in Ghana has not been very successful. The rate of drilling a successful borehole is reported to be below 60%, yet over 67% of the potable water supply to communities in the basin comes from groundwater (Agyekum & Asare, 2016b;

Asante & Amuakwa-Mensah, 2015). This high dependence on groundwater in the region is as a result of the quick drying of surface water bodies caused by extreme temperatures, high evapotranspiration, and prolonged drought (Banoeng-Yakubo et al., 2011; Dapaah-Siakwa & Gyau-Boakye, 2000) and further worsened by the apparent impacts of climate change manifesting in the form of irregular rainfall patterns. The combined effects of the erratic rainfall patterns and prolonged drought periods affect agricultural activities, thus increasing poverty levels in the area. The high failure rate associated with drilling wells coupled with the highly variable yields of the shallow aquifers (100 meters and less) have necessitated deeper (greater than 100 meters) subsurface investigations integrating multiple geophysical approaches.

The study area is located between the latitudes 10° 28'N and 9° 29'N and longitudes 0° 30'E and 0° 45'E and covers part of the Northern and Northeast Regions of Ghana.

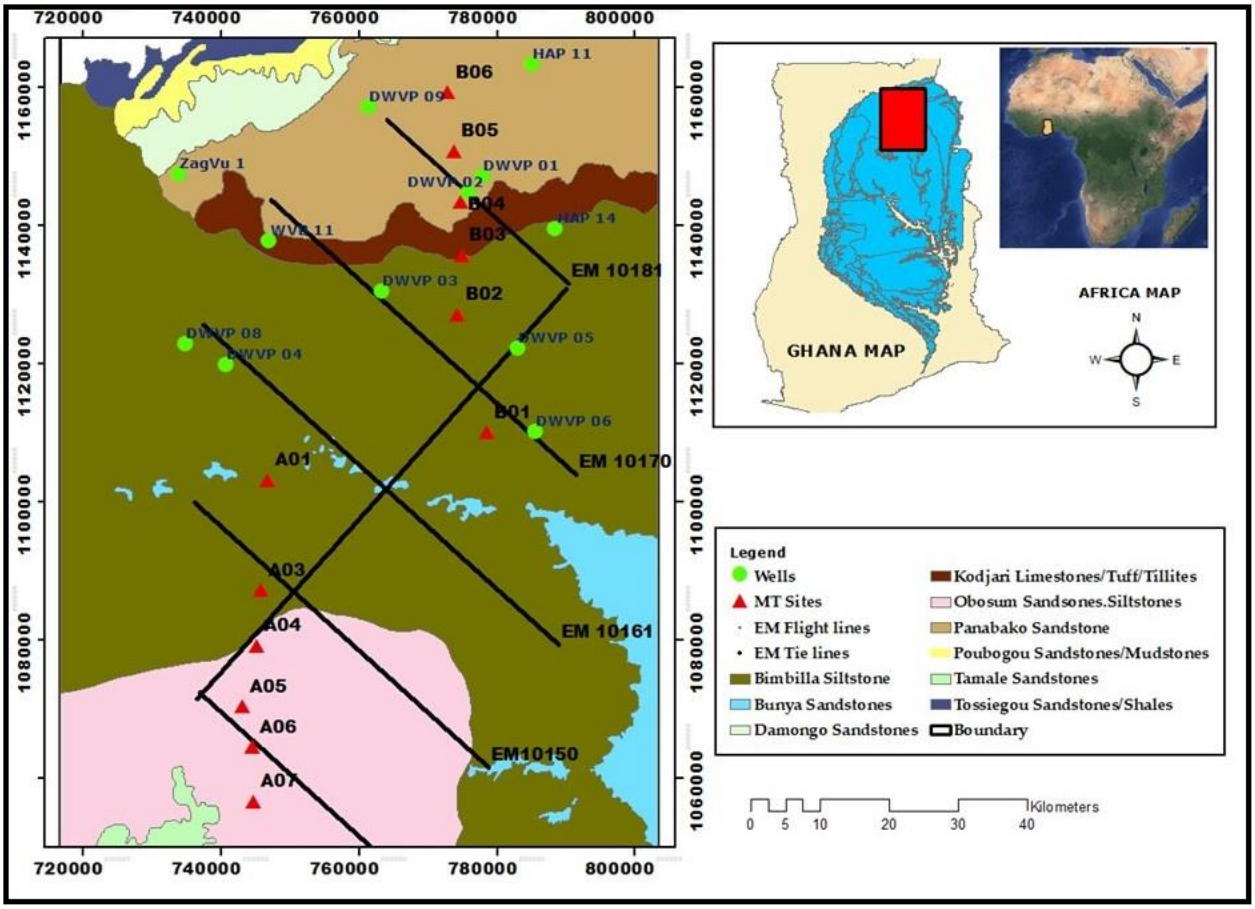

Figure 5. 1: Geological map (modified after Carney et. al., 2010), showing AEM flight lines (black) and MT sites (Red triangles), groundwater wells (green circles) with an inset, map of Ghana defining the study area in red rectangle.

The main vegetation is the Savanna grassland consisting of clusters of shrubs and drought-resistant trees such as the shea nut and the baobab trees. Climate conditions are hot and dry with

the area experiencing only one rainy season starting from May to October each year followed by a prolonged dry season from November to April. The average annual rainfall is about 750 to 1300 mm with temperatures ranging as low as 14°C at night and 40°C during the day (Dickson & Benneh, 2004). The terrain is generally flat lying with low relief to the south and high elevations to the north (Fig 5.2). It is drained mainly by the Nasia and Nabogo rivers (Fig. 5.2) which are both tributaries of the White Volta River.

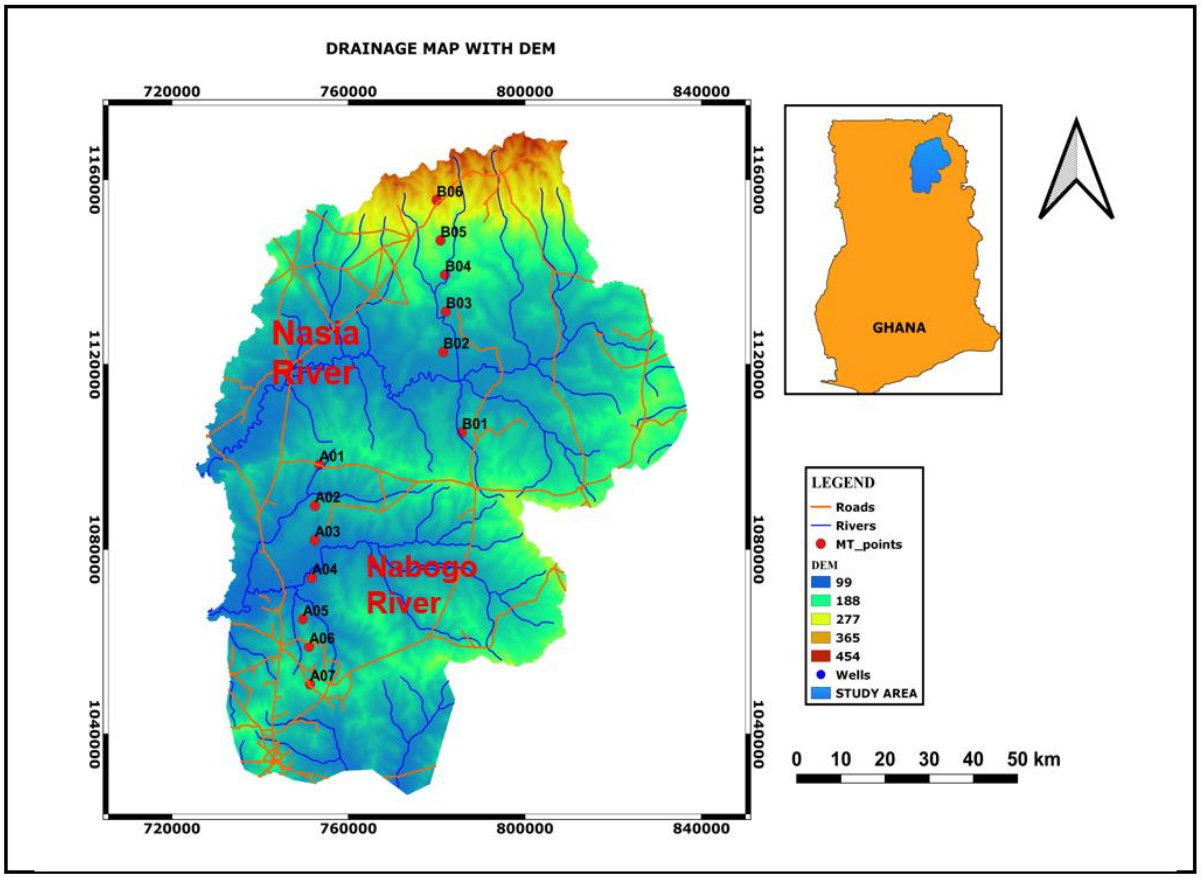

Figure 5. 2: Digital elevation model showing drainage patterns (blue), road network (yellow lines) and MT stations (Red dots) in the area. The ends coordinates are in UTM. The shape of this map delimits the boundaries Nasia and Nabogo sub-basins of the white Volta basin and represent the study area.

5.1.1 Geology and Hydrogeology

The Neoproterozoic VSB, which underlies the study area is among a series of smaller depositional basins located at the eastern margin of the Leo-man shield of the West African craton (Carney, et al., 2010). This geological province, the Voltaian Supergroup comprises

three main groups namely; Bombouka, Oti-Pendjari and the Obosum Groups (Fig. 5.1) and underlies about 45% of the total landmass of Ghana (Carney et al., 2010; Kesse, 1985). Each of the Groups is divided into formations comprising various lithological units. A recent lithostratigraphic classification of the Supergroup (Carney et al., 2010) indicates six rock formations with different lithologies within the study area. They include the Obosum Formation, Bimbilla Formation, Kodjari, Panabako Sandstones, Poubogou Formation and the Tossiegou shales and sandstones.

The Obosum Group is the youngest found in the study area and rests unconformably on the Bimbilla Formation (of the Oti-Pendjari Group). This Group includes highly distinctive lithic, feldspar-rich arenites and conglomerates deposited as terrestrial molasse at the final stage of the uplift of the Dahomeyide orogen (Carney et al. 2010; Kalsbeek et al. 2008). It occurs to the south of the study area (Fig. 5.1) and consists of variegated mudstones and siltstone with locally thick beds of sandstones mostly known as the Tamale sandstones.

The Bimbilla Formation has two sandstone members occurring at the base and the uppermost boundaries which are the major unifying features of the formation. The formation consists of green to khaki, micaceous laminated mudstones, siltstones and tabular, sharp-based sandstones representing a continuous foreland basin deposition. The siltstones often occur in thin, tabular beds with wind-rippled tops and low angle cross-bedding. The sandstones are thinly intercalated within the mudstones and siltstone units forming the Chereponi and Bunya end members (Jordan et al., 2009).

The Kodjari Formation forms the basal member of the of the Oti-Pendjari Group of the Voltaian Supergroup and comprises a distinctive triad of tuff, cap carbonate (Buipe limestone) and tillites which lie unconformably on the Panabako Formation in the area (Carney et al., 2010). The tillites of this group fill an erosional and slightly angular unconformity of glacial origin. Also, Barfod et al. (2004) suggest that the Kodjari consists mainly of shales and siltstones, and lenses of various facies of sandstones, greywackes, limestones, silexites and tuffs.

The thickness of the Panabako sandstones in the study area ranges between 150m to 200 m with an average of about 175 m. It is made up of hard, well-cemented, well-sorted, medium-grained, quarzitic sandstones, which are particularly indurated and appear crystalline in the north of the area. Overlying the unit is a typically thin, gravelly laterite, sometimes capped by thin iron oxide cement (Carney et al., 2010; Jordan et al., 2009).

The Poubogou formation underlies the Panabako sandstones in the study area and it comprises mudstones and Siltstones, which outcrop towards the north along the Gambaga escarpment with an average thickness of 170 m. It grades into the overlying nearshore facies quartz arenites of the Panabako Sandstone Formation (Carney et al., 2010). Also, Ayite, et al. (2008), noted that Poubogou Formation consists of green-grey micaceous mudstones and siltstones with thin intercalations of fine-grained sandstone.

The rocks of the Supergroup have lost their primary porosities and permeabilities as a result of the Pan-African tectonic event which caused the sediments to be partially metamorphosed. Groundwater occurrence and storage in the basin is therefore aided by the presence of secondary porosities such as fractures, joints, faults, and fissures (Kesse, 1985). Well yields in the basin generally vary and decrease in the order of sandstones, limestones, siltstones (mudstones), and shales (Acheampong and Hess 1998; Agyekum and Asare 2016). Regional hydrogeological studies revealed that the fractures in the basin are erratic and in certain areas, they are dried and non-productive (Chegbeleh et al., 2009). Borehole yields range from 5 to 1200 l/min, static water levels (SWL) from 1 to 20 m and water table fluctuation averages about 4m. Dapaah-Siakwa and Gyau-Boakye (2000) indicated that the success rates of well drilling is less than 60% and groundwater storage and transmission is controlled by the presence of discrete entities which vary significantly in lateral extent.

The average well depth in the area is about 55 m with the most productive fractures observed between 13 m and 80 m (Bannerman, 1990). The productivity of the aquifers is generally low to moderate with transmissivity ranging between 0.3 and 267 m^2 /day, with a mean of 11.9 m^2 /day (Carrier, 2008; Banoeng-Yakubo et al., 2011) with most of the aquifers in the area being semi-confined (Chegbeleh et al., 2009). Groundwater recharge estimated in the area using chloride mass balance (CMB) method averages about 94 mm/year and ranges between 73 – 110 mm/year. Groundwater recharge occurs vertical through piston flow in the area (Addai et al., 2016).

5.2 DATA AND METHODS

5.2.1 Airborne data

Airborne geophysical data comprising magnetic, and electromagnetic (AEM) data were obtained from the Ghana Geological Survey Authority (GGSA). The airborne data was initially acquired by the Fugro Airborne Survey (FAS) Limited for the purposes of mineral exploration under the mining sector support program with funding from the European Union (Fugro

Airborne Survey, 2009a). Using the Casa-212 aircraft, FAS conducted the survey over the Volta and Keta basins of Ghana (Fugro Airborne Survey, 2009b). The AEM was acquired using a GEOTEM 20 channel multiple systems which consist of a transmitter (vertical loop 6 turns) and a receiver for transmitting and detecting signals. The AEM data was measured at a nominal flying altitude of 120 m above the ground. The aeromagnetic measurements were done utilizing the Scintrex CS-2 single-cell cesium vapor magnetometer with a sensitivity of 0.01 nT. The aeromagnetic data was acquired along NW-SE flight lines spaced at 500 m at a surveying height of 75m. Similarly, the AEM data was recorded at 20 km flight line spacing in a NW – SE direction (black lines in Fig. 1). Aside from the 20 km line spacing, AEM data with significantly denser line spacing of 200 m was also collected by FAS. However, we were, unable to get that data due to new data restrictions at the GGSA. The data acquisition company, FAS performed all the necessary data treatment and reduction and subsequently stored the datasets in Geosoft private format (geodatabase), consisting of different channels for different data parameters.

5.2.2 Aeromagnetic

The airborne datasets were subjected to different processing and filtering techniques using the Oasis Montaj version 2021.2 (Geosoft Inc., 2021). The purpose of geophysical data filtering is to eliminate unwanted features and enhance desired characteristics that are diagnostic of the geology (Hayatudeen et al., 2021). To improve the visibility and separate anomalies of shallow sources from deep sources, filters were applied on the resultant grid of the total magnetic intensity generated for the study area. Reduce to equator (RTE) techniques (Luo et al., 2010; Aina, 1986), Euler deconvolution (Thompson, 1982), and derivatives filters (Cooper & Cowan, 2004) were extensively used to delineate structural trends at different depth scales likely to control groundwater in the area. The RTE (Supplementary Fig. 5.1 in appendix 7) was carried out on the magnetic data to remove asymmetry caused by magnetic inclination.

The RTE technique repositions the magnetic anomalies directly above the causative bodies for better interpretation at low geomagnetic latitudes (Mohamed & Ella, 2021). The RTE map produced illustrates high and low magnetic intensity anomalies in the area with values ranging about 190 – 320nT. The prevailing long wavelength anomalies with spatial scale of several kilometers are undoubtedly due to deep seated basement materials. The map (Supplementary Fig. 5.1) shows the study area is made of different magnetic regions probably distinguished by the difference in strength of magnetic response. The north and central parts are categorized with low magnetic response while the southern portions show high magnetic response representing long wavelength features perhaps from a deeper source. Small amplitude wavelength anomalies

are superimposed on these large wavelength features and may only be exposure by suppressing the regional long wavelength features through derivative filtering.

The total horizontal derivative (THD) filter measures the lateral rate of change of the measured field. Thus, the derivative is a vector filter which gives additional information on the directional variations of the total field (Christensen & Dransfield, 2002; Salem et al., 2008) and are crucial for delineating linear features such as faults and dykes from magnetic data. The THD technique (Fig. 5.3) are most useful in highlighting edges and discontinuity patterns in potential field data. The THD is calculated by the Pythagorean sum of the gradients in orthogonal directions (Oni et al., 2020; Cordell and Grauch, 1985). The application of this technique demonstrates anomalies of high and low values with dominant E-W, NE-SW and NW-SE trends. The linear structures that have been significantly exposed could have been due to past tectonic such as the Pan African event that affected the area (Kesse, 1985). The THD filter highlights lithological contacts locations. It is also effective in detecting shallow magnetic sources (Ibraheem et al. 2019). Banded iron formation within the crust has been stated as the possible source of magnetization within the West Africa sub-region (Launay et al., 2018).

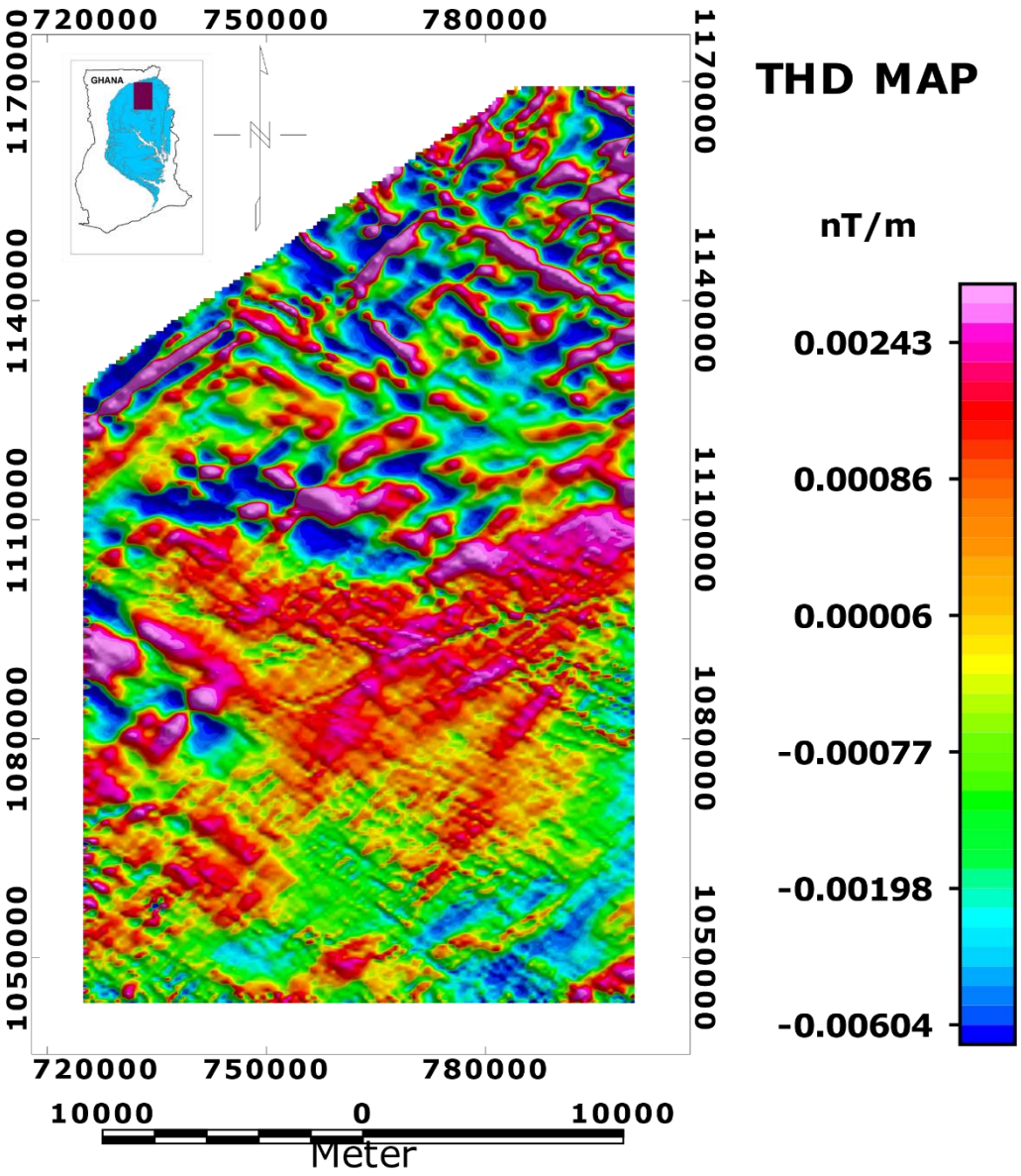

Figure 5. 3: Total horizontal derivative maps showing variational direction of linear structure with inset map of Ghana showing coverage of the VSB and location the current study.

The first vertical derivatives (FVD) is essentially a high pass-filter suppressing long wavelength signals. Its application to magnetic data helps to enhance the details of short wavelength signals and sharpens the geophysical anomalies for better interpretation as it significantly improves the resolution of closely spaced and superposed anomalies (Fig. 5.4). It is a very good technique for determining anomalies over distinct structures in total magnetic intensity data and remarkably suppresses the regional signals of the data. The application of FVD to magnetic data over the area revealed several linear structures predominantly to the north, west and

southern parts of the area. These structures can significantly improve on the hydrogeological fortunes of the area if their positions could be properly and precisely inferred. The application of the FVD and THD to the magnetic data acquired for the area revealed several structures which aided the selection of suitable sites for magnetotellurics (MT) field campaign.

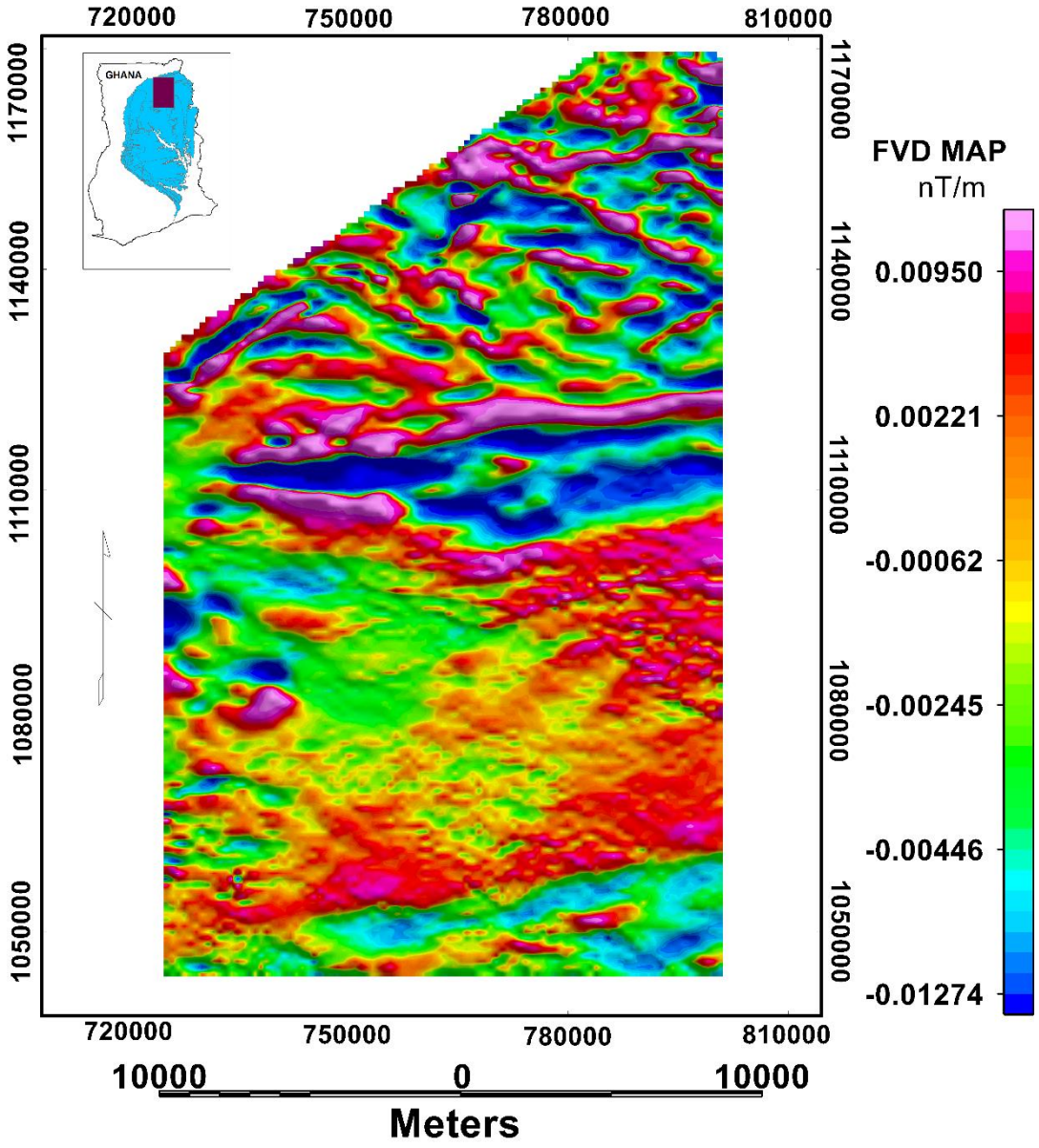

Figure 5. 4: First vertical derivative map showing presence of short wavelength structures and inset map of Ghana showing coverage of the VSB and location the current study.

The 3D Euler method (Fig. 5.5) was used to estimate the source-depth of the linear structures revealed by the FVD and THD techniques. The Euler deconvolution methods is based on the concept that anomalous magnetic fields of localized structures are homogeneous functions of the source coordinates and therefore satisfy the Euler homogeneity equation (Reid et al. 1990; Thompson 1982). The application of this method has emerged as a powerful tool for determining the depth and source geometry in magnetic data interpretation (Barbosa et al. 1999). In Euler deconvolution, a slide window operator is moved in piecewise manner over the whole data set.

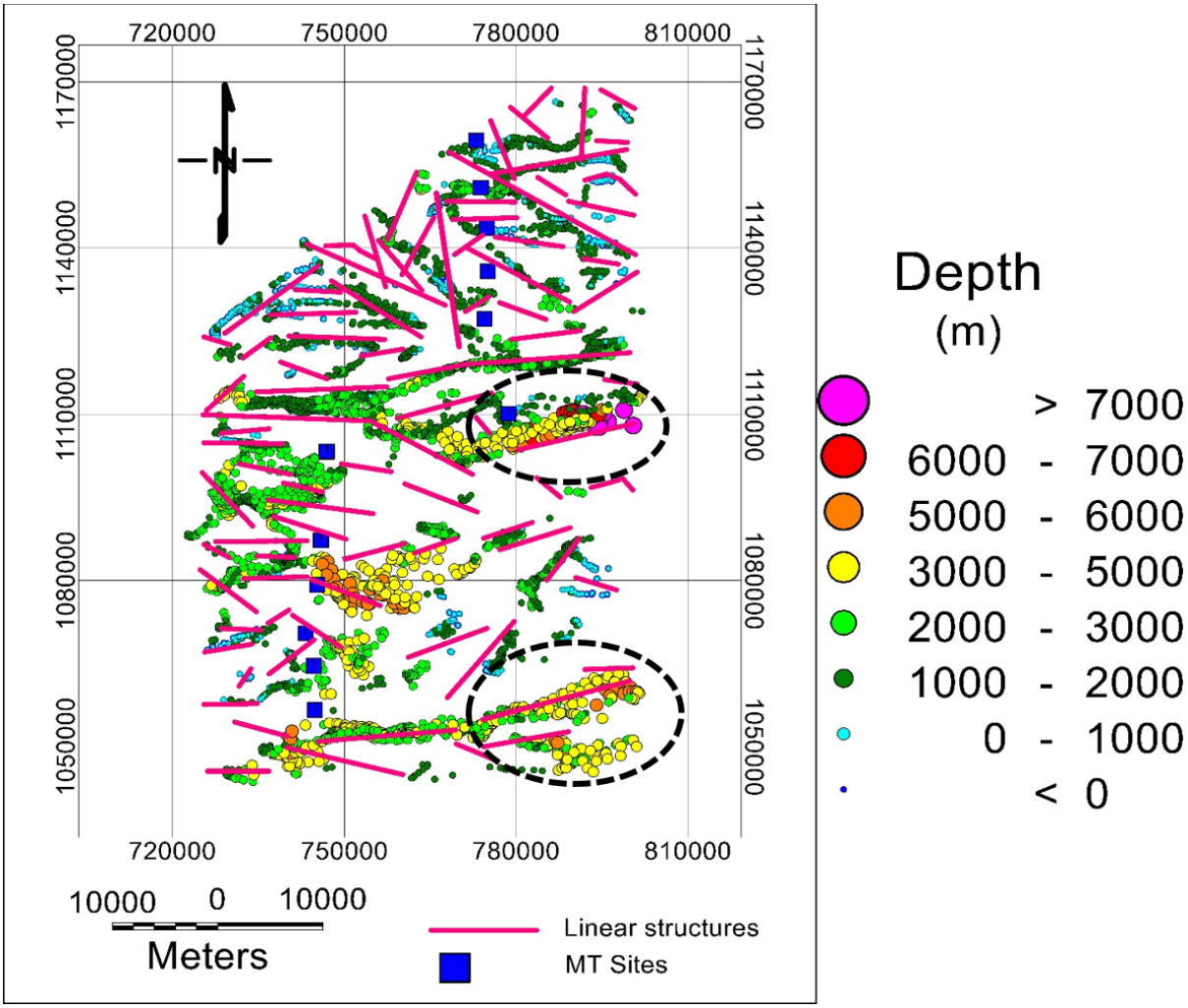

Figure 5. 5: Linear structural map deduced from combination derivative filters (pink lines represent linear structures deduced from FVD and THD maps) and Euler deconvolution (colored dots) techniques. (a) the blue squares are the locations where MT data was recorded (b) broken-circle shows locations of possible sub-vertical structures as same structures reflect varying colors with depths.

The measured data inside the window are then solved using the Euler deconvolution homogeneity equation linearly to estimate the depth to source of the magnetic bodies. The technique was applied to the gridded magnetic data in the region to determine the source-depth location of the anomalies. The source-depth estimation and type of structure depends on the structural index which has been determined by Thompson (1982) and Reid et. al., (1990) to range from 0 to 3 for a certain type of structures. Structural index (SI) of 1 was found to give better solution after several attempt and was used in this analysis. A structural index of 1 is most effective in characterizing linear features such as faults, dykes, sills and contacts (Alan et al. 2014). Therefore, the choice of a structural index of 1 was appropriate since structures such as faults and lithological contacts were of interest in this current study. Although no prior knowledge about the anomalous source of magnetization is required, the technique still has some setbacks. It is important to state that, the Euler technique produces large amount of solutions which increases uncertainties and making interpretation difficult. This large amount of solutions generated by the technique contains some invalid solutions caused by interference of adjacent field source (background field data) (Cooper, 2004). The interference caused by the background field data affects the accuracy of the technique leading to inconsistency in the source positioning (Q. Liu et al., 2023). However, to improve the accuracy of the results, the large amount of solutions and uncertainties were regulated by reducing the window size, the maximum depth tolerance to allow and the maximum depth to accept. A window size of $8 \times 8m$ was used and a maximum depth tolerance allowed was set to 10%. The maximum depth beyond which solution was rejected was set at 8000m based on prior information on the basin thickness.

5.2.2 Airborne Electromagnetic (AEM) data

The AEM data provided by GGSA (shown as black lines in Fig. 5.1) were in the form of resistivity depth array in geosoft database format. The data acquisition company, FAS processed and inverted the Bz coil data from the GEOTEM system into resistivity depth images (RDI). The GEOTEM data were inverted using a software known as AIRBEO (Rachie, 1998). The program uses single measurement points along the flight line together with a simple layered earth resistivity model. The model may be in any number of layers but the last layer is an infinite half space. The AIRBEO algorithm uses a 1-D singular value decomposition inversion (Rachie, 1998). The inversion process simply, compare the theoretical electromagnetic field from the

layered earth model to the observed data. This process is repeated until a goodness of fit is achieved, which is generally measured by the least square error of the fit between the measured and the calculated. The AIRBEO application allows for some flexibility to control the inversion process in an attempt to find a good fit between the observed and the computed data from the layered model. The process however, is non-linear and can reach a number of reasonable data fit. The result is sensitive to the initial layer model used. The final individual layered inversion results can then be plotted along the survey lines to create a 2-D map view representation of the subsurface resistivity and layer thickness variations over the area of study (Slattery & Andriashek, 2012). The RDI data obtained was used to plot cross-sections (Fig. 5.9 and Supplementary Fig. 5.5) along the lines to show variations in resistivity from the surface down to a few hundred of meters. The distance between sampling points along the flight lines ranges between 13m-15m hence cross-sections were plotted along the survey lines due to good sampling density. The sections were plotted for flight lines intersected by the MT field profiles for purposes of comparison with MT results.

5.3 Magnetotellurics (MT)

The processing and filtering of the aeromagnetic data helped in the selection of areas where MT field campaign was carried out. Magnetotelluric as a passive electromagnetic (EM) method uses the natural time variations of the earth's electric and magnetic field at the surface to make inferences about the electrical resistivity of the subsurface. The subsurface resistivity inferred can be related to pore fluids, tectonic, geology or geologic structures (Oskooi, 2006; Simpson & Bahr, 2005). The measured horizontal components of the natural EM field are used through a series of processes to construct the full complex impedance tensor, Z, as a function of frequency (Simpson & Bahr, 2005). The Z is defined by the 2 by 2 matrix,

$$Z = \begin{pmatrix} Z_{xx} & Z_{xy} \\ Z_{yx} & Z_{yy} \end{pmatrix} \quad (1)$$

representing the lateral and vertical variations of electrical conductivity of the subsurface at a given MT measurement site.

A total of 13 MT soundings (red triangles shown in Figure 5.1) were recorded along two north-south profile lines at the northern and southern portions of the study area. The horizontal electric and magnetic time-series components were measured within a frequency range of 1000 to 0.001Hz using two ADU-08e acquisition systems by Metronix Geophysics (Metronix, 1998).

The electric potentials were measured using non-polarizable $Cl_2 – PbCl_2$ electrodes with typical separation of 100m. The electric and magnetic fields were recorded in the magnetic north, *x*, and east, *y*, directions. The spacing between stations was approximately 8 Km covering roughly about 96 km length of profiles from north to south. The two recording systems were deployed simultaneously to allow for cross remote-referencing for the computation of robust MT impedance (Gamble et al. 1979). The horizontal electric (E_x, E_y) to the horizontal magnetic (B_x, B_y) components of the MT impedance was determined using the robust remote processing method of Chave and Thompson, (1989).

5.3.1 MT Inversion

All the MT stations were sited away from communities to avoid interference from culture noise and electric noise from power lines. The data recorded was therefore of good quality leading to precise MT impedance tensors with small error bars (Fig 5.6) for all periods. Some examples are shown in Figure 5.6 and the rest in supplementary section Figure 3 in appendix 7. The nature and character as revealed by the impedance indicates that the structures at depth are heterogeneous at the long periods and therefore 3D inversion was performed using an in-house inversion code known as MINIM3D (Hautot et al., 2007) to characterize the apparent resistivity of the subsurface.

The 3-D inversion technique used in this study is based on an iterative procedure of minimizing the misfit between the observed data and computed model response using the non-linear steepest gradient method (Hautot & Tarits, 2000; Hautot et. al., 2007). The 3-D model was parameterized into blocks in the x, y, and z directions with a minimum horizontal dimension of mesh of 3.5 x 3.5 Km. A starting model with an average resistivity of 200-ohm m was used for the inversion, and after a number of iterations the resistivity in the blocks were adjusted until a minimum misfit was obtained (e.g. Fig. 5.6). The four components of the MT impedance tensor of all sites were inverted at all available periods. A regularization term was introduced to provide stability to the objective function to obtain a unique solution to the inversion. The root-mean-square (rms) misfit of the model was reduced from an initial value of 22.9 to a final misfit value of 3.3 due of small error floors, namely 2% for the off diagonal and 5% for the diagonal indicating a good agreement between the data and the model responses for all sites (e.g. Figure 5.6). The rest of the figures are presented in the supplementary section (Supplementary Fig. 3 in appendix 7).

Because of the small number of data points, the resistivity grid in 3-D is coarse (Supplementary Fig. 5.2). It is possible to improve locally the vertical resolution using 1-D inversion of an averaged MT tensor provided the dimensionality is not too severe (Rung-Arunwan et al. 2016). The 3-D resistivity model can then be used to validate the 1-D inversion, which gives much better vertical resolution than 3-D. The 1-D inversion was ran using the Berdichevsky average of the invariant determinant at each site. The 1-D inversion was executed using a robust code known as MINIM1D (Tarits, 1986).

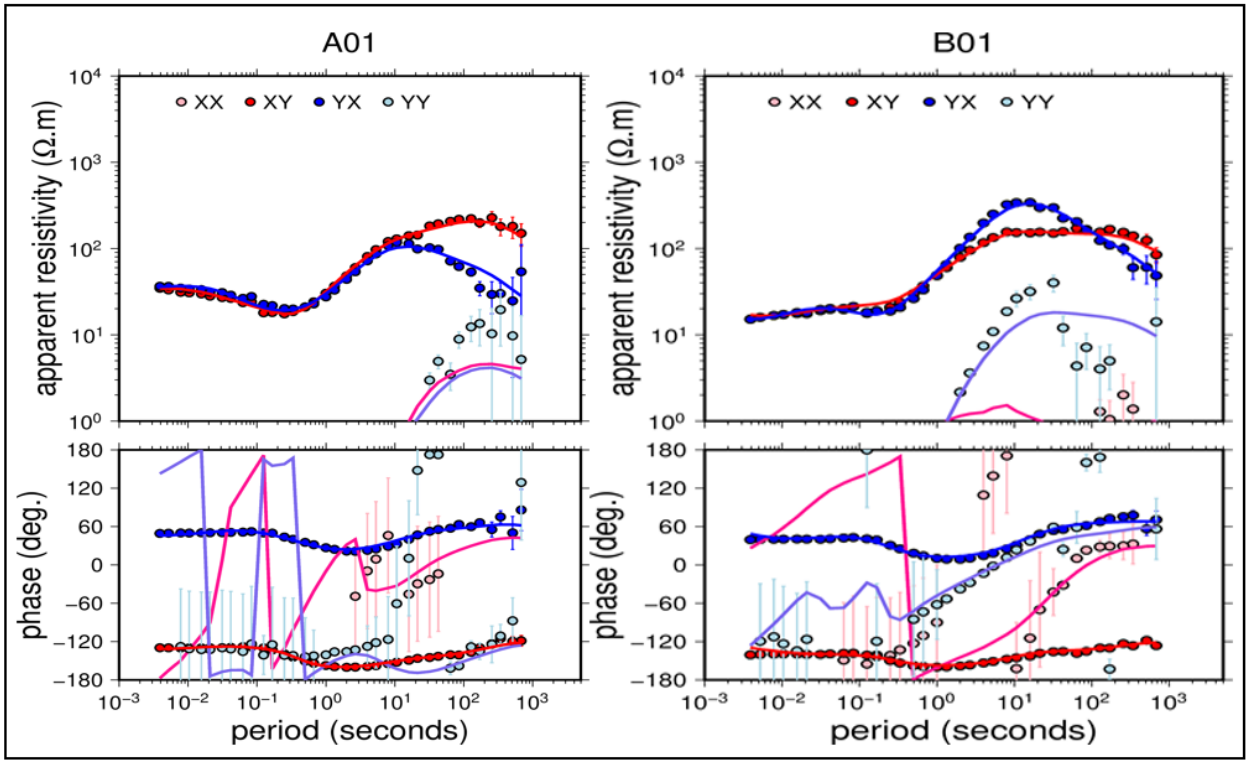

Figure 5. 6: Comparison between observed data (dots) and 3-D model response (solid lines) of apparent resistivity and phases for all four components of the MT tensor for both profiles (A and B).

5.4 RESULTS AND DISCUSSION

5.4.1 Airborne

The derivative filtering techniques and Euler deconvolution were used jointly to delineate and produce a linear structural map (Figure 5.5) over the research area. Linear structures such as faults, folds and joints are often credited to an unexpected discontinuity of the magnetic units and sudden adjustment in depth to magnetic source as well as the geometry of the magnetic source (Hayatudeen et al., 2021). These geologic features are expressed as linear narrow magnetic low (associated with weathering) anomalies within a magnetic high (Fairhead, 2007).

Most of the structures are observed as sub-vertical structures which is explained by same structures showing different colours representing different depths revealed in the Euler deconvolution technique (e.g. structures in broken circle in Fig. 5.5). This observation agrees with Acheampong and Hess (1998) who suggest that the structures in the basin are mostly sub-vertical and appear to control groundwater occurrence. Several of the structures traced from the integration of the FVD and the THD techniques correctly fit when superimposed on the Euler structures, suggesting a good agreement among the techniques and proper structural resolution. The superimposed structures of shallow origin (FVD) on that of the Euler technique which gave both shallow and deeper structures further buttress the sub-vertical nature of the structures in the area. It also suggests a possible connection between the basin and basement structures and could be indicative of good sources for groundwater provided their spatial location and geometry are well characterized. The presence of such linear structures in the basin are attributed to past tectonic events which affected the area (Kesse, 1985). Similar structures within the basin have been previously observed by Crowe & Jackson-Hicks, (2008) while investigating intra-basin structures of the basin. They described the identified linear structures as brittle faults mostly trending east-west at the central part of the basin. The structures observed in this study could serve as reliable indicators and guides for natural resources exploration. They are particularly vital in groundwater exploration and programs for groundwater development in the area should be designed with the structures in mind. The linear structures observed occurred mostly to the north and west of the area which were the key reasons for the location of the MT profile lines.

5.4.2 MT Results

The final resistivity distribution maps of the 3-D models are presented in Figures 5.7 and supplementary section Figure 4 in appendix 7. The profile B at the north of the study area transect lithologic formations of the Kwaku-Bombouaka and the Oti-Pendjari Groups of the Voltaian Supergroup. Relatively resistive areas (black broken circles) revealed in Figure 5.7a near the surface along the profile to the north represents the Panabako sandstones as noted by Carney et al., (2010) and correlates well with resistive features seen in some AEM sections (Fig. 5.9). The quartz-arenite-rich sandstone formation of the Panabako has a suggested thickness of 150-200 m according to Carney et al., (2010) and overlies the Poubogou Formation. However, this thickness has been observed to range from 200 – 320 m based on possible lithologic contacts revealed through 3-D and 1-D MT models (Fig. 5.7 and 5.8). The Poubogou Formation grades upward into the Panabako with an increase in proportion of

sandstone relative to argillaceous material (Carney et al., 2010; Jordan et al., 2009). Ayite et al., (2008) observed the existence of several sedimentary structures such as flute casts fissures and slumps at the upper part of the Poubogou coming in contact with the Panabako sandstones in the area. These sedimentary structures could increase the porosity of the rocks at the lithologic contacts and thereby increase the water storage capacity. The contacts relating to distinct lithological boundaries and intercalation of lithologic units are described as good indicators of groundwater availability within the Nasia sub-catchment of the VSB (Aliou et al., 2022). Also, in geologic environment where permeability and porosity of suitable outcrops is lacking, the interpretation of geophysical results for groundwater prospecting should be targeted at sections that can indicate permeabilities associated with fractures and other discontinuities (Aliou et al., 2022; Yidana, et al., 2020). The southern end of profile B, is underlain by lithologies of the Oti-Pendjari Group of the Voltaian Supergroup Group. The basal formation of the Oti-Pendjari Group, the basal limestones of the Kodjari (black polygon) probably accounts for the relatively resistive features observed (Fig. 5.7a). Below the resistive Panabako sandstone Formation down to the contact between the Poubogou Formation (averaging 250 m), a structure of relatively low resistivity (black polyline in Fig. 5.7b) is observed traceable across the major geologic units underlying the profile.

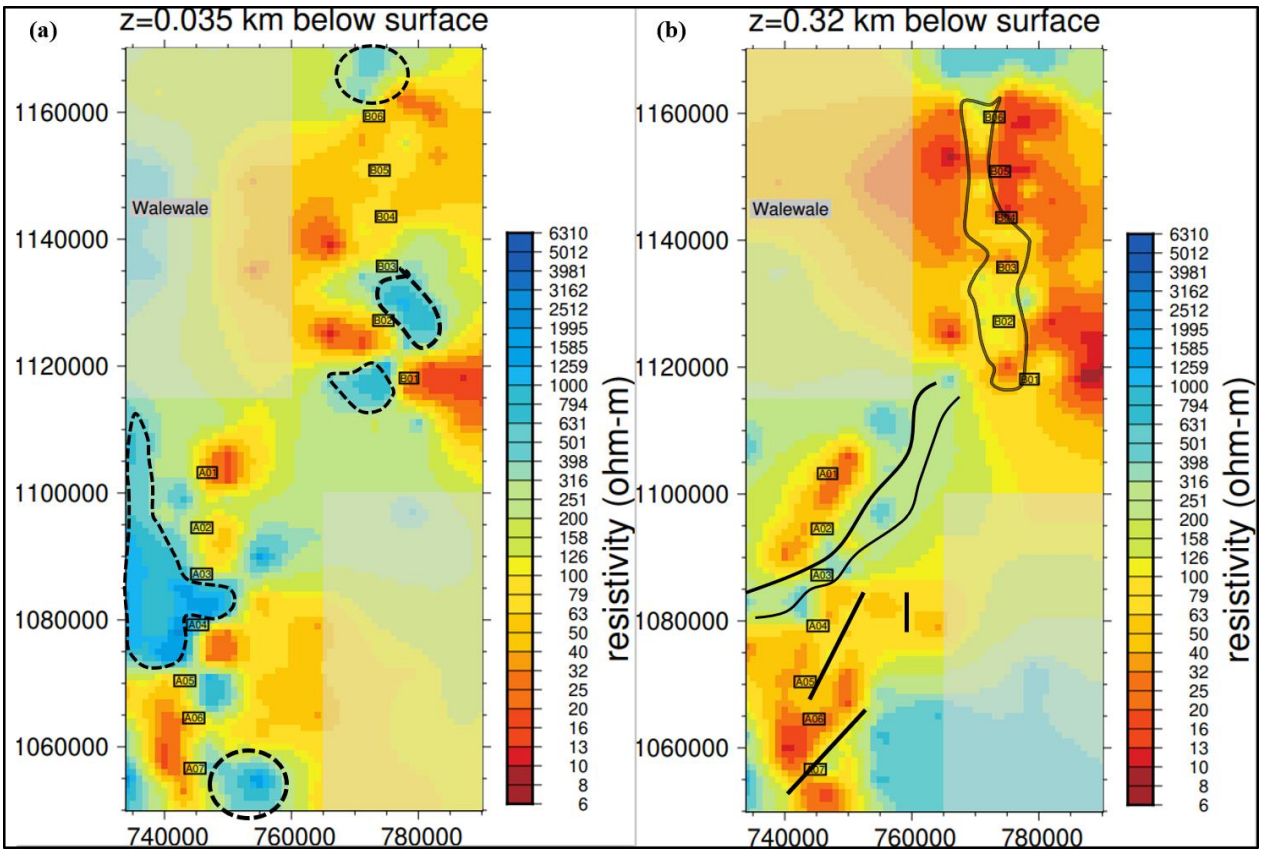

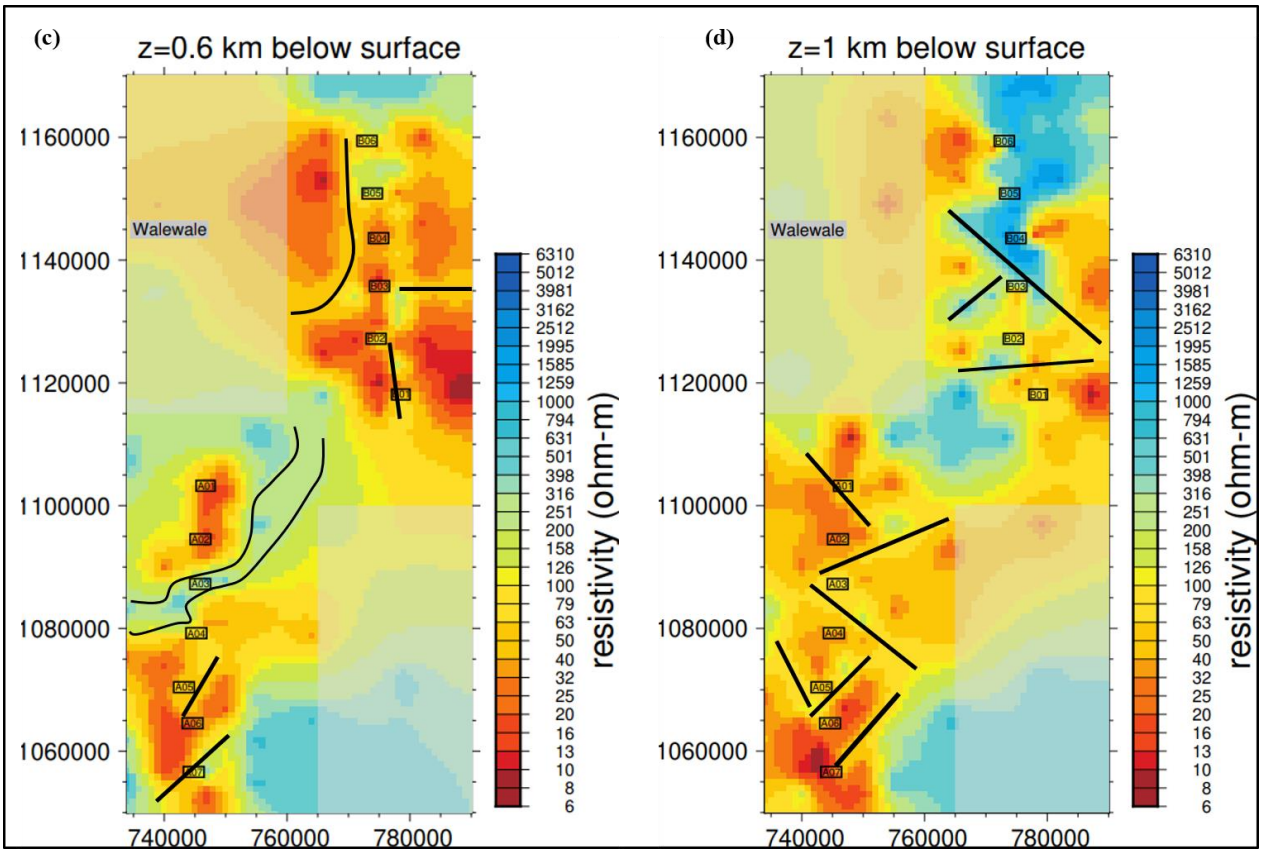

Figure 5. 5 3-D MT resistivity maps at different depths with a transparent layer added at areas not well covered by the data: (a) at 35m below ground indicating resistive sandstones units (broken circles) along both profile lines (profile B to the north and profile A to the south), (b) at 320m depth showing possible contact fractures (black curvy lines) at the contact between the Panabako sandstones and the Poubogou formation as defined by the most recent stratigraphy of the area (Carney et al., 2010). (c) shows a NE-SW contact fracture (black curvy lines) around profile A (also observed in Fig. b) and other fractures (black solid lines) at 600m. (d) shows fractural entities (black solid lines) at 1000m respectively.

The characteristic features (pattern and resistivity range) of the structure suggest it is pervasive and therefore cannot be a representative feature of one lithologic formation in the area hence it is identified as a contact structure. This structure with resistivity values ranging between 40 – 160 ohm-m is an extensive fracture with an average length of approximately 45 km and trending north-south in the area. The range of resistivities of the identified fracture matches that of the resistivity values of freshwater (Palacky, 1988) and similar to the values reported by Aliou et al., (2022) for productive boreholes in the area. The contact fracture was traced on the 1-D resistivity curves which gives better vertical resolution at each individual MT site (Fig. 5.8a). Several researchers (e.g. Acheampong and Hess 1998; Aliou et al. 2022; Chegbeleh et al. 2009;

Dapaah-Siakwa and Gyau-Boakye 2000) have indicated that the occurrence of groundwater in the basin is largely controlled by subsurface fractures.

Profile A is located in the southern part (Fig. 5.1) of the study area and covers the Bimbilla Formation of the Oti-Pendjari Group, as well as the outcrops of Obosum Group. Both the 3-D maps (Fig. 5.7) and the 1-D resistivity sections (Fig. 5.8b) were observed to have relatively low resistivity signatures reflecting the predominant geology of argillaceous strata interbedded with highly immature wacke-type sandstone underlying the profile. Some resistive features were however, observed at near surface (Figure 5.8a) towards the south of the profile and correlate well with the Tamale sandstones of the Obosum Group which are said to show relatively high resistivity values (Carney et al., 2010). According to Archie, (1942), low resistivity values of a rock are directly linked with its porosity and the conductivity of pore water within them, and this perhaps is the reason why low resistivity readings often imply the occurrence of groundwater. Whilst this relationship could be true and has been used extensively in most cases, it does not work entirely well for clay-rich formations (Clarke & Smout, 2018) such as in the Bimbilla Formation. Clay-rich formations have high porosity and high surface conductivity caused by cation exchange capacity which allows current to travel along their grain surfaces thereby making them conductive (Wilson, 1994). Mudstones and siltstones which are formed from clay, are good at retaining groundwater due to high porosities, but incapable of releasing the water owing to low permeability and are mostly referred to as aquicludes (MacDonald & Davies, 2000). However, they can be productive where a network of fractures exists. The presence of interconnected fractures allows groundwater to flow freely even in a clay dominated environment (MacDonald et al. 2005). The main control as to whether such robust fractures could exist in a clay-rich formation depends on the presence of the type of clay mineral known as illite (Abouelresh et al., 2016; Clarke & Smout, 2018). Illite is dominant in argillaceous rocks and is formed by the weathering of silicate minerals such as feldspar. According to Yidana et al., (2011), silicate mineral weathering is the most pervasive factor controlling groundwater hydrochemistry in VSB which is apparently due to the abundance of silicate minerals almost everywhere in the basin. The determination of the conductivity of illite shows that it is less conductive than other clay minerals (Kriaa et al., 2014). Therefore, proper delineation of groundwater productive zones in such environments will require targeting subordinate lithologies showing less conductivity likely to be a robust network of fractures. This will mean targeting moderately resistive zones as against low resistivity areas in groundwater exploration. Electromagnetic methods such as the MT method can appropriately identify such targets and

map steeply dipping fracture networks in the subsurface (Hazell et at. 1988) in such environments.

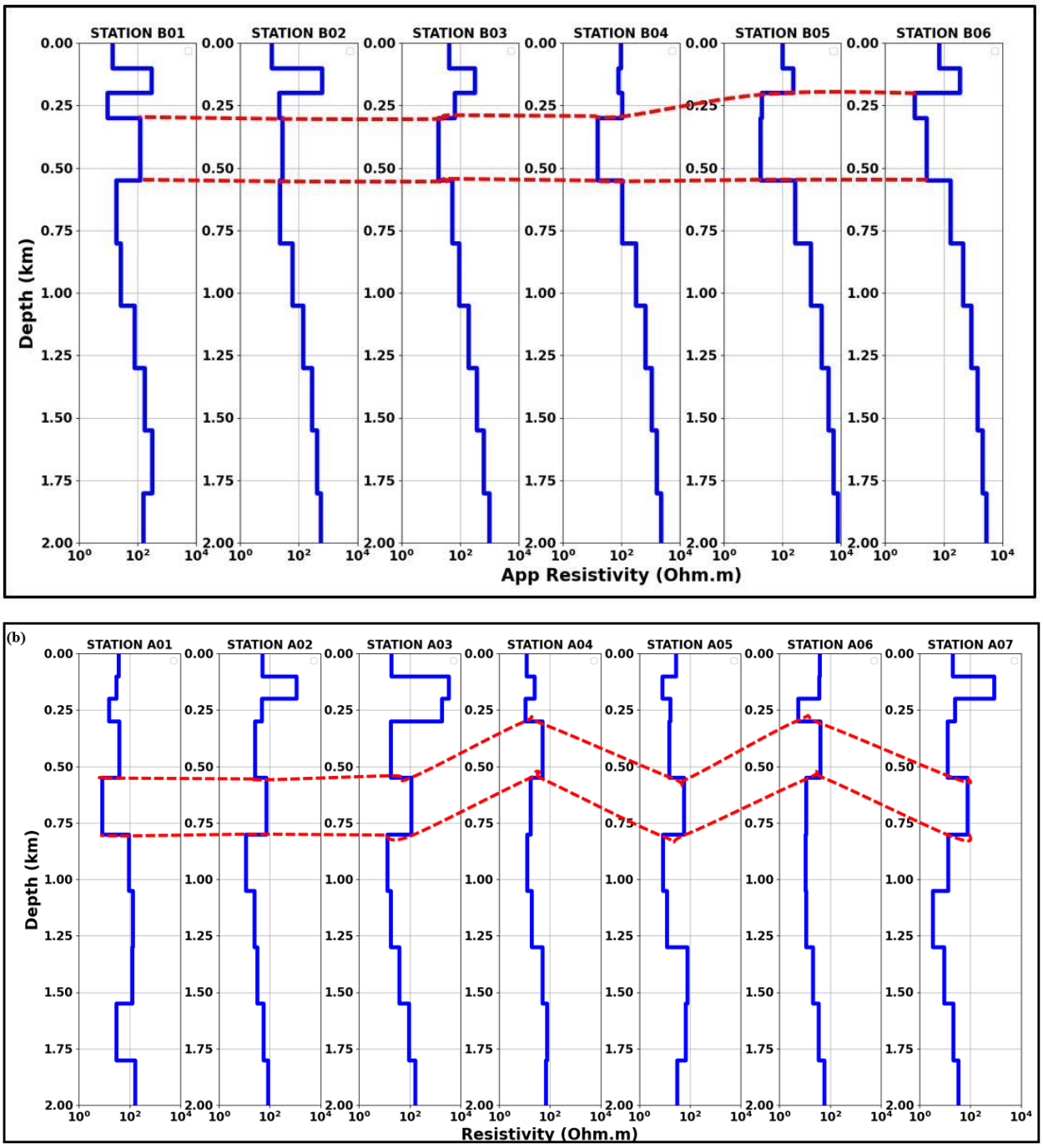

Figure 5. 6: 1-D resistivity map showing possible lithologic contact structures (red broken lines) underneath MT sites along the profiles: (a) 1D resistivity sections arranged from south to north for the profile B. (b) 1-D resistivity sections arranged from north to south along profile A within a highly conductive argillaceous material south in the study area.

Several fractural entities with moderately low conductivities (Fig. 5.7b, c and d) are observed within the more conductive argillaceous materials underlying profile A. These fractures with

resistivity range of 40-102 ohm-m occur at different depths along the profile forming a network of fractures which were probably developed and preserved within the sediments during their formation in the last tectonic event that affected the area. The range of resistivity values observed for the layer agreed with that suggested for freshwater by Palacky, (1988). Clarke and Smout, (2018) indicated that such range of resistivity (40-102 ohm.m) in a clay dominated environment could be attributed to the abundance of illite. Illite clay unlike smectite is resistant and strong enough to withstand deformation therefore a robust network of water-bearing fractures can exist in them. Illite is formed when soft and weak clay (smectite) is exposed to heat and pressure in an irreversible reaction. Rocks of the Voltaian supergroup are generally consolidated and are not inherently permeable (Kesse, 1985) hence groundwater occurrence is controlled by secondary fractures (Acheampong and Hess 1998; Chegbeleh et al. 2009).

5.5 DISCUSSION

There is no unique interpretation of geophysical models because the relationship between geophysical parameters and the geology are poorly known. Therefore comprehensive interpretation of the models requires adequate knowledge of the underlying geology especially in terrains such as the VSB (Agarwal et al. 1993; Aliou et al. 2022). The lack of outcrops in the northern parts of the VSB posed a major challenge in interpreting the geology. Nonetheless, Carney et al., (2010) and Dzikunoo et al., (2020) provided regional stratigraphic insights using a combination of field visits and remote sensing data and airborne EM respectively. In 3-D MT, the resolution of the resistivity maps was affected due to limited number of MT sites and large spacing (~8 to 10 Km) between sites, hence a transparency layer was added to areas poorly constrained by the data. The resistivity maps in Figures 5.7 and supplementary section Figure S4 presented show variations in resistivity reflecting the diverse geologic and possible fracture units in the area.

In generally, different fractures influence and control groundwater occurrence in the subsurface differently by acting as either low permeability zones (barrier) or high permeability zones (conduits). When a fault is filled with an impermeable material such as silt and clay, they act as barriers or aquitard/aquicludes (Elhag & Elzien, 2013). For example, if a fracture is open, it acts as a conduit allowing direct flow in the path of the fracture similar to a flowing stream (Mulwa et al., 2005). A stream (Fig. 5.2) observed close to the profile B, flows in the same direction as the trend of the identified fracture thus suggesting the fracture is a conduit and perhaps hydrologically connected to the stream. The stream survives the high temperatures and the extreme evapotranspiration even in the protracted dry season while others dry up. Hence

the fracture could be an aquifer located at the contact between the Panabako and the Poubogou Formation in the area and hydraulically connected to the stream to replenish and sustain perennial flow.

In profile A, the moderate resistive structures observed were visible across different horizontal depth slices in 3-D (Fig. 5.7b, c & d) probably due to the sub-vertical nature of the structures. In 1-D vertical sections (Fig. 5.8b) validated by the 3-D model and compared with AEM cross sections (Fig. 5.9), the structures are observed as a continuous low conductive layer with uniform thickness but varies in depth across the traverse. The nature and pattern of the layer could be due to the presence of faults network (Fig. 5.5) at that location (Crowe & Jackson-Hicks, 2008). This moderately resistive layer and fractures could be targeted for groundwater development in the area as focus on the interpretation of very low resistivity reading have not yielded much success in terms of the groundwater exploration and exploitation (Agyekum & Asare, 2016b). Aliou et al. (2022) considered a moderately resistive area for borehole drilling within the Bimbilla Formation and was successful in their attempt. The characteristic pattern of the layer in 1-D (Fig 5.8b) is also an indication of a possible paleo channel environment. The presence of such a structure in the area could be of significant interest in terms of hydrogeology (Dzikunoo et al., 2020) and placer deposit prospecting. Paleo river channels may be found exposed on the surface or buried, depending on the post-depositional environment. Buried paleo channels may have properties very similar to those of aquifers but are distinguished by their low width-to-length ratio (Chandra et al., 2019).

Figure 5.9 and supplementary Figure 5 shows the cross sections of the AEM resistivity from airborne data acquired for the area. The choice of available flight lines (Fig. 5.1) for the sections were based on their proximity to the MT sites and or whether the AEM lines intersect the MT profiles. The variations in resistivity revealed by the AEM cross sections when compared with the MT stations sited in proximity show strong correlation with the MT resistivity sections (Fig. 5.7) and borehole geophysical log (Fig. 5.10) (Klitten & Agyekum, 2021). Resistive features observed in the research area are more resolved and extensive in the 1-D MT (Fig. 5.8) than in the AEM sections for same locations.

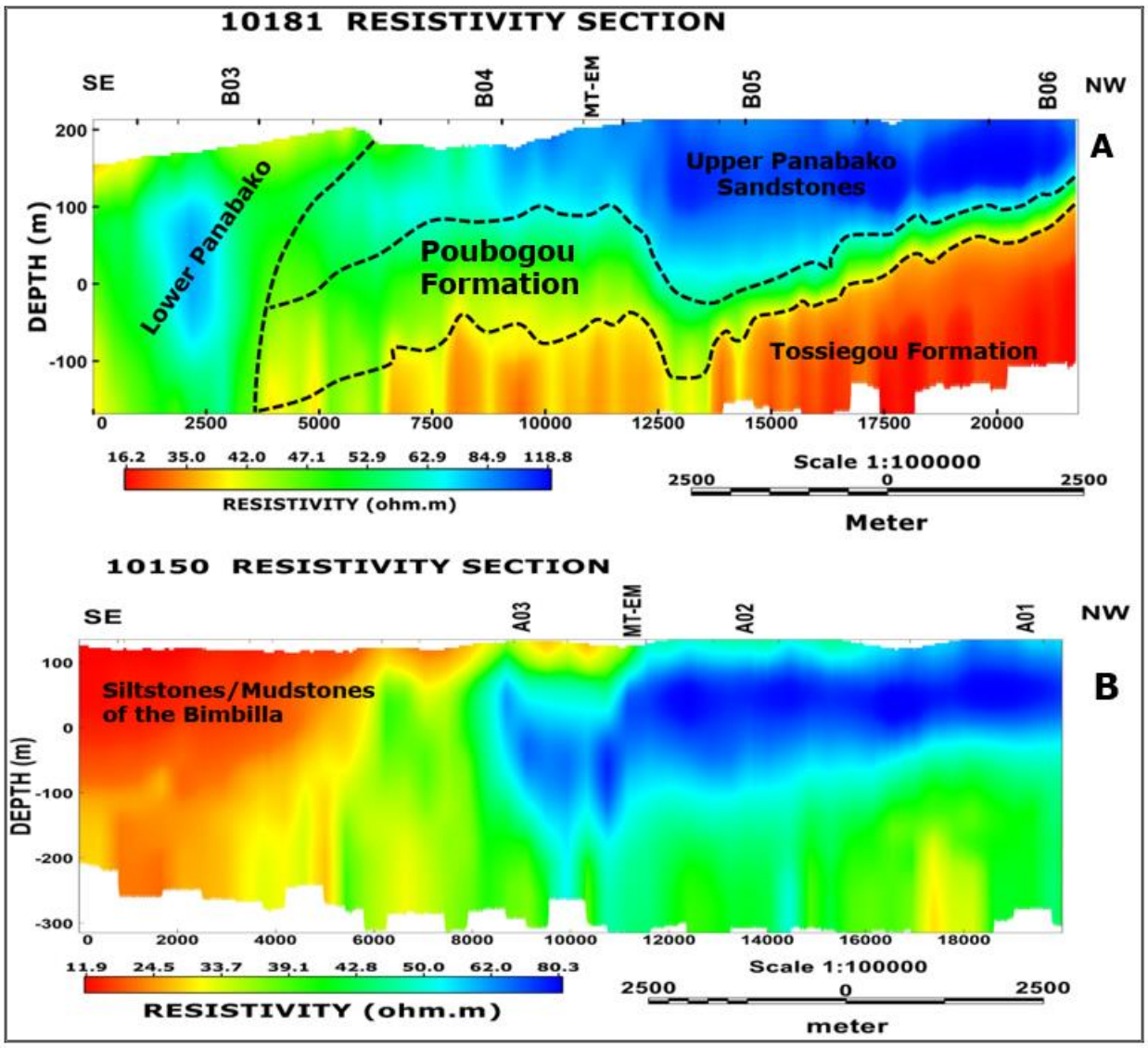

Figure 5. 7: Resistivity cross section of airborne electromagnetic (AEM) data showing variation in resistivity along flight line (a) 10180 and (b)10150 depicting lithologic contacts (black dash-lines) for the different formations as defined by Dzikunoo et. al., (2020). The sections were plotted using Oasis montaj program in Geosoft.

For example, B04 sited close to DWVP 02 (well with geophysical log) on the Panabako sandstones were compared to AEM section 10181 (Fig. 5.9a) crossing same lithologic unit, and all showed relatively high resistivity except at the depth 54-100 m where the geophysical log reported a fracture (Fig. 5.10). The reported fracture has a yield of about 132 l/min (Aliou et al., 2022) was intercepted by the MT station B04 at the same depth as revealed by the both drilling and geophysical wireline logging (Klitten & Agyekum, 2021). Similar comparison and correlation can be deduced between the MT site B03 (in Fig. 5.8a) and AEM cross section 10181 (Fig. 5.9a) at least up to the depth of investigation penetrated by the AEM data. Again,

along the profile A, a good correction can be observed between the AEM (Figure 5.9b) and the MT site A03 (in Figure 5.8b). These comparisons have clearly explored and demonstrate the sync of MT results with the geology which is evident by the good agreement between the MT, borehole logs, and AEM.

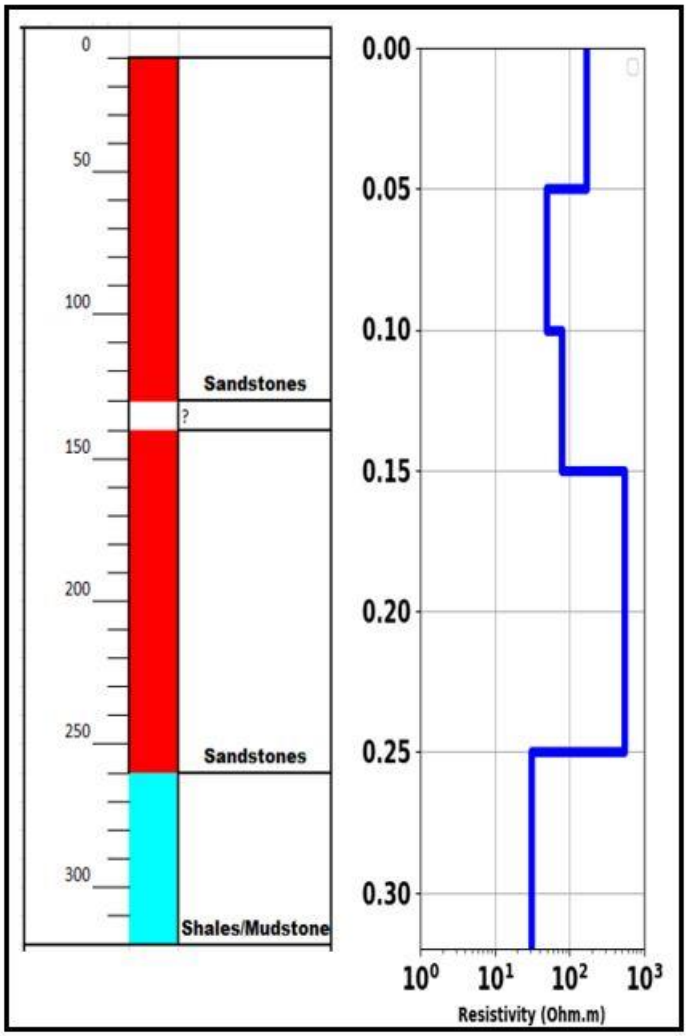

Figure 5. 8: Comparison between a borehole drill log (red) and MT site B04 resistivity (blue) close to the borehole in the study area.

The AEM data in combination with remote imagery and fieldwork were used to revise the current accepted lithostratigraphy and nomenclature of the Voltaian supergroup (Carney et al., 2010; Jordan et al., 2009) based on which our interpretations are derived.

5.6 CONCLUSIONS

The study demonstrates the efficacy of using an integration of geophysical techniques to characterize the subsurface structures in the sedimentary Voltaian Supergroup. The integration of techniques clearly defines the contact structures of the various formations, particularly in the

Bombouaka and Oti-Pendjari Groups. The thicknesses indicated by this current study is approximately are 250 m for the Panabako Formation and 200 m for the Poubogou Formation. This revised stratigraphic thickness indicates that the sediments in the area are deeper than what was proposed. The presence of other deep subsurface structures in the basin that have never been targeted for groundwater development have also been identified at various depths. The low success rate of the basin in terms of the groundwater potential could be improved if the deeper structures mapped in this research are targeted as against the previous focus on the relatively shallow subsurface.

The analysis revealed a low resistive structure at the interface between the Panabako sandstones and the Poubogou Formation which is indicative of groundwater potential. The structure is roughly 45 kilometers long and runs parallel to the river channel going north-south, implying that it is an open fracture that serves as a conduit for groundwater and hence could be a fractured aquifer. A fissured layer and fractures detected in profile A could be part of an aquifer system formed by a network of faults. The spatial distribution, pattern, and characteristics of the layer indicate that it is a paleo channel, which could have implications for hydrogeology and placer deposit exploration in the basin. MT as an EM technique has proven to be very sensitive to fracture zones as it revealed conductive structures with groundwater potential in a consolidated and partially metamorphose sedimentary terrain.

Findings from the study are expected to serve as a guide for all stakeholders in the groundwater enterprise as the deep structures could help improve the groundwater developmental efforts in the terrain. It will significantly reduce investment losses made in drilling unsuccessful wells. Further analysis will however be required to delineate these structures at a local scale as the study is more regional.

ACKNOWLEDGEMENT

The authors wish to thank the French government through the French embassy (Ghana) and the Ghana government for the financial support which made this work possible. Also, we express our gratitude to the DANIDA White Volta Project (file number 14-P02-GHA) of University of Ghana and Ghana Geological Survey Authority for assisting us with secondary data. Our sincere appreciation also goes to Ge-Ocean laboratory of the Universite de Bretagne Occidentale (UBO) for providing funding for the fieldwork.

REFERENCES

Abdel Moneim, A. A. (2005). Overview of the geomorphological and hydrogeological characteristics of the Eastern Desert of Egypt. *Hydrogeology Journal, 13 (2),* 416–425.

Abdelaal, G. Z., Mousa, M. K. M., & Ebraheem, M. O. (2021). Estimate the depth to basement from the interpretation of aeromagnetic data at the northwestern part of Egypt. *Journal of Multidisciplinary Sciences, 3*(1), 27–38. https://doi.org/10.33888/jms.2021.314

Abdul Azeez, K. K., Patro, P. K., Harinarayana, T., & Sarma, S. V. S. (2017). Magnetotelluric imaging across the tectonic structures in the eastern segment of the Central Indian Tectonic Zone: Preserved imprints of polyphase tectonics and evidence for suture status of the Tan Shear. *Precambrian Research, 298*, 325–340. https://doi.org/10.1016/j.precamres.2017.06.018

Abdul Azeez, K. K., Veeraswamy, K., Gupta, A. K., Babu, N., Chandrapuri, S., & Harinarayana, T. (2015). The electrical resistivity structure of lithosphere across the Dharwar craton nucleus and Coorg block of South Indian shield: Evidence of collision and modified and preserved lithosphere. *Journal of Geophysical Research: Solid Earth 120.* https://doi.org/10.1002/2014JB011854

ABEM. (2010). *International Manual Terrameter LS.* ABEM Instruments, Stockholm, Sweden.

Aboud, E., Saud, R., Asch, T., Aldamegh, K., & Mogren, S. (2014). Water exploration using magnetotellurics and gravity data analysis; Wadi Nisah, Riyadh, Saudi Arabia. *NRIAG Journal Astronomy and Geophysics*, *3*, 184–191.

Abouelresh, M., D., B., Babalola, L., K., K., & Omer, M. (2016). *Factors Controlling Natural Fracture development in the Qusaiba Hot Shale, Northwest Saudi Arabia; Outcrop Approach*.

Aboyeji, O. S., & Eigbokhan, S. F. (2016). Evaluations of groundwater contamination by leachates around Olusosun open dumpsite in Lagos metropolis, southwest Nigeria. *Journal of Environmental Management*, *183*, 333–341. https://doi.org/10.1016/j.jenvman.2016.09.002

Acheampong, S., & Hess, J. (2000). Origin of the shallow grounwater system in the sothern Voltaian Sedimentary Basin of Ghana: An isotopic approach. *Journal of Hydrology*, 37–53.

Acheampong, S., Y., & Hess, J. W. (1998). Hydrogeologic and hydrochemical framework of the shallow groundwater system in the southern Voltaian Sedimentary Basin, Ghana. *Hydrogeology Journal*, *6*, 527–537. https://doi.org/10.1007/s100400050173

Adam, A. B., & Appiah-Adjei, E. K. (2019). Groundwater potential for irrigation in the Nabogo basin, Northern Region of Ghana. *Groundwater for Sustainable Development*, *9*, 100274. https://doi.org/10.1016/j.gsd.2019.100274

Addai, M. O., Yidana, S. M., Chegbeleh, L. P., Adomako, D., & Banoeng-Yakubo, B. (2016). Groundwater recharge processes in the Nasia sub-catchment of the White Volta Basin: Analysis of porewater characteristics in the unsaturated zone. *Journal of African Earth Science*, *122*, 4–14.

Affaton, P., Sougy, J., & Trompette, R. (1980). The tectono-stratigraphic relationships between the Upper Precambrian and Lower Paleozoic Volta Basin and the Pan-African Dahomeyide orogenic belt (West Africa). *America Journal of Science*, *280*, 224–248.

Agarwal, A. K., Poll, H. E., & Weaver, J. T. (1993). One- and two-dimensional inversion of magnetotelluric data in continental regions. *Physics of the Earth and Planetary Interiors*, *18*, 155–176.

Agyekum, W. A., & Asare, E. B. (2016a). Challenges associated with ground water resources development in northern Ghana. *Ghana Journal of Science*, *56*, 39–51. https://doi.org/10.4314/gjs.v56i1

Agyekum, W. A., & Asare, E. B. (2016b). Challenges Associated with groundwater resources development in Northern Ghana. *Ghana Journal of Science*, *56*, 39–51.

Agyekum, W. A., Dark, P. K., & Dapaa-Siakwan, S. (2006). *Annual summary of groundwater monitoring in the White Volta River basin.* [Technical Report]. Water Research Institute.

Agyekum, W., Klitten, K., Armah, T., Banoeng-Yakubo, B., & Amartey, E. O. (2013). Geophysical borehole logging for control of driller's records: Hydrogeological case study from Voltaian sedimentary rocks in northern Ghana. *Applied Water Science*, *3*(2), 491–500. https://doi.org/10.1007/s13201-013-0097-y

Aina, A. (1986). Reduction to Equator, Reduction to Pole and Orthogonal Reduction of Magnetic Profiles. *Exploration Geophysics - EXPLOR GEOPHYS*, *17*. https://doi.org/10.1071/EG986141

Aizebeokhai, A. P., Oyeyemi, D. K., & Joel, S. E. (2016). Groundwater potential assessment in a sedimentary terrain, southwestern Nigeria. *Arabian Journal of Geoscience*, *9*, 496.

Akankpo, O., & Igboekwe, M. U. (2011). Monitoring Groundwater Contamination Using Surface Electrical Resistivity and Geochemical Methods. *Journal of Water Resource and Protection*, *3*(5), Article 5. https://doi.org/10.4236/jwarp.2011.35040

Akinremi, S., Fadel, I., & van der Meijde, M. (2022). Crustal and Upper Mantle Imaging of Botswana Using Magnetotelluric Method. *Frontiers in Earth Science*, *10*. https://www.frontiersin.org/articles/10.3389/feart.2022.840703

Ako, J., & Wellman, P. (1985). The margin of the West African craton: The Voltaian basin. *Journal of the Geological Society of London*, *142*, 625-632.

Akpan, O. U. (2019, June 24). Crustal structure of some tectonic region in West Africa. *Geodesy and Geodynamics*. CTBT Science and Technology 2019 Conference, Hofburg, Vienna, Austria.

Akudago, J. A., Chegbeleh, L. P., Nishigaki, M., Nanedo, N. A., Ewusi, A., & Kankam-Yeboah, K. (2009). Borehole Drying: A Review of the Situation in the Voltaian Hydrogeological System in Ghana. *Journal of Water Resource and Protection*, *1*(3), Article 3. https://doi.org/10.4236/jwarp.2009.13020

Al-Amoush, H., Al-Tarazi, E., Rajab, J. A., Al-Dwyeek, Y., Al-Atrash, M., & Shudiefat, A. (2015). Geophysical Investigation Using Time Domain Electromagnetic Method (TDEM) at Wadi Deir Al-Kahaf Area/Jordan for Groundwater Artificial Recharge Purposes. *Journal of Water Resource and Protection*, *07*(03), Article 03. https://doi.org/10.4236/jwarp.2015.73012

Al-Amri, A. M. (2015). Lithospheric structure of the Arabian shield from joint inversion of P and S-wave receiver functions and dispersion velocities. *Acta Geod Geophysics*, *65 (2)*, 229–245.

Al-Badani, M. A., & Al-Wathaf, Y. M. (2018). Using the aeromagnetic data for mapping the basement depth and contact locations, at southern part of Tihamah region, western Yemen. *Egyptian Journal of Petroleum*, *27*(4), 485–495. https://doi.org/10.1016/j.ejpe.2017.07.015

Al-Garni, M. A. (2009). Geophysical investigations for groundwater in a complex subsurface terrain, Wadi Fatima, KSA: A case history",. *Jordan Journal of Civil Engineering, Vol. 3, No. 2*, 118-136.

Al-Ibiari, M. G., Ismail, A. A. M., El-Khafeef, A. A., Basheer, A. A., El-laban, A. M. M., & Tarek, Y. (2017). Analysis and interpretation of aeromagnetic data for Wadi Zeidun area, Central Eastern Desert, Egypt. *Egyptian Journal of Petroleum*, *27*(3), 285–293. https://doi.org/10.1016/j.ejpe.2017.04.002

Aliou, A. S., Dzikunoo, E. A., Yidana, S. M., Loh, Y., & Chegbeleh, L. P. (2022). Investigation of Geophysical Signatures for Successful Exploration of Groundwater in Highly Indurated Sedimentary Basins: A Look at the Nasia Basin, NE Ghana. *Natural Resources Research*. https://doi.org/10.1007/s11053-022-10125-9

Al-saadi, O., Abd, N., Hijab, B., & Mustafa, B. (2021). *Subsurface Investigation Using Electrical Resistivity Imaging for Proposed Industrial Site near Erbil-Kirkuk Borders, Northern Iraq*. *54*, 198–209. https://doi.org/10.46717/igj.54.2E.14Ms-2021-11-30

Alshehri, F., & Abdelrahman, K. (2022). Groundwater aquifer detection using the time-domain electromagnetic method: A case study in Harrat Ithnayn, northwestern Saudi Arabia. *Journal of King Saud University - Science*, *34*(1), 101684. https://doi.org/10.1016/j.jksus.2021.101684

Ametepey, S. T., Cobbina, S. J., Akpabey, F. J., Duwiejuah, A. B., & Abuntori, Z. N. (2018). Health risk assessment and heavy metal contamination levels in vegetables from Tamale Metropolis, Ghana. *International Journal of Food Contamination*, *5*(1), 5. https://doi.org/10.1186/s40550-018-0067-0

Amponsah, T. Y., Danuor, S. K., Wemegah, D. D., & Forson, E. D. (2022). Groundwater potential characterisation over the Voltaian basin using geophysical, geological, hydrological and topographical datasets. *Journal of African Earth Sciences*, *192*, 104558. https://doi.org/10.1016/j.jafrearsci.2022.104558

Annan-Yorke, R. (1971). Geology of the Voltaian Basin (summary of current ideas). In: Cudjoe, J.E. (Ed.), Special Bulletin for Oil Exploration. *Geological Survey Depart Ment, Accra, Ghana, p*.

Apesegah, E. (2008). Hydrocarbon Potential of the Voltaian Basin (Post-Premuase-1 Well). *Voltaian Workshop Report*, 75–77.

Aplin, C. A., Flete, J. A., & Macquaker, H. S. J. (1999). *Muds and mudstones: Physical and fluid-flow properties* (Vol. 158). Geological Soceity of London.

Appiah, I., Wemegah, D. D., Asare, S. V.-D., Danuor, K. S., & Forson, E. D. (2018). Integrated geophysical characterisation of Sunyani municipal solid waste disposal site using magnetic gradiometry, magnetic susceptibility survey and electrical resistivity tomography. *Journal of Applied Geophysics*, *153*, 143–153. https://doi.org/10.1016/j.jappgeo.2018.02.007

Aquaterrex. (2023). Deep Seated Water. *AquaterreX*. https://aquaterrex.com/deep-seated-water/

Arafa-Hamed, T., Marzouk, H., Elbarbary, S., & Abdel Zaher, M. (2023). A geophysical investigation of the urban-expanding area over the seismologically active Dahshour region, Egypt. *Acta Geophysica*. https://doi.org/10.1007/s11600-023-01131-3

Archie, G. E. (1942). The electrical resistivity log as an aid to determine some reservoir characteristics. *Trans.Am.Inst.Mining Met. Eng*, *146*, 54–62.

Arhin, E., Kazapoe, R. W., & Salami, F. (2020). Linking geology to the prevalence of non-communicable diseases: A case study of the Voltaian sedimentary basin, Ghana. *Ecofeminism and Climate Change*, *2*(1), 26–41. https://doi.org/10.1108/EFCC-05-2020-0014

Aristodemou, E., & Thomas-Betts, A. (2000). DC resistivity and induced polarisation investigations at a waste disposal site and its environments. *Journal of Applied Geophysics*, *44*(2), 275–302. https://doi.org/10.1016/S0926-9851(99)00022-1

Armah, F., Obiri, S., Yawson, D., ANM, P., & B, A. (2010). Mining and Heavy Metal Pollution: Assessment of Aquatic Environments in Tarkwa (Ghana) using Multivariate Statistical Analysis. *Journal of Environmental Statistics*, *1*, 1–13.

Asante, F., & Amuakwa-Mensah, F. (2015). *Climate change Variability in Ghana: Stocktaking. 3(1)*, 78–99.

Asuma, O. (2013). Leachate characterization and assessment of groundwater and surface water qualities near municipal solid waste dump site in Effurun, Delta state, Nigeria. *Journal of Environmental and Public Health*, *3(9)*, 126–135.

Atitsogbey, P., Steiner_Aseidu, M., Nti, C., & Ansong, R. (2018). The impact of climate change on household food security in the Bongo District of the UpperEast Region of Ghana. *Ghana Journal of Agric Science*, *52*, 145–153.

Attias, E., Thomas, D., Sherman, D., Ismail, K., & Constable, S. (2020). Marine electrical imaging reveals novel freshwater transport mechanism in Hawai‘i. *Science Advances*, *6*(48), eabd4866. https://doi.org/10.1126/sciadv.abd4866

Ayite, A., Awua, F., & Kalvig, P. (2008). Lithostratigraphy of the Gambaga massif. *The Voltaian Basin Ghana Workshop and Excursion*, 41.

Azaiez, H., Gabtni, H., & Bédir, M. (2021). Joint Gravity and Seismic Reflection Methods to Characterize the Deep Aquifers in Arid Ain El Beidha Plain (Central Tunisia, North Africa). *Water*, *13*. https://doi.org/10.3390/w13091310

Bahr, K. (1988). Interpretadon of the magnetotelluric impedance tensor: Regional induction and local telluric distortion. *Journal of Geophysics*, *62*, 119–127.

Bai, E., Guo, W., Zhang, D., Tan, Y., Guo, M., & Zhao, G. (2019). Using the Magnetotelluric Method for Detecting Aquifer Failure Characteristics under High-Intensity Mining of Thick Coal Seams. *Energies*, *12*(22), Article 22. https://doi.org/10.3390/en12224397

Balwant, P., Pujari, P. R., Dhyani, S., Bramhanwade, K., & Jyothis, V. (2022). Geophysical Methods for Assessing Microbial Processes in Soil: A Critical Review. *Indian Journal of Pure and Applied Scinece*, *60*, 707–715. https://doi.org/10.56042/ijpap.v60i8.63548

Banerjee, A., & Ahmed Salim, A. M. (2020). Seismic attribute analysis of deep-water Dangerous Grounds in the South China Sea, NW Sabah Platform region, Malaysia. *Journal of Natural Gas Science and Engineering*, *83*, 103534. https://doi.org/10.1016/j.jngse.2020.103534

Bannerman, R. R. (1990). *Appraisal of hydrogeological conditions and analysis of boreholes in the Nanumba and Western Gonja Districts—Northern Region, Ghana: Assessment of groundwater potential for hand dug wells. Final report for rural action NORRIP/GTZ.*. NORRIP.

Banoeng-Yakubo, B., & Armah, T. (2001). *Hydrogeological and geophysical test investigation in the Afram plain, Ghana.* [DANIDA-CWSA, Project,]. Department of Geology,University of Ghana.

Banoeng-Yakubo, B., Yidana, S. M., Ajayi, J. O., Loh, Y., & Aseidu, D. K. (2011). Hydrogeology and groundwater resources of Ghana: A review of the hydrogeology and groundwater hydrochemistry of Ghana. *In J. M. McMann (Ed.), Potable Water and Sanitation. Nova Science Publishers.*

Baranov, A., & Bobrov, A. (2018). Crustal structure and properties of Archean cratons of Gondwanaland: Similarity and difference. *Russian Geology and Geophysics*, *59*, 512–524. https://doi.org/10.1016/j.rgg.2018.04.005

Baranwal, V., & Rønning, J. (2020). *Airborne Geophysical Surveys and Their Integrated Interpretation* (pp. 377–400). https://doi.org/10.1007/978-3-030-28909-6_14

Barberio, M. D., Gori, F., Barbieri, M., Boschetti, T., Caracausi, A., Cardello, G. L., & Petitta, M. (2021). Understanding the Origin and Mixing of Deep Fluids in Shallow Aquifers and Possible Implications for Crustal Deformation Studies: San Vittorino Plain, Central Apennines. *Applied Sciences*, *11*(4), Article 4. https://doi.org/10.3390/app11041353

Barbosa, V., Silva, J., & Medeiros, W. (1999). Stability analysis and improvement of structure index estimation in Euler deconvolution. *Geophysics*, *64*, 48–60.

Barfod, G. H., Vervoort, J. D., Montanez, I. P., & Reibold, S. (2004). *Lu-Hf geochronology of phosphates in ancient sediments*. 5–11.

Bauer, P., Supper, R., Zimmermann, S., & Kinzelbach, W. (2006). Geoelectrical imaging of groundwater salinization in the Okavango Delta, Botswana. *Journal of Applied Geophysics*, *60*(2), 126–141. https://doi.org/10.1016/j.jappgeo.2006.01.003

Baumle, R., & Himmelsbach, T. (2018). Exploration of deep, previously unknown semi-fossil aquifers of the Kalahari Basin (southern Africa). *Grundwasser*. http://dx.doi.org/10.1007/s00767-017-0378-8

Becken, M., & Burkhardt, H. (2004). An ellipticity criterion in magnetotelluric tensor analysis. *Geophysical Journal International*, *159*(1), 69–82. https://doi.org/10.1111/j.1365-246X.2004.02376.x

Beinabaj, H. S. M., Heydariyan, H., Mohammad Aleii, H., & Hosseinzadeh, A. (2023). Concentration of heavy metals in leachate, soil, and plants in Tehran's landfill: Investigation of the effect of landfill age on the intensity of pollution. *Heliyon*, *9*(1), e13017. https://doi.org/10.1016/j.heliyon.2023.e13017

Bellali, A., Jarraya Horriche, F., Gabtni, H., & Bédir, M. (2018). Seismic reflection and structuring characterization of deep aquifer system in the Dakhla syncline (Cap Bon, North-Eastern Tunisia). *Journal of African Earth Sciences*, *140*, 134–150. https://doi.org/10.1016/j.jafrearsci.2017.12.012

Benson, A. K. (1995). Applications of ground penetrating radar in assessing some geological hazards: Examples of groundwater contamination, faults, cavities. *Journal of Applied Geophysics*, *33*(1), 177–193. https://doi.org/10.1016/0926-9851(95)90040-3

Berdichevskiy, M. N., & Dmitriev, V. I. (1976). DISTORTION OF MAGNETIC AND ELECTRICAL FIELDS BY NEAR-SURFACE LATERAL INHOMOGENEITIES. *Acta Grodaet. Geophys. Et Mantanist. Acad. Sci. Hung.*, *11*, 217–221.

Bernard, J., Lemine, M., Diagana, B., & Ricolvi, M. (2004). Combination of electrical resistivity and magnetic resonance sounding data for mapping an aquifer layer in Mauritania. In *SEG Technical Program Expanded Abstracts 2004* (pp. 1381–1384). Society of Exploration Geophysicists. https://doi.org/10.1190/1.1839667

Bernardo, B., Candeias, C., & Rocha, F. (2022). Characterization of the Dynamics of Leachate Contamination Plumes in the Surroundings of the Hulene-B Waste Dump in Maputo, Mozambique. *Environments*, *9*, 19. https://doi.org/10.3390/environments9020019

Bertoni, C., Lofi, J., Micallef, A., & Moe, H. (2020). Seismic Reflection Methods in Offshore Groundwater Research. *Geosciences*, *10*(8), Article 8. https://doi.org/10.3390/geosciences10080299

Binley, A., Hubbard, S. S., Huisman, J. A., Revil, A., Robinson, D. A., Singha, K., & Slater, L. D. (2015). The emergence of hydrogeophysics for improved understanding of subsurface processes over multiple scales. *Water Resources Research*, *51*(6), 3837–3866. https://doi.org/10.1002/2015WR017016

Binley, A., & Kemna, A. (2005). *DC Resistivity and Induced Polarization Methods* (Vol. 50, pp. 129–156). https://doi.org/10.1007/1-4020-3102-5_5

Blakely, R. J. (1996). *Potential theory in gravity and magnetic application.* Cambridge, University press.

Blakely, R. J., & Simpson, R. W. (1986). Approximating edges of source bodies from magnetic or gravity anomalies. *Geophysics*, *51*, 1494–1498.

Boerner, D. E. (1992). Controlled source electromagnetic deep sounding: Theory, results and correlation with natural source results. *Surveys in Geophysics*, *13*, 435–488. https://doi.org/10.1007/BF01903486

Booker, J. R. (2014). The Magnetotelluric Phase Tensor: A Critical Review. *Surveys in Geophysics*, *35*(1), 7–40. https://doi.org/10.1007/s10712-013-9234-2

Bosum, W., Damaske, D., Roland, N. W., Behrendt, J., & Saltus, R. (1989). The Ganovex IV Victoria Land/Ross Sea aeromagnetic survey: Interpretation of anomalies. *Geologisches Jahrbuch*, *38*, 153–230.

Bourgeois, B., Mathieu, F., Vachette, C., & Vaubourg, P. (1994). AMT measurements compared with gravimetry and magnetometry for structural study of a sedimentary basin: Letlhakeng-Botlhapatlou groundwater project, Botswana. *Journal of Applied Geophysics*, *31*, 7–25. https://doi.org/10.1016/0926-9851(94)90044-2

Boyd, T., & Burnley, P. (2020). *GEOL 452/652—Geophysics* [SEG]. UNLV, Department of Geoscience. https://pburnley.faculty.unlv.edu/GEOL452_652/index.html

Bradford, J. H. (2002). Depth characterization of shallow aquifers with seismic reflection, Part I—The failure of NMO velocity analysis and quantitative error prediction. *GEOPHYSICS*, *67*(1), 89–97. https://doi.org/10.1190/1.1451362

Bravo-Osuna, A. G., Gómez-Treviño, E., Cortés-Arroyo, O. J., Delgadillo-Jauregui, N. F., & Arellano-Castro, R. F. (2021). Reframing the magnetotelluric phase tensor for monitoring applications: Improved accuracy and precision in strike determinations. *Earth, Planets and Space*, *73*(1), 34. https://doi.org/10.1186/s40623-021-01354-y

Bruno, P. P. G., & Vesnaver, A. (2021). Groundwater characterization in arid regions using seismic and gravity attributes: Al Jaww Plain, UAE. *Frontiers in Earth Science*, *8*. https://www.frontiersin.org/articles/10.3389/feart.2020.575019

Buddies, S. (2016). *How Dirt Cleans Water*. Scientific American. https://www.scientificamerican.com/article/how-dirt-cleans-water/

Bugan, R., Tredoux, G., Jovanovic, N., & Israel, S. (2018). Pollution Plume Development in the Primary Aquifer at the Atlantis Historical Solid Waste Disposal Site, South Africa. *Geosciences*, *8*(7), Article 7. https://doi.org/10.3390/geosciences8070231

Cagniard, L. (1953). Basic theory of mag netotelluric method of geophysical prospecting. *Society of Exploration Geophysics*, *18*, 605–635.

Caldwell, T. G., Bibby, H. M., & Brown, C. (2004). The magnetotelluric phase tensor. *Geophysical Journal International*, *158*(2), 457–469. https://doi.org/10.1111/j.1365-246X.2004.02281.x

Carbonell, R., Levander, A., & Kind, R. (2013). The Mohorovičić discontinuity beneath the continental crust: An overview of seismic constraints. *Tectonophysics*, *609*, 353–376. https://doi.org/10.1016/j.tecto.2013.08.037

Carney, J. N., Jordan, C. J., Thomas, C. W., Condon, D. J., Kemp, S. J., & Duodo, J. A. (2010). Lithostratigraphy, sedimentation and evolution of the Volta Basin in Ghana. *Precambrian Research, Volume 183*(Issue 4), 701–724. https://doi.org/10.1016/j.precamres.2010.08.012

Carrier, M. A., Lefebvre, R., Racicot, J., & Asare, E. B. (2008). *Northern Ghana hydrogeological assessment project*. 33rd WEDC International Conference., Accra, Ghana.

Carrier, M.-A., Lefebvre, R., & Asare, E. (2011). *Hydrogeological Assessment Project of the Northern Regions of Ghana (HAP): Final technical report : Water Resources Database Development.* (R1327; Issue R1327). INRS, Centre Eau, Terre et Environnement. https://espace.inrs.ca/id/eprint/1648/

Carrier, R. (2008). *Northern Ghana Hydrogeological Assessment Project*. https://www.academia.edu/20699400/Northern_Ghana_Hydrogeological_Assessment_Project

Carvajal-Flórez, E., & Cardona-Gallo, S.-A. (2019). Technologies applicable to the removal of heavy metals from landfill leachate. *Environmental Science and Pollution Research*, *26*(16), 15725–15753. https://doi.org/10.1007/s11356-019-04888-7

Caselle, C., Bonetto, S., & Comina, C. (2019). Comparison of laboratory and field electrical resistivity measurements of a gypsum rock for mining prospection applications. *International Journal of Mining Science and Technology*, *29*(6), 841–849. https://doi.org/10.1016/j.ijmst.2019.09.002

Castaneda, S. S., Sucgang, R. J., Almoneda, R. V., Mendoza, N. D. S., & David, C. P. C. (2012). Environmetal isotopes and major ions for tracing leachate contamination from a municipal landfillin Metro Manlia, Philippines. *Journal Environmental and Radioactivity*, *110*, 30–37.

Castillo-Widener, M. P. (2013). *Using ground penetrating radar in the investigation of LNAPL contamination within a controlled environment*. https://doi.org/10.13140/RG.2.1.3228.6565

Chandra, S., Ahmed, S., Auken, E., Pedersen, B. J., Singh, A., & Verma, S. (2016). 3D aquifer mapping employing airborne geophysics to meet the india's water future. *CSIR-NGRI.*

Chandra, S., Choudhury, J., Maury, P., Ahmed, S., Auken, E., & Verm, S. (2019). Geological significance of delineating paleochannels with AEM. *Exploration Geophysics*, 1834–7533.

Chandrasekhar, E., Fontes, S. L., Flexor, J. M., Rajaram, M., & Anand, S. P. (2009). Magnetotelluric and aeromagnetic investigations for assessment of groundwater resources in Parnaiba basin in Piaui State of North-East Brazil. *Journal of Applied Geophysics*, *68*(2), 269–281. https://doi.org/10.1016/j.jappgeo.2008.12.001

Chave, A. D., & Jones, A. G. (2012). The Magnetotelluric Method, Theory and Practice. *Cambridge University Press*.

Chave, A. D., & Thompson, D. J. (1989). Some comments on magnetotelluric response function estimation. *Journal of Geophysical Research*, *94*, 14202–14215.

Chegbeleh, L. P., Akudago, J. A., Nishigaki, M., & Edusi, S. N. (2009). ELECTROMAGNETIC GEOPHYSICAL SURVEY FOR GROUNDWATER EXPLORATION IN THE VOLTAIAN OF NORTHERN GHANA. *Journal of Environmental Hydrology*, *17*.

Chen, Y., Chen, Y., Liu, Q., & Liu, X. (2023). Quantifying common major and minor elements in minerals/rocks by economical desktop scanning electron microscopy/silicon drift detector energy-dispersive spectrometer (SEM/SDD-EDS). *Solid Earth Sciences*, *8*(1), 49–67. https://doi.org/10.1016/j.sesci.2022.12.002

Cheunteu Fantah, C. A., Mezoue, C. A., Mouzong, M. P., Tokam Kamga, A. P., Nouayou, R., & Nguiya, S. (2022). Mapping of major tectonic lineaments across Cameroon using potential field data. *Earth, Planets and Space*, *74*(1), 59. https://doi.org/10.1186/s40623-022-01612-7

Christensen, A., & Dransfield, M. (2002). Airborne vector magnetometry over banded iron formation. *In: 72nd Annual International Meeting of SEG.*, 13-16.

Christensen, T. H., Kjeldsen, P., Bjerg, P. L., Jensen, D. L., Christensen, J. B., Baun, A., Albrechtsen, H.-J., & Heron, G. (2001). Biogeochemistry of landfill leachate plumes. *Applied Geochemistry*, *16*(7), 659–718. https://doi.org/10.1016/S0883-2927(00)00082-2

Ciudad, D., Cobos, P., Sanchez, P., & Aroca, C. (2010). *RFID in Metal Environments: An Overview on Low (LF) and Ultra-Low (ULF) Frequency Systemsled*. https://doi.org/10.5772/7978

Clarke, G., & Smout, I. (2018). *Clay, Conductivity, and Rural Water supply: A hydrogeological investigation.* (Dissertation B221637; pp. 2–5). Loughborough Uni.

Connard, G., Couch, R., & Gemperle, M. (1983). Analysis of aeromagnetic measurements from the Cascade Range in central Oregon. *Geophysics*, *48*, 376–390.

Conti, P., Pistis, M., Bernardinetti, S., Barbagli, A., Zirulia, A., Serri, L., T., C., Guastaldi, E., & Ghiglieri, G. (2021). Tectonic Setting of the Kenya Rift in the Nakuru Area, Based on Geophysical Prospecting. *Geosciences*, *11*, 80. https://doi.org/10.3390/geosciences11020080

Cooper, G. (2004). Euler Deconvolution Applied to Potential Field Gradients. *Exploration Geophysics*, *35*. https://doi.org/10.1071/EG04165

Cooper, G., & Cowan, D. R. (2004). Filtering using variable order vertical derivatives. *Computers and Geosciences*, *30*, 455–459. https://doi.org/10.1016/j.cageo.2004.03.001

Cordell, L., & Grauch, V. J. S. (1985). Mapping Basement Magnetization zones from aeromagnetic data in the San Juan Basin, New Mexico, in Hinze, W.J., Ed., the Utility of Regional Gravity and Magnetic Anomaly Maps. *Society of Exploration Geophysics*, 181–197.

Coulibaly, N., Coulibaly, T. J. H., Mpakama, Z., & Savané, I. (2018). The Impact of Climate Change on Water Resource Availability in a Trans-Boundary Basin in West Africa: The Case of Sassandra. *Hydrology*, *5*(1), Article 1. https://doi.org/10.3390/hydrology5010012

Crawford, M. M., Bryson, L. S., Woolery, E. W., & Wang, Z. (2018). Using 2-D electrical resistivity imaging for joint geophysical and geotechnical characterization of shallow landslides. *Journal of Applied Geophysics*, *157*, 37–46. https://doi.org/10.1016/j.jappgeo.2018.06.009

Crowe, W. A., & Jackson-Hicks, S. (2008). Intrabasin deformation of the Volta Basin,. *The Voltaian Basin, Workshop and Excursion*, 31–38.

Dahlin, T. (1996). 2D resisitivity surveying for enviromental and engineering applications. *First Break*, *14*, 275–283.

Dapaah-Siakwa, S., & Gyau-Boakye, P. (2000). Hydrogeological framework and borehole yield in Ghana. *Hydrogeology Journal*, 8: 405-415.

Dawoud, A. M. (2011). Using Airborne Geophysical Survey for Exploring and Assessment of Groundwater Potentiality in Arid Regions. *Journal of King Abdulaziz, 22 (3)*, 207–220.

Day-Lewis, F. D., Slater, L. D., Robinson, J., Johnson, C. D., Terry, N., & Werkema, D. (2017). An overview of geophysical technologies appropriate for characterization and monitoring at fractured-rock sites. *Journal of Environmental Management*, *204*, 709–720. https://doi.org/10.1016/j.jenvman.2017.04.033

de Groot-Hedlin, C., & Constable, S. (1990). Occam's inversion to generate smooth two-dimensional models from magnetolluric data. *Geophysics*, *55*, 1613–1624.

de Jong, S. M., Heijenk, R. A., Nijland, W., & van der Meijde, M. (2020). Monitoring Soil Moisture Dynamics Using Electrical Resistivity Tomography under Homogeneous Field Conditions. *Sensors*, *20*(18), Article 18. https://doi.org/10.3390/s20185313

Demidova, T. A., Yegorov, I. V., & Yanikyan, V. O. (1985). Galvanic distortions of the magnetotelluric field of the lower Caucasus. *Geomagnetic Aeron.*, *25*, 391–396.

Demirci, İ., Gündoğdu, N. Y., Candansayar, M. E., Soupios, P., Vafidis, A., & Arslan, H. (2020). Determination and Evaluation of Saltwater Intrusion on Bafra Plain: Joint Interpretation of Geophysical, Hydrogeological and Hydrochemical Data. *Pure and Applied Geophysics*, *177*(11), 5621–5640. https://doi.org/10.1007/s00024-020-02573-2

Deng, Y., Byrnes, J. S., & Bezada, M. (2021). New Insights Into the Heterogeneity of the Lithosphere-Asthenosphere System Beneath South China From Teleseismic Body-Wave Attenuation. *Geophysical Research Letters*, *48*(6), e2020GL091654. https://doi.org/10.1029/2020GL091654

Dentith, M., & Mudge, S. T. (2014). *Geophysics for the Mineral Exploration Geoscientist* (First edition). Cambridge University Press.

Dickson, K. B., & Benneh, G. A. (2004). New geography of Ghana. Longmans Group Ltd. *Longman Group Ltd.*

Dunlop, D. J., & Ozdemir, O. (2007). Geomagnetism. In *Sedimentology and structures of the Earth* (Vol. 1).

Dzikunoo, E. A., Vignoli, G., Jorgensen, F., Yidana, S. M., & Banoeng-Yakubo, B. (2020). New regional stratigraphic insights from a 3D geological model of the Nasia sub-basin, Ghana, developed for hydrogeological purposes and based on reprocessed B-field data originally collected for mineral exploration. *Solid Earth*, *11*, 349–361.

Edokpayi, J. N., Rogawski, E. T., Kahler, D. M., Hill, C. L., Reynolds, C., Nyathi, E., Smith, J. A., Odiyo, J. O., Samie, A., Bessong, P., & Dillingham, R. (2018). Challenges to Sustainable Safe Drinking Water: A Case Study of Water Quality and Use across Seasons in Rural Communities in Limpopo Province, South Africa. *Water*, *10*(2), 159. https://doi.org/10.3390/w10020159

Edwards, L. S. (1977). A modified pseudosection for resistivity and IP. *Geophysics*, *42(5)*, 1020–1036.

Egbueri, J. C., Agbasi, J. C., Ayejoto, D. A., Khan, M. I., & Khan, M. Y. A. (2023). Extent of anthropogenic influence on groundwater quality and human health-related risks: An integrated assessment based on selected physicochemical characteristics. *Geocarto International*, *38*(1), 2210100. https://doi.org/10.1080/10106049.2023.2210100

Eke, K. T., & Igboekwe, M. U. (2011). Geoelectric Investigation of Groundwater in Some Villages in Ohafia Locality, Abia State, Nigeria. *Current Journal of Applied Science and Technology*, 190–203. https://doi.org/10.9734/BJAST/2011/600

Elhag, A. B., & Elzien, S. M. (2013). Structures controls on groundwater occurrence and flow in crystalline bedrocks: A case study of the El Obeid area, Western Sudan. *Global Advanced Research Journal*, *2(2)*, 37–46.

Ersoy, A., & Waller, M. D. (1995). Textural characterisation of rocks. *Engineering Geology*, *39*(3), 123–136. https://doi.org/10.1016/0013-7952(95)00005-Z

Evans, R. L., Elsenbeck, J., Zhu, J., Abdelsalam, M. G., Sarafian, E., Mutamina, D., Chilongola, F., Atekwana, E. A., & Jones, A. G. (2019). Structure of the Lithosphere Beneath the Barotse Basin, Western Zambia, From Magnetotelluric Data. *Tectonics*, *38*(2), 666–686. https://doi.org/10.1029/2018TC005246

Ewusi, A., Seidu, J., & Ansah, E. (2020). Efficacy of Geophysical Techniques for Groundwater Exploration in the Volta Basin, Northern Region of Ghana. *Ghana Mining Journal*, *20*, 10–19.

Fairhead, J. D. (2007). Gravity and magnetics in today's oil and mineral industry. *GETECH Group Plc. Kitson House. Elmete Hall Roundhay, Leed. LS821J UK.*

Faleiro, E., Asensio, G., Denche, G., Garcia, D., & Moreno, J. (2019). Wenner Soundings for Apparent Resistivity Measurements at Small Depths Using a Set of Unequal Bare Electrodes: Selected Case Studies. *Energies*, *12*, 695.

Farag, K. S. I., Howari, F. M., & Abdelmalik, K. W. (2019). Imaging of hydrothermal altered zones in Wadi Al-Bana, in southern Yemen, using remote sensing techniques and very low frequency–electromagnetic data. *Arabian Journal of Geosciences*, *12*(18), 554. https://doi.org/10.1007/s12517-019-4702-8

Ferguson, G., Mcintosh, J., Perrone, D., & Jasechko, S. (2018). Competition for shrinking window of low salinity groundwater. *Environmental Research Letters*. https://doi.org/10.1088/1748-9326/aae6d8

Feroci, M., Orlando, L., Balia, R., Bosman, C., Cardarelli, E., & Deidda, G. (1986). Some consideration on shallow seismic reflection survey. *Journal of Applied Geophysics*, *2000*, 127–139. https://doi.org/10.1016/S0926-9851(00)00024-0

Fetter, C. W. (2002). *Applied Hydrogeology*. upper Sadle River.

Fiandaca, G., Doetsch, J., Vignoli, G., & Auken, E. (2015). Generalized focusing of time-lapse changes with applications to direct current and time-domain induced polarization inversions. *Geophysical Journal International*, *203*(2), 1101–1112. https://doi.org/10.1093/gji/ggv350

Filho, J. H., Salazar, F. R. dos S., Capri, M. da R., Neto, C. A., Alcantara, A. K. M., & Peixoto, L. de C. (2012). *State-of-the-Art and Trends in Atomic Absorption Spectrometry*. IntechOpen.com.

Fugro Airborn Survey. (2009b). *Fugro Airborne Surveys Interpretation: Airborne Geophysical Sur vey over the Volta River Basin and Keta Basin Geological Inter pretation Summary Report* (FCR2350/Job 1769). GGSA.

Fugro Airborn Survey. (2009a). *Fugro Airborne Surveys: Logistics and Processing Report, Airborne Magnetic and GEOTEM Survey, Areas 1 to 8* (92). GGSA.

Fugro Airborne Surveys. (2009b). *Airborne Geophysical Survey over the Volta River Basin and Keta Basin Geological Interpretation Summary Report,* (FCR2350/Job No.1769).

Fukushima, K., Kabir, M., Kanda, K., Obara, N., Fukuyama, M., & Otsuki, A. (2022). Simulation of Electrical and Thermal Properties of Granite under the Application of Electrical Pulses Using Equivalent Circuit Models. *Materials*, *15*(3), 1039. https://doi.org/10.3390/ma15031039

Gamble, T. D., Goubau, W. M., & Clarke, J. (1979). Magnetotellurics with a remote magnetic reference. *Geophysics*, *44*(1), 53–68. https://doi.org/10.1190/1.1440923

Ganiyu, S. A., Badmus, B. S., Idowu, O. A., oladunjoye, M. A., & Olurin, T. (2015). 2D Electrical Resistivity Imaging Investigation of Open Dump Site in Basement Complex Formation. *African Review of Physics*.

Garcia, X., Seillé, H., Elsenbeck, J., Evans, R. L., Jegen, M., Hölz, S., Ledo, J., Lovatini, A., Marti, A., Marcuello, A., Queralt, P., Ungarelli, C., & Ranero, C. R. (2015). Structure of the mantle beneath the Alboran Basin from magnetotelluric soundings. *Geochemistry, Geophysics, Geosystems*, *16*(12), 4261–4274. https://doi.org/10.1002/2015GC006100

Genchi, G., Sinicropi, M. S., Lauria, G., Carocci, A., & Catalano, A. (2020). The Effects of Cadmium Toxicity. *International Journal of Environmental Research and Public Health*, *17*(11), 3782. https://doi.org/10.3390/ijerph17113782

George, D. W., Selby, C. M., & Scolnik, R. (1947). Electrical Characteristics of Quartz-Crystal Units and Their Measurement. *Journal of Research of the National Bureau of Standards*, *38*.

Geosoft Inc., O. M. (2021). *Data Processing and Analysis Systems for Earth Science Application.* (2021.2) [English]. Seequent.

Geotomo-Software. (2002). *Geoelectrical Imaging 2D and 3D Geotomo Software Manual*. ABEM Instrument, Bromma, Sweden.

Geris, J., Comte, J.-C., Franchi, F., Petros, A. K., Tirivarombo, S., Selepeng, A. T., & Villholth, K. G. (2022). Surface water-groundwater interactions and local land use control water quality impacts of extreme rainfall and flooding in a vulnerable semi-arid region of Sub-Saharan Africa. *Journal of Hydrology*, *609*, 127834. https://doi.org/10.1016/j.jhydrol.2022.127834

Giroux, B., Chouteau, M., & Descloitres, M. (1997). Use of magnetotellurics methods in the study of deep Maestrichitian aquifer in Senegal. *Journal of Applied Geophysics*, 77-96.

Golshadi, Z., KarbalaeiRamezanali, A., & Kafaei, K. (2016). Interpretation of magnetic data in the Chenar-e Olya area of Asadabad, Hamedan, Iran, using analytic signal, Euler deconvolution, horizontal gradient and tilt derivative methods. *Bollettino Di Geofisica Teorica Ed Applicata*, *57*, 329–342. https://doi.org/10.4430/bgta0182

Grauch, V. J. S., Paul, W. B., & Keith, I. K. (2004). Preliminary interpretation of high resolution aeromagnetic data near Taos New Mexico. *5th Field Conference Geology of the Taos Region*, 244–256.

Greenfield, R. J., & Stoyer, C. H. (1976). Monitoring ground-water contamination with geophysical methods. *Trans. Soc. Min. Eng. AIME; (United States)*, *260:1*. https://www.osti.gov/biblio/7346030

Griffiths, D. H., & Barker, R. D. (1993). Two-dimensional resistivity imaging and modelling in areas of geology. *Journal of Applied Geophysics*, *29*, 211–226.

Grisey, B., & Aleya, L. (2016). Assessing the impact of leachate plumes on groundwater quality in Etueffont landfill (Belfort France). *Environmental Earth Sciences*, *75*, 913.

Groom, R., & Bailey, R. (1989). Decomposition of the Magnetotelluric impedance tensor in the presence of local three-dimensional galvanic distortion. *Journal of Geophysical Research*, *94, B2*, 1913–1925. https://doi.org/10.1029/JB094iB02p01913

Guireli Netto, L., Barbosa, A. M., Galli, V. L., Pereira, J. P. S., Gandolfo, O. C. B., & Birelli, C. A. (2020). Application of invasive and non-invasive methods of geo-environmental investigation for determination of the contamination behavior by organic compounds. *Journal of Applied Geophysics*, *178*, 104049. https://doi.org/10.1016/j.jappgeo.2020.104049

Gunn, D. A., Chambers, J., Uhlemann, S., Wilkinson, P. B., Meldrum, P., Dijkstra, T., Haslam, E., Kirkham, M., Wragg, J., Holyoake, S., Hughes, P., Hen-Jones, R., & Glendinning, S. (2014). Moisture monitoring in clay embankments using electrical resistivity tomography. *Construction and Building Materials*, *92*. https://doi.org/10.1016/j.conbuildmat.2014.06.007

Günther, T., & Müller-Petke, M. (2012). Hydraulic properties at the North Sea island of Borkum derived from joint inversion of magnetic resonance and electrical resistivity soundings. *Hydrology and Earth System Sciences*, *16*(9), 3279–3291. https://doi.org/10.5194/hess-16-3279-2012

Gyau-Boakye, P., & Dapaa-Siakwan, S. (1999). GROUNDWATER: SOLUTION TO GHANA'S RURAL WATER SUPPLY INDUSTRY? *The Ghana Engineer*.

Han, D., Tong, X., Currell, M. J., Cao, G., Jin, M., & Tong, C. (2014). Evaluation of the impact of an uncontrolled landfill on surrounding groundwater quality, Zhoukou, China.

Journal of Geochemical Exploration, *136*, 24–39. https://doi.org/10.1016/j.gexplo.2013.09.008

Han, K., & Clark, S. M. (2021). Review of calculating the electrical conductivity of mineral aggregates from constituent conductivities. *Solid Earth Sciences*, *6*(2), 111–128. https://doi.org/10.1016/j.sesci.2021.02.003

Hanneson, C., & Unsworth, M. J. (2023). Regional-scale resistivity structure of the middle and lower crust and uppermost mantle beneath the southeastern Canadian Cordillera and insights into its causes. *Geophysical Journal International*, *234*(3), 2032–2052. https://doi.org/10.1093/gji/ggad183

HAP. (2011). *Water resource atlas of the northern regions of Ghana-hydrogeological assessment project (HAP).* [HAP]. Water resource commission.

Harinarayana, T. (2008). Applications of Magnetotelluric Studies in India. *Memoir Geological Society of India*, *68*.

Harris, C. R., Millman, K. J., Van der Walt, S. J., Gommers, R., Virtanen, P., Cournapeau, D., & Oliphat, T. E. (2020). Array programming with NumPy. *Nature*, *585*, 357–362. https://doi.org/10.1038/s41586-020-2649-2

Hasan, M., Shang, Y., & Jin, wj. (2018). Delineation of weathered/fracture zones for aquifer potential using an integrated geophysical approach: A case study from South China. *Journal of Applied Geophysics*, *157*, 47–60. https://doi.org/10.1016/j.jappgeo.2018.06.017

Hautot, S., Single, R. T., Waston, J., Harrop, N., Jerram, D. A., Tarits, P., Whaler, K., & Dawes, G. (2007). 3-D magnetotelluric inversion and model validation with gravity data for the investigation of flood basalts and associated volcanic rifted margins. *Geophysics Journal International*, *170*, 1418–1430.

Hautot, S., & Tarits, P. (2000). Deep structure of the Baringo Rift Basin (central Kenya) from three-dimensional magnetotelluric imaging' Implications for rift evolution. *Journal of Geophysical Research*, *105*, 23493–23518.

Hautot, S., Tarits, P., Perrier, F., Tarits, C., & Trique, M. (2002). Groundwater electromagnetic imaging in complex geological and topographical regions: A case study of a tectonic boundary in the French Alps. *GEOPHYSICS*, *67*(4), 1048–1060. https://doi.org/10.1190/1.1500365

Hayatudeen, M., Rasaq, B., Onaolapo, R. I., & Olummide, A. (2021). FIRST HORIZONTAL AND FIRST VERTICAL DERIVATIVES FROM HIGH RESOLUTION AEROMAGNETIC DATA OVER THE GONGOLA BASIN UPPER BENUE TROUGH NORTHEASTERN NIGERIA. *Global Journal of Pure and Applied Science*, *27, 2021*, 181–192. https://dx.doi.org/10.4314/gjpas.v27i2.10

Hazell, J. R. T., Cratchley, C. R., & Preston, A. M. (1988). The location of aquifers in crystalline rocks and alluvium in Northern Nigeria using combined electromagnetic and resistivity techniques. *Quarterly Journal of Engineering Geology, Vol.*, 159–175.

Heather, L. R.-S., Beth, A. S., Jeffrey, L. L. P. G., & Jeffrey, J. W. (1999). ELECTRICAL IMAGING: A Method for Identifying Potential Collapse and other Karst Features Near Roadways. *Science Application International Corporation*.

Hepburn, E., Madden, C., Szabo, D., Coggan, T. L., Clarke, B., & Currell, M. (2019). Contamination of groundwater with per- and polyfluoroalkyl substances (PFAS) from

legacy landfills in an urban re-development precinct. *Environmental Pollution (Barking, Essex: 1987), 248*, 101–113. https://doi.org/10.1016/j.envpol.2019.02.018

Hossain, M. A., Haque, M. I., Parvin, M. A., & Islam, M. N. (2023). Evaluation of iron contamination in groundwater with its associated health risk and potentially suitable depth analysis in Kushtia Sadar Upazila of Bangladesh. *Groundwater for Sustainable Development*, *21*, 100946. https://doi.org/10.1016/j.gsd.2023.100946

Hubbard, S. S., Rubin, Y., & Majer, L. E. (1999). Spatial correlation structure estimation using geophysical and hydrogeological data. *Water Resource Research*, *35*, 1809–1825.

Ibraheem, I. M., Haggag, M., & Tezkan, B. (2019). Edge Detectors as Structural Imaging Tools Using Aeromagnetic Data: A Case Study of Sohag Area, Egypt. *Geosciences*, *9*(5), Article 5. https://doi.org/10.3390/geosciences9050211

Igboekwe, M. U., Agada, I. O., & Amos-Uhegbu, C. (2021). Investigation of Dumpsite Leachate using Electrical Resistivity Tomography at Umueze-Ibeku, Umuahia, South-Eastern Nigeria. *Journal of Scientific and Engineering Research, 8(4)*, 71–80.

Ishizu, K., & Ogawa, Y. (2021). Offshore-onshore resistivity imaging of freshwater using a controlled-source electromagnetic method: A feasibility study. *GEOPHYSICS*. https://doi.org/10.1190/geo2020-0906.1

Iwmi, G., Rao, V., Padalu, G., Dhakate, R., & Sarma, V. S. (2013). Application of electrical resistivity tomography methods for delineation of groundwater contamination and potential zones. *Arabian Journal of Geosciences*, *7*. https://doi.org/10.1007/s12517-013-0835-3

Jiang, Z., Mallants, D., Peeters, L., Gao, L., Soerensen, C., & Mariethoz, G. (2019). High-resolution paleovalley classification from airborne electromagnetic imaging and deep neural network training using digital elevation model data. *Hydrology and Earth System Sciences*, *23*(6), 2561–2580. https://doi.org/10.5194/hess-23-2561-2019

Joel, E. S., Olasehinde, P. I., De, D. K., & Maxwell. (2016). Regional groundwater studies using aeromagnetic technique. *Society of Exploration Geophysics*.

Jones, A. (1988). Static-shift of magnetotelluric data and its removal in a sedimentary environment. *Geophysics*, *53*, 967–978. https://doi.org/10.1190/1.1442533

Jones, A., Ledo, J., & Ferguson, I. (2005). Electromagnetic images of the Trans-Hudson Orogen: The North American Central Plains anomaly revealed. *Canadian Journal of Earth Sciences*, *42*, 457–478. https://doi.org/10.1139/e05-018

Jordan, C. J., Carney, J. N., Thomas, C. W., McDonnell, P., Turner, P., McNanus, K., & McEvoy, F. M. (2009). Ghana Airborne Geophysics Project: BGS Final Report. British Geological Survey Commissioned Report, CR/09/02. 325 pp. *Ghana Geological Survey Department, Accra*.

Jørgensen, F., Sandersen, P. B. E., & Auken, E. (2003). Imaging buried Quaternary valleys using the transient electromagnetic method. *Journal of Applied Geophysics*, *53*(4), 199–213. https://doi.org/10.1016/j.jappgeo.2003.08.016

Kabir, M. (2023). *Impacts of anthropogenic activities & climate change resulting from increasing concentration of Carbon dioxide on environment in 21st Century; A Critical Review*.

Kalmár, D., Hetényi, G., & Bondár, I. (2019). Moho depth analysis of the eastern Pannonian Basin and the Southern Carpathians from receiver functions. *Journal of Seismology*, *23*(5), 967–982. https://doi.org/10.1007/s10950-019-09847-w

Kalsbeek, F., Frei, D., & Affaton, P. (2008). Constraints on provenance, stratigraphic correlation and structural context of the Volta basin, Ghana, from detrital zircon geochronology: An Amazonian connection. *Sedimentary Geology, Volume 212*(Issues 1–4,), 86–95. https://doi.org/10.1016/j.sedgeo.2008.10.005

Kalsbeek, F., & Frei, R. (2010). Geochemistry of Precambrian sedimentary rocks used to solve stratigraphical problems: An example from the Neoproterozoic Volta basin, Ghana. *Precambrian Research*, *176*(1–4), 65–76. https://doi.org/10.1016/j.precamres.2009.10.004

Kamiński, M., Zientara, P., & Krawczyk, M. (2023). Application of airborne laser scanning and electrical resistivity tomography in the study of an active landslide and geology of the cliff, Jastrzębia Góra, Poland. *Bulletin of Engineering Geology and the Environment*, *82*(4), 131. https://doi.org/10.1007/s10064-023-03153-z

Kanthiya, S., Mangkhemthong, N., & Morley, K. C. (2019). Structural interpretation of Mae Suai Basin, Chiang Rai Province, based on gravity data analysis and modelling. *Heliyon*, *5*.

Kearey, P., Brook, M., & Hill, I. (2002). *An Introduction to Geophysical Exploration* (Third Edition). Blackwell Scientific Publications.

Kearey, P., & Brooks, M. (1991). *An Introduction to Geophysical Exploration, 2nd Edition*. Blackwell Scientific Publications.

Keller, G. V., & Frischknecht, F. C. (1966). *Electrical methods in geophysical prospecting.* Pergamon Press Ltd.

Kenworthy, A. (2016, January 10). Top Five Reasons to Use Geophysics in Environmental Projects. *Seequent*. https://www.seequent.com/top-five-reasons-to-use-geophysics-in-environmental-projects/

Kesse, G. O. (1985). *The mineral and rock resources of Ghana.* Balkema.

Khalil, M. H. (2014). Detection of Magnetically Susceptible Dyke Swarms in a Fresh Coastal Aquifer. *Pure and Applied Geophysics*, *171*(8), 1829–1845. https://doi.org/10.1007/s00024-013-0696-4

Khan, A., Connolly, J. A. D., Maclennan, J., & Mosegaardl, K. (2007). Joint inversion of seismic and gravity data for lunar composition and thermal state. *Geophysical Journal International*, *168*, 243–258.

Khoza, T. D., Jones, A. G., Muller, M. R., Evans, R. L., Miensopust, M. P., & Webb, S. J. (2013). Lithospheric structure of an Archean craton and adjacent mobile belt revealed from 2-D and 3-D inversion of magnetotelluric data: Example from southern Congo craton in northern Namibia. *Solid Earth*. https://doi.org/10.1002/jgrb.50258

Kirkby, A. L., Zhang, F., Peacock, J., Hassan, R., & Duan, J. (2019). The MTPy software package for magnetotelluric data analysis and visualisation. *Journal of Open Source Software*, *4*(37), 1358. https://doi.org/10.21105/joss.01358

Kivior, I., & Boyd, D. (1998). Interpretation of the aeromagnetic experimental survey in Euromanga-Cooper basin. *Journal of Canadian ExplorationGeophysics*, *34*, 58–66.

Klitten, K., & Agyekum, W. A. (2021). *Geophysical Wire-line Logging of Boreholes in Nasia River Catchment Basin.* (Danida Project ID 14-P02-GHA; Groundwater Development and Sustainable Agriculture in White Volta Basin of Ghana, pp. 15–45). GEOLOGICAL SURVEY OF DENMARK AND GREENLAND.

Knight, R. (2000). Seeing into the Earth: Noninvasive Characterization of the Shallow Subsurface for Environmental and Engineering Applications. *National Academy Press, Washington, D.C.* http://dx.doi.org/10.17226/5786, 148p

Knight, R., Smith, R., Asch, T., Abraham, J., Cannia, J., Viezzoli, A., & Fogg, G. (2018). Mapping Aquifer Systems with Airborne Electromagnetics in the Central Valley of California. *Ground Water*, *56*(6), 893–908. https://doi.org/10.1111/gwat.12656

Kpiebaya, P., & Abdul-Ganiyu, S. (2020). *Hydrogeological Study of Groundwater for Dry Season Farming in Northern Region of Ghana*. *15*, 187–196.

Kriaa, A., Hajji, M., Jamoussi, F., & Hamzaoui, A. H. (2014). Electrical Conductivity of 1:1 and 2:1 Clay Minerals. *Euro-Mediterranean Journal for Environmental Integration*, 78–88.

Krieger, L., & Peacock, J. R. (2014). MTpy: A Python toolbox for magnetotellurics. *Computers & Geosciences*, *72*, 167–175. https://doi.org/10.1016/j.cageo.2014.07.013

Kumar, A., Fernàndez, M., Vergés, J., Torne, M., & Jiménez-Munt, I. (2021). Opposite Symmetry in the Lithospheric Structure of the Alboran and Algerian Basins and Their Margins (Western Mediterranean): Geodynamic Implications. *Journal of Geophysical Research: Solid Earth*, *126*(7), e2020JB021388. https://doi.org/10.1029/2020JB021388

Kumar, V. P. V., Rao, S. P. B. V., Singh, A. K., Kumar, A., & Rao, R. P. (2021). Dimensionality and directionality analysis of magnetotelluric data by using different techniques: A case study from northern part of Saurashtra region, India. *Journal of Earth System Science*, *130*, 102. https://doi.org/10.1007/s12040-021-01596-0

LANGEO. (2023). *Summary of different array types of electrical method_Langeo Geophysical Instruments*. http://www.langeoinstrument.com/bolg/2016/0824/105.html

Launay, N., Quesnel, Y., Rochette, P., & Demory, F. (2018). Iron Formations as the Source of the West African Magnetic Crustal Anomaly. *Frontiers in Earth Science*, *6*. https://www.frontiersin.org/articles/10.3389/feart.2018.00032

Le Pape, F., Jones, A. G., Jessell, M. W., Hogg, C., Siebenaller, L., Perrouty, S., Touré, A., Ouiya, P., & Boren, G. (2021). The nature of the southern West African craton lithosphere inferred from its electrical resistivity. *Precambrian Research*, *358*, 106190. https://doi.org/10.1016/j.precamres.2021.106190

Le Pape, F., Jones, A. G., Jessell, M. W., Perrouty, S., Gallardo, L. A., Baratoux, L., Hogg, C., Siebenaller, L., Touré, A., Ouiya, P., & Boren, G. (2017). Crustal structure of southern Burkina Faso inferred from magnetotelluric, gravity and magnetic data. *Precambrian Research*, *300*, 261–272. https://doi.org/10.1016/j.precamres.2017.08.013

Lei, J. (2011). Seismic tomographic imaging of the crust and upper mantle under the central and western Tien Shan orogenic belt. *Journal of Geological Research*, *116*, B09305.

Levander, A., & Miller, M. (2012). Evolutionary aspects of lithosphere discontinuity structure in the Western U.S. *Geochemistry Geophysics Geosystems*, *13*. https://doi.org/10.1029/2012GC004056

Li, H., Li, H., Wang, K., & Liu, C. (2018). Effect of rock composition microstructure and pore characteristics on its rock mechanics properties. *International Journal of Mining Science and Technology*, *28*(2), 303–308. https://doi.org/10.1016/j.ijmst.2017.12.008

Lilley, F. E. M., & Weaver, J. T. (2010). Phases greater than 90° in MT data: Analysis using dimensionality tools. *Journal of Applied Geophysics*, *70*(1), 9–16. https://doi.org/10.1016/j.jappgeo.2009.08.007

Lissah, S. Y., Ayanore, M. A., Krugu, J. K., Aberese-Ako, M., & Ruiter, R. A. C. (2021). Managing urban solid waste in Ghana: Perspectives and experiences of municipal waste company managers and supervisors in an urban municipality. *PLOS ONE*, *16*(3), e0248392. https://doi.org/10.1371/journal.pone.0248392

Liu, H., Liang, Y., Zhang, D., Wang, C., Liang, H., & Cai, H. (2010). Impact of MSW landfill on the environmental contamination of phthalate esters. *Waste Management*, *30*(8), 1569–1576. https://doi.org/10.1016/j.wasman.2010.01.040

Liu, Q., Shu, Q., Gao, W., Luo, Y., Li, Z., Yang, J., & Xu, W. (2023). Automatic Interpretation of Potential Field Data Based on Euler Deconvolution with Linear Background. *Applied Sciences*, *13*(9), Article 9. https://doi.org/10.3390/app13095323

Local Gov. Minstry. (2023, July 16). Tamale Metropolitan Assembly. *Ghana District.Com*. http://ghanadistricts.com/Home/District/139

Loke, M. (2001). *Tutorial: 2-D and 3-D Electrical Imaging Surveys*.

Loke, M., & Barker, R. (1996). Rapid least-squares inversion of apparent resistivity pseudo-sections by quasi-Newton method. *Geophysics Prospect.*, *44*, 131–152.

Lubang, J., Liu, H., & Chen, R. (2023). Combined Application of Hydrogeological and Geoelectrical Study in Groundwater Exploration in Karst-Granite Areas, Jiangxi Province. *Water*, *15*, 865.

Luo, Y., Xue, D.-J., & Wang, M. (2010). Reduction to the Pole at the Geomagnetic Equator. *Chinese Journal of Geophysics*, *53*(6), 1082–1089. https://doi.org/10.1002/cjg2.1578

Luparello, C., Sirchia, R., & Longo, A. (2011). Cadmium as a transcriptional modulator in human cells. *Critical Reviews in Toxicology*, *41*(1), 75–82. https://doi.org/10.3109/10408444.2010.529104

MacDonald, A. M., & Davies, J. (2000). *A brief review of groundwater for rural water supply in Sub-saharan Africa*. (BGS Technical Report WC/00/33; Overseas Geology Series). British geological survey.

MacDonald, A. M., Kemp, S. J., & Davies, J. (2005). Transmissivity variations in Mudstones. *Groundwater Journal*, *43*(no.2), 259–269.

Mackie, R. L., Madden, T. R., & Wannamaker, P. E. (1993). Three-dimensional magnetotelluric modelling using difference equations—Theory and com parisons to integral equation solutions. *Geophysics*, *58*, 215–226.

Mainoo, P. A., Manu, E., Yidana, S. M., Agyekum, W. A., Stigter, T., Duah, A. A., & Preko, K. (2019). Application of 2D-Electrical resistivity tomography in delineating groundwater potential zones: Case study from the voltaian super group of Ghana. *Journal of African Earth Sciences*, *160*, 103618. https://doi.org/10.1016/j.jafrearsci.2019.103618

Maithya, J., & Fujimitsu, Y. (2019). Analysis and interpretation of magnetotelluric data in characterization of geothermal resource in Eburru geothermal field, Kenya. *Geothermics*, *81*, 12–31. https://doi.org/10.1016/j.geothermics.2019.04.003

Malleswari, D., Veeraswamy, K., Abdul-Azeez, K. K., Gupta, A. K., Babu, N., Patro, P. K., & Harinarayana, T. (2019). *Magnetotelluric investigation of lithospheric electrical structure beneath the Dharwar Craton in south India: Evidence for mantle suture and plume-continental interaction | Elsevier Enhanced Reader*. https://doi.org/10.1016/j.gsf.2018.10.011

Manfredi, E. C., Flury, B., Viviano, G., Thakuri, S., Khanal, S. N., Jha, P. K., Maskey, R. K., Kayastha, R. B., Kafle, K. R., Bhochhibhoya, S., Ghimire, N. P., Shrestha, B. B., Chaudhary, G., Giannino, F., Cartenì, F., Mazzoleni, S., & Salerno, F. (2010). Solid Waste and Water Quality Management Models for Sagarmatha National Park and Buffer Zone, Nepal. *Mountain Research and Development*, *30*(2), 127–142. https://doi.org/10.1659/MRD-JOURNAL-D-10-00028.1

Manzella, A., Volpi, G., Zaja, A., & Meju, M. (2004). Combined TEM-MT investigation of shallow-depth resistivity structure of Mt Somma-Vesuvius. *Journal of Volcanology and Geothermal Research*, *131*(1), 19–32. https://doi.org/10.1016/S0377-0273(03)00313-5

Martí, A., Queralt, P., Ledo, J., & Farquharson, C. (2010). Dimensionality imprint of electrical anisotropy in magnetotelluric responses. *Physics of the Earth and Planetary Interiors*, *182*(3), 139–151. https://doi.org/10.1016/j.pepi.2010.07.007

Martinho, E., & Dionísio, A. (2014). Main geophysical techniques used for non-destructive evaluation in cultural built heritage: A review. *Journal of Geophysics and Engineering*, *11*(5), 053001. https://doi.org/10.1088/1742-2132/11/5/053001

Martorana, R., Capizzi, P., Pisciotta, A., Scudero, S., & Bottari, C. (2023). An Overview of Geophysical Techniques and Their Potential Suitability for Archaeological Studies. *Heritage*, *6*(3), Article 3. https://doi.org/10.3390/heritage6030154

Maurice, L., Taylor, R., Tindimugaya, C., Macdonald, A., Johnson, P., Kaponda, A., Owor, M., Sanga, H., Bonsor, H., Darling, W., & Gooddy, D. (2018). Characteristics of high-intensity groundwater abstractions from weathered crystalline bedrock aquifers in East Africa. *Hydrogeology Journal*, *27*. https://doi.org/10.1007/s10040-018-1836-9

McNeice, W. G., & Jones, G. A. (2001). Multisite, multifrequency tensor decomposition of magnetotelluric data. *GEOPHYSICS*, *66*, 158–173.

McNeill, J. D., & Snelgrove, F. B. (1995). Electromagnetic Geophysical Methods applied to to Groundwater Exploration and Evaluation.. *Geonics Limited*.

Meju, M. A., Fontes, S. L., Oliveira, M. F. B., Lima, J. P. R., Ulugergerli, E. U., & Carrasquilla, A. A. (1999). Regional aquifer mapping using combined VES-TEM-AMT/EMAP methods in the semiarid eastern margin of Parnaiba Basin, Brazil. *GEOPHYSICS*, *64*(2), 337–356. https://doi.org/10.1190/1.1444539

Mensah, J. K., Ofosu, E. A., Akpoti, K., Kabo-Bah, A. T., Okyereh, S. A., & Yidana, S. M. (2022). Modeling current and future groundwater demands in the White Volta River Basin of Ghana under climate change and socio-economic scenarios. *Journal of Hydrology: Regional Studies*, *41*, 101117. https://doi.org/10.1016/j.ejrh.2022.101117

Metronix, G. (1998). Metronix geophysics and magnetotellurics. *Appex*. https://www.metronix.de/metronixweb/en/geophysiks/contact/

Michot, D., Benderitter, Y., Dorigny, A., Nicoullaud, B., King, D., & Tabbagh, A. (2003). Spatial and temporal monitoring of soil water content with an irrigated corn crop cover using surface electrical resistivity tomography. *Water Resources Research*, *39*(5). https://doi.org/10.1029/2002WR001581

Miensopust, M. P., Jones, A. G., Muller, M. R., Garcia, X., & Evans, R. L. (2011). Lithospheric structures and Precambrian terrane boundaries in northeastern Botswana revealed throughmagnetotelluric profiling as part of the Southern African Magnetotelluric Experiment. *Journal of Geophysical Research, 116,* B02401. https://doi.org/10.1029/2010JB007740.

Miller, R., Pullan, S., Waldner, J., & Haeni, F. (1986). Field comparison of shallow seismic sources. *GEOPHYSICS*, *51*, 2067–2092. https://doi.org/10.1190/1.1442061

Min, G., Yuan, H., Wang, X., Wang, K., Li, C., Liu, K., & Hu, S. (2023). Crustal and upper mantle electrical structure and uplift mechanism of the Liupanshan orogenic belt in the NE Tibetan Plateau. *Tectonophysics*, *853*, 229–799.

Mockler, E. M., O'Loughlin, F. E., & Bruen, M. (2016). Understanding hydrological flow paths in conceptual catchment models using uncertainty and sensitivity analysis. *Computers & Geosciences*, *90*, 66–77. https://doi.org/10.1016/j.cageo.2015.08.015

Mohamaden, M. I. I., & Ehab, D. (2017). Application of electrical resistivity for groundwater exploration in Wadi Rahaba, Shalateen, Egypt. *NRIAG Journal of Astronomy and Geophysics*, *6*(1), 201–209. https://doi.org/10.1016/j.nrjag.2017.01.001

Mohamed, A., & Abu El Ella, E. (2021). Magnetic Applications to Subsurface and Groundwater Investigations: A Case Study from Wadi El Assiuti, Egypt. *International Journal of Geosciences*, *12*, 77–101. https://doi.org/10.4236/ijg.2021.122006

Mohamed, A., Al Deep, M., Othman, A., Taha, A. I., Alshehri, F., & Abdelrady, A. (2022). Integrated Geophysical Assessment of Groundwater Potential in Southwestern Saudi Arabia. *Frontiers in Earth Science*, *10*. https://www.frontiersin.org/articles/10.3389/feart.2022.937402

Mohamed, A., & Ella, E. A. (2021). Magnetic application to subsurface and groundwater investigations: A case study from the Wadi El Assiuti, Egypt. *International Journal of Geoscience*, *12*, 77–101.

Mohamed, H. S., Senosy, Mahmoud. M., & Abdel Zaher, M. (2016). Interactive interpretation of airborne gravity, magnetic, and drill-hole data within the crustal framework of the northern Western Desert, Egypt. *Journal of Applied Geophysics*, *134*, 291–302. https://doi.org/10.1016/j.jappgeo.2016.09.002

Mokgatle, T., & Fourie, F. (2017). Groundwater exploration in the Tsineng area using airborne and ground base geophysical methods. *15th Biennial Groundwater Conference*, 14–18.

Moorkamp, M. (2007). Comment on 'The magnetotelluric phase tensor' by T. Grant Caldwell, Hugh M. Bibby and Colin Brown. *Geophysical Journal International*, *171*(2), 565–566. https://doi.org/10.1111/j.1365-246X.2007.03490.x

Morales-Ocaña, C., Bohoyo, F., Escutia, C., Marín-Lechado, C., Rey-Moral, C., Druet, M., Galindo-Zaldívar, J., & Maestro, A. (2023). 3D Geophysical and Geological Modeling of the South Orkney Microcontinent (Antarctica): Tectonic Implications for the Scotia Arc Development. *Tectonics*, *42*(4), e2022TC007602. https://doi.org/10.1029/2022TC007602

Mulwa, J. K., Gaciri, S. J., Barongo, J. O., Opiyo-Akech, N., & Kianji, G. K. (2005). GEOLOGICAL AND STRUCTURAL INFLUENCE ON GROUNDWATER DISTRIBUTION AND FLOW IN NGONG AREA, KENYA. *African Journal of Science and Technology*, *6*, 105–115.

Nagarajan, R., Thirumalaisamy, S., & Lakshumanan, E. (2012). Impact of leachate on groundwater pollution due to non-engineered municipal solid waste landfill sites of erode city, Tamil Nadu, India. *Iranian Journal of Environmental Health Science & Engineering*, *9*(1), 35. https://doi.org/10.1186/1735-2746-9-35

Naif, S., Selway, K., Murphy, S. B., Egbert, G., & Pommier, A. (2021). Electrical conductivity of the lithosphere-asthenosphere system. *Physics of the Earth and Planetary Interiors*, *313*.

Nazari, S., Rochlitz, R., & Günther, T. (2023). Optimizing Semi-Airborne Electromagnetic Survey Design for Mineral Exploration. *Minerals*, *13*(6), Article 6. https://doi.org/10.3390/min13060796

NGA, N. G. A. Inc. (2004). *GM-SYS: Gravity/Magnetic Modeling software User Guide.* Corvallis.

Niwas, S., & Celik, M. (2012). Equation estimation of porosity and hydraulic conductivity of Ruhrtal aquifer in Germany using near surface geophysics. *Journal of Applied Geophysics*, *84*, 77–85. https://doi.org/10.1016/j.jappgeo.2012.06.001

Nurit, T.-G. (2022). Minerals Observed by Scanning Electron Microscopy (SEM), Transmission Electron Microscopy (TEM) and High Resolution Transmission Electron Microscopy (HRTEM). In *Electron Microscopy*. IntechOpen. https://doi.org/10.5772/intechopen.102477

Okpoli, C. (2013). Application of 2D Electrical Resistivity Tomography in Landfill Site: A Case Study of Iku, Ikare Akoko, Southwestern Nigeria. *Journal of Geological Research*, *2013*. https://doi.org/10.1155/2013/895160

Omosuyi, G. O., Adeyemo, A., & Adegoke, A. O. (2007). Investigation of Groundwater Prospect Using Electromagnetic and Geoelectric Sounding at Afunbiowo, near Akure, Southwestern Nigeria. *The Pacific Journal of Science and Technology*, *8*, 172.

Oni, A. G., Eniola, P. J., Olorunfemi, M. O., Okunubi, M. O., & Osotuyi, G. A. (2020). The magnetic method as a tool in groundwater investigation in a basement complex terrain: Modomo Southwest Nigeria as a case study. *Applied Water Science*, *10*(8), 190. https://doi.org/10.1007/s13201-020-01279-z

Oryński, S., Jóźwiak, W., Nowożyński, K., & Klityński, W. (2022). Comparison of 3D, 2D, and 1D Magnetotelluric Inversion Results on the Example of Data from Fore-Sudetic Monocline. *International Journal of Geophysics*, *2022*, e3400950. https://doi.org/10.1155/2022/3400950

Osagie, A. U., Eshanibli, A., & Adepelumi, A. A. (2021). Structural trends and basement depths across Nigeria from analysis of aeromagnetic data. *Journal of African Earth Sciences*, *178*, 104184. https://doi.org/10.1016/j.jafrearsci.2021.104184

Osinowo, O. O., Adabanija, M. A., Adewoye, O. A., Osinowo, O. O., Adabanija, M. A., & Adewoye, O. A. (2019). Structural Interpretation and Depth Estimation from Aeromagnetic Data of Abigi-Ijebu-Waterside area of Eastern Dahomey Basin, Southwestern Nigeria. *Geofísica Internacional*, *58*(4), 259–277.

Osinowo, O. O., Agbaje, M. A., & Ariyo, S. O. (2020). Integrated geophysical investigation techniques for mapping cassava effluent leachate contamination plume, at a dumpsite in Ilero, southwestern Nigeria. *Scientific African*, *8*, e00374. https://doi.org/10.1016/j.sciaf.2020.e00374

Oskooi, B. (2006). 1D interpretation of the Magnetotelluric data from Travale Geothermal Field in Italy. *Journal of the Earth and Space Physics*, *32*, 1–16.

Palacky, G. (1988). Resistivity characteristics of geologic targets in electromagnetic methods in applied geophysics. *Society of Exploration Geophysics*, *1*, 53–129.

Park, S. K. (1985). Distortion of magnetotelluric sounding curves by three-dimensional structures. *GEOPHYSICS*, *50(5)*, 785–797.

Park, S., Shin, S., Lee, D. K., Kim, C. R., & Son, J.-S. (2016). *Relationship between Electrical Resistivity and Physical Properties of Rocks*. https://doi.org/10.3997/2214-4609.201602101

Paterson, N. R., & Bosschart, R. A. (1987). Airborne Geophysical Exploration for Ground Water. *Groundwater*, *25*(1), 41–50. https://doi.org/10.1111/j.1745-6584.1987.tb02114.x

Pedersen, L. B. (1991). Relations between potential field and some equivalent sources. *Geophysics*, *56*, 961–971.

Pellerin, L., & Hohmann, G. (1990). Transient electromagnetic inversion: A remedy for magnetotelluric static shifts. *Geophysics*, *55*. https://doi.org/10.1190/1.1442940

Perozzi, L., Guglielmetti, L., & Moscariello, A. (2021). Quantitative uncertainty analysis of gravity disturbance. The case of the Geneva Basin (Switzerland). *Journal of Applied Geophysics*, *193*, 104431. https://doi.org/10.1016/j.jappgeo.2021.104431

Peter, E. A., Alkali, A., & Udensi, E. E. (2017). *DETERMINATION OF THE DEPTH TO MOHOROVICIC DISCONTINUITY IN THE MINNA AREA IN NIGERIA USING BOUGUER GRAVITY DATA*. http://repository.futminna.edu.ng:8080/jspui/handle/123456789/4616

Pirttijarvi, M., Saartenoja, A., & Korkeakangas, P. (2022). Drone-based electromagnetic survey system ... | Open Research Europe. *Earth and Environmental Science Gateway*. https://open-research-europe.ec.europa.eu/articles/2-3

Porsani, J., Filho, W., Shimeles, F., Dourado, J., & Moura, J. (2004). The use GPR and VES in delineating a contaminating plume in a landfill site: A case study in SE Brazil. *Journal of Applied Geophysics*, *55(3-4)*, 199-209.

Pranata, E., Irawati, S. M., & Niasari, S. W. (2017). Magnetotelluric Data Analysis using Swift Skew, Bahr Skew, Polar Diagram, and Phase Tensor: A Case Study in Yellowstone, US. *Pakistan Academy of Sciences*, *54(3)*, 311–317.

Puopiel, F., & Owusu-Ansah, J. (2014). Solid Waste Management in Ghana: The Case of Tamale Metropolitan Area. *Journal of Environment and Earth Science*, *4*.

Rachie, A. (1998). Modelling the time-domain response of AEM systems. *Exploration Geophysics*, *29*, 103–106.

Raji, W. O., & Adeoye, T. O. (2017). Geophysical mapping of contaminant leachate around a reclaimed open dumpsite. *Journal of King Saud University - Science*, *29*(3), 348–359. https://doi.org/10.1016/j.jksus.2016.09.005

Ramalho, E. C., Francés, A. P., Santos, F. M., & Victorino, A. da M. (2023). 3D electrical structure definition of aquifer systems in the Kalahari basin in Southern Angola based on legacy data reprocessing. *Journal of Applied Geophysics*, *211*, 104968. https://doi.org/10.1016/j.jappgeo.2023.104968

Rapti-Caputo, D., & Vaccaro, C. (2006). Geochemical evidences of landfill leachate in groundwater. *Engineering Geology*, *85*(1), 111–121. https://doi.org/10.1016/j.enggeo.2005.09.032

Rathod, M., Mishra, H., & Karmarkar, S. (2013). Leachate Characterization and Assessment of Water Pollution near Municipal Solid Waste Landfill site. *International Journal of Chemical and Physical Science*, *2*, 186–199.

Rehman, F., Harbi, M. H., Azeem, T., Naseem, A. A., Ullah, M. F., Rehman, S. ur, Riaz, O., Rehman, F., & buelnaga, H. S. O. (2021). Shallow geophysical and hydrological investigations to identify groundwater contamination in Wadi Bani Malik dam area Jeddah, Saudi Arabia. *De Gruyter*, *13*, 272–279. https://doi.org/doi.org/10.1515/geo-2020-0176

Reid, A., Allsop, J., Granser, H., Millet, A., & Somerton, I. (1990). Magnetic interpretation in three dimensions using Euler Deconvolurion. *Geophysics, Vol. 55*, 80–91.

Reid, A., Ebbing, J., & Webb, S. (2014). Egregious Euler Errors – The Use and Abuse of Euler Deconvolution Applied to Potential Fields. *Geophysical Prospecting*, *62*. https://doi.org/10.1111/1365-2478.12119

Reynolds, J. M. (2011). *An Introduction to Applied and Environmental Geophysics* (2nd Edition). John Wiley & Sons.

Roch, J. (2007). Airborne Geophysics. *India Geophysical Union*, *11*, 1–28.

Rodriguez, D. B., Deszcz-Pan, M., & Sawyer, A. D. (2001). *Electromagnetic Studies and Subsurface Mapping of Electrical Resistivity in the La Bajada Constriction Area, New Mexico* (1720–F; The Cerrillos Uplift, the La Bajada Constriction, and Hydrogeologic Framework of the Santo Domingo Basin, Rio Grande Rift, New Mexico, p. 27). U.S. Geological Survey.

Romo, J., Flores, C., Vega, R., Vazquez, R., A. Pérez Flores, M., Gómez Treviño, E., J. Esparza, F., E. Quijano, J., & H. García, V. (1997). A closely-spaced magnetotelluric study of the Ahuachapán-Chipilapa geothermal field, El Salvador. *Geothermics*, *26*(5), 627–656. https://doi.org/10.1016/S0375-6505(97)00014-X

Rubin, Y., & Hubbard, S. S. (2005). *Hydrogeophysics.* Springer.

Rung-Arunwan, T., Siripunvaraporn, W., & Utada, H. (2016). On the Berdichevsky average. *Physics of the Earth and Planetary Interiro*, *253*, 1–4.

Saad, R., & Tonnizam, E. (2012). Groundwater Detection in Alluvium Using 2-D Electrical Resistivity Tomography (ERT). *Electronic Journal of Geotechnical Engineering*, *17*.

Saibi, H., Khosravi, S., Cherkose, B. A., Smirnov, M., Kebede, Y., & Fowler, A.-R. (2021). Magnetotelluric data analysis using 2D inversion: A case study from Al-Mubazzarah Geothermal Area (AMGA), Al-Ain, United Arab Emirates. *Heliyon*, *7*(6), e07440. https://doi.org/10.1016/j.heliyon.2021.e07440

Salameh, E. (2021). The Hydrogeological Consequences of the Proposed Extraction of the Deep Groundwater in Jordan. *Journal of Geoscience and Environment Protection*, *9*(8), Article 8. https://doi.org/10.4236/gep.2021.98007

Salem, A., William, S., Fairhead, D., Smith, R., & Ravat, D. (2008). Interpretation of magnetic data using tilt-angle derivatives. *Society of Exploration Geophysics*, *Vol. 7*, 1–10.

Samouëlian, A., Cousin, I., Tabbagh, A., Bruand, A., & Richard, G. (2005). Electrical resistivity survey in soil science: A review. *Soil and Tillage Research*, *83*(2), 173–193. https://doi.org/10.1016/j.still.2004.10.004

Saul, J., Kumar, M. R., & Sarkar, D. (2000). Lithospheric and upper mantle structure of the Indian shield, from teleseismic receiver functions. Geophys. Res. Lett. 27, 2357–2360. *Geophysical Research Letters*, *27*, 2357–2360.

Schulz, B., Sandmann, D., & Gilbricht, S. (2020). SEM-Based Automated Mineralogy and Its Application in Geo- and Material Sciences. *Minerals*, *10*, 1004.

Selway, K. (2014). On the causes of electrical conductivity anomalies in tectonically stable lithosphere. *Survey in Geophysics*, *35*, 219–257.

Sendrós, A., Urruela, A., Himi, M., Alonso, C., Lovera, R., Tapias, J. C., Rivero, L., Garcia Artigas, R., & Casas, A. (2021). Characterization of a Shallow Coastal Aquifer in the Framework of a Subsurface Storage and Soil Aquifer Treatment Project Using Electrical Resistivity Tomography (Port de la Selva, Spain). *Applied Sciences*, *11*, 2448. https://doi.org/10.3390/app11062448

Senos Matias, M., Marques da Silva, M., Ferreira, P., & Ramalho, E. (1994). A geophysical and hydrogeological study of aquifers contamination by a landfill. *Journal of Applied Geophysics*, *32*(2), 155–162. https://doi.org/10.1016/0926-9851(94)90017-5

Severin, P. K. (2004). *Energy Dispersive Spectrometry of Common Rock Forming Minerals*. Kluwer Academic Publishers.

Shahin, M. (2002). Hydrology and Water Resources of Africa. *Kluwer Academic Publishers*.

Shaji, B. (2021). AQUIFER MAPPING USING AEM SKYTEM. *International Journal of Engineering Applied Sciences and Technology*, *6*. https://doi.org/10.33564/IJEAST.2021.v06i03.040

Shao, S., Gao, C., Guo, X., Wang, Y., Zhang, Z., Yu, L., & Tang, H. (2019). Mapping the contaminant plume of an abandoned hydrocarbon disposal site with geophysical and geochemical methods, Jiangsu, China. *Environmental Science and Pollution Research International*, *26*(24), 24645–24657.

Sharma, V. P. (1997). *Environmental and Engineering Geophysics*. Cambridge University Press.

Shawky, H. A., Said, M. M., El-Aassar, A. M., Kotp, Y. H., & Abdel Mottaleb, M. S. A. (2012). *Study the chemical characteristics of groundwater to determine the suitable localities desalination processesin the area between Mersa Alam and Ras Banas, Red sea Coast Eastern Desert, Egypt.*

Siddiqua, A., Hahladakis, J. N., & Al-Attiya, W. A. K. A. (2022). An overview of the environmental pollution and health effects associated with waste landfilling and open dumping. *Environmental Science and Pollution Research*, *29*(39), 58514–58536. https://doi.org/10.1007/s11356-022-21578-z

Siemon, B. (2009). Levelling of helicopter-borne frequency-domain electromagnetic data. *Journal of Applied Geophysics*, *67*(3), 206–218. https://doi.org/10.1016/j.jappgeo.2007.11.001

Siemon, B., Auken, E., & Christiansen, Vest. A. (2009). Laterally constrained inversion of helicopter-borne frequency-domain electromagnetic data. *Journal of Applied Geophysics*, *67*, 259–268.

Siemon, B., Ibs-von Seht, M., Steuer, A., Deus, N., & Wiederhold, H. (2020). Airborne Electromagnetic, Magnetic, and Radiometric Surveys at the German North Sea Coast Applied to Groundwater and Soil Investigations. *Remote Sensing*, *12*(10), Article 10. https://doi.org/10.3390/rs12101629

Silahtar, A., Kanbur, M., & Beyhan, G. (2020). Investigation of a sedimentary basin by using gravity and seismic reflection data in the Isparta basin, southwestern Turkey. *Bulletin of Engineering Geology and the Environment*, *79*. https://doi.org/10.1007/s10064-020-01804-z

Simpson, F., & Bahr, K. (2005). Practical Magnetotellurics. *CambridgeUniversity Press*.

Singh, P. S., Chaubey, S., Dwivedi, D. R., Yadav, R., & Chaurasia, S. K. (2019). Case Study of Solid Waste Management in Gorakhpur city. *Arabian Journal Geoscience*, *7*, 1246–1251.

Slattery, S. R., & Andriashek, L. D. (2012). *Overview of Airborne-Electromagnetic and - Magnetic Geophysical Data Collection Using the GEOTEM® Survey in the Sylvan Lake Area, Central Alberta* (ERCB/AGS Open File Report 2012-08; pp. 18–120).

Smith, J. T. (1995). Understanding telluric distortion matrices. *Gophysics Journal Internation*, *122*, 219–226.

Soussa, H., El Feel, A. A., Alfy, S. Z., & Yousif, M. S. M. (2012). Flood hazard in Wadi Rahbaa area, Egypt . *Arabian Journal Geoscience*, *5*, 45–52.

Spector, A., & Grant, F. S. (1970). Statistical models for interpreting aeromagnetic data. *Geophysics*, *32(2)*, 293–302.

Spratt, J. E., Skulski, T., Craven, J. A., Jones, A. G., Snyder, D. B., & Kiyan, D. (2009). Megnetotelluric investigations of the lithosphere beneath the central Rae craton, mainland Nunavut, Canada. *Journal of Geophysical Research*, *119*, 2415–2439.

Srena, B. F., Gavin, F., Charles, J., & Lemckert, C. (2011). Field and modelling investigations of fresh-water plume behaviour in response to infrequent high-precipitation events, Sydney Estuary, Australia. *Estuarine Coastal and Shelf Science - ESTUAR COAST SHELF SCI*, *92*, 389–402. https://doi.org/10.1016/j.ecss.2011.01.013

St. Johns River Water Management District. (2023). Florida's aquifers. *SJRWMD*. https://www.sjrwmd.com/water-supply/aquifer/

Stagpoole, V. M., Bennie, S. L., Bibby, H. M., Dravitzki, S., & Ingham, M. R. (2009). Deep structure of a major subduction back thrust: Magneto-telluric investigations of the Taranaki Fault, New Zealand. *Tectonophysics*, *463*(1), 77–85. https://doi.org/10.1016/j.tecto.2008.09.035

Stavrev, P., & Reid, A. (2007). Degrees of homogeneity of potential fields and structural indices of Euler deconvolution. *GEOPHYSICS*, *72*(1), L1–L12. https://doi.org/10.1190/1.2400010

Stephen, J., Gokarn, S. G., Manoj, C., & Singh, S. B. (2003). Effects of galvanic distortions on magnetotelluric data: Interpretation and its correction using deep electrical data. *NAtional Geopysical Research Institute*, *112*, 27–36.

Sternberg, B. K., Washburne, J. C., & Pellerin, L. (1988). Correction for the static shift in magnetotellurics using transient electromagnetic soundings | GEOPHYSICS. *GEOPHYSICS*, *53*(11). https://library.seg.org/doi/10.1190/1.1442426

Sumanovac, F. (2012). *Magnetotelluric method in the exploration of deep aquifers.* 3–5.

Swift, C. M. (1967). *A magnetotelluric investigation of an electrical conductivity anomaly in the southwestern United States* [Thesis, Massachusetts Institute of Technology, Dept. of Geology and Geophysics]. http://hdl.handle.net/1721.1/38346

Talwani, M., & Hiertzler, J. R. (1964). Computation of magnetic anomalies caused by two dimensiona bodies of arbitrary shape. *Geological Science*, *9*, 464–480.

Talwani, M., Worzel, J. L., & Landisman, M. (1959). Rapid gravity computations for 2 dimensional bodies with application to the Mendocino submarine fracture zone. *Journal of Geological Research*, *64*, 49–59.

Tarits, P. (1986). Conductivity and fluids in oceanic upper mantle. *Physics of the Earth and Planetary Interiors*, *42*, 215–226.

Telford, W. M., Geldart, L. P., & Sheriff, R. E. (1990, October 26). *Applied Geophysics*. Higher Education from Cambridge University Press; Cambridge University Press. https://doi.org/10.1017/CBO9781139167932

Thaw, M., GebreEgziabher, M., Villafañe-Pagán, J. Y., & Jasechko, S. (2022). Modern groundwater reaches deeper depths in heavily pumped aquifer systems. *Nature Communications*, *13*(1), Article 1. https://doi.org/10.1038/s41467-022-32954-1

Thomas, S., Fountain, D., & Watts, T. (2007). Airborne Geophysics-Evolution and Revolution. *Proceedings of Exploration 07: Fifth Decennial Internation Conference on Mineral Exploration*, 19–37.

Thompson, D. (1982). EULDPH: A new technique for making computer-assisted depth estimated from magnetic data. *Geophysics*, *Vol. 47*, 31–37.

Tian, J., Ye, G., Ding, Z., Wu, Q., Wei, W., Jin, S., & Xie, C. (2019). A study of the deep electrical structure of the northern segment of the Tan Lu fault zone, NE China. *Journal of Asian Earth Sciences*, *170*, 118–127.

Tinivella, U., Giustiniani, M., & Cassiani, G. (2013). Geophysical Methods for Environmental Studies. *International Journal of Geophysics*, *2013*, e950353. https://doi.org/10.1155/2013/950353

Tripathi, K., & Dwivedi, A. K. (2021). Impact of dumping on groundwater: A review. *International Journal of Creative Research Thoughts (IJCRT)*, *9*, 2320–2882.

Tuğrul, A., & Zarif, I. H. (1999). Correlation of mineralogical and textural characteristics with engineering properties of selected granitic rocks from Turkey. *Engineering Geology*, *51*(4), 303–317. https://doi.org/10.1016/S0013-7952(98)00071-4

Twort, A. C., Ratnayaka, D. D., & Brandt, M. J. (Eds.). (2000). 4—Groundwater supplies. In *Water Supply (Fifth Edition)* (pp. 114–II). Butterworth-Heinemann. https://doi.org/10.1016/B978-034072018-9/50006-0

Vadoodi, R., & Rasmussen, T. M. (2022). Joint Interpretation of Magnetotelluric and Potential Field Data From North-Eastern Norrbotten, Sweden. *Pure and Applied Geophysics*, *179*(3), 1069–1088. https://doi.org/10.1007/s00024-022-02959-4

Vanegas-Espinosa, L. I., Vargas-Del-Río, D., Ochoa-Covarrubias, G., & Grindlay, A. L. (2022). Flood Mitigation in Urban Areas through Deep Aquifer Recharge: The Case of

the Metropolitan Area of Guadalajara. *International Journal of Environmental Research and Public Health*, *19*(6), 3160. https://doi.org/10.3390/ijerph19063160

Vaudelet, P., Schmutz, M., Pessel, M., Franceschi, M., Guérin, R., Atteia, O., Blondel, A., Ngomseu, C., Galaup, S., Rejiba, F., & Bégassat, P. (2011). Mapping of contaminant plumes with geoelectrical methods. A case study in urban context. *Journal of Applied Geophysics*, *75*(4), 738–751. https://doi.org/10.1016/j.jappgeo.2011.09.023

Veeraswamy, K., Azeez, K. K. A., Patro, P. K., Gupta, A. K., & Babu, N. (2020). Electrical resistivity structure across the Jaisalmer Basin (Rajasthan, NW India) derived from magnetotelluric data: Inferences on basin architecture and basement morphology. *Journal of Applied Geophysics*, *181*, 104147. https://doi.org/10.1016/j.jappgeo.2020.104147

Vest Christiansen, A., & Auken, E. (2012). A global measure for depth of investigation. *GEOPHYSICS*, *77*(4), WB171–WB177. https://doi.org/10.1190/geo2011-0393.1

Viezzoli, A., Tosi, L., Teatini, P., & Silvestri, S. (2010). Surface water–groundwater exchange in transitional coastal environments by airborne electromagnetics: The Venice Lagoon example. *Geophysical Research Letters*, *37*(1). https://doi.org/10.1029/2009GL041572

Vignoli, G., Cassiani, G., Rossi, M., Deiana, R., Boaga, J., & Fabbri, P. (2012). Geophysical characterization of a small pre-Alpine catchment | Elsevier Enhanced Reader. *Journal of Applied Geophysics*, *80*, 32–42. https://doi.org/10.1016/j.jappgeo.2012.01.007

Vignoli, G., Fiandaca, G., Christiansen, A. V., Kirkegaard, C., Auken, E., Vignoli, Fiandaca, Christiansen, A. V., Kirkegaard, & Auken. (2015). Sharp spatially constrained inversion with applications to transient electromagnetic data. *Geophysical Prospecting*, *63*(1), Article 1. https://doi.org/10.1111/1365-2478.12185

Viljanen, A. (2012). 3B. Description of the magnetospheric/ionospheric sources. In A. D. Chave & A. G. Jones (Eds.), *The Magnetotelluric Method: Theory and Practice* (pp. 96–121). Cambridge University Press. https://doi.org/10.1017/CBO9781139020138.005

Vozoff, K. (1972). The magnetotelluric method in the exploration of sedimentary basins. *Geophysics*, *37*, 980–1041.

Vozoff, K. (1990). Magnetotelluric: Principles and practice. *Indian Academy of Science, 99(4)*, 441–471.

Wagner, F. M., & Uhlemann, S. (2021). Chapter One—An overview of multimethod imaging approaches in environmental geophysics. In C. Schmelzbach (Ed.), *Advances in Geophysics* (Vol. 62, pp. 1–72). Elsevier. https://doi.org/10.1016/bs.agph.2021.06.001

Wahaab, F. A., Lawal, S. K., & Adebayo, L. L. (2017). *Spectral Analysis of Higher Resolution Aeromagnetic Data over Some Part of Kwara State, Nigeria*. *Vol. 6*(Issue 03), 2278–0181.

Waldron, W. F. J., & Snyder, M. (2020). *Geological Structures: A Practical Introduction*. Pressbooks.

Wannamaker, P. E., Hasterok, D. P., Johnston, J. M., Stodt, J. A., Hall, D. B., Sodergren, T. L., Pellerin, L., Maris, V., Doerner, W. M., Groenewold, K. A., & Unsworth, M. J. (2008). Lithospheric dismemberment and magmatic processes of the Great Basin–Colorado Plateau transition, Utah, implied from magnetotellurics. *Geochemistry, Geophysics, Geosystems*, *9*(5). https://doi.org/10.1029/2007GC001886

Wannamaker, P. E., Hohmann, G. W., & Ward, S. H. (1984). Magnetotelluric response of three-dimensional bodies in layered earth. *GEOPHYSICS, 49(9)*, 1517–1533.

Water Resource Commission, W. (2011). *Final Technical Report: Hydrogeological Assement of the Northern Region of Ghana Project (HAP).* Water resource commission.

Webster, R. J., Kight, P. R., Winburn, S. R., & Cool, A. C. (2003). HEAVY MINERAL ANALYSIS OF SANDSTONES BY RIETVELD ANALYSIS. *International Center for Diffraction Data*, *46*, 198.

WHO, W. H. O. (2022). *Guidelines for drinking-water quality*. (pp. 240–265). World Health Organization.

Wiederhold, H., Kallesøe, A. J., Kirsch, R., Mecking, R., Pechnig, R., & Skowronek, F. (2021). Geophysical methods help to assess potential groundwater extraction sites. *Grundwasser*, *26*(4), 367–378. https://doi.org/10.1007/s00767-021-00495-x

Wijekoon, P., Koliyabandara, P. A., Cooray, A. T., Lam, S. S., Athapattu, B. C. L., & Vithanage, M. (2022). Progress and prospects in mitigation of landfill leachate pollution: Risk, pollution potential, treatment and challenges. *Journal of Hazardous Materials*, *421*, 126627. https://doi.org/10.1016/j.jhazmat.2021.126627

Wilson, M. J. (1994). Clay mineralogy: Spectroscopic and chemical determinative methods. *Chapman and Hall, London, ISBN: 9780412533808*.

Won, I. J., & Bevis, M. (1987). Computing the gravitational and magnetic anomalies due to a polygon: Algorithms and Fortran subroutines. *Geophysics*, *52*, 232–238.

Yadav, K., Shah, M., & Sircar, A. (2020). Application of magnetotelluric (MT) study for the identification of shallow and deep aquifers in Dholera geothermal region. *Groundwater for Sustainable Development*, *11*, 100472. https://doi.org/10.1016/j.gsd.2020.100472

Yan, B., Qiu, S., Xiao, C., & Liang, X. (2019). Characteristics of Mineral Fluids and Geothermal Reservoir in Changbai Mountain, Northeast of China. *Geochemistry International*, *57*, 83–97. https://doi.org/10.1134/S0016702919010038

Yaramanci, U., Lange, G., & Hertrich, M. (2002). Aquifer characterization using surface NMR jointly with other geophysical techniques at the Nauen/Berlin test site. *Journal of Applied Geophysics*, *50*, 47–65. https://doi.org/10.1016/S0926-9851(02)00129-5

Ye, X., Yu, Z., Zhang, Y., Kang, J., Wu, S., Yang, T., & Gao, P. (2022). Mineral Composition Impact on the Thermal Conductivity of Granites Based on Geothermal Field Experiments in the Songliao and Gonghe Basins, China. *Minerals*, *12*(2), Article 2. https://doi.org/10.3390/min12020247

Yidana, S. M., Banoeng-Yakubo, B., Aliou, A.-S., & Akabzaa, T. M. (2012). Groundwater quality in some Voltaian and Birimian aquifers in northern Ghana—Application of mulitvariate statistical methods and geographic information systems. *Hydrological Sciences Journal*, *57*(6), 1168–1183. https://doi.org/10.1080/02626667.2012.693612

Yidana, S. M., Dzikunoo, E. A., Aliou, A. S., Adams, R. M., Chegbeleh, L. P., & Anani, C. (2020). The geological and hydrogeological framework of the Panabako, Kodjari, and Bimbilla Formations of the Voltaian Supergroup—Revelations from groundwater hydrochemical data. *Applied Geochemistry*, *115*, 104533.

Yidana, S., Yiran, G., Sakyi, P., Nude, P., & Banoeng-Yakubo, B. (2011). Groundwater evolution in the Voltaian basin, Ghana-an application of multivariate analyses to hydrochemical data. *Natural Science*, *3*, 837–854.

Yousef, A. F., Salem, A. A., Baraka, A. M., & Aglan, O. sh. (2009). The impact of geological setting on groundwater occurrence in some Wadis in Shalatein—Abu Ramad Area, South Eastern Desert, Egypt. *European Water Resource Association*, *25 (26)*, 53–68.

Yusuf, T. U. (2016). *Overview of Effective Geophysical Methods Used in the Study of Environmental Pollution by Waste Dumpsites.* (41; African Research Review, pp. 123–143). College of Agriculture, Mokwa, Niger state.

Zaru, N., Rossi, M., Vacca, G., & Vignoli, G. (2023). Spreading of Localized Information across an Entire 3D Electrical Resistivity Volume via Constrained EMI Inversion Based on a Realistic Prior Distribution. *Remote Sensing*, *15*(16), Article 16. https://doi.org/10.3390/rs15163993

Zayed, A. M. (2021). Geoeletrical exploration of groundwater by using vertical eletrical sounding technique at Wadi Morra, south Sinai, Egypt. *Austin Publishing Group*, *4*, 1025.

Zhang, W., Sun, Q., Hao, S., Geng, J., & Lv, C. (2016). Experimental study on the variation of physical and mechanical properties of rock after high temperature treatment. *Applied Thermal Engineering*, *98*, 1297–1304. https://doi.org/10.1016/j.applthermaleng.2016.01.010

CHAPTER SIX

INVESTIGATING NEAR-SURFACE SUBSURFACE STRUCTURES USING HIGH FREQUENCY MT AND BOREHOLE GEOPHYSICAL LOG DATA

6.0 INTRODUCTION

The interpretation of the first MT data presented in Chapter Five revealed several subsurface structures at varying depths including features interpreted as a fractured aquifer that appeared to be hydraulically connected to a surface stream via some shallow sub-vertical structures. Based on this relationship a second field survey with more localized intent was designed to utilize high frequencies MT to optimize relatively shallow subsurface structures and precisely defining the geometry of the shallow structures at the northern part of the study area (Figure 6.1). The hydrogeologic characteristics of subsurface structures make application of geophysical techniques such as MT suitable. As an electromagnetic technique that leverages the natural time variations of the Earth's magnetic and electrical field (Vozoff, 1990), it is sensitive to temperature, porosity, permeability, with the presence of fluids (Manzella et al., 2004) and therefore can effectively delineate steeply dipping subsurface structures (Hazell et al., 1988). The use of high-frequency measurements enables the acquisition of good-resolution data of near-surface characteristics. This will ensure effective and proper interpretation of the data and delineation of shallow structures if any. Delineating structural entities which could likely constitute productive aquifers at much shallower surfaces will be much more important in the rural areas as it may be cost effective in terms of drilling. The knowledge of such structural characteristics will help to understand and develop a more sustainable groundwater management plan for the basin. In most rural communities in northern Ghana, the main economic activities are crop cultivation and the rearing of animals. These activities are being encouraged by both the government and non-governmental organizations (NGOs) as a poverty reduction measure as a means to improve the livelihood of rural communities. The challenge to the realization of this policy in the northern part of the Voltaian basin however is the lack of reliable sources of water. Most surface water sources in the basin are ephemeral while rainfall patterns are erratic due to the impact of climate change. Groundwater therefore remains the only reliable alternative in the face of depleting surface water sources and unreliable precipitation (Adam & Appiah-Adjei, 2019). However, groundwater development in the basin has not been successful due to the use of what is refer to as conventional groundwater siting techniques (Ewusi et al., 2020). In hard rock terrain where the occurrence of groundwater is largely controlled by discrete fractures, conventional techniques such as the electrical resistivity method and EM-34 are ineffective (Chegbeleh et al., 2009). The electrical resistivity method is

useful for delineating groundwater zones but broad current electrode spacing is required to penetrate deep. Whereas the EM-34 can detect steeply dipping fractures but limited in penetration depth. The use of state-of-the-art deep penetrating geophysical technique with the ability to detect steeply dipping fractures such as the MT will therefore be appropriate in delineating good potential zones for groundwater development in the basin.

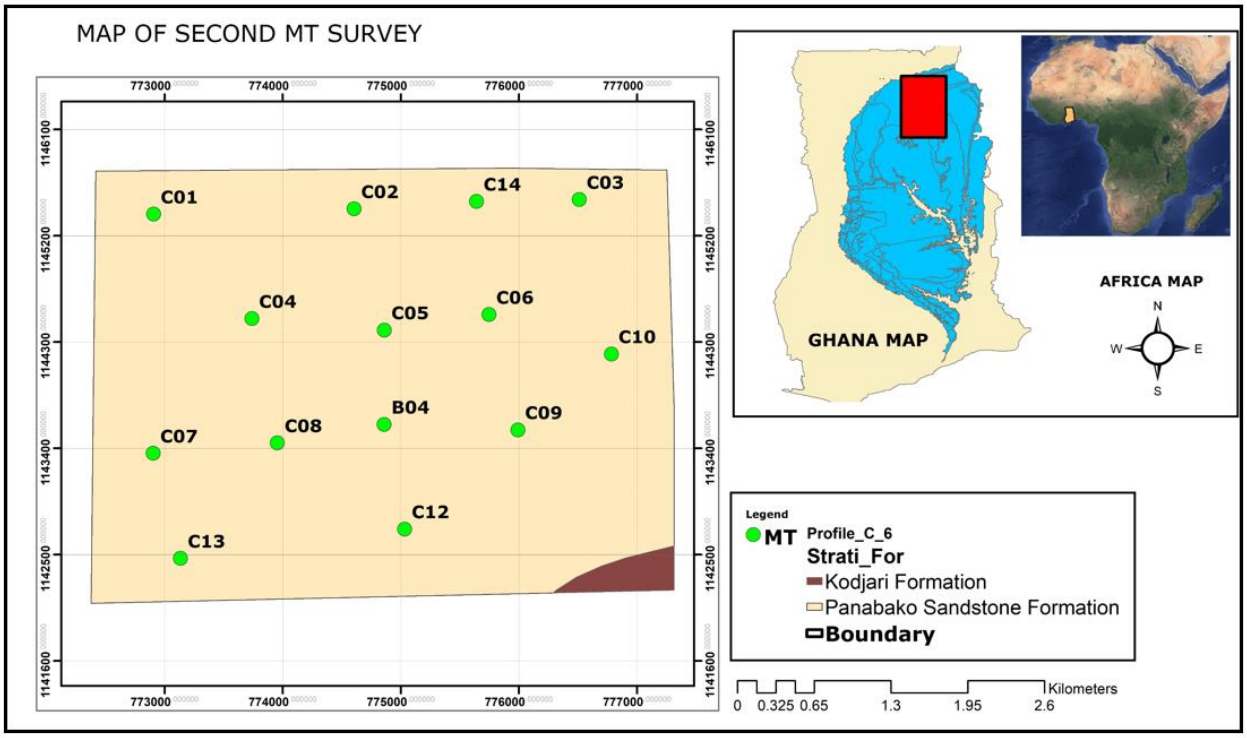

Figure 6. 1: Geological map showing locations of MT stations with inset map of Africa and Ghana (blue color represents the voltaian basin and red rectangle represent study area).

The objective of this work is to utilize high frequency data of the MT survey to investigate and map discrete fractures with good potential for groundwater development in the hard rock Voltaian sedimentary basin in the northern part of Ghana. This current work is a follow up study on the findings of first MT campaign that suggested a possible connection between a surface stream and a potential contact fracture observed at relatively deeper depth (Chapter Four) in the area. The relatively deep contact fracture trending N-S appeared to truncate towards south of the area prompted further campaign to investigate and to attempt to delineate the geometry of possible aquifers around the fracture.

6.1 DATA ACQUISITION AND PROCESSING

The procedure for the data acquisition and processing followed precisely the format as in the first survey which is discussed in the previous chapters (Chapter 2 and 5). This current survey

was conducted between March to April 2023 with the MT stations at regular intervals of approximately 1 Km throughout the area (Figure 6.1). The MT measurements were performed simultaneously with two ADU-08e acquisition systems synchronized by a GPS clock. The simultaneous recording of the data allows for remote referencing during data processing (Gamble et al., 1979). The recording lasted for about 12 hours at each site. The quality of most of the data collected was good except for stations C02, and C03 (Figure 6.2) which were affected by some cultural noise. The observed noise in the sites mentioned could be attributed to the location of the stations situated close to feeder roads on which there is a constant movement of vehicles and motorcycles. The noise produces characteristic offsets in both apparent resistivity and phase within the frequency range of 100 – 1000 Hz and were removed prior to the inversion modeling to avoid incorrect geological interpretations.

6.1.1 Dimensionality of the MT data

Most of the measured field data shown in Figure 6.3 exhibit fairly 1-D and 3-D characters with the off-diagonal components of the impedance tensor showing high values of apparent resistivity except for periods less than one second across all sites. Multiple sites exhibit 1-D at short periods (less than 1s) but for the long periods the patterns revealed are more likely an origin caused by regional 3D features. The resulting apparent resistivity and phases follow consistent curves, with standard errors reflecting the presence of noise observed in some sites. The apparent resistivity and phase data shown in Figure 6.2 are typical of all the measurement sites for the survey and suggest a conductive layer lying on a resistive layer underneath. The curves of apparent resistivity and phase typically separate at periods of about 1s due to the influence of distant 3D structure.

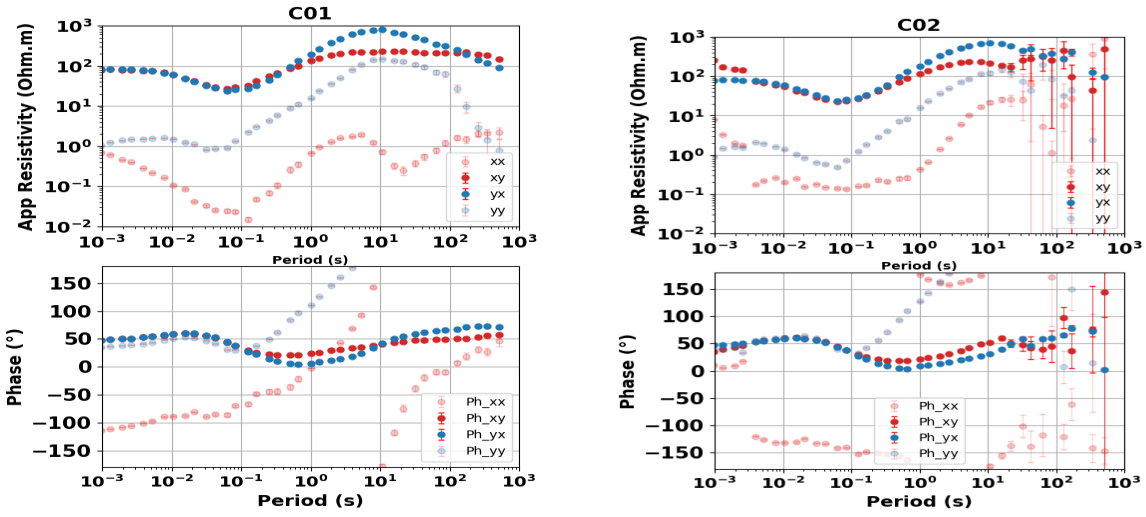

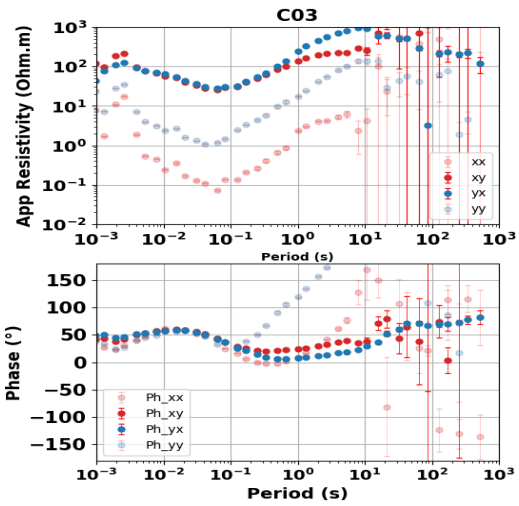
C03
App Resistivity (Ohm.m)
xx
xy
yx
yy
Period (s)
Phase (°)
Ph_xx
Ph_xy
Ph_yx
Ph_yy
Period (s)

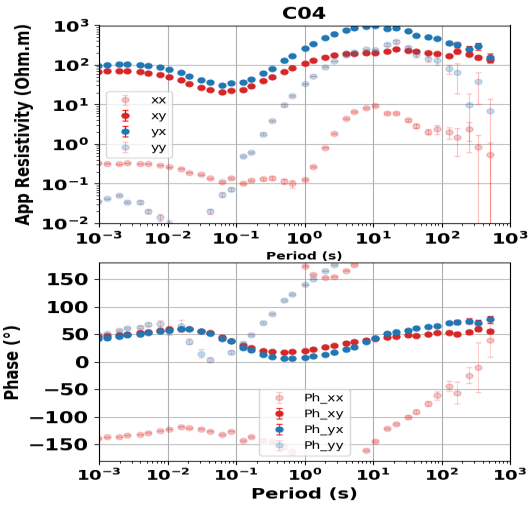
C04
App Resistivity (Ohm.m)
xx
xy
yx
yy
Period (s)
Phase (°)
Ph_xx
Ph_xy
Ph_yx
Ph_yy
Period (s)

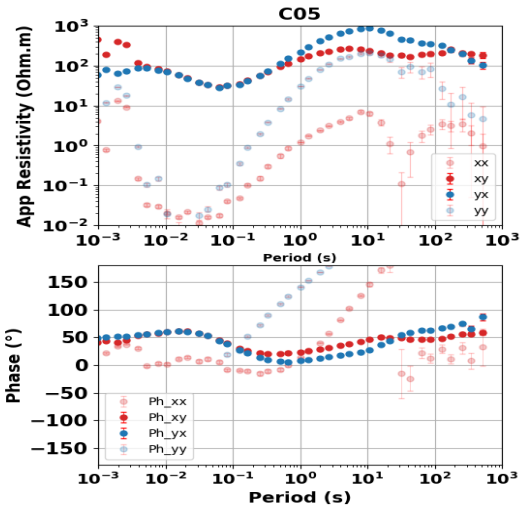
C05
App Resistivity (Ohm.m)
xx
xy
yx
yy
Period (s)
Phase (°)
Ph_xx
Ph_xy
Ph_yx
Ph_yy
Period (s)

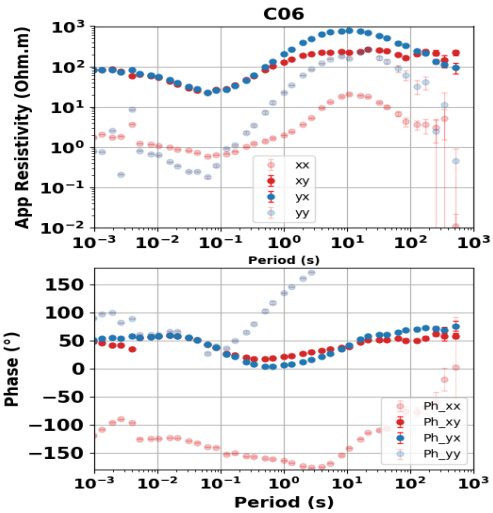
C06
App Resistivity (Ohm.m)
xx
xy
yx
yy
Period (s)
Phase (°)
Ph_xx
Ph_xy
Ph_yx
Ph_yy
Period (s)

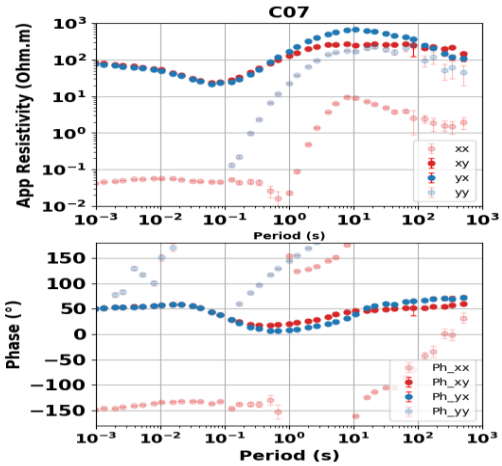
C07
App Resistivity (Ohm.m)
xx
xy
yx
yy
Period (s)
Phase (°)
Ph_xx
Ph_xy
Ph_yx
Ph_yy
Period (s)

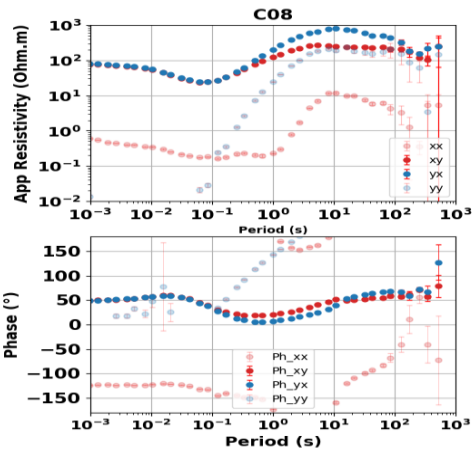
C08
App Resistivity (Ohm.m)
xx
xy
yx
yy
Period (s)
Phase (°)
Ph_xx
Ph_xy
Ph_yx
Ph_yy
Period (s)

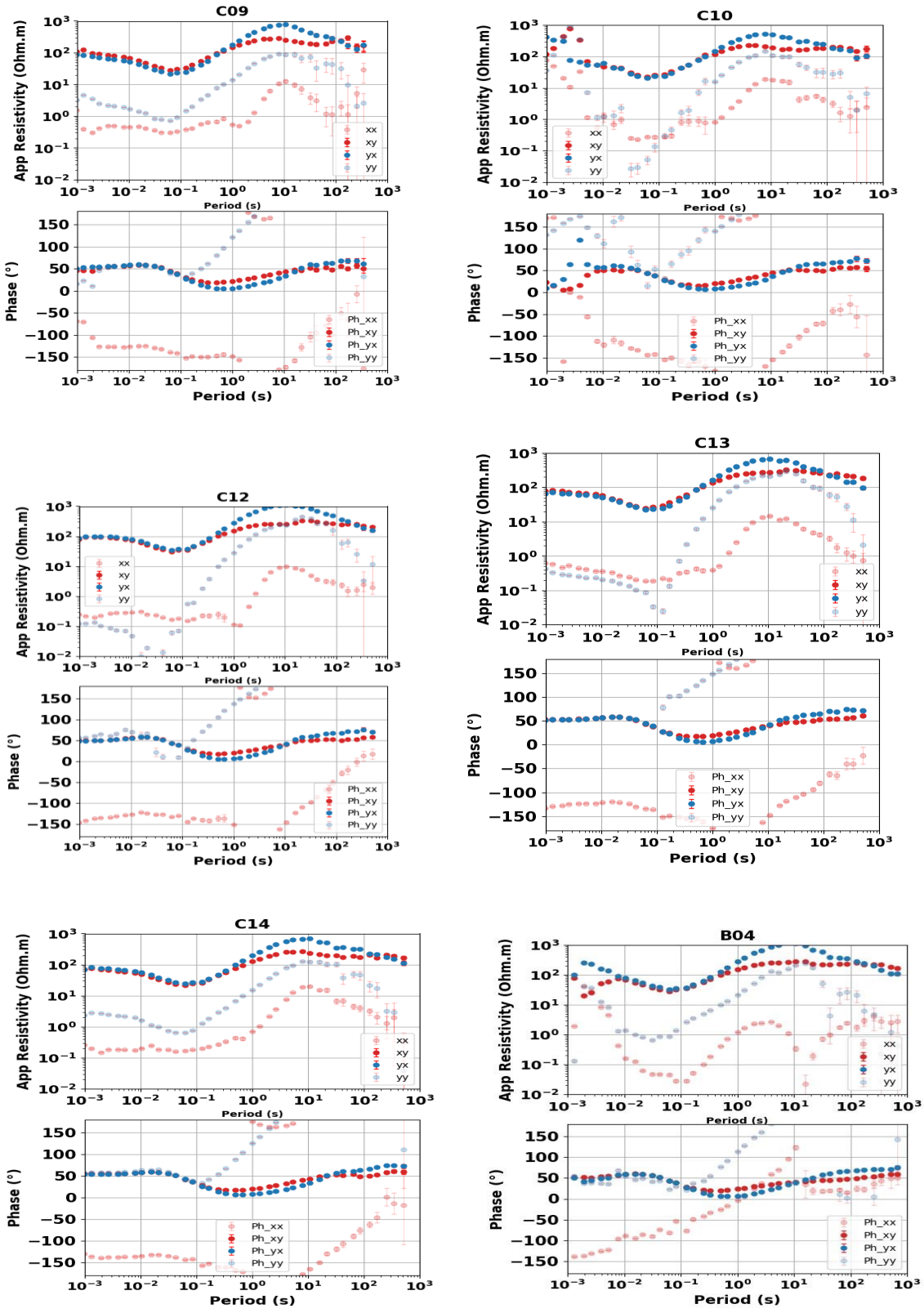

Figure 6. 2: Impedance tensor of all 14 sites with diagonal components: xx and yy represented by dull colors and off-diagonal components: xy and yx, represented by bright colors). The amplitudes expressed as resistivity and phases are plotted against period at each site.

The Swift skew (Swift, 1967) and Bahr skew (Bahr, 1988) were used to investigate the dimensionality of the subsurface resistivity structure. The skew values calculated for both Swift and Bahr skew are shown in Figure 6.3. The Swift skew analysis returned most values less than 0.3 and only a few are more than 0.3, indicating 1-D and 3-D features. The Bahr skew (Phase sensitive skew) on the other hand produced results which were mostly over 0.3 and a few times below 0.3, indicating the presence of 3-D character of the resistivity structure. Following the understanding of the dimensionality of the resistivity structure, the data was inverted in 3-D to describe the general structure and in 1-D to locally improve the vertical resolution.

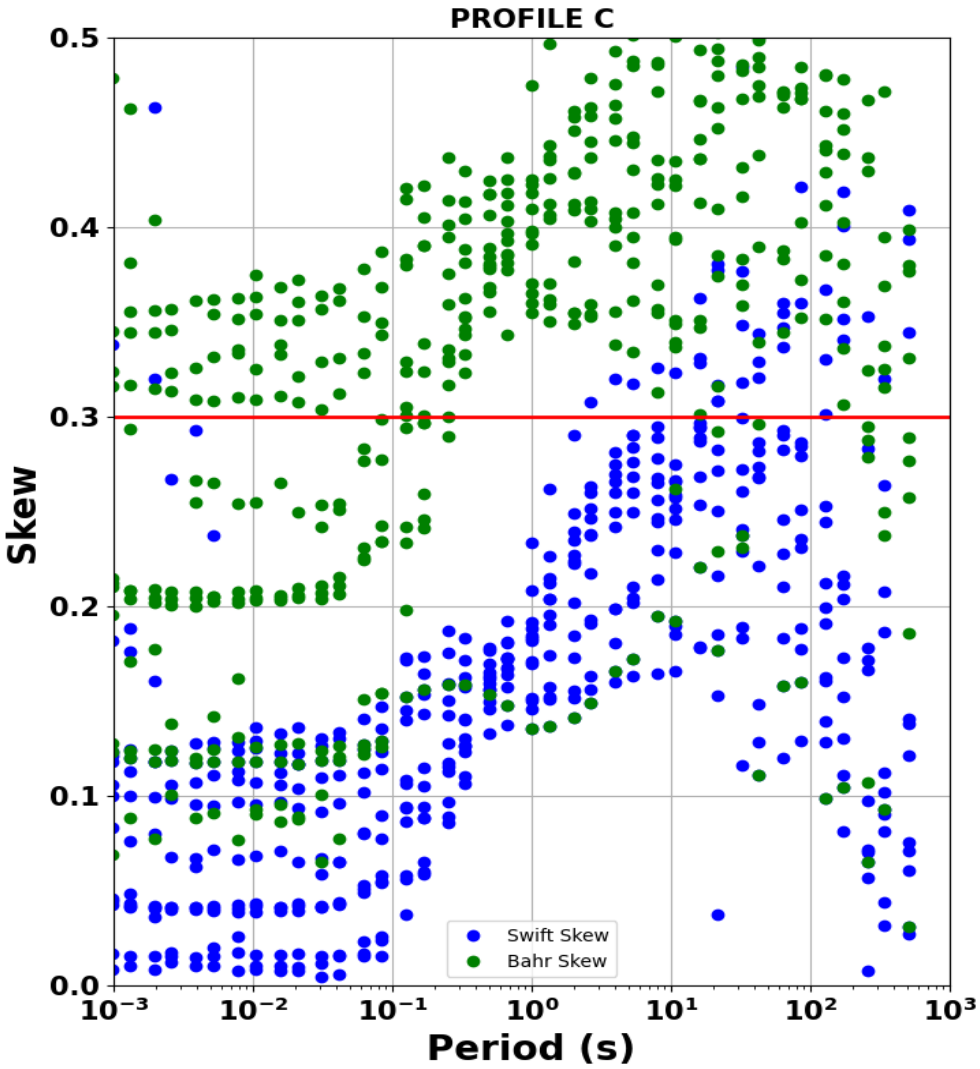

Figure 6. 3: A plot showing skewness as a measure of dimensionality of the MT data. Red straight line indicates the threshold for the determination of dimensionality. Blue and green dots represent Swift and Bahr skew respectively.

6.1.2 Inversion of MT data

The details of the procedure for inverting the data in 1-D and 3-D have already been discussed in the Chapter two. However, this survey was designed in a 3-D array with focus on high frequency part of the data to optimized good resolution of subsurface structures at near surface. A total of 14 sites were inverted with a minimum horizontal grid dimension of 400 x 400 m and a total depth 7 km (Figure 6.4).

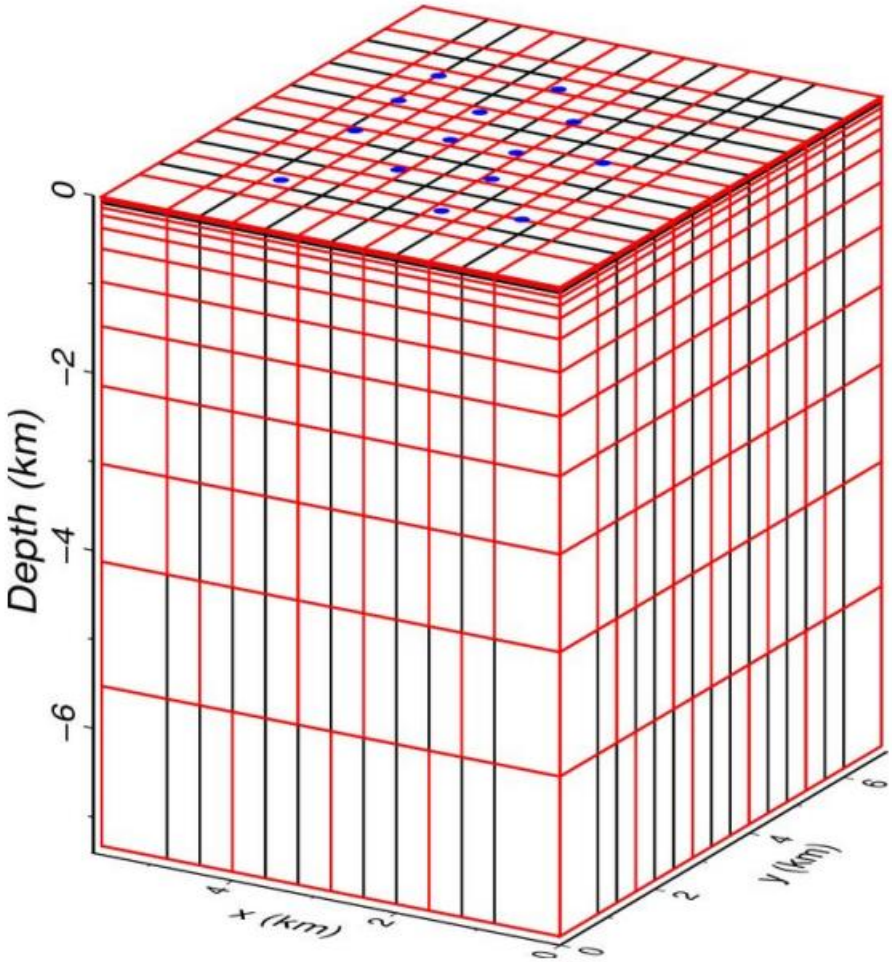

Figure 6. 4: 3-D grid showing model dimensions with blue dots at the showing MT array used for the survey.

An initial homogeneous half space model of 100 Ωm was used for the modeling reducing the initial root mean square (rms) error from 16.1 to 2.8 indicating good fit between observed data and computed model (Figure 6.5). All four components of the MT impedance were inverted simultaneously at periods between 1/3072 – 64 seconds. Given that the aim of the study was to get good resolution in the near surface, longer periods were not considered in the present work. Depth slices as well as vertical cross sections through the 3-D model are shown and discussed

in the next section (Figure 6.6). The 1-D inversion was obtained using the average of the determinant of the impedance as explained in chapter two. The 1-D results were again validated by the robust 3-D inversion results.

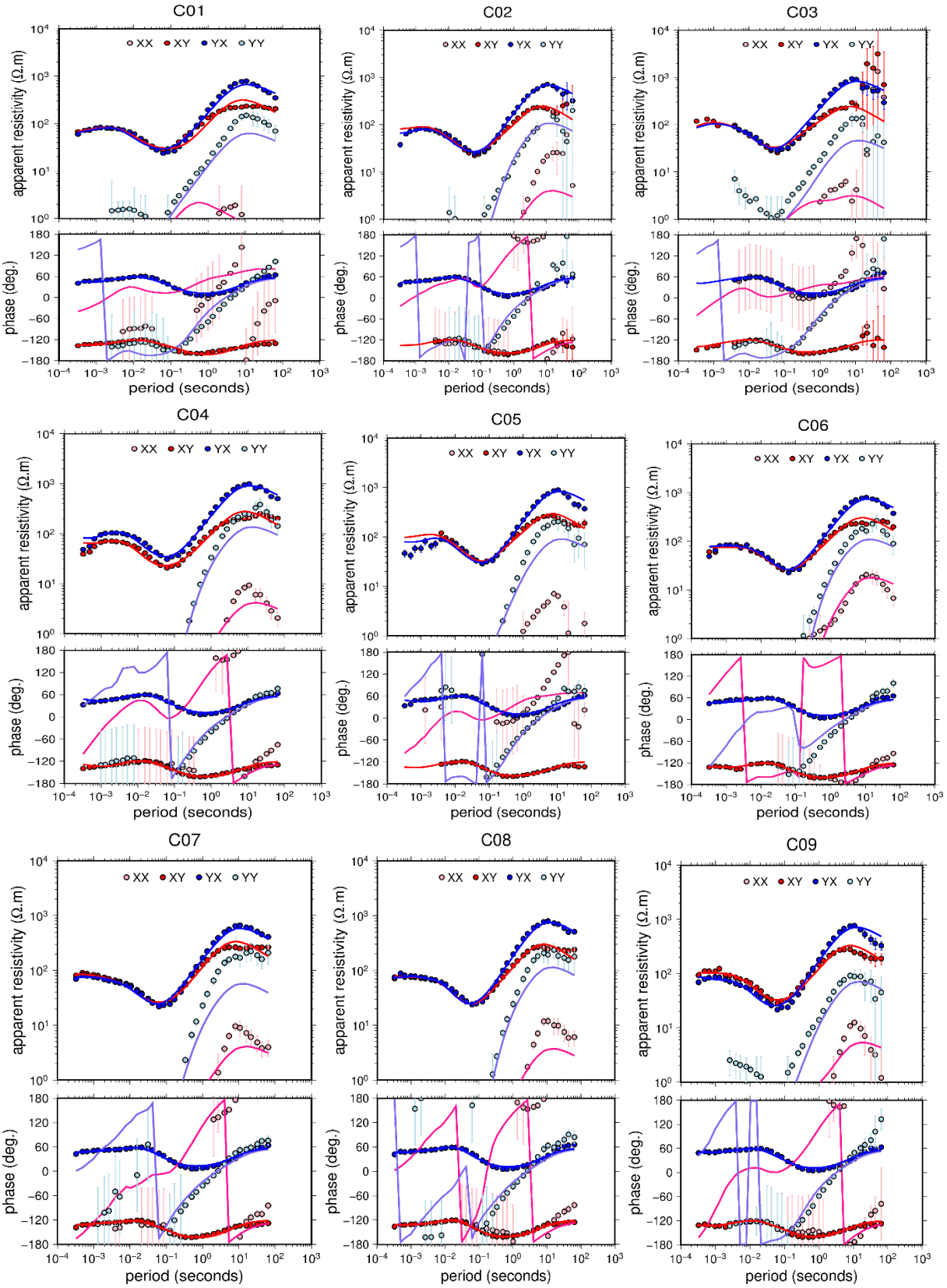

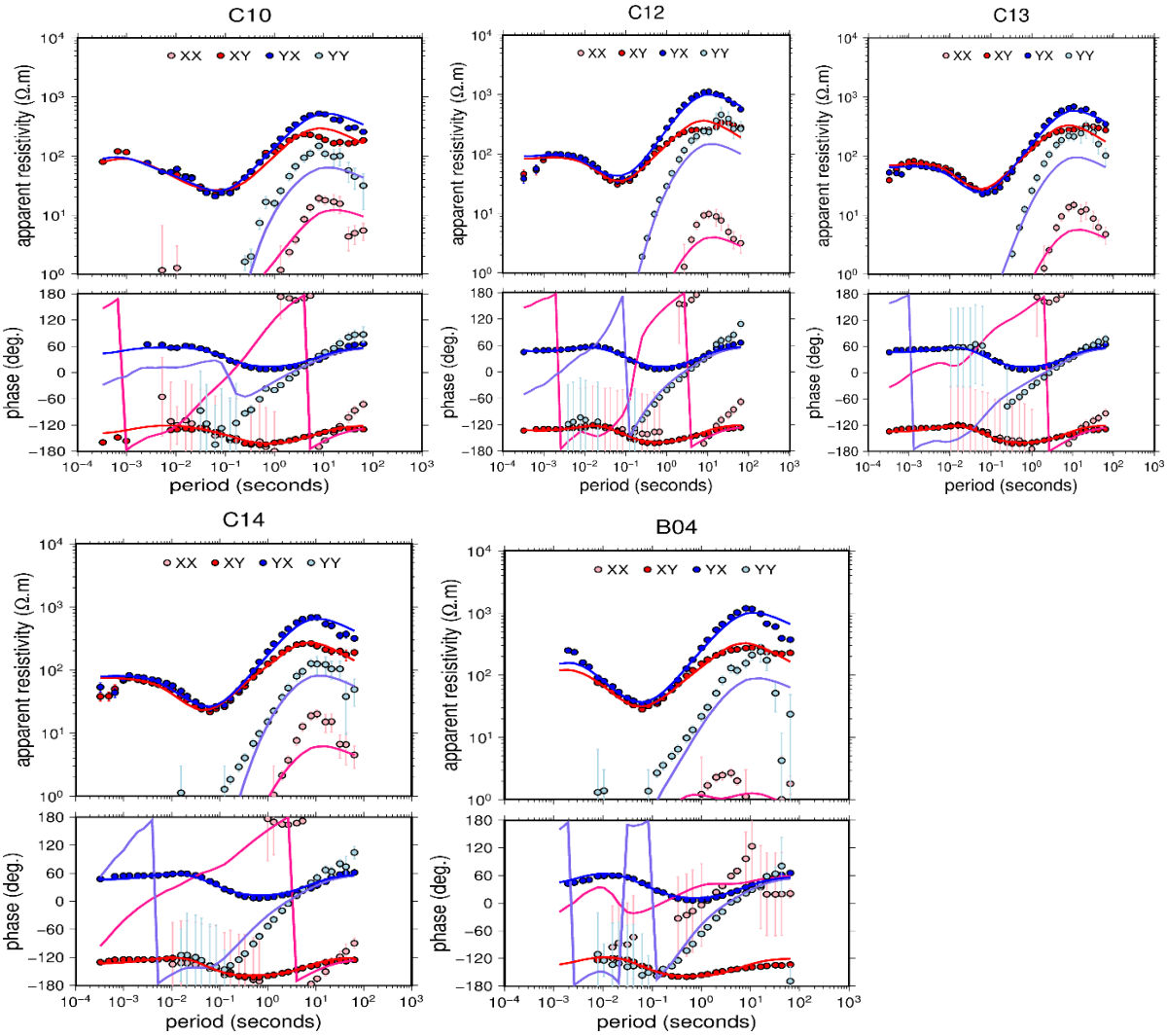

Figure 6. 5: Comparison between observed data (dots) and 3-D model response (solid lines) of apparent resistivity and phases for all components of the MT tensor for all 14 sites.

6.2 RESULTS AND DISCUSSION

The 3-D geophysical inversion of the MT data yielded horizontal slices at varied depths as well as vertical cross-sections for qualitative evaluation of subsurface lithological succession for the investigated terrain as shown in Figure 6.6 and 6.7. The horizontal depth slices and sections show variations in resistivity signatures often interpreted as lithology and/or clay content produced by weathering of rock minerals as well as subsurface structural entities containing pore fluids. The models exhibit the true resistivity distribution of the subsurface with strong spatial correlation with the known localized geology underlying the MT sites. The spatial variability in resistivity signatures with geology reflect the physical properties of rocks of the subsurface. In Figure 6.7, the first 0.7 Km reflects the sedimentary basin with a level of accuracy that is satisfactory and matches the lithostratigraphic thickness estimated for the area

(Apesegah, 2008; Carney et al., 2010; Dzikunoo et al., 2020). The sedimentary cover consists of three distinct strata resting unconformably on a highly resistive Paleoproterozoic basement. The sedimentary rocks of the basin have lost nearly their primary porosity and permeability as a consequence of sedimentary process such as consolidation and cementation (Chegbeleh et al., 2009; Dapaah-Siakwa & Gyau-Boakye, 2000) and some episodes of partial metamorphism that affected the area (Kesse, 1985). As a result, the occurrence and storage of groundwater in the basin is aided mostly by discrete structural entities such as faults, joints and lithological contacts as well as weathering rock minerals.

According to Carney et al (2010) the surface geology underlying the research area is the Panabako sandstone formation (Figure 6.1) which has an average thickness of about 200 m. In some parts of the basin, the Panabako sandstones forms a hardpan of lateritic material on the surface associated with weathering of sandstones in such climatic regions. The impermeable lateritic layer prevents infiltration of water during rainfall. This layer in addition to the consolidated nature of the formation sediments has resulted in high resistivity readings of the sandstones (Agyekum et al., 2013; Dzikunoo et al., 2020; Jordan et al., 2009). Therefore, potential groundwater zones will be areas indicating low resistivity signatures as such areas could be related to fractures or claystone described as possible aquifers in the area (Aliou et al., 2022). The range of resistivity values observed in the models varies from <10 Ωm to >1000 Ωm. Four units of resistivity can be identified in the 3-D models.

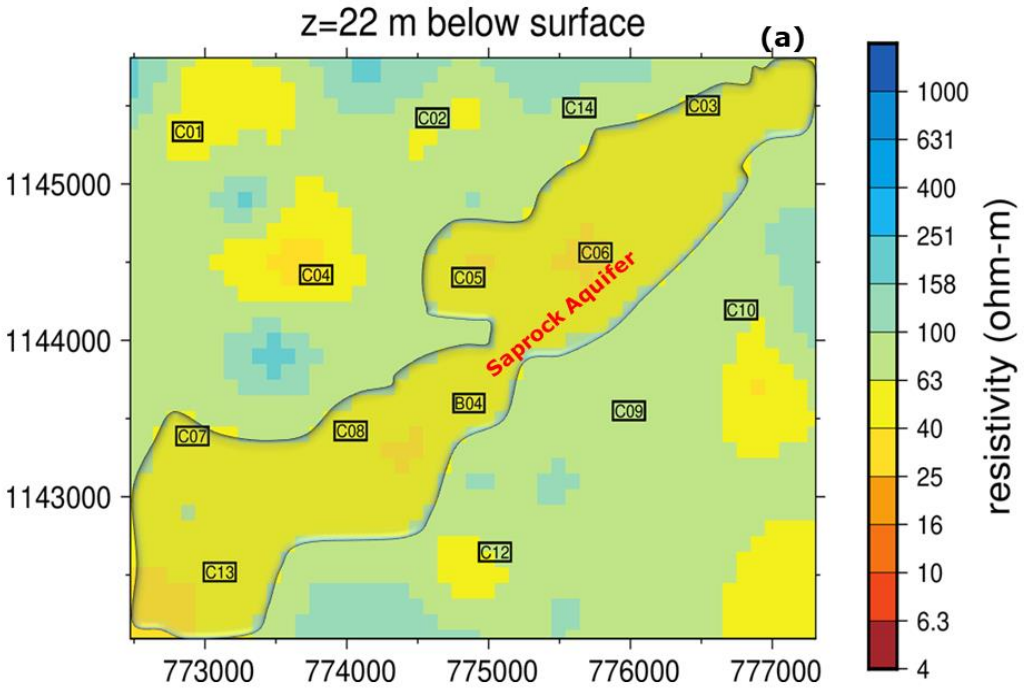

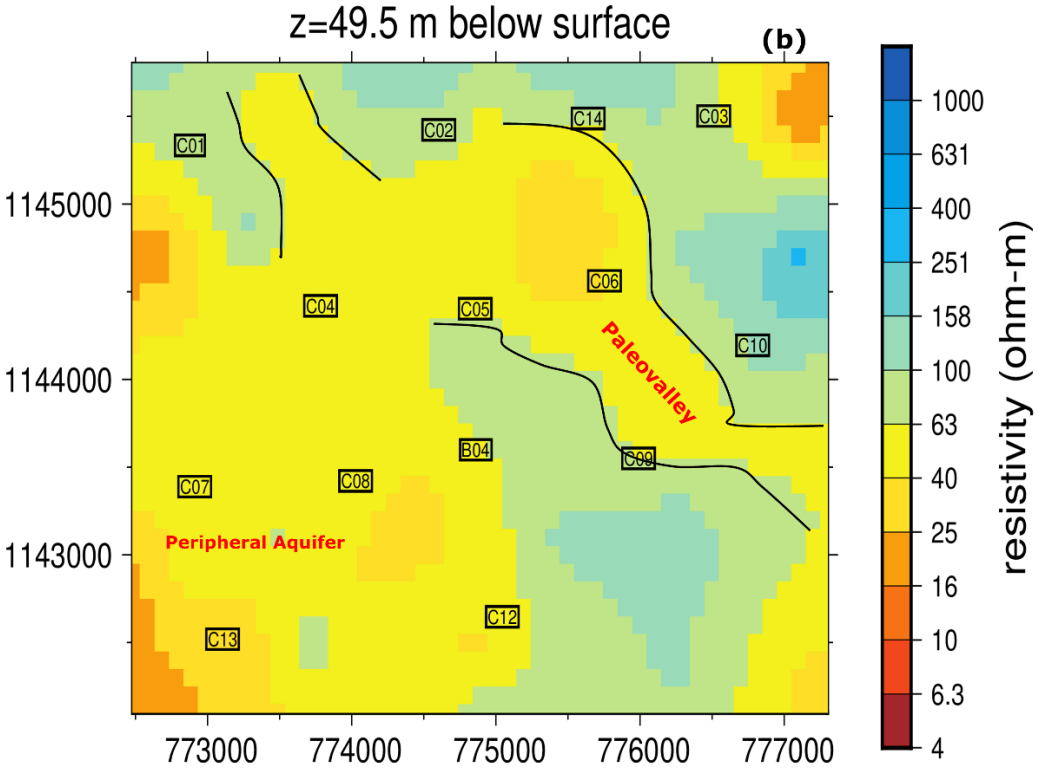
z=49.5 m below surface
(b)
C01
C02
C14
C03
C04
C05
C06
C10
C07
C08
B04
C09
C12
C13
Paleovalley
Peripheral Aquifer
1145000
1144000
1143000
773000
774000
775000
776000
777000
1000
631
400
251
158
100
63
40
25
16
10
6.3
4
resistivity (ohm-m)

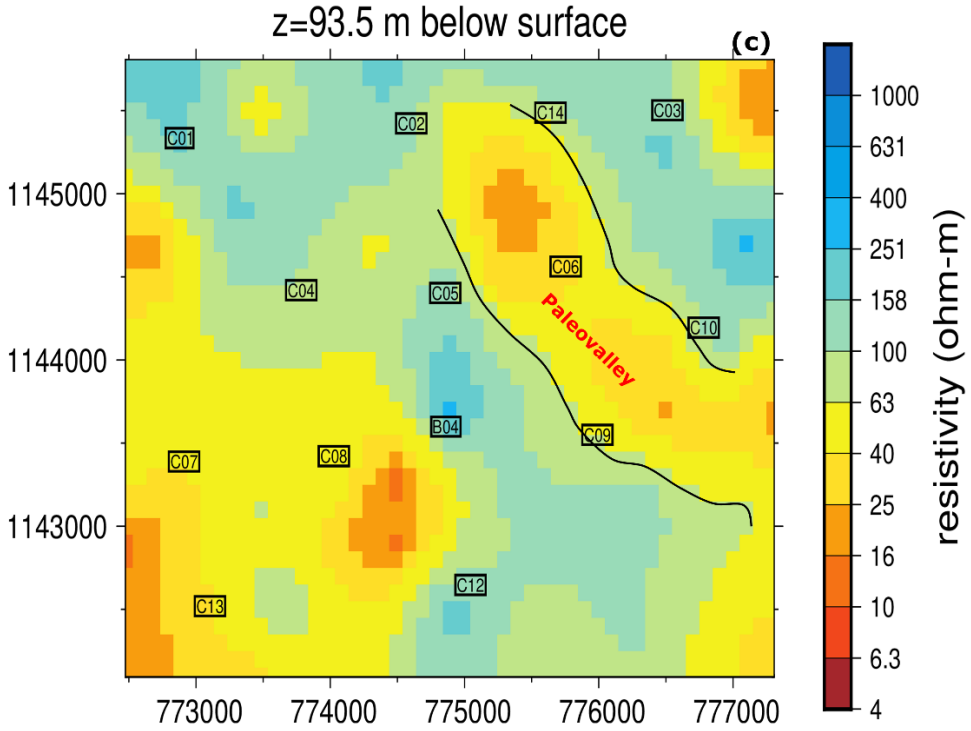
z=93.5 m below surface
(c)
C01
C02
C14
C03
C04
C05
C06
C10
C07
C08
B04
C09
C12
C13
Paleovalley
1145000
1144000
1143000
773000
774000
775000
776000
777000
1000
631
400
251
158
100
63
40
25
16
10
6.3
4
resistivity (ohm-m)

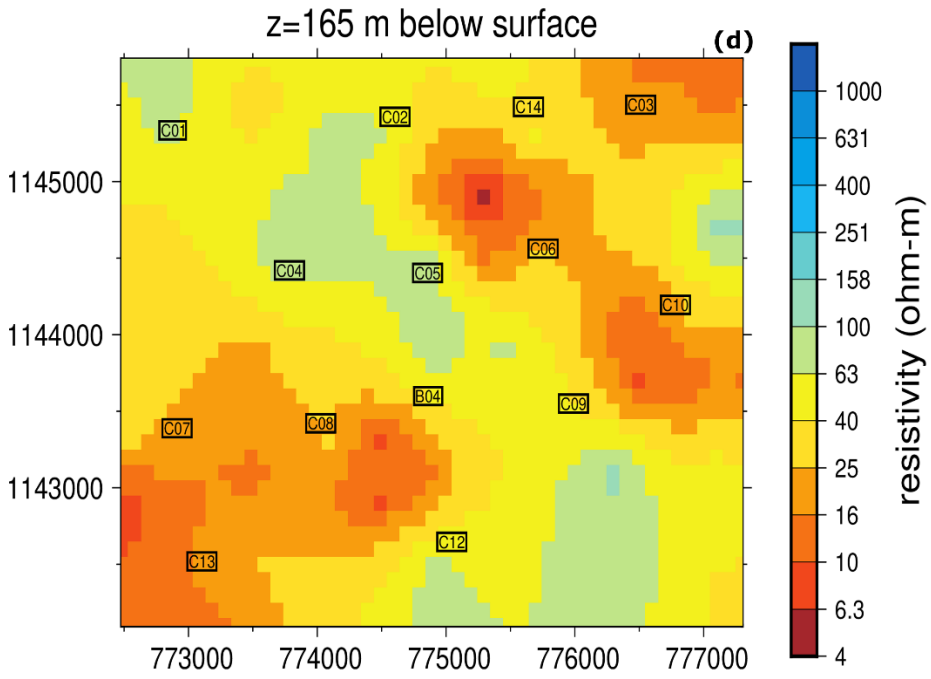

Figure 6. 6: Horizontal depth slices showing of 3-D resistivity model: (a) potential saprock aquifer trending NE-SW (b) NW-SE paleovally at 50m identified by erstwhile Dzikunoo et al. (2020) connect to extended network of fractures forming a potential peripheral aquifer (c) NW-SE paleovally at ~94m (d) potential groundwater productive unit formed from network of fractures at 165m deep.

The first resistivity layer (unit) consists of resistivity values <25 Ωm and is interpreted as argillaceous materials as the range of resistivity is consistent with saturated clay (Gunn et al., 2014). Clays materials have a porosity of 30% or higher (Twort et al., 2000), but their low permeability due their fine grained structure makes them incapable of yielding much water. This makes such formation not suitable targets for groundwater development, as it may be difficult characterizing prolific aquifers within such formations. The unit of argillaceous material is observed at different depths within the research area but is more pronounced at around 300 m and congruous with the mudstones and shales of Poubogou formation (Carney et al., 2010). Borehole geophysical logs (Figure 6.8a) in the area also indicate significant intercalating layers of clay in the Panabako formation which aligns well with the observation in the 3-D models (Figure 6.6&6.7).

The second unit has a moderately low resistivity range of 25 Ωm to <200 Ωm and could be a suitable target for groundwater exploration within the sandstone formation. This unit can be interpreted as fractures with high of porosity and permeability found within the otherwise resistive sandstone formation. The moderately low resistivity values could be attributable to

fractures filled with fresh groundwater which has the ability to facilitate the flow of electrical charges thereby lowering the resistivity of their host formation. The range of resistivity indicated by this unit are compatible to that of the resistivity of fresh groundwater stated for the basin (Aliou et al., 2022; Kpiebaya & Abdul-Ganiyu, 2020; Mainoo et al., 2019). According to Carrier et al (2011) underlying fracture zones in the Voltaian basin are generally developed in the bedrock at depth of 20 m below the ground surface. This assertion appeared to be the case as a well-defined NE-SW fracture with resistivity similarly to the resistivity values suitable for groundwater in the basin is observed at 22m in the 3-D model (Figure 6.6a). The fracture is likely located within the sap rock as it occurs at the base of regolith and could act as a recharge channel for deeper lying fractures. A saprock is the fractured part of the fresh bedrock usually occurring between the saprolite and bedrock. It is thin and contains less clay compare to the saprolite thereby making it good zone for storing and transmitting groundwater (Maurice et al., 2018). Information from geophysical borehole logging in the area indicates a productive fracture at depth between 44 to 62 m (Figure 6.7b) (Klitten & Agyekum, 2021). The geophysical log data also suggests an increase in inflow of water at around 78 m. These observations are in line with the resistivity patterns noted in the 3-D models at approximately 50m and 94m (Figure 6.6b&c). The geophysical logging was done by the water research institute (WRI) as part of the DANIDA white Volta basin manage by University of Ghana.

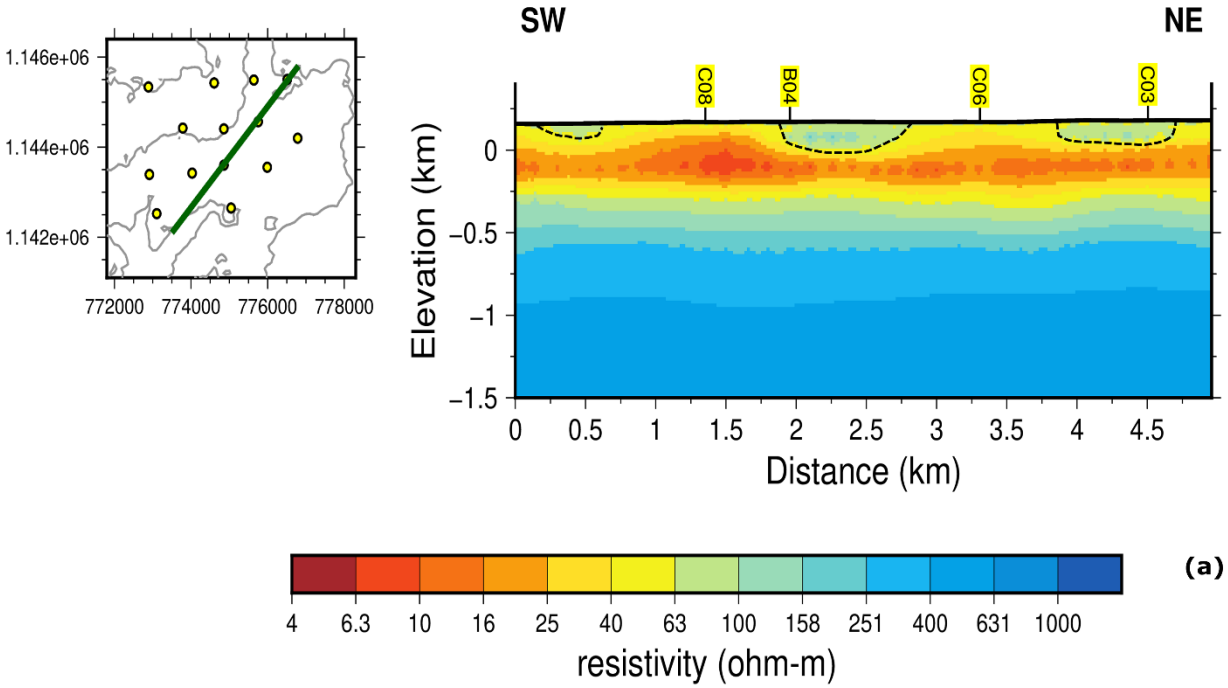

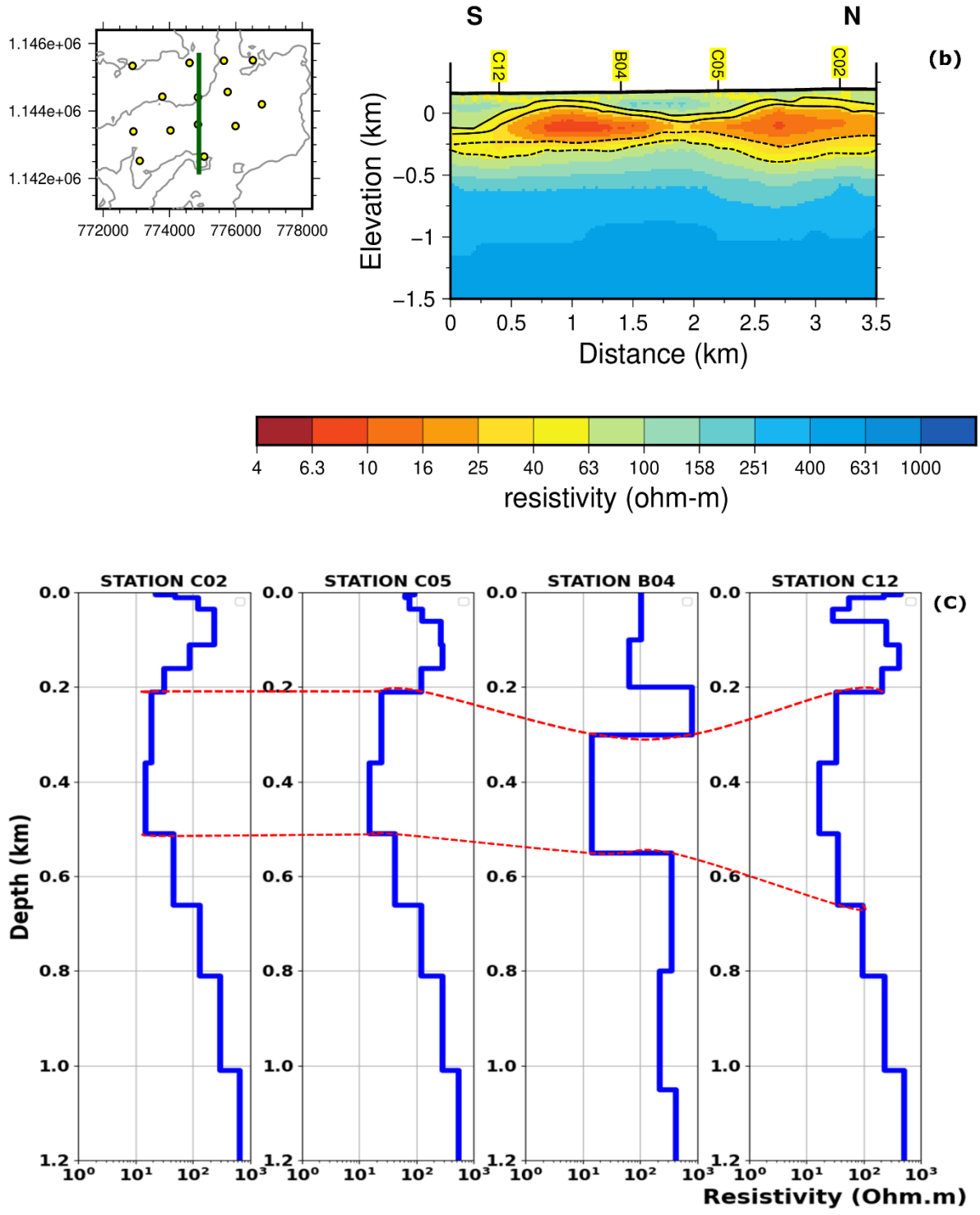

Figure 6. 7: Subsurface resistivity models (a) 3-D model showing the location of the paleovalleys in U-shape dotted lines, first two to the right have been identified by Dzikunoo et al. (2020) and the third one observed in this current study. (b) 3-D model showing the positions of the lithological boundaries potential aquifers at 280-300m (black solid lines), and 470m (black dotted lines). (c) 1-D models showing lithological contacts (red dotted lines) observed in b.

The structures at 50m and 94m aligned well with the paleovalleys identified in the area by Dzikunoo et al (2020) in terms orientation, depth and location. At 50m the paleovalley connect extensively with other structural entities with similar potential outside the perimeter of the channel forming a network of potential aquifers within the terrain (Figure 6.6b). Available borehole yield information in the basin suggest that, yield of wells generally increases with increasing depth (Mainoo et al., 2019; Water Resource Commission, 2011) and supports the observation made with the geophysical logging data (Figure 6.8) (Klitten & Agyekum, 2021). Following same argument, similar fractures are observed at depths of about 165m (Figure 6.6d), 250-300m and 470 m (Figure 6.7b). The depths of the structures matches lithological contacts within the Bombouaka group of the Voltaian sedimentary basin (Carney et al., 2010). According to Aliou et al. (2022), lithological boundaries and intercalations of claystones within the basin constitute significant water-bearing zones and should be targeted for groundwater development in the area. The structure at 250-300m has been well characterized and discussed in the models of the first MT campaigned in the basin (Chapter Five). The structures as observed within the lithological boundaries could therefore constitute prolific aquifers that could be key in addressing the water challenges in the basin. It is important also to noted that, the 3-D model has significantly resolved layer thickness of the Bombouaka formations in the area with much accuracy. The model indicates thicknesses of units which are deeper than first proposed suggesting a reclassification of the layer's thicknesses. The fractural entities and thicknesses observed at the lithological contacts are well resolved in the 1-D (Figure 6.7c) which gives better vertical resolution at the MT sites across the study area.

The third unit has a resistivity range of >200 Ωm to 1000 Ωm. This unit plausible represent the sandstones of the Bombouaka group which have been described as relatively resistive due to their consolidated nature and compositions (Chapter Three). Mineralogical composition analysis of the sandstone's samples under both polarized microscope and scanning electron microscope (Chapter Three) indicates that the dominant mineral is quartz which are known to show high resistivity. The quartz under thin section appeared stretched and interlocking probably due to recrystallization of the mineral from past tectonic events of the which affect the sediments (Kesse, 1985) hence making them hard and increasing their resistivity. It is important to note that, discrete fractures and intergranular spaces at certain locations within the units causes the unit to become moderately resistive.

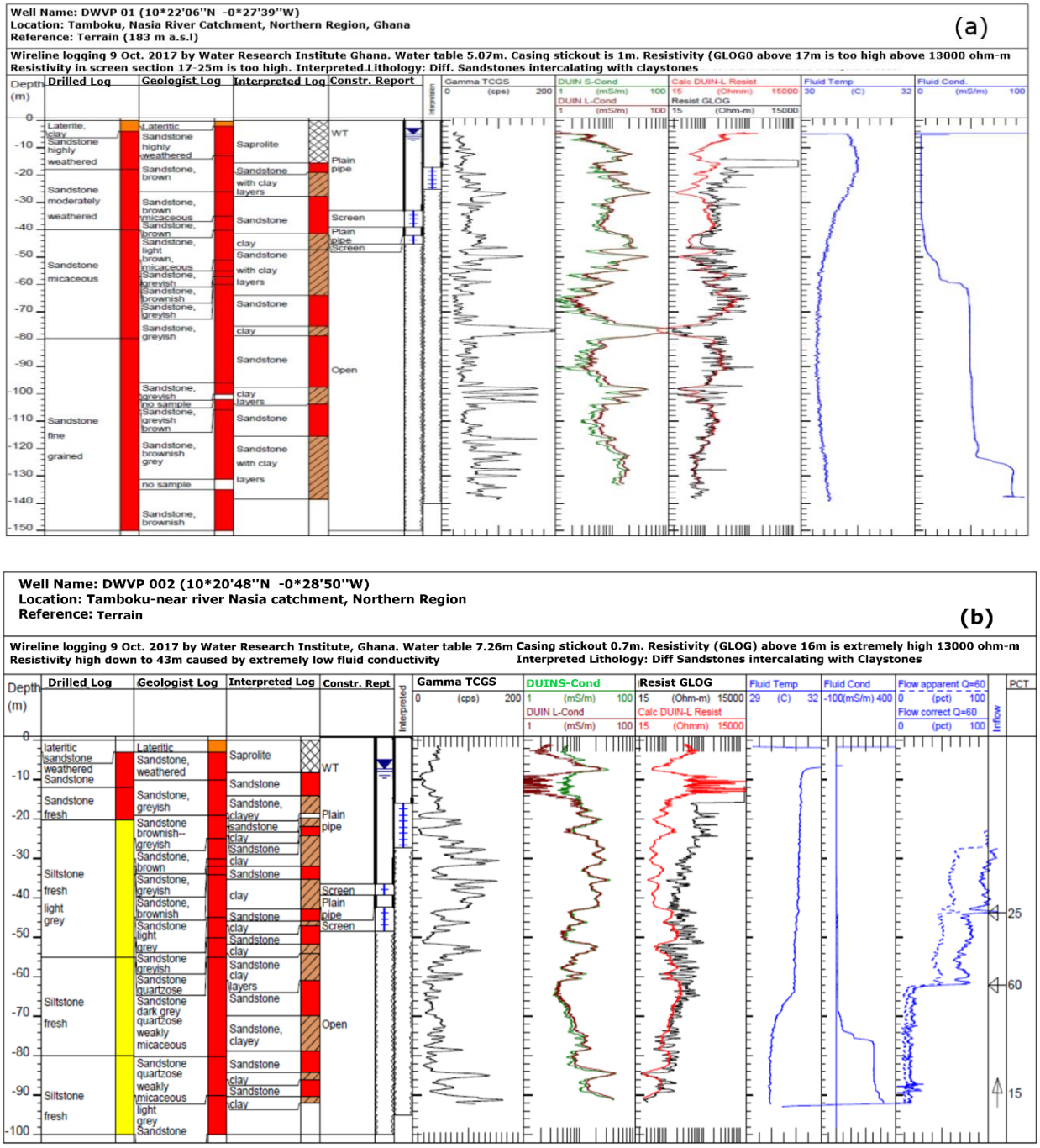

Figure 6. 8: Borehole geophysical logs indicating different rock types down hole within the Panabako Sandstone Formation; (a) DWVP 01 showing sandstones (red color) intercalating clay (brow color) and (b) DWVP 02 showing identified sandstones in red color with intercalating clay stones in brown color. The site geologist log represented in yellow color.

The final unit with resistivity >1000 Ωm likely represents the Paleoproterozoic basement material or highly impermeable duricrust usually form on the surface of sedimentary basin in similar climatic conditions. The high resistivity of the basement materials could be due to compaction cause by weight of overlying materials as well as recrystallization of the rock

minerals due to increases in temperature at such depths. The recrystallization of the rock constituents results in interlocking crystals leaving no voids that could host pore fluids and increase conductivity of the rocks. The impervious lateritic top layer also lacks pore spaces and therefore unable to conduct current leading to its high resistive nature.

The potential groundwater units that have been observed as aquifers formed by nexus of fractural entities, lithological contacts and paleovalleys within the quartz-arenite sandstones and the underlying formations of the Voltaian sedimentary basin, may prove crucial in addressing the water challenges in the basin. Paleovalleys or paleochannels are buried old river channels that often form prolific aquifers especially in semi-arid and arid regions such as Ghana (Jiang et al., 2019). The aquifer formed by the network of fractures are observed as an extension outside the perimeter of the paleochannel while the potential structures at the lithological contacts occur below the paleochannels. Their spatial location and orientation make them significant targets for groundwater development in the basin. Groundwater is touted as a resilient measure for climate change adaptation that could be harnessed for irrigation to improve the livelihood of rural dwellers across many communities in sub-Sahara Africa. Agricultural activities which is the mainstay of the rural economy in northern part of the basin have been hampered by adverse effects of climate change causing more rural-urban migration. Efforts by authorities to address these challenges have seen many attempts made using conventional groundwater exploration techniques in the basin which yielded little success. This is because most conventional geophysical techniques are only effective at delineating groundwater zones where a good contrast exist between the weathered zone and the bedrock. In the case of the Voltaian basin, groundwater occurrence is controlled by discrete fractural entities (Acheampong & Hess, 2000; Agyekum & Asare, 2016; Aliou et al., 2022) which might not readily be detected by these conventional techniques. For instance, the reinversion of the airborne electromagnetic data in area identified the paleovalleys also seen this study but could not detect the possible aquifer formed by the network of discrete fractural that extend at the peripherals of the paleochannel. The deployment of the MT however, effectively delineate zones with high promising groundwater potential in the basin. MT as an EM techniques is effective at mapping steeply dipping structures (Chegbeleh et al., 2009; Hazell et al., 1988) where other techniques may fall short.

6.3 CONCLUSION

The present work has emphasized on the importance of utilizing more robust deep penetration subsurface imaging technique which has the ability to detect subtle changes in resistivity of the subsurface structures particularly in hard rock terrain. The results demonstrate that the MT technique when combined with borehole data and geological information can characterize and map the depth and extent of subsurface fracture network and their associated hydrogeological pathways. The study has identified potential productive structures at different depths that can be targeted for groundwater development to improve the resilience of rural communities in basin. A NE-SW fracture with good groundwater potential was observed at 22m coinciding with the depth of saprock described in the area. A nexus of fractures described as an aquifer system has also been delineated at depths of about 50m and 165m in addition to the erstwhile paleovalleys identified at 50m and 94m in the terrain. A promising structure at the lithological boundaries (250m-300m) which underlies the paleovalleys in the basin has been intercepted in an earlier MT survey in the area. The unit which has been described as a potential fracture aquifer is hydrologically linked with a N-S flowing surface stream that defies the extreme temperatures in the basin and could hold the key to addressing the water challenges in the area. Knowledge of the observed fractures network in the hard rock terrain of the Voltaian sedimentary basin would be useful in understanding the hydrogeology of the basin which has so far been described as complex. The information could serve as crucial inputs to simulate the groundwater flow system and develop a sustainable groundwater management plan for the basin.

CHAPTER SEVEN

DEEP BASIN, CRUST AND MANTLE STRUCTURES REVEALED BY THE JOINT INTERPRETATION OF 3-D MT AND AIRBORNE DATA

7.0 Investigating the Sediment Thickness in the Study Area.

The interpretation of sedimentary thickness is of paramount interest to gain insight into subsurface structures which are vital for natural resource exploration. Subsurface structures of the earth's crust are concealed with a lot of different natural resources that when discovered and harnessed, could be of economic importance to national development. However, the sediment thickness of the geological complex Neoproterozoic Voltaian Sedimentary Basin (VSB) in Ghana has remained a subject of controversy for decades. Some scholars have attempted to interpret the sediment basement thickness of the basin using various approaches. For instance, Annan-Yorke, (1971) and Ako and Wellman, (1985) through a review of geophysical data and geology indicated that the depth to the basement of the Supergroup (Chapter one section 1.5.3) is 5000 m and 6000 m respectively. Apesegah, (2008) estimated the thickness of the sediments to exceed 7000 m based on seismic and well-log data. The lack of consensus, therefore, makes it imperative to conduct further investigations in an attempt to ascertain the proper thickness of the sedimentary cover of the basin.

Additionally, the crustal thickness of the area has remained largely under-explored, aside from recent work done by Le Pape et al., (2021) on the lithospheric structure in southern Burkina Faso which extended to some parts of northern Ghana. However, their investigations remain inconclusive on the crustal thickness (Moho discontinuity) in the area. Understanding the crustal thickness provides valuable insights into the stability of the lithosphere in relation to the tectonic movement (Kalmár et al., 2019; Peter et al., 2017). The improvement in technology and the science of geophysics, which has enhanced the utility of geophysical techniques in subsurface geology and the recent hike in exploration activity in the basin to uncover the natural resource potential of the basin constitute the basis for this investigation.

7.1 Airborne Data

The details of the airborne datasets (aerogravity and aeromagnetic) have been explained in the previous chapters two and five. Therefore, only the methods for depth investigation and 2-D modelling relating to the airborne are presented and explained in the subsequent sections.

7.1.1 Radial Average Spectrum Analysis of Aeromagnetic data

One of the most significant steps in the interpretation of aeromagnetic data is to determine the depth to source of the magnetic anomaly (Al-Ibiari et al., 2017; Liu et al., 2023). The total magnetic intensity grid reduced to the equator was used to determine the depth to magnetic sources within VSB using statistical spectral analysis. The entire study area (Figure 1.2a) was

considered as a single block and the plot of logarithm of spectral power (energies) against wavenumbers (frequencies) obtained for the area is shown in figure 7.1a below. The slope of the different segment of the graph was then calculated after the data was exported from Oasis Montaj software (Geosoft Inc., 2021) (Figure 7.1b) and using equation 2.14. The results of the spectral analysis show the presence of shallow source bodies at depths of about 0.6 km below datum while the deep sources are at an approximately 6.9 km depth in the area. The shallow results represent the spectral analysis of magnetic data of regions where magnetic source (basement rocks) exist very close to the ground surface. The essence of this enhancement technique is to define the depth to the basement in order to have a fair understanding regarding the possible depth of subsurface structures revealed by the derivative filters. These structures are of paramount interest in this studies as they have been suggested to controlled groundwater flow in the basin (Acheampong & Hess, 2000; Aliou et al., 2022; Carrier et al., 2011; Chegbeleh et al., 2009; Mainoo et al., 2019).

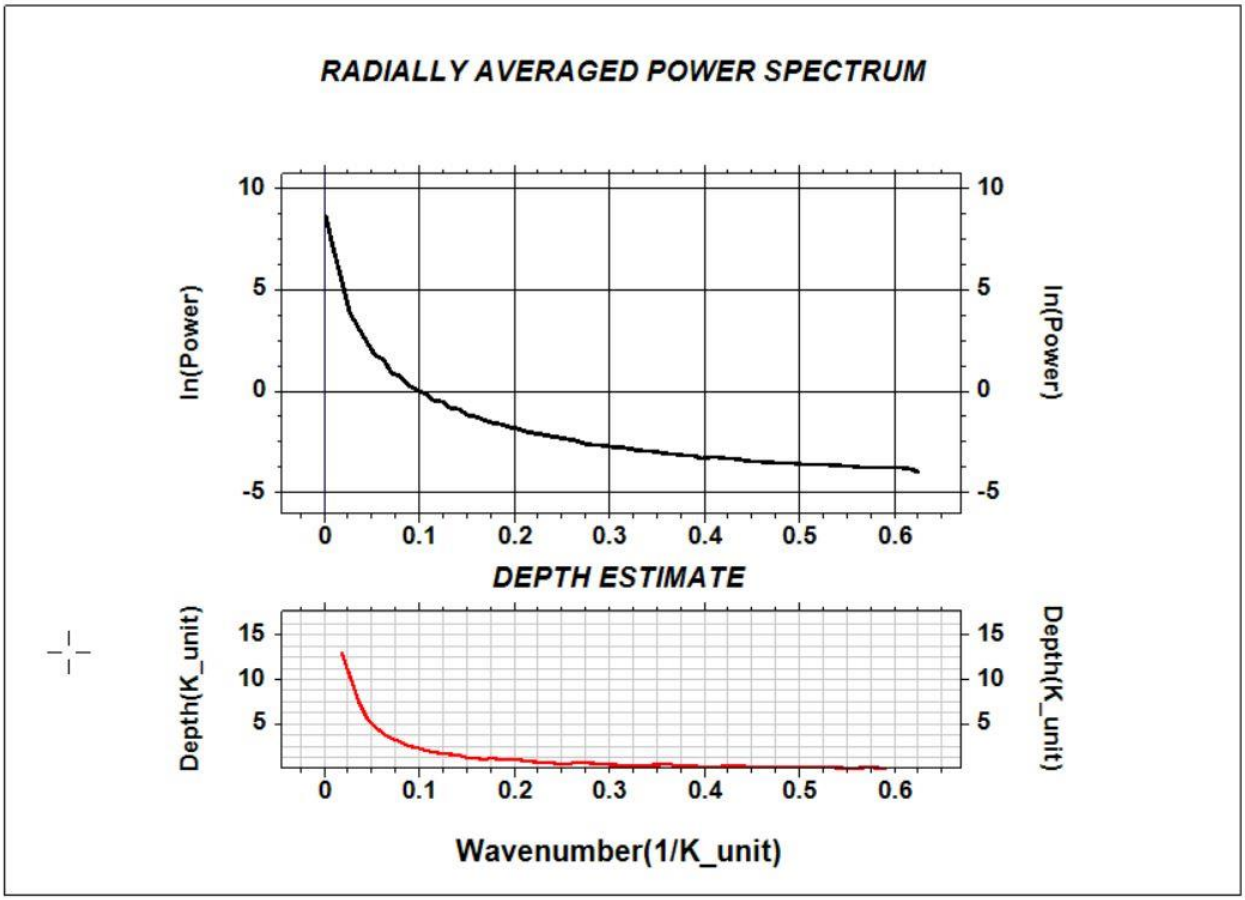

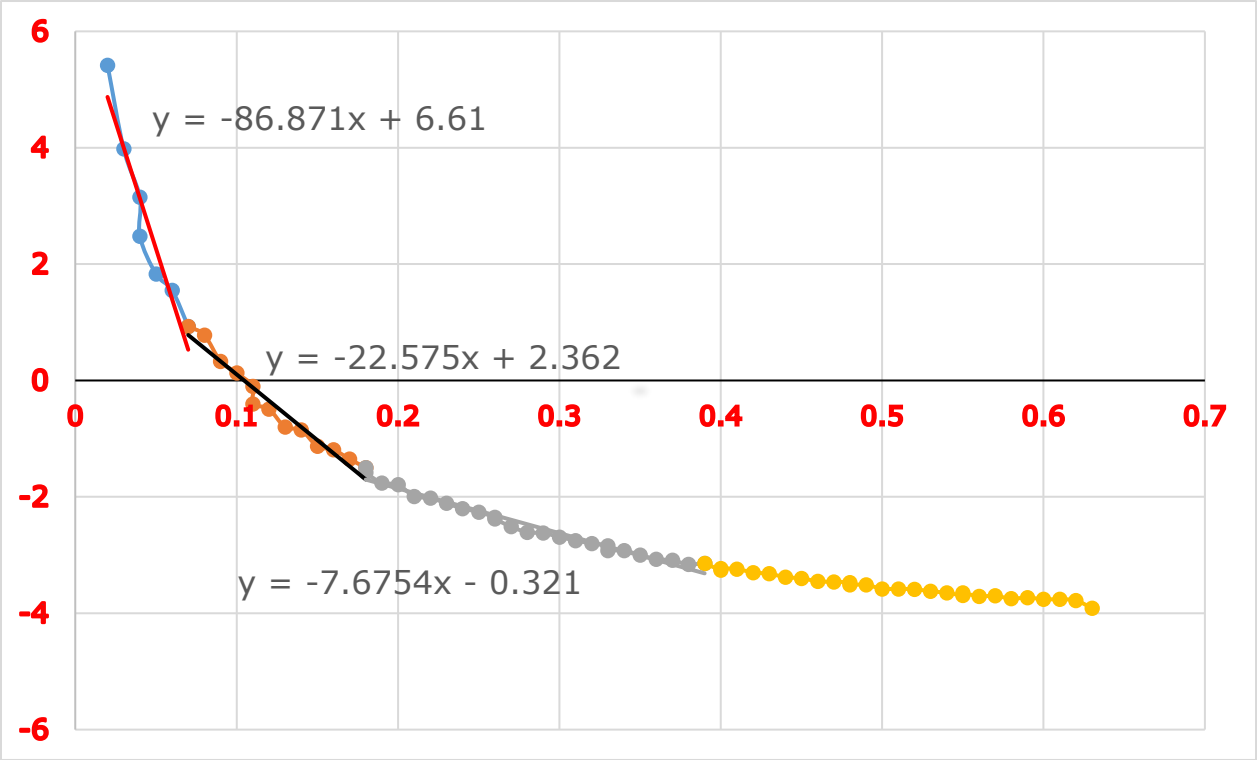

Figure 7. 1: Radial Average Spectrum Analysis (a) a plot of log power (energies) versus the wavenumber and the estimate depths for the whole area (b) regeneration of the energies versus wavenumbers plot fitted with straight-line segments to determine the slope which is related to the depth to source of the spectral energies in the study area. Different colors represent different depth segments.

In spectra analysis, if the area under investigation is large, it is advisable to divide it into smaller blocks before applying the technique to estimate the depth to source of each block. However, the study area is relatively small, and was considered as a unit block for the analysis. By considering the area as a single block, the technique is unable to differentiate locations of shallow depths from deep depths. To distinguish the different depths locations over the area, 2-D GM-SYS forward modelling of aeromagnetic and aerogravity data was performed. The initial depth of the 2-D GM-SYS was set based on the depth information derived from the spectral analysis.

7.1.2 Two-Dimensional Forward Modelling of Aerogravity and Aeromagnetic Data

The GM-SYS tool in Oasis Montaj Gesoft version 2021.2 was used to undertake two-dimensional forward modeling of three selected profiles shown in figure 7.2 (black solid lines) extracted from interpolated grids of the aerogravity (Figure 7.3a) and aeromagnetic (Figure 7.3b) data to characterize the sediments basement interface. The gravity data was acquired along wide line spacing (5000m) hence the interpolation of the data could introduce

uncertainties in the grid (Perozzi et al., 2021). To reduce uncertainties and improve model results, aerogravity data was model sequentially with the much denser high-resolution aeromagnetic data (Figure 7.3b).

After importing the extracted grids into the program, the subsurface was divided into two layers with the sedimentary basin at the top and the basal basement complex at the bottom. The initial depth of the interface between the sediments and basement for each of the profiles was set based on prior information derived from spectra analysis of aeromagnetic data and initial values of density and susceptibility assigned to each layer. The defined interface was then continually adjusted to obtain a best fit between the observed data and the computed model. The orientations of the profiles were selected to match the profiles orientation of deep MT sounding profiles.

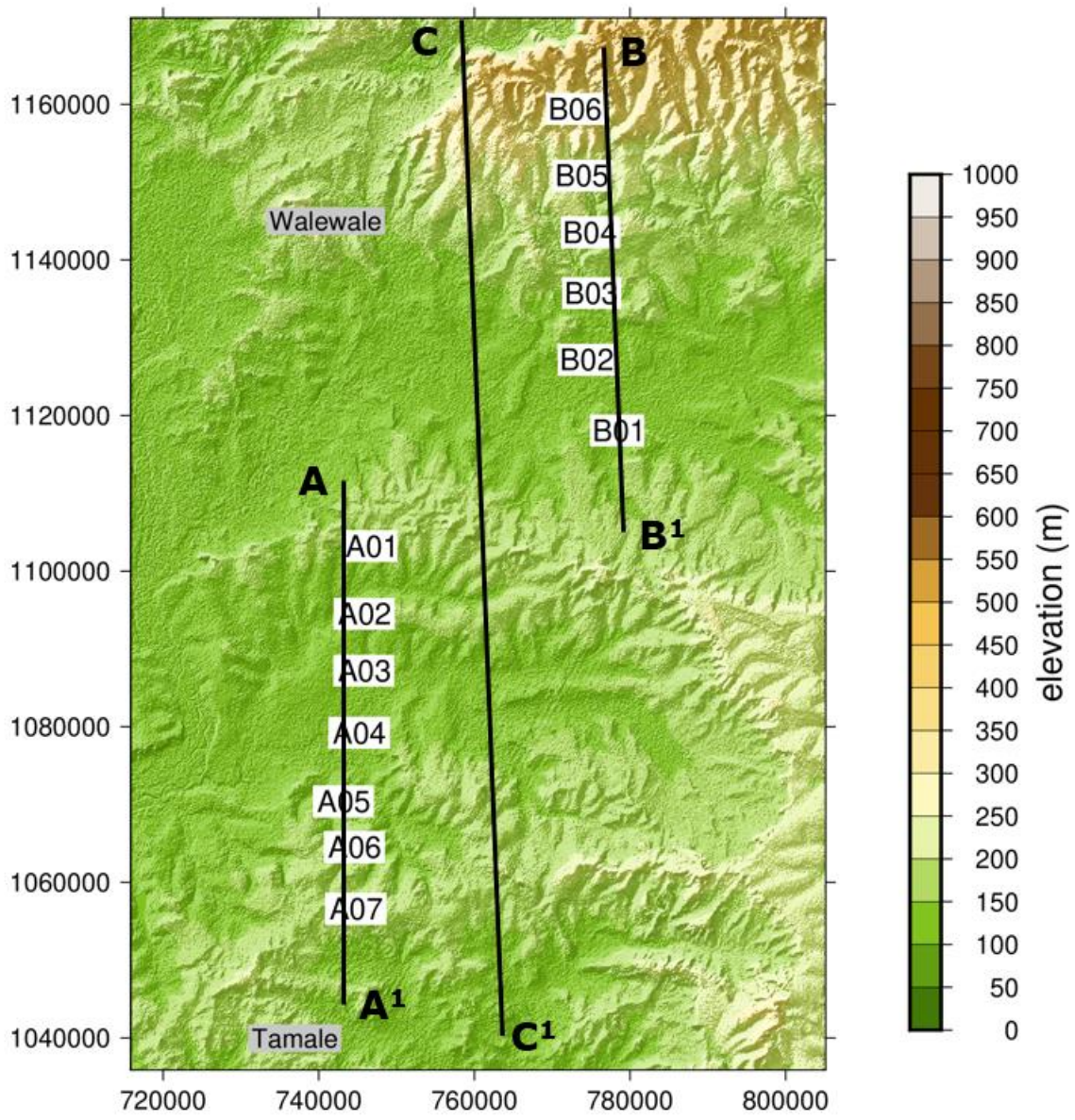

Figure 7. 2: Location of selected profiles used for 2-D forward modelling of aerogravity and aeromagnetic, plotted on topographic map of the study area (DEM from a satellite dataset. The profiles (solid black lines) to match MT survey stations and regional trend of the basin.

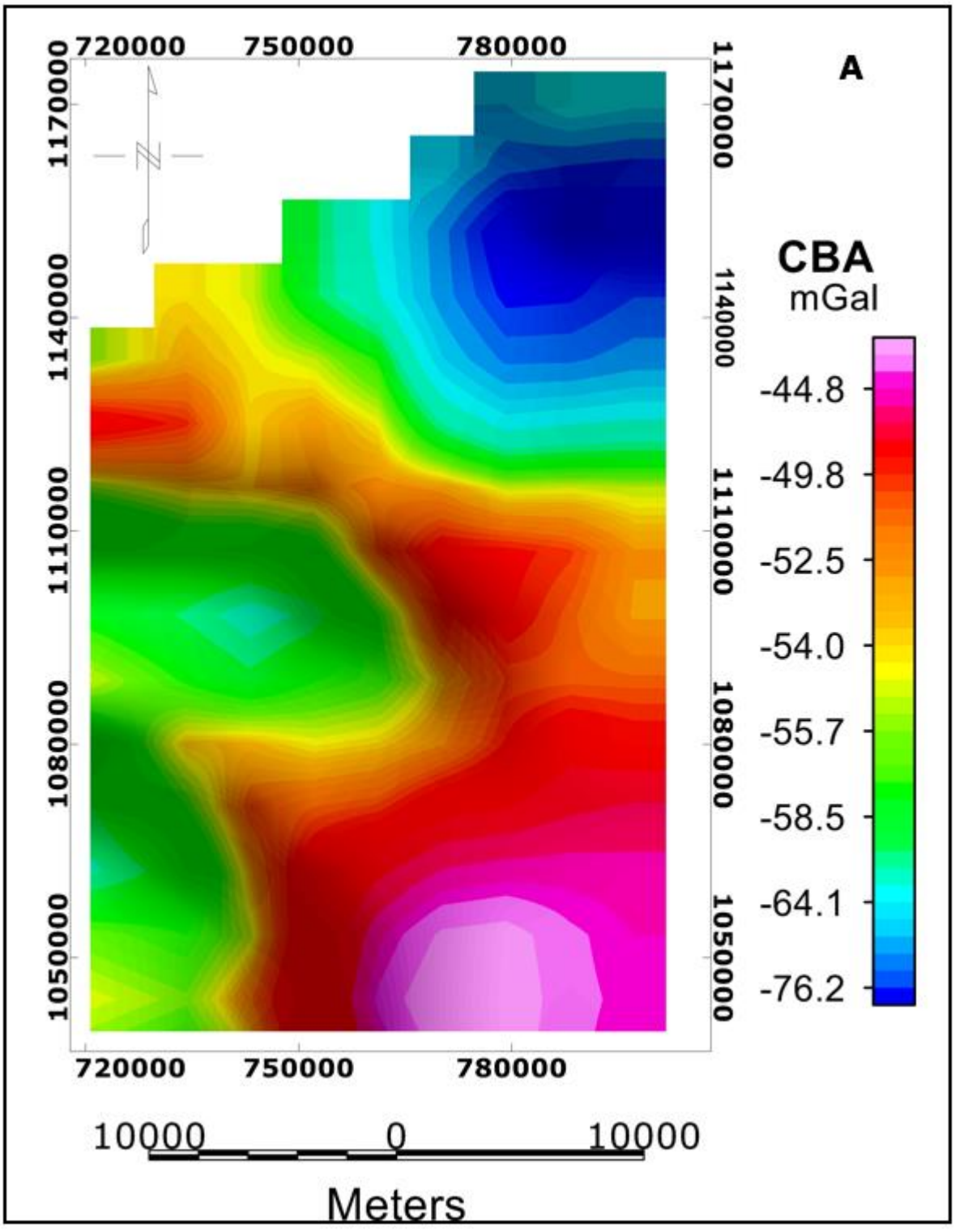
A
720000
750000
780000
1170000
1140000
1110000
1080000
1050000
CBA
mGal
-44.8
-49.8
-52.5
-54.0
-55.7
-58.5
-64.1
-76.2
10000
0
10000
Meters

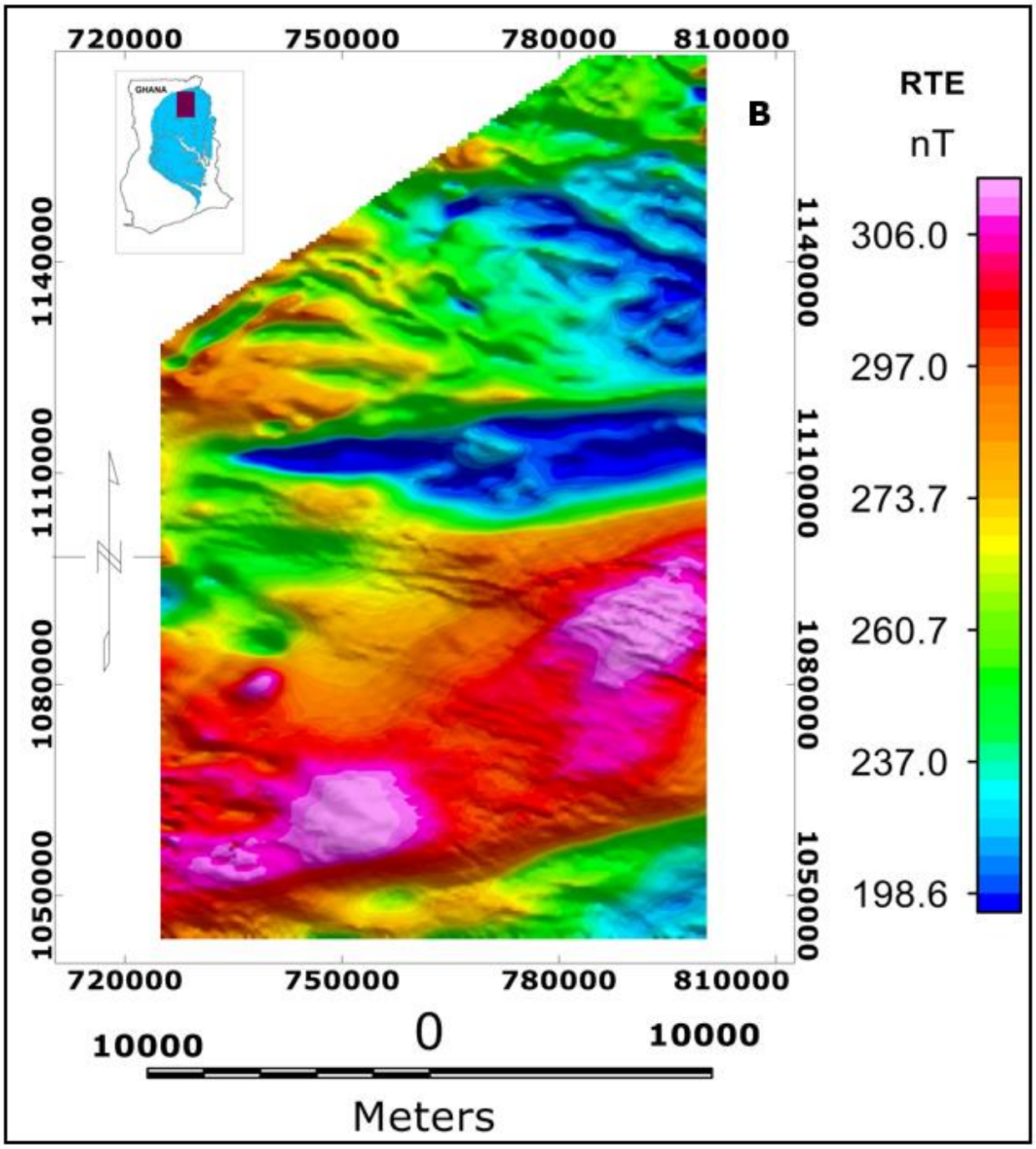

Figure 7. 3: Maps of (a) Bouguer anomaly and (b) magnetic intensity anomaly with inset map of Ghana showing the VSB and the study area (brown color in inset map). The shape of the maps at the top left is due to unavailability of data.

7.1.3 Basement Morphology and Sedimentary Thickness

The basement geometry and morphology and the sedimentary thickness of the VSB in the study area was investigated using 2-D forward modelling of airborne data (aerogravity and aeromagnetic) supported with 3-D inversion of MT results. The sequential modelling of

aerogravity and aeromagnetic provides a constrained in the interpretation of the model results as oppose to modelling each data separately (Kanthiya et al., 2019; Mohamed et al., 2016). This is because different physical properties of the different rocks are modelled together thereby reducing ambiguity in the models. Further validations of the models were carried out with prior geological information for the area before interpretation. The 2-D cross sections derived from profiles of aerogravity and aeromagnetic are presented in figure 7.4. The root means square errors between the observed data and the computed models obtained after the modelling were considerably low indicating a good fit. The modeling was done along north-south orientated profiles to enable comparison with the 3-D MT models. The directions of the MT profiles were determined following subsurface structural interpretation of the aeromagnetic data (Chapter Five). All the 2-D models show varying depths and basement morphology along the interface between the sedimentary cover and underlying basement material (Figure 7.4). A maximum depth of approximately 7.3 km was estimated to the south of profile AA^1 and CC^1 (Figure 7.4a and c) while the minimum depths of about 0.6 Km were found towards the north in profile BB^1(Figure 7.4b). The deepest sediment-basement boundary interpreted based on the 2-D GM-SYS forward modeling of the aerial data is consistent with Apesegah, (2008) assessment of the basin sediments thickness. The models however revealed thicker sediments than the thicknesses proposed by both Ako and Wellman, (1985) and Annan-Yorke, (1971) for the basin. These difference in sediment thickness estimation could be attributed to improved data quality as well modeling techniques. The recent improvement in the science of geophysics has resulted in improved resolution of geophysical techniques and equipment leading to more quality data acquisition. The results of the models are compatible with geological information of the area. The Voltaian Supergroup is described as shallow at its margins, with an irregular interface between the sediments and basement boundary (Affaton et al., 1980; Carney et al., 2010; Kalsbeek & Frei, 2010). The fringes correspond to the locations that showed minimum sediment thicknesses for the 2-D GM-SYS models (Figure 7.4) and 3-D MT inversion models (Figure 7.8). Similarly, the deepest areas of the basin are in line with the maximum sedimentary thicknesses estimated.

AA' PROFILE (a)

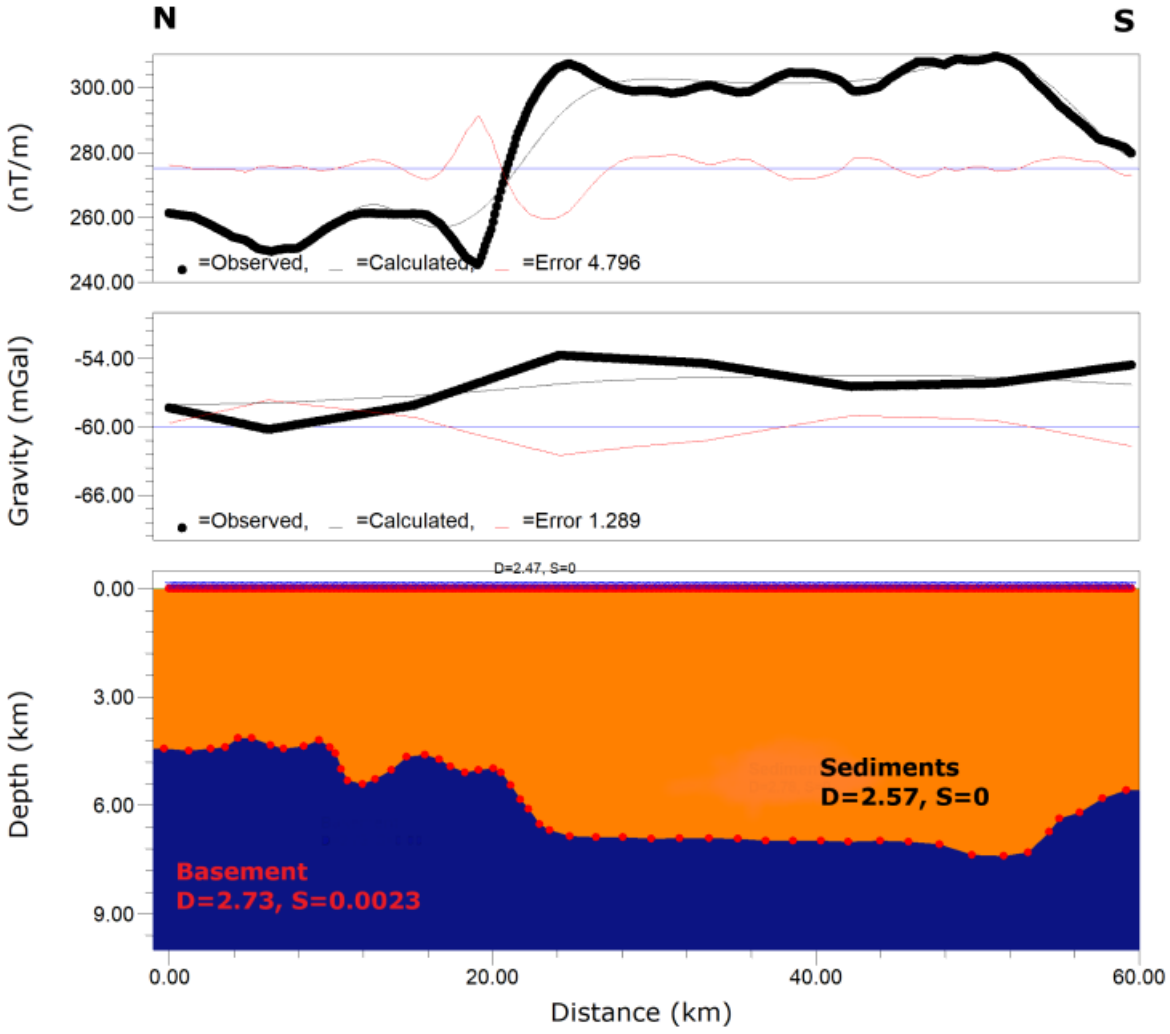
N
S
(nT/m)
300.00
280.00
260.00
240.00
=Observed,
=Calculated,
=Error 4.796
Gravity (mGal)
-54.00
-60.00
-66.00
=Observed,
=Calculated,
=Error 1.289
D=2.47, S=0
Depth (km)
0.00
3.00
6.00
9.00
Sediments
D=2.57, S=0
Basement
D=2.73, S=0.0023
0.00
20.00
40.00
60.00
Distance (km)

BB' PROFILE (b)

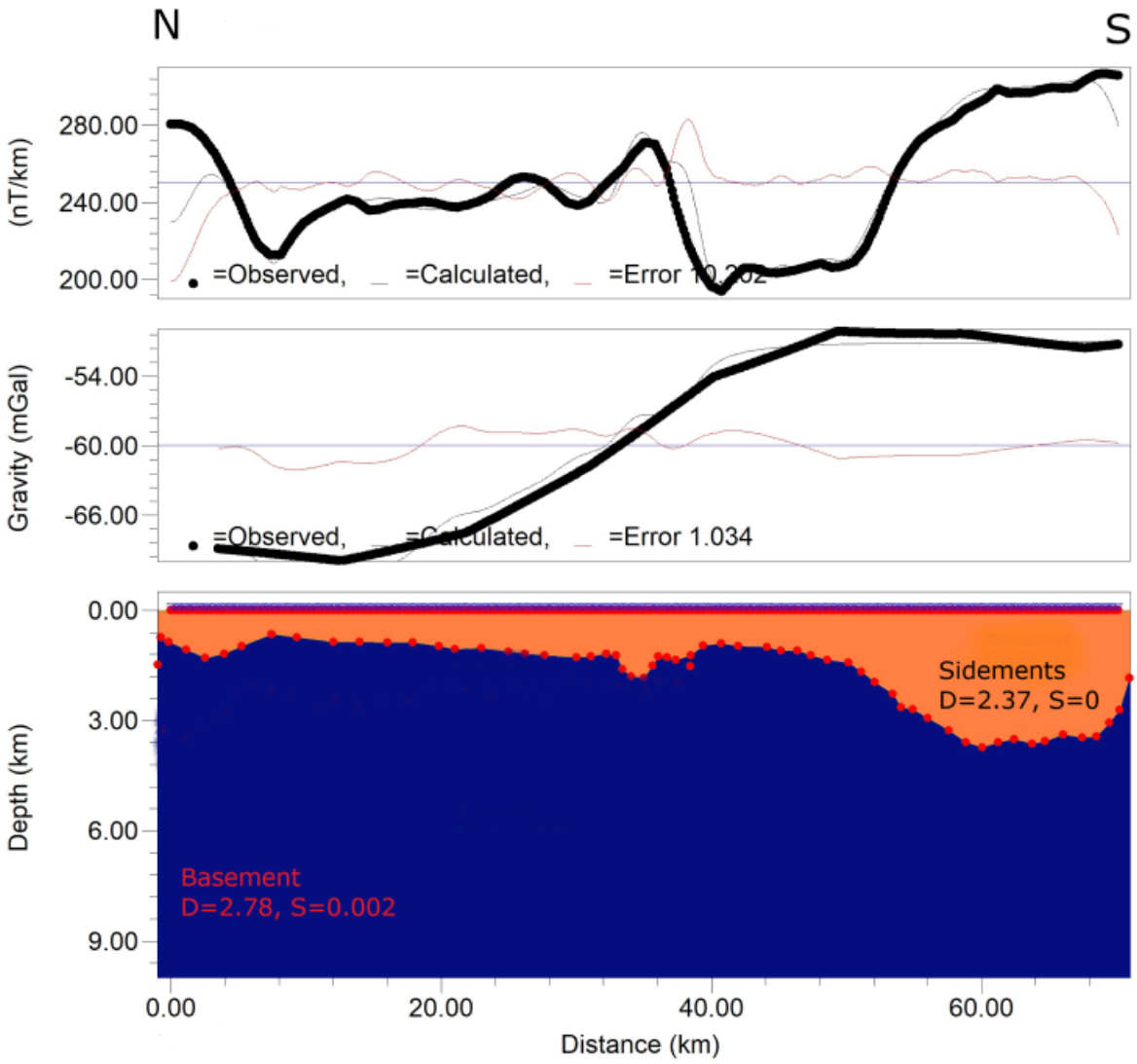
N
S
(nT/km)
280.00
240.00
200.00
=Observed,
=Calculated,
=Error 1.034
Gravity (mGal)
-54.00
-60.00
-66.00
=Observed,
=Calculated,
=Error 1.034
Depth (km)
0.00
3.00
6.00
9.00
Sidements
D=2.37, S=0
Basement
D=2.78, S=0.002
0.00
20.00
40.00
60.00
Distance (km)

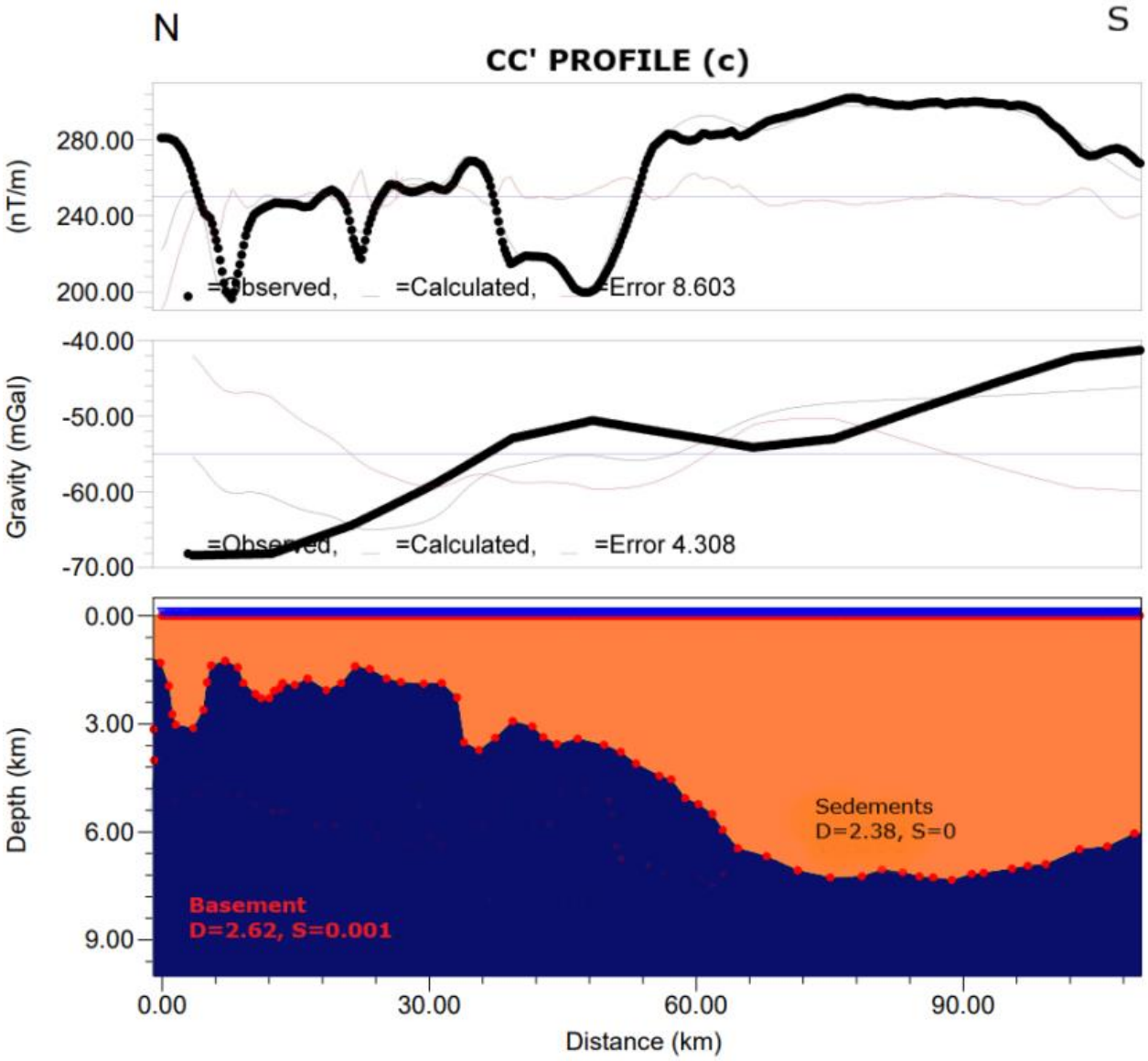

Figure 7. 4: 2-D models of aerogravity and aeromagnetic data showing sediment-basement boundary and morphology of the basement along three NS profiles: (a) AA^1 Profile, (b) BB^1 Profile and (c) CC^1 Profile.

7.2MT DATA

7.2.1 Dimensionality Analysis of the MT Data.

Prior to MT inversion (Chapter Two Section 2.3.5), dimensionality analysis was carried out to determine whether the computed responses (from observation data at all frequencies) correspond to 1-D, 2-D and or 3-D geoelectrical structures. This is because the inversion can be ambiguous if the dimensionality of the model differs from the dimensionality of the data. Performing dimensionality analysis therefore help to reduce the ambiguity of the model leading to precise modelling and interpretation of the data (Pranata et al., 2017). The analysis allows

for identification and quantification of distortions (Groom & Bailey, 1989; A. Kumar et al., 2021; Lilley & Weaver, 2010; McNeice & Jones, 2001; Smith, 1995) as well as recovery of the strike of the subsurface structures (Kumar et al., 2021). Dimensionality analysis of the MT response was done utilizing Swift and Bahr skew and phase tensors ellipticity criterion (Arafa-Hamed et al., 2023; Becken & Burkhardt, 2004; Caldwell et al., 2004). An ellipse is used to graphically illustrate the phase tensor (Arafa-Hamed et al., 2023).

7.2.1.1 Swift and Bahr Skew Analysis

Generally, skew values that are less than 0.3 (<0.3) are indication of 1-D or 2-D structure of the subsurface while skew values greater than 0.3 (>0.3) indicates 3-D subsurface resistivity or conductivity structure. Swift and Bahr skew were calculated for both profiles in the northern part of the VSB and are presented Figure 7.5 and 7.6 respectively. At short periods most of the skew values calculated using the Swift approach were less than 0.3 suggesting a 1-D or 2-D structure of the subsurface resistivity structures for both profiles. Few of the Swift skew values however plotted above 0.3 at long periods indicating the presence a 3-D structure (Figure 7.5). The phase-sensitive approach used by Bahr was applied to the data which revealed majority of the skew values for profile A (Figure 7.6a), plotted below 0.3 at short periods, showing 1-D or 2-D character of the subsurface structure while few were plotted above 0.3 at long periods indicating some 3-D structure present (Figure 7.6a). In profile B (Figure 7.6b) most of the Bahr skew values plotted above 0.3 at long periods showing clearly 3-D subsurface structure underneath the profile. This clearly means that, inverting the data in 2-D could lead to misinterpretation as the model will be ambiguous and may not account for the 3-D character as observed in the data. Heterogeneities of the subsurface structure are better resolved with 3-D inverse modelling of the MT data (Hautot et al., 2007).

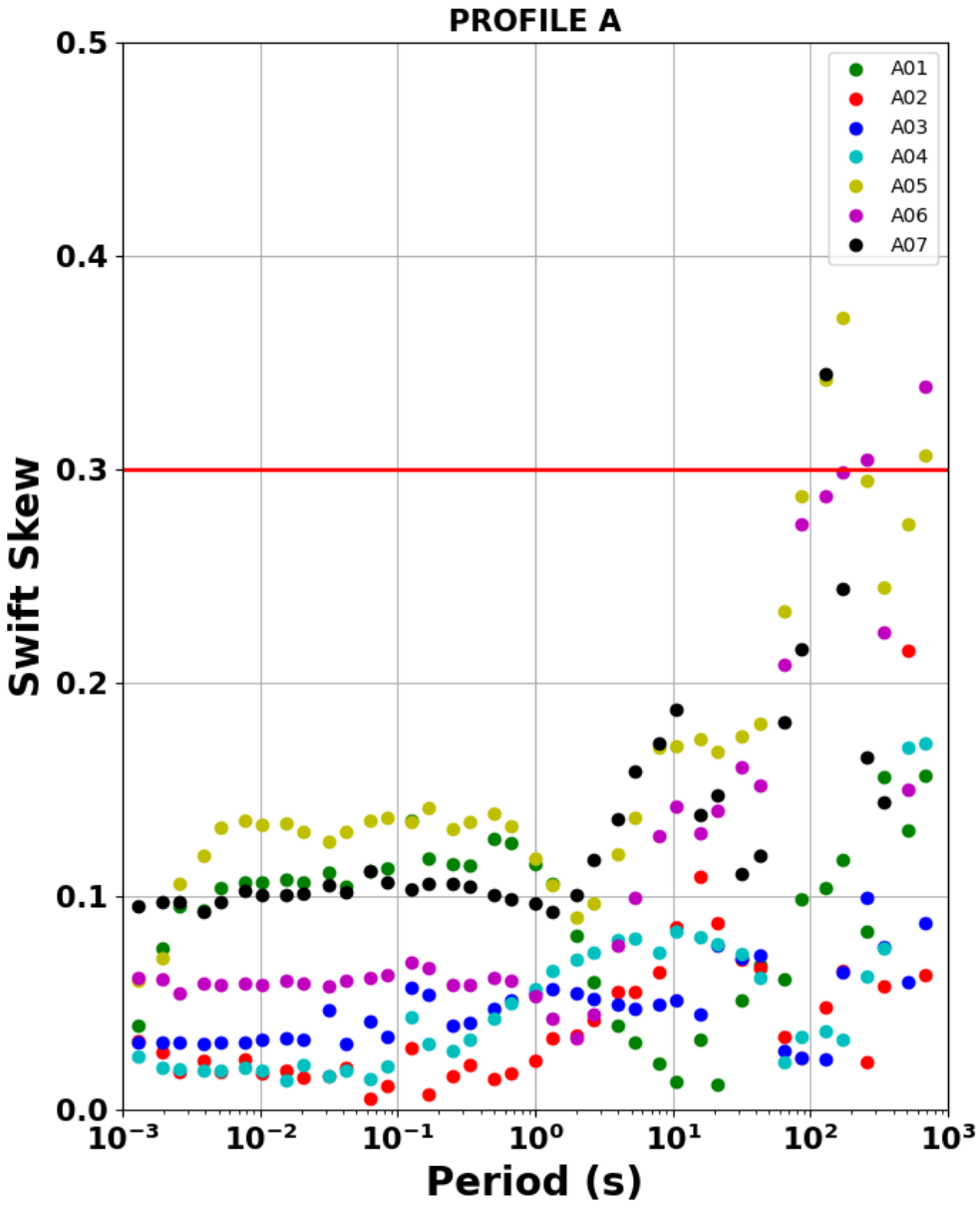
PROFILE A
A01
A02
A03
A04
A05
A06
A07
Swift Skew
0.0
0.1
0.2
0.3
0.4
0.5
10^{-3}
10^{-2}
10^{-1}
10^{0}
10^{1}
10^{2}
10^{3}
Period (s)

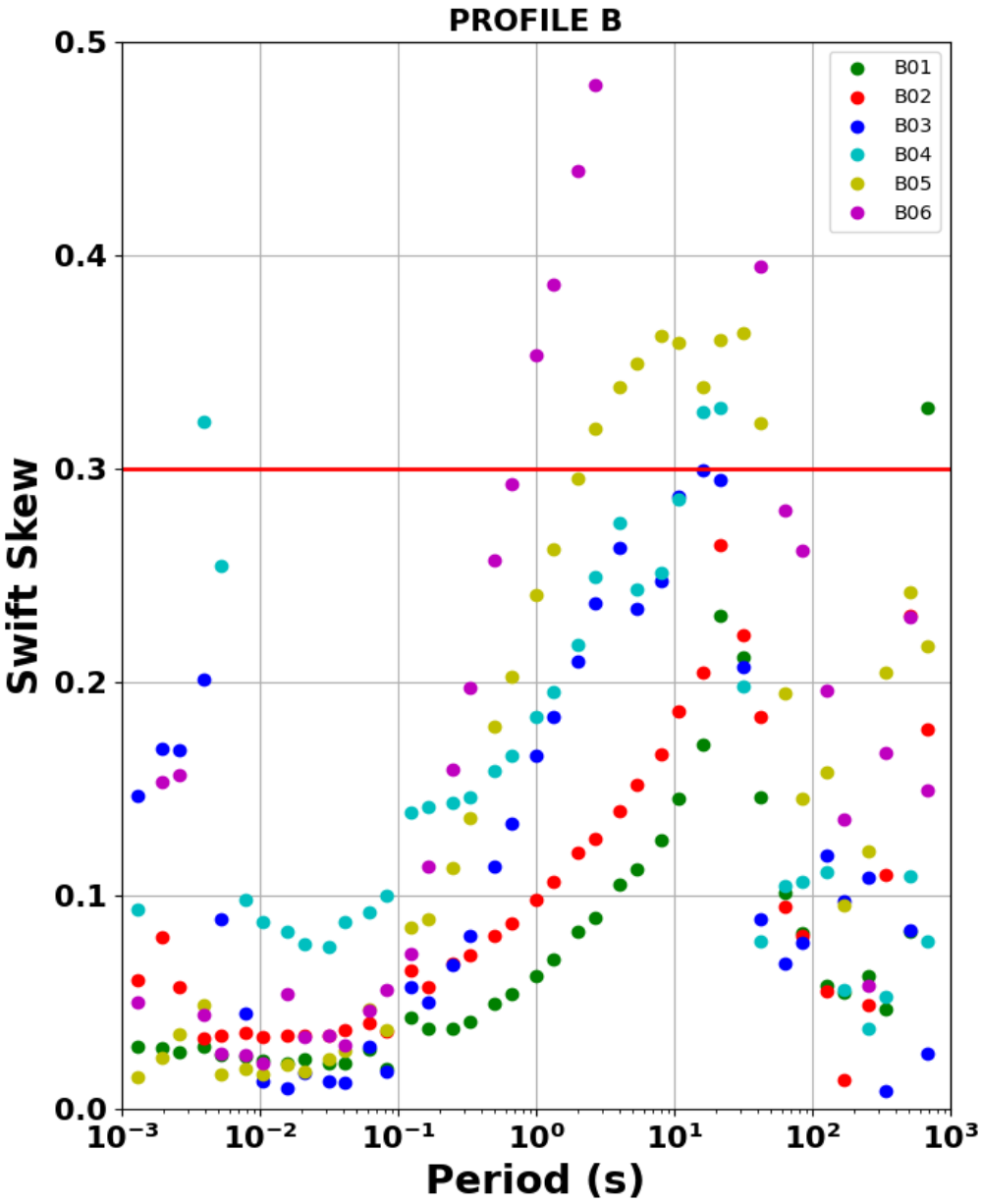

Figure 7. 5: Swift skew values for all sites with different colors representing different MT sounding stations shown in legend of the graphs. (a) most sites in profile A plotted below 0.3 threshold (red solid line) at short periods (b) shows all sites along profile B with majority of skew values plotting below 0.3 indicating 1-D or 2-D structure. 3-D structure is observed at long periods shown few skew values plotting above 0.3 for both profiles.

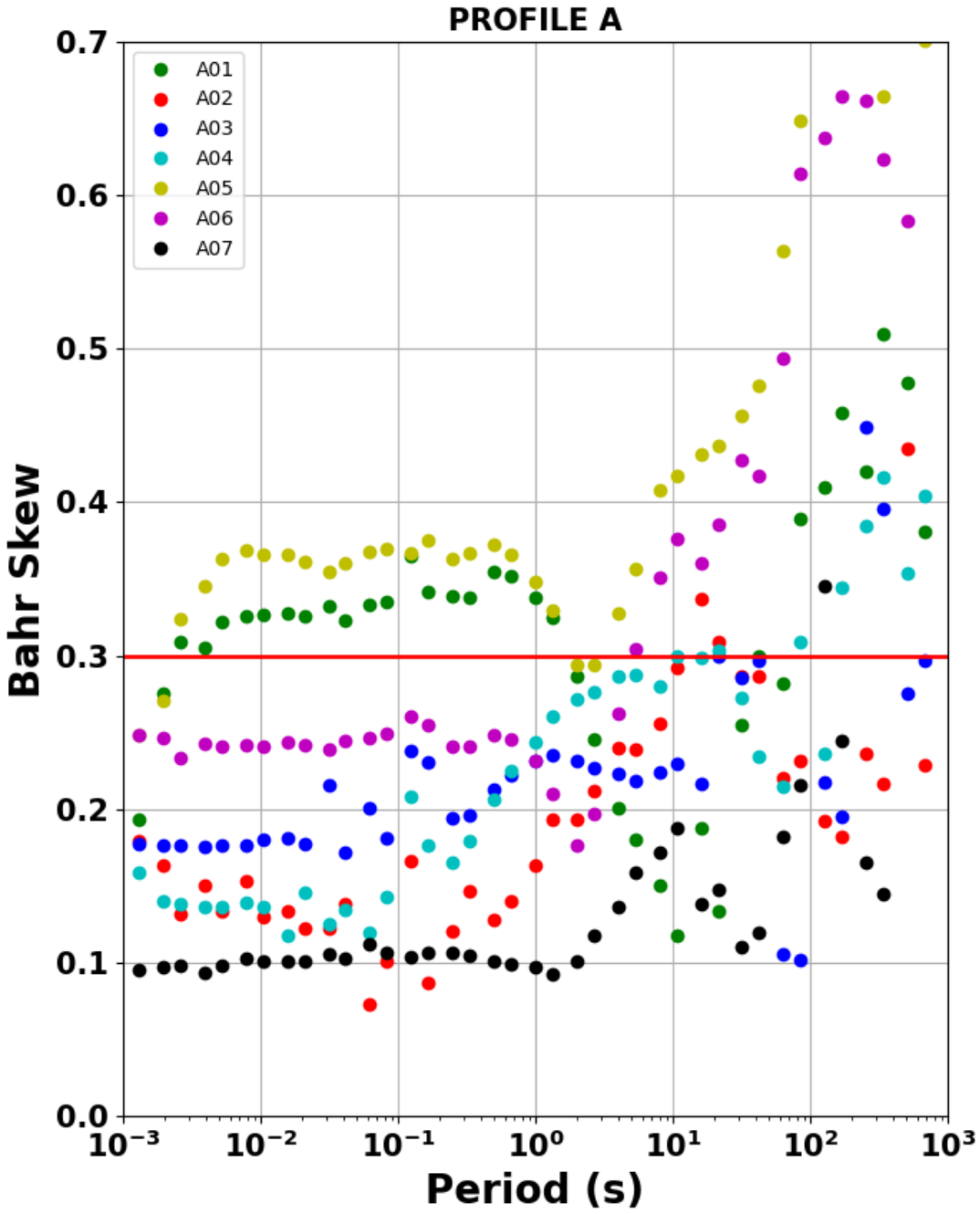
PROFILE A
A01
A02
A03
A04
A05
A06
A07
Bahr Skew
0.0
0.1
0.2
0.3
0.4
0.5
0.6
0.7
10^{-3}
10^{-2}
10^{-1}
10^{0}
10^{1}
10^{2}
10^{3}
Period (s)

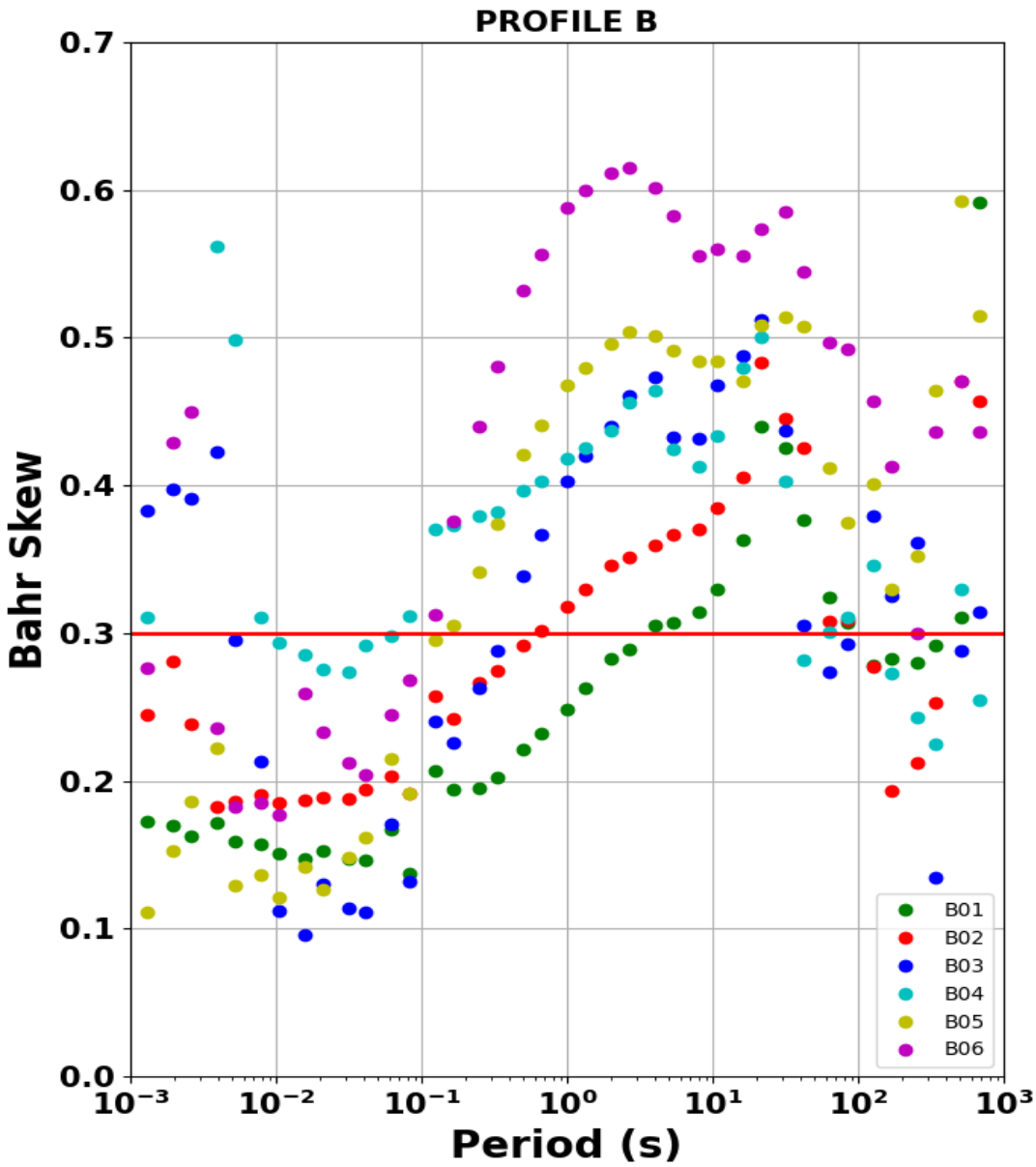

Figure 7. 6: Bahr skew values of all sites represented by different colors; (a) most of the sites along profile A plotted below 0.3 suggesting a 1-D or 2-D structure at short periods while a significant number of the values plotted above 0.3 indicating a 3-D structure present. (b) few sites are plotted below 0.3 at short periods whilst to most sites plotted above 0.3 at long periods indicating a 3-D subsurface structure.

7.2.1.2 Phase Tensor Analysis

Figure 7.7 represent the ellipse of the phase tensors for the MT data for the two profiles in the study area. The MTpy open source package in python (Kirkby et al., 2019; Krieger & Peacock, 2014) was used to plot the pseudo-sections. The cross sections are plotted in such a way that the horizontal axis correspond to north-south orientation. The phase tensor ellipses are reflected in various colors representing the MT response of dimensionality throughout the profiles. In profile A (Figure 7.7a) the different color scheme and shape of ellipses shown characterized the subsurface dimensionality or heterogeneity. At short periods, the phase tensor ellipses are nearly circular with skew angles close to zero along the profile, indicating a 1-D structure. The 1-D character of the subsurface structure is observed at periods less than ten seconds (<10 s) for station A01, A02, A03 and A04. In station A05, A06 and A07 however, the 1-D structure is observed at periods less than 1 second (< 1 s) before changing. As the periodicity increases, the circles become more ellipsoidal and asymmetrical in nature suggesting a 2-D or 3-D structure. According to Lilley and Weaver, (2010) 2-D structures correspond to asymmetry caused by mid-crustal inhomogeneities resulting in low phase tensor angles. However, the phase tensor skew angle values observed in the MT data for profile A are large and exceed the range of -5° – 5° for significant number of periods surpassing the 2-D approximation. Furthermore, in a 2D setting the orientation of the ellipses would be expected to remain consistent across stations and periods, but that is not the case for sites along the profile (Figure 7.7a) hence the structure could be 3-D in character. Le Pape et al., (2021) noted that, the complex 3D signatures of the phase tensor ellipses previously observed for southern Burkina Faso extend to northern Ghana as well at longer periods and could be the case for the study area. This changing pattern of the phase angle is stated by Stagpoole et al., (2009) to correspond to rapid change in resistivity within the subsurface.

In profile B (Figure 7.7b), the ellipticity of the phase tensor and the skew angle (β) are near zero at periods less than 0.1 seconds indicating 1-D structure at near surface for all sites across the profile. But for periods greater than 0.1 seconds the azimuth of the principal axis of the phase tensor varies with increasing periods suggesting the structure is 3-D at greater depths in the area. The 3-D structure is observed at a much shallow (taken less time = 0.01 seconds) depth in profile B as compared to profile A (greater than =1 s). This is probably due to the influence of the shallow basement underneath profile B. The relatively wide range of phase tensor skew angle values (values exceeding -5° - 5°) at long periods also suggest the possible presence of a 3-D structure beneath the profile.

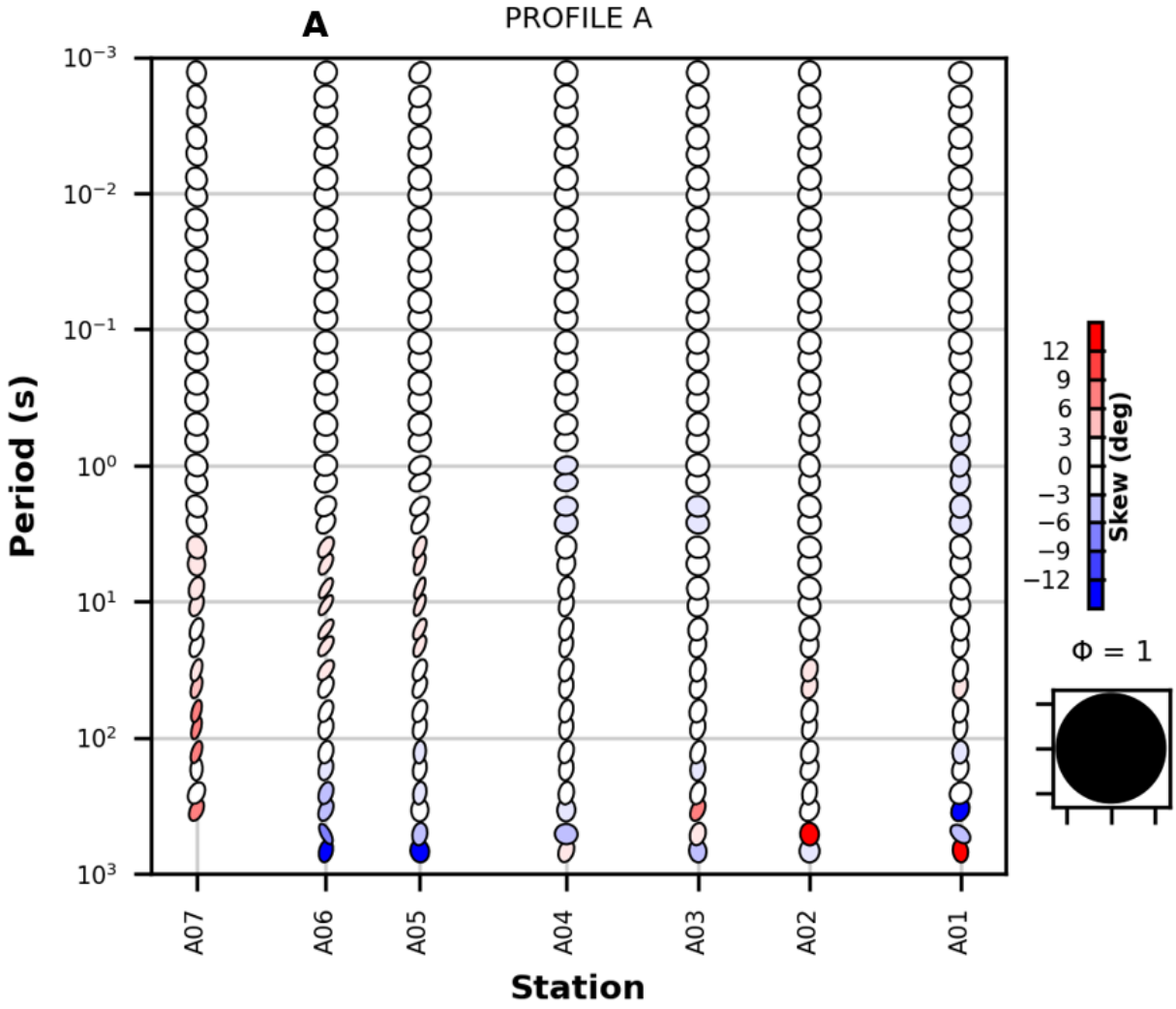
A
PROFILE A
Period (s)
10^{-3}
10^{-2}
10^{-1}
10^{0}
10^{1}
10^{2}
10^{3}
A07
A06
A05
A04
A03
A02
A01
Station
12
9
6
3
0
−3
−6
−9
−12
Skew (deg)
Φ = 1

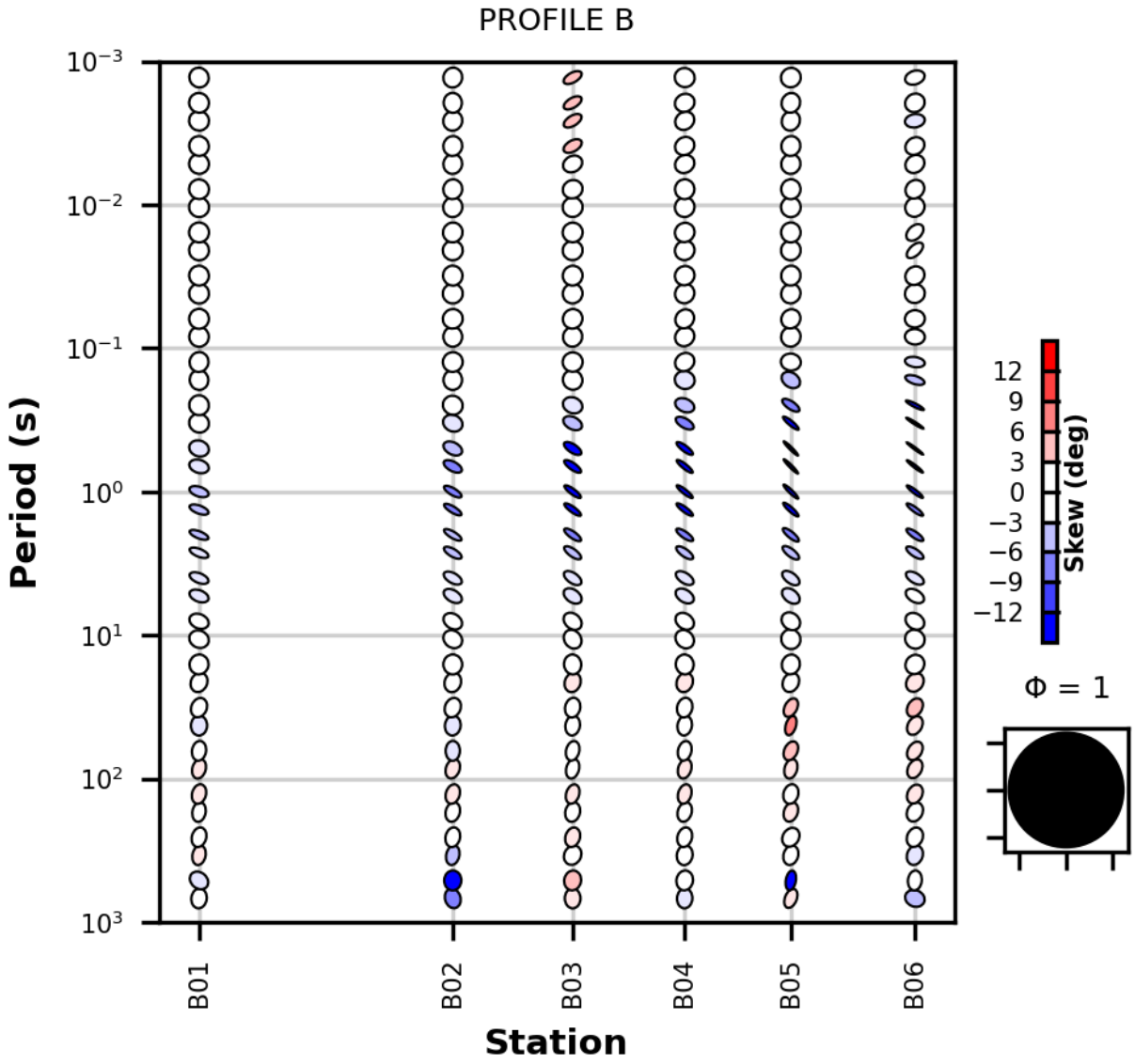

Figure 7. 7: Phase tensor pseudo-section plotted for all periods of MT data using MTpy (Kirkby et al., 2019; Krieger & Peacock, 2014): (a) profile A located south of the study area and showing 1-D structures at short periods and 3-D structure at long periods. (b) profile B located to the north in the study area and showing 1-D structures at periods less than 1 second. At long periods the data revealed a 3-D structure of the subsurface.

In general, the recorded MT data for the area showed more circular or rounded ellipses at near surface indicating 1-D structure with small phase tensor skew angles. At long periods however, the analysis revealed more of 3-D structure which supported by both the Swift and Bahr skew values computed for the study area. The dimensionality analysis by all three approaches suggest the inversion of the MT data in 3-D is required, hence 3-D inversion was performed to understand the geo-electrical structure of the area in this study. The 3-D model was then used

to validate the 1-D resistivity models at the individual sites which gives much better vertical resolution.

7.2.2 Static Shift Correction

Static shift is a possible source of distortion caused by resistivity heterogeneity at near electric dipoles (Maithya & Fujimitsu, 2019; Simpson & Bahr, 2005). The field recorded appeared not show static shift as no significant split was observed in the apparent resistivity curves at high frequencies for all sites. The sediment cover at near surface are relatively conductive which perhaps filtered the static shift effect in the data as observed. Also, by carrying the inversion in 3-D, the code used for the modeling accounts for static shift effects.

7.2.3 Basement Thickness and Morphology from MT Perspective

The 3D geo-electric resistivity structure across the northern Voltaian basin shows a low resistivity (6 - <126 Ωm) structure occurring at near surface and at deeper depth (> 50 Km). The low resistivity upper layer sits on a highly resistive (>1000 Ωm) formation beneath (Figure 7.8). The low resistivity upper layer (C1) clearly characterizes the sedimentary basin of the study area in which Neoproterozoic sediments unconformably overlies a Paleoproterozoic basement (R). The overlying conductive formation thus represents the sedimentary column along the profiles. The resistive structure below the conductive sediments aligns well with highly crystalline basement rocks of the area (Le Pape et al., 2021). It should be noted that the resolution of MT technique is high when constraining the top of conductors, but significantly decreases when constraining the bottom of conductive structure, especially for a thick conductive layer, due to the diffusive nature of MT signals (Abdul Azeez et al., 2017; Veeraswamy et al., 2020). In order to resolve clearly the depth to the top of the basement (thickness of sediments), different horizontal depth sections of the resistivity structure were presented in figure 7.9. The 3-D model shows that the resistive crystalline basement formation occurs at depth less than one kilometer (<1 Km) to the north of the area along the MT profile (Figure 7.9a) whereas to the south, the basement is observed deeper than 7 Km (Figure 7.9b). The observation suggests that the thickness of sediments in the basin varies and exceeds 7 Km at some locations in the area. Based on the difference in resistivity along the profiles, we can attempt to delineate the interface between the sediments and the basement. In figure 7.8 therefore, we proposed the sediment-basement interface (black broken line) which also shows the corresponding basement morphology across the traverse from north to south. The interface as defined ranges from a minimum of about 0.7 Km at the north to a maximum of about 7.4Km in the south in the upper crust.

The sediments basement interface for the area has been investigated using an integrated approach. The maximum depth to basement is estimated to be 6.9 km for the spectra technique, 7.3 km GM-SYS modelling and 7.4 km for the MT method. The variation in the sediment thickness estimated by the different techniques is within a range of $\pm 1\ km$ indicating a good agreement and emphasizes the need for the integration of geophysical techniques and data sets. The basement interface is asymmetrical as proposed by earlier researchers with shallow depths toward the margins of the basin. Understanding sediments thickness of the basin is crucial as it serve to guide the exploration efforts in the basin.

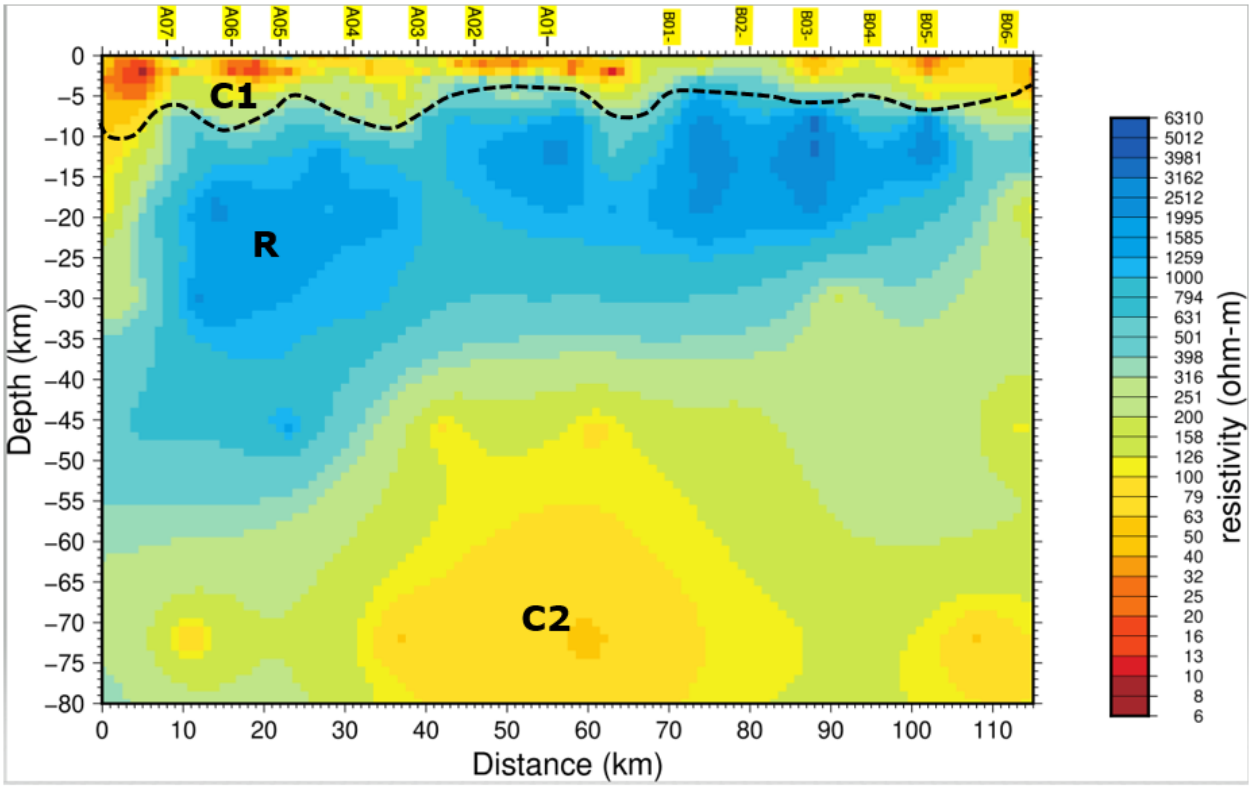

Figure 7. 8: Vertical section of 3-D model showing the geo-electrical resistivity structure along a NS profile with an inserted boundary defining possible sediment-basement interface and morphology of the basin. Black label C1 refers Conductive layer one, C2 refers to conductive zone two and R refers to Resistivity zone as defined in the model.

7.3 3-D Geo-Electric Structure of the Crustal and Mantle

The electrical structure of the subsurface is an intrinsic material property that is sensitive to temperature, composition, porosity, volatile and/or melt content and other physical properties relevant to the solid Earth (Naif et al., 2021). Investigating the electrical structure of the crust

and mantle is important as it provides valuable information on the physical and chemical state of the lithospheric system (Deng et al., 2021; Naif et al., 2021). Some of the most common and widely used methods for investigating the deep crust and mantle include seismological methods such as receiver function (Banerjee & Ahmed Salim, 2020; Lei, 2011; Saul et al., 2000). Also, joint inversion using multiple geophysical datasets (e.g., joint inversion with seismic and MT or seismic and gravity) have been used by several researchers (e.g. Al-Amri, 2015; Hautot et al., 2007; Khan et al., 2007; Moorkamp, 2007; Silahtar et al., 2020; Vadoodi & Rasmussen, 2022) to investigate lithospheric thickness in different parts of the world. The MT technique has also been used independently to effectively image the electrical structure of crust and mantle (e.g. Abdul Azeez et al., 2015; Evans et al., 2019; Khoza et al., 2013; Malleswari et al., 2019; Min et al., 2023; Selway, 2014; Spratt et al., 2009; Tian et al., 2019) and has contributed to a better understanding of the tectonic processes associated with the geodynamic evolution. The MT technique is effective and provide in-situ subsurface physical conditions which can be linked to tectonic processes through measurement of the naturally occurring time varying signals of electric and magnetic field (Abdul Azeez et al., 2015; Chave & Jones, 2012; Hautot et al., 2002; Malleswari et al., 2019; Miensopust, et al., 2011). The technique is highly subtle to high conductive structures, which might arise from different mechanisms taking place within the subsurface such as the presence of fluids, partial melts, and metallic minerals.

In the north of the VSB, the 3-D electrical structure of the transect has characteristic of lateral segmentation and vertical stratification (Figure 7.8). This perhaps represent different geo-electric units showing different resistivity signatures (Tian et al., 2019). The units within the profiles show stratified electrical characteristics. Specifically, a large scale high resistive body (R) occurs underneath the sedimentary cover (C1). The highly resistive body appeared to be largely within the middle crust and extend deeper towards the southern part of the study area. The middle crust consists of crystalline basement belonging to the Birimian formation in Ghana. In the northern part of the transect however, this resistive body is abridged by a conductive layer (<100 Ωm) which constitute another geo-electric unit (C2) at about 18 Km deep (Figure 7.9c). The massive conductor is observed at relatively shallow depth to north but spread steadily towards the south (Figure 7.9d) in a similar fashion like the highly resistive body (R). Le Pape et al., (2021) observed similar conductive structure in the north most part of the VSB following an east-west MT profile. They concluded that the structure was essentially within the crust. While it could be true that the conductive structure is within the crust, it tends have some form of link with deep lying materials probably beyond the limits of the crustal thickness of the area

as suggested by Le Pape et al., (2021). The crustal thickness estimated for the West Africa craton ranges from 37 Km to about 43 Km (Baranov & Bobrov, 2018).

According to Akpan, (2019), the average crustal thickness of the Birimian formation and the Dahomiyde mobile belt which boarded the eastern side of the VSB in Ghana, is 43 Km. The thickness of the resistive crust underlying the profile in this study exceed 41 Km in the south and gradually decrease in resistivity with depth, indicating a possible transition from the lower crust into the upper mantle (Figure 7.9). However, the lack of sharp contrast in resistivity makes it difficult to estimate the Moho in the area. The characteristics of the Moho boundary is influenced by the geology and tectonic evolution (Carbonell et al., 2013).

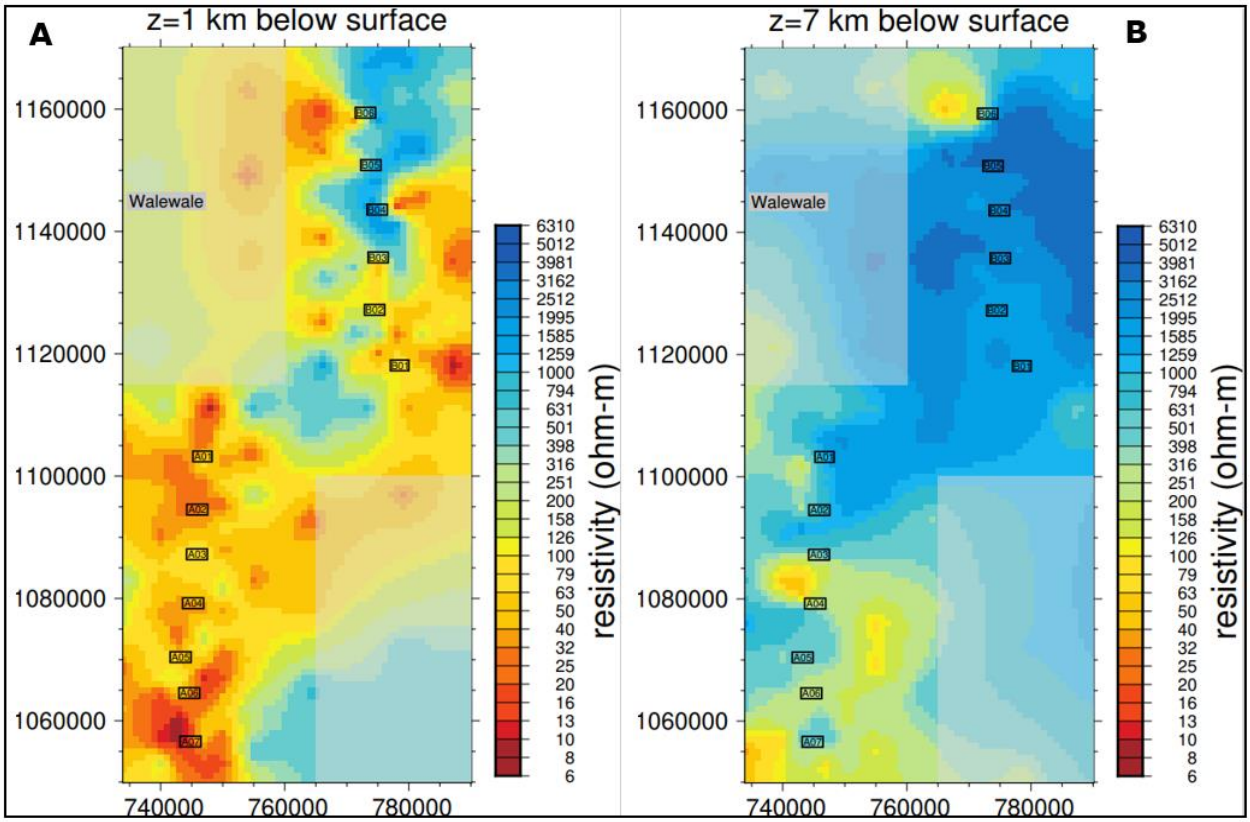

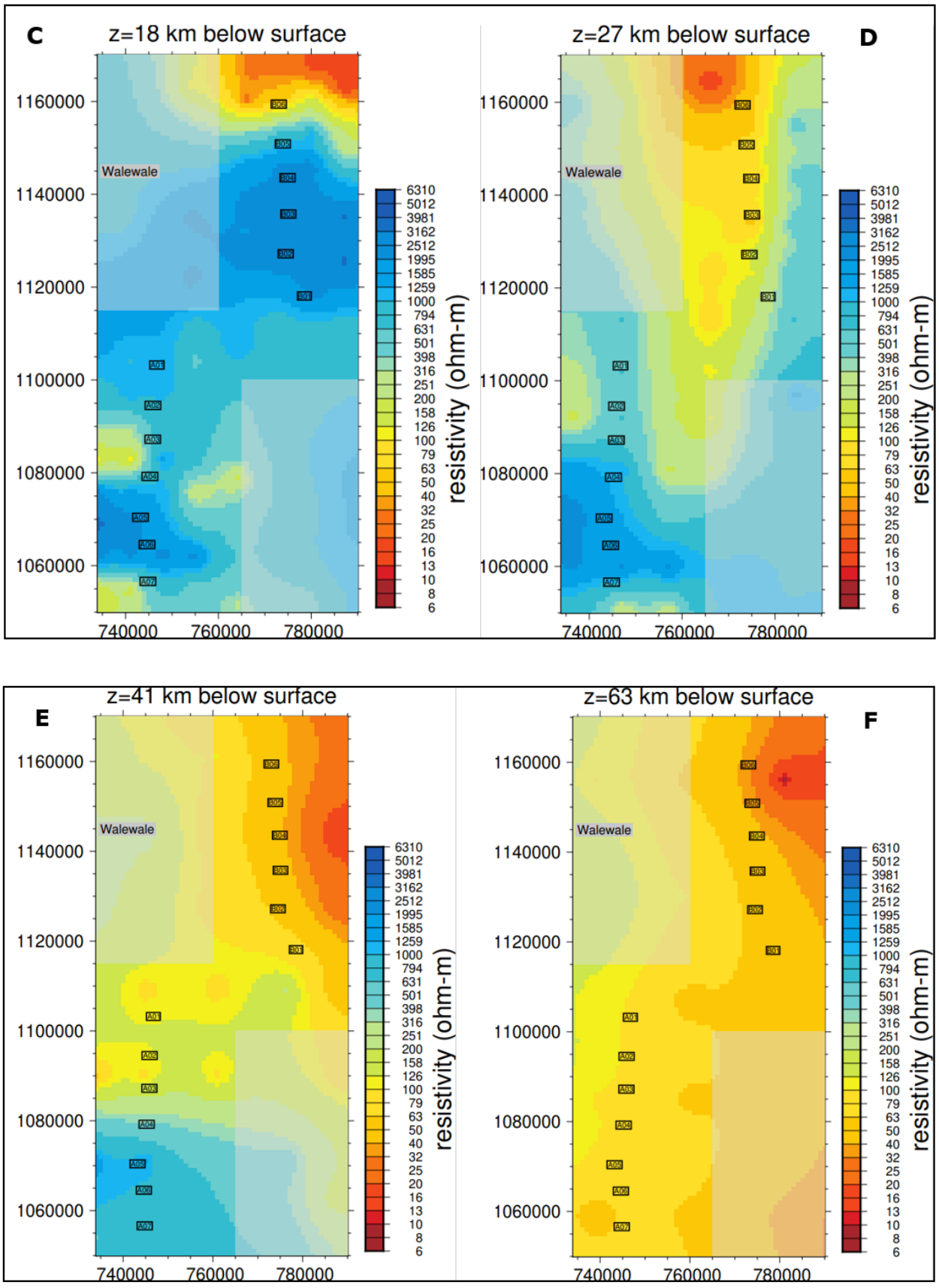

Figure 7. 9: Horizontal slice of the 3-D model showing the resistivity structure at different depths.

The origin of the Moho and its relationship to the crust-mantle interface are likely to be better constrained by careful investigation of its internal details which can be complex and spatially diverse (Carbonell et al., 2013; Levander & Miller, 2012). Unlike the oceanic Moho which is formed in a relatively simple, well understood process, the continental Moho can be subject to a wide range of tectonic events, making generalization about the continental Moho challenging (Carbonell et al., 2013).

The enhanced conductivity of the lower crust and upper mantle have been reported by many investigators using magnetotelluric (Akinremi et al., 2022; Hanneson & Unsworth, 2023; Jones et al., 2005; Khoza et al., 2013; Le Pape et al., 2017). A number of factors can account for the high conductivity in the lower crust and upper mantle. Anomalous conductive structure in the lower crust could be attributed to the presence of graphite or aqueous fluids (Jones et al., 2005). In some places, sulphide and other metalliferous ore deposits or magmatic event contribute to high conductivity in the lower crust (Le Pape et al., 2021; Wannamaker et al., 2008). Also, regions that are spatially close to shear zones or fault zones have high conductive features due to the crustal weakening at such locations (Akinremi et al., 2022; Jones et al., 2005). High conductivity features in the mantle can be attributed to high temperature, partial melting, hydration, or mineralization of the mantle material from magmatic intrusion (Akinremi et al., 2022; Jones et al., 2005; Khoza et al., 2013; Le Pape et al., 2017). Le Pape et al., (2021) noted that, a positive Bouguer anomaly peak along an MT profile in southern Burkina Faso in the Baule-Mossi Dormain that extends under the Voltaian basin, coincide with the conductive feature observed in northern Ghana in Voltaian basin. This led to their conclusion that the conductive zone in the crust could favor presence of magmatic sulphide deposits in the area. Our observation agreed with their assessment however, the feature seemed to extend deeper into the upper mantle towards the south, hence it could also be due to contribution from high temperature, hydration or iron enrichment from magmatic intrusion. The upper mantle beneath the profile is conductive and tend to have a connection with the conductive structure observed at a relatively shallow depth (~18 Km) to the north (mid-lower crust). According to Malleswari et al (2019), such shallow conductors with link to the upper mantle could be due to migration of Archean magmatism through weak channels (Fault/Shear zones) which are often caused by ductile deformation at greater depth. The structure is N-S orientated similar to the structure observed in southern Burkina Faso and northern Ghana (Le Pape et al., 2017, 2021).

7.4 CONCLUSION

In geologically complex terrains such as the VSB, the modeling and interpretation of MT data can be quite challenging, nonetheless the 3-D model explained the resistivity structure of the basin. The conductive layer at near surface is interpreted as the sedimentary basin that overlies a crystalline resistive basement. At the north of profile, a conductive body is observed at a relatively shallow depth compared to the south. The conductive body in the north tend to have some form of connection with a deep lying conductor (possibly in the upper mantle) towards the south. The interpretation of the conductivity of the lower most crust and upper mantle favors magmatic sulphide ore deposit and migration of magmatism along weak channels probably caused by ductile deformation at greater depths. The lack of apparent contrast in resistivity between the lower and upper mantle hindered the estimation of the Moho boundary estimation for the area. The study has revealed the geoelectrical framework of the basin and the underlying Paleoproterozoic basement and could form a major step in understanding the architecture and tectonic settings of the area.

CHAPTER EIGHT

CONCLUSIONSnAND RECOMMENDATIONS

8.0 CONCLUSIONS

The overall objective of this research was to characterize subsurface structures at different scales to improve on environmental management relative to groundwater development in the northern part of the Voltaian sedimentary basin (VSB). The first specific objective was to understand the likely perils posed by municipal waste dumps and their interaction with possible groundwater zones in the shallow part of the basin. The second was to investigate the assertion of the barrenness of the basin in relation to groundwater occurrence by characterizing the basin at different depths in search of possible fractures that could enhance the hydrogeologic conditions of the basin. These two specific objectives will be crucial in improving the resilience of communities in the basin as they will enhance the development of clean and quality groundwater (Sustainable development goal 6) in the northern part of the basin. In addition to the main objective stated above, the research also contributed to the long-disputed architectural framework of the basin by attempting to estimate the sediment thickness and investigate the overall electrical structure. To achieve these objectives, the electrical resistivity tomography (ERT) technique was deployed to collect data at some selected dump sites while airborne data sets were processed to delineate possible structure locations, and then proceeded with magnetotellurics (MT) techniques field campaign to ascertain the relative depth positions and geometry of the structural entities across varying depth in the area.

The analysis of the dumpsite ERT results reveals potential conductive fluids (leachates) steadily migrating both laterally and vertically into the shallow subsurface in the vicinity of the waste dumps. In some locations, the leachate plumes had infiltrated to depths possibly beyond the weathered zones. The presence of sub-vertical fractures observed appeared to aid leachate movement from the hybrid waste dumps and could potentially contaminate the already scarce shallow groundwater table in the area. To investigate this, groundwater samples were collected at the vicinity of the waste dumps to analyze for heavy metals concentration. This analysis revealed the concentration of cadmium (Cd) and iron (Fe) to exceed the permissible limits stated by WHO suggesting some form of leachate infiltration. The results of the ERT also helped to delineate the regolith thickness along the survey traverse, which coincides with the regolith depths previous reported for the basin. The findings from the waste dump study suggest it is probably impractical to continue exploring the shallow part of the basin, particularly in residential communities where leachate poses an imminent health threat. Already, the shallow (depths <100m) part of the basin has been reported to be less successful in terms of its

groundwater potential hence exploring for deep aquifer will make more sense as have been indicated.

Furthermore, a multi-scale approach using an integration of airborne magnetic, EM derived from B-field, and MT was utilized to delineate subsurface structures and defined lithological boundaries of the Bombouaka and Oti-Pendjari groups of the Voltaian Supergroup. The thicknesses indicated by this current research are approximately 250m for the Panabako Formation and 200m for the Poubogou Formation. This revised stratigraphic thickness indicates that the sediments in the area are deeper than what was earlier reported. Several other subsurface structures in the basin that have never been targeted for groundwater development have been identified at various depths. At least one of the structures could be hydraulically replenishing a stream and therefore was delineated as a fractured aquifer. The spatial pattern and characteristics of the network of structures suggest aquifer systems that could significantly improve the fortunes of the hydrogeology and groundwater exploration in the basin.

The scale of investigation and frequency of the MT were adjusted in a follow-up campaign with an aim to properly delineate shallow subsurface structures in a more localized study. The results of the MT were interpreted along with geophysical well logs, and geology to map potential structures that could have good hydrogeological implications in the basin at near the surface. Among the findings was a NE-SW fracture identified as a saprock aquifer at about 22m deep. The identification of this unit is significant within the sandstone formation as regional hydrogeological studies in the basin point to the expediency of the saprock to groundwater development. The results of this investigation also revealed an interplay of fractures at varying depths that could serving as potential aquifers and could hydraulically link the relatively deep-lying contact fracture to the flowing stream in the area. Additionally, three paleo-channels were characterized two of which have been revealed by an earlier investigator in the same area.

Our contribution to the long-disputed sediment thickness suggested an average thickness of 7.2 km and its towards the south and south-eastern end of the area. The sediment layer is thinner towards the margins of the basin and thickest towards the center and to the east. Also, the electrical structure of the basin revealed huge conductive bodies observed in the middle crust down into the mantle towards. While these deep conductors are still work in progress, we interpreted them as possible magnetic sulfide ore deposits and migration of magmatism along weak channels caused by deformation resulting geodynamic processes. The Moho boundary was not clearly defined due to lack of sharp contrast in resistivity between the lower crust and the upper mantle as observed in the area. However, the Moho could between 39-42 km which may align well with a regional Moho boundary estimation for the West Africa sub-region. The

investigation of the sediment basement interface and the crustal thickness of the basin forms a significant basis for understanding the basin's architecture and tectonics settings.

8.1 RECOMMENDATIONS

- Government and local authorities should as a matter of urgency enact regulations to curb the indiscriminate disposal of municipal solid disposal across communities in the basin in order to prevent possible contamination of the shallow groundwater table.
- Properly engineered landfills of modern standards must be adopted for waste management in the area.
- A drilling program should be carried out on the identified structures to properly characterize their yields and perhaps mechanize them for irrigation farming purposes as a poverty reduction strategy.
- More localized studies should be conducted throughout the basin using the MT technique to attempt to delineate the aquifer units across the entire basin in Ghana.
- We recommend the adoption and deployment of the MT technique for regional study of the geology of the basin in Ghana. The technique will help to better characterize the geology particularly the lithostratigraphic thicknesses of the various formations as lack outcrop exposures in the basin has hampered proper understanding of the local geology.

REFERENCES

Abdel Moneim, A. A. (2005). Overview of the geomorphological and hydrogeological characteristics of the Eastern Desert of Egypt. *Hydrogeology Journal, 13 (2),* 416–425.

Abdelaal, G. Z., Mousa, M. K. M., & Ebraheem, M. O. (2021). Estimate the depth to basement from the interpretation of aeromagnetic data at the northwestern part of Egypt. *Journal of Multidisciplinary Sciences*, *3*(1), 27–38. https://doi.org/10.33888/jms.2021.314

Abdul Azeez, K. K., Patro, P. K., Harinarayana, T., & Sarma, S. V. S. (2017). Magnetotelluric imaging across the tectonic structures in the eastern segment of the Central Indian Tectonic Zone: Preserved imprints of polyphase tectonics and evidence for suture status of the Tan Shear. *Precambrian Research*, *298*, 325–340. https://doi.org/10.1016/j.precamres.2017.06.018

Abdul Azeez, K. K., Veeraswamy, K., Gupta, A. K., Babu, N., Chandrapuri, S., & Harinarayana, T. (2015). The electrical resistivity structure of lithosphere across the Dharwar craton nucleus and Coorg block of South Indian shield: Evidence of collision and modified and preserved lithosphere. *Journal of Geophysical Research: Solid Earth 120*. https://doi.org/10.1002/2014JB011854

ABEM. (2010). *International Manual Terrameter LS.* ABEM Instruments, Stockholm, Sweden.

Aboud, E., Saud, R., Asch, T., Aldamegh, K., & Mogren, S. (2014). Water exploration using magnetotellurics and gravity data analysis; Wadi Nisah, Riyadh, Saudi Arabia. *NRIAG Journal Astronomy and Geophysics*, *3*, 184–191.

Abouelresh, M., D., B., Babalola, L., K., K., & Omer, M. (2016). *Factors Controlling Natural Fracture development in the Qusaiba Hot Shale, Northwest Saudi Arabia; Outcrop Approach*.

Aboyeji, O. S., & Eigbokhan, S. F. (2016). Evaluations of groundwater contamination by leachates around Olusosun open dumpsite in Lagos metropolis, southwest Nigeria. *Journal of Environmental Management*, *183*, 333–341. https://doi.org/10.1016/j.jenvman.2016.09.002

Acheampong, S., & Hess, J. (2000). Origin of the shallow grounwater system in the sothern Voltaian Sedimentary Basin of Ghana: An isotopic approach. *Journal of Hydrology*, 37–53.

Acheampong, S., Y., & Hess, J. W. (1998). Hydrogeologic and hydrochemical framework of the shallow groundwater system in the southern Voltaian Sedimentary Basin, Ghana. *Hydrogeology Journal*, *6*, 527–537. https://doi.org/10.1007/s100400050173

Adam, A. B., & Appiah-Adjei, E. K. (2019). Groundwater potential for irrigation in the Nabogo basin, Northern Region of Ghana. *Groundwater for Sustainable Development*, *9*, 100274. https://doi.org/10.1016/j.gsd.2019.100274

Addai, M. O., Yidana, S. M., Chegbeleh, L. P., Adomako, D., & Banoeng-Yakubo, B. (2016). Groundwater recharge processes in the Nasia sub-catchment of the White Volta Basin: Analysis of porewater characteristics in the unsaturated zone. *Journal of African Earth Science, 122*, 4–14.

Affaton, P., Sougy, J., & Trompette, R. (1980). The tectono-stratigraphic relationships between the Upper Precambrian and Lower Paleozoic Volta Basin and the Pan-African Dahomeyide orogenic belt (West Africa). *America Journal of Science*, *280*, 224–248.

Agarwal, A. K., Poll, H. E., & Weaver, J. T. (1993). One- and two-dimensional inversion of magnetotelluric data in continental regions. *Physics of the Earth and Planetary Interiors*, *18*, 155–176.

Agyekum, W. A., & Asare, E. B. (2016a). Challenges associated with ground water resources development in northern Ghana. *Ghana Journal of Science*, *56*, 39–51. https://doi.org/10.4314/gjs.v56i1

Agyekum, W. A., & Asare, E. B. (2016b). Challenges Associated with groundwater resources development in Northern Ghana. *Ghana Journal of Science*, *56*, 39–51.

Agyekum, W. A., Dark, P. K., & Dapaa-Siakwan, S. (2006). *Annual summary of groundwater monitoring in the White Volta River basin.* [Technical Report]. Water Research Institute.

Agyekum, W., Klitten, K., Armah, T., Banoeng-Yakubo, B., & Amartey, E. O. (2013). Geophysical borehole logging for control of driller's records: Hydrogeological case study from Voltaian sedimentary rocks in northern Ghana. *Applied Water Science*, *3*(2), 491–500. https://doi.org/10.1007/s13201-013-0097-y

Aina, A. (1986). Reduction to Equator, Reduction to Pole and Orthogonal Reduction of Magnetic Profiles. *Exploration Geophysics - EXPLOR GEOPHYS*, *17*. https://doi.org/10.1071/EG986141

Aizebeokhai, A. P., Oyeyemi, D. K., & Joel, S. E. (2016). Groundwater potential assessment in a sedimentary terrain, southwestern Nigeria. *Arabian Journal of Geoscience*, *9*, 496.

Akankpo, O., & Igboekwe, M. U. (2011). Monitoring Groundwater Contamination Using Surface Electrical Resistivity and Geochemical Methods. *Journal of Water Resource and Protection*, *3*(5), Article 5. https://doi.org/10.4236/jwarp.2011.35040

Akinremi, S., Fadel, I., & van der Meijde, M. (2022). Crustal and Upper Mantle Imaging of Botswana Using Magnetotelluric Method. *Frontiers in Earth Science*, *10*. https://www.frontiersin.org/articles/10.3389/feart.2022.840703

Ako, J., & Wellman, P. (1985). The margin of the West African craton: The Voltaian basin. *Journal of the Geological Society of London*, *142*, 625-632.

Akpan, O. U. (2019, June 24). Crustal structure of some tectonic region in West Africa. *Geodesy and Geodynamics*. CTBT Science and Technology 2019 Conference, Hofburg, Vienna, Austria.

Akudago, J. A., Chegbeleh, L. P., Nishigaki, M., Nanedo, N. A., Ewusi, A., & Kankam-Yeboah, K. (2009). Borehole Drying: A Review of the Situation in the Voltaian Hydrogeological System in Ghana. *Journal of Water Resource and Protection*, *1*(3), Article 3. https://doi.org/10.4236/jwarp.2009.13020

Al-Amoush, H., Al-Tarazi, E., Rajab, J. A., Al-Dwyeek, Y., Al-Atrash, M., & Shudiefat, A. (2015). Geophysical Investigation Using Time Domain Electromagnetic Method (TDEM) at Wadi Deir Al-Kahaf Area/Jordan for Groundwater Artificial Recharge Purposes. *Journal of Water Resource and Protection*, *07*(03), Article 03. https://doi.org/10.4236/jwarp.2015.73012

Al-Amri, A. M. (2015). Lithospheric structure of the Arabian shield from joint inversion of P and S-wave receiver functions and dispersion velocities. *Acta Geod Geophysics*, *65 (2)*, 229–245.

Al-Badani, M. A., & Al-Wathaf, Y. M. (2018). Using the aeromagnetic data for mapping the basement depth and contact locations, at southern part of Tihamah region, western Yemen. *Egyptian Journal of Petroleum*, *27*(4), 485–495. https://doi.org/10.1016/j.ejpe.2017.07.015

Al-Garni, M. A. (2009). Geophysical investigations for groundwater in a complex subsurface terrain, Wadi Fatima, KSA: A case history",. *Jordan Journal of Civil Engineering*, *Vol. 3, No. 2*, 118-136.

Al-Ibiari, M. G., Ismail, A. A. M., El-Khafeef, A. A., Basheer, A. A., El-laban, A. M. M., & Tarek, Y. (2017). Analysis and interpretation of aeromagnetic data for Wadi Zeidun area, Central Eastern Desert, Egypt. *Egyptian Journal of Petroleum*, *27*(3), 285–293. https://doi.org/10.1016/j.ejpe.2017.04.002

Aliou, A. S., Dzikunoo, E. A., Yidana, S. M., Loh, Y., & Chegbeleh, L. P. (2022). Investigation of Geophysical Signatures for Successful Exploration of Groundwater in Highly Indurated Sedimentary Basins: A Look at the Nasia Basin, NE Ghana. *Natural Resources Research*. https://doi.org/10.1007/s11053-022-10125-9

Al-saadi, O., Abd, N., Hijab, B., & Mustafa, B. (2021). *Subsurface Investigation Using Electrical Resistivity Imaging for Proposed Industrial Site near Erbil-Kirkuk Borders, Northern Iraq*. *54*, 198–209. https://doi.org/10.46717/igj.54.2E.14Ms-2021-11-30

Alshehri, F., & Abdelrahman, K. (2022). Groundwater aquifer detection using the time-domain electromagnetic method: A case study in Harrat Ithnayn, northwestern Saudi Arabia. *Journal of King Saud University - Science*, *34*(1), 101684. https://doi.org/10.1016/j.jksus.2021.101684

Ametepey, S. T., Cobbina, S. J., Akpabey, F. J., Duwiejuah, A. B., & Abuntori, Z. N. (2018). Health risk assessment and heavy metal contamination levels in vegetables from Tamale Metropolis, Ghana. *International Journal of Food Contamination*, *5*(1), 5. https://doi.org/10.1186/s40550-018-0067-0

Amponsah, T. Y., Danuor, S. K., Wemegah, D. D., & Forson, E. D. (2022). Groundwater potential characterisation over the Voltaian basin using geophysical, geological, hydrological and topographical datasets. *Journal of African Earth Sciences*, *192*, 104558. https://doi.org/10.1016/j.jafrearsci.2022.104558

Annan-Yorke, R. (1971). Geology of the Voltaian Basin (summary of current ideas). In: Cudjoe, J.E. (Ed.), Special Bulletin for Oil Exploration. *Geological Survey Depart Ment, Accra, Ghana, p.*

Apesegah, E. (2008). Hydrocarbon Potential of the Voltaian Basin (Post-Premuase-1 Well). *Voltaian Workshop Report*, 75–77.

Aplin, C. A., Flete, J. A., & Macquaker, H. S. J. (1999). *Muds and mudstones: Physical and fluid-flow properties* (Vol. 158). Geological Soceity of London.

Appiah, I., Wemegah, D. D., Asare, S. V.-D., Danuor, K. S., & Forson, E. D. (2018). Integrated geophysical characterisation of Sunyani municipal solid waste disposal site using magnetic gradiometry, magnetic susceptibility survey and electrical resistivity

tomography. *Journal of Applied Geophysics*, *153*, 143–153. https://doi.org/10.1016/j.jappgeo.2018.02.007

Aquaterrex. (2023). Deep Seated Water. *AquaterreX*. https://aquaterrex.com/deep-seated-water/

Arafa-Hamed, T., Marzouk, H., Elbarbary, S., & Abdel Zaher, M. (2023). A geophysical investigation of the urban-expanding area over the seismologically active Dahshour region, Egypt. *Acta Geophysica*. https://doi.org/10.1007/s11600-023-01131-3

Archie, G. E. (1942). The electrical resistivity log as an aid to determine some reservoir characteristics. *Trans.Am.Inst.Mining Met. Eng*, *146*, 54–62.

Arhin, E., Kazapoe, R. W., & Salami, F. (2020). Linking geology to the prevalence of non-communicable diseases: A case study of the Voltaian sedimentary basin, Ghana. *Ecofeminism and Climate Change*, *2*(1), 26–41. https://doi.org/10.1108/EFCC-05-2020-0014

Aristodemou, E., & Thomas-Betts, A. (2000). DC resistivity and induced polarisation investigations at a waste disposal site and its environments. *Journal of Applied Geophysics*, *44*(2), 275–302. https://doi.org/10.1016/S0926-9851(99)00022-1

Armah, F., Obiri, S., Yawson, D., ANM, P., & B, A. (2010). Mining and Heavy Metal Pollution: Assessment of Aquatic Environments in Tarkwa (Ghana) using Multivariate Statistical Analysis. *Journal of Environmental Statistics*, *1*, 1–13.

Asante, F., & Amuakwa-Mensah, F. (2015). *Climate change Variability in Ghana: Stocktaking. 3(1)*, 78–99.

Asuma, O. (2013). Leachate characterization and assessment of groundwater and surface water qualities near municipal solid waste dump site in Effurun, Delta state, Nigeria. *Journal of Environmental and Public Health*, *3(9)*, 126–135.

Atitsogbey, P., Steiner_Aseidu, M., Nti, C., & Ansong, R. (2018). The impact of climate change on household food security in the Bongo District of the UpperEast Region of Ghana. *Ghana Journal of Agric Science*, *52*, 145–153.

Attias, E., Thomas, D., Sherman, D., Ismail, K., & Constable, S. (2020). Marine electrical imaging reveals novel freshwater transport mechanism in Hawai‘i. *Science Advances*, *6*(48), eabd4866. https://doi.org/10.1126/sciadv.abd4866

Ayite, A., Awua, F., & Kalvig, P. (2008). Lithostratigraphy of the Gambaga massif. *The Voltaian Basin Ghana Workshop and Excursion*, 41.

Azaiez, H., Gabtni, H., & Bédir, M. (2021). Joint Gravity and Seismic Reflection Methods to Characterize the Deep Aquifers in Arid Ain El Beidha Plain (Central Tunisia, North Africa). *Water*, *13*. https://doi.org/10.3390/w13091310

Bahr, K. (1988). Interpretadon of the magnetotelluric impedance tensor: Regional induction and local telluric distortion. *Journal of Geophysics*, *62*, 119–127.

Bai, E., Guo, W., Zhang, D., Tan, Y., Guo, M., & Zhao, G. (2019). Using the Magnetotelluric Method for Detecting Aquifer Failure Characteristics under High-Intensity Mining of Thick Coal Seams. *Energies*, *12*(22), Article 22. https://doi.org/10.3390/en12224397

Balwant, P., Pujari, P. R., Dhyani, S., Bramhanwade, K., & Jyothis, V. (2022). Geophysical Methods for Assessing Microbial Processes in Soil: A Critical Review. *Indian Journal of Pure and Applied Scinece*, *60*, 707–715. https://doi.org/10.56042/ijpap.v60i8.63548

Banerjee, A., & Ahmed Salim, A. M. (2020). Seismic attribute analysis of deep-water Dangerous Grounds in the South China Sea, NW Sabah Platform region, Malaysia. *Journal of Natural Gas Science and Engineering*, *83*, 103534. https://doi.org/10.1016/j.jngse.2020.103534

Bannerman, R. R. (1990). *Appraisal of hydrogeological conditions and analysis of boreholes in the Nanumba and Western Gonja Districts—Northern Region, Ghana: Assessment of groundwater potential for hand dug wells. Final report for rural action NORRIP/GTZ.*. NORRIP.

Banoeng-Yakubo, B., & Armah, T. (2001). *Hydrogeological and geophysical test investigation in the Afram plain, Ghana.* [DANIDA-CWSA, Project,]. Department of Geology,University of Ghana.

Banoeng-Yakubo, B., Yidana, S. M., Ajayi, J. O., Loh, Y., & Aseidu, D. K. (2011). Hydrogeology and groundwater resources of Ghana: A review of the hydrogeology and groundwater hydrochemistry of Ghana. *In J. M. McMann (Ed.), Potable Water and Sanitation. Nova Science Publishers.*

Baranov, A., & Bobrov, A. (2018). Crustal structure and properties of Archean cratons of Gondwanaland: Similarity and difference. *Russian Geology and Geophysics*, *59*, 512–524. https://doi.org/10.1016/j.rgg.2018.04.005

Baranwal, V., & Rønning, J. (2020). *Airborne Geophysical Surveys and Their Integrated Interpretation* (pp. 377–400). https://doi.org/10.1007/978-3-030-28909-6_14

Barberio, M. D., Gori, F., Barbieri, M., Boschetti, T., Caracausi, A., Cardello, G. L., & Petitta, M. (2021). Understanding the Origin and Mixing of Deep Fluids in Shallow Aquifers and Possible Implications for Crustal Deformation Studies: San Vittorino Plain, Central Apennines. *Applied Sciences*, *11*(4), Article 4. https://doi.org/10.3390/app11041353

Barbosa, V., Silva, J., & Medeiros, W. (1999). Stability analysis and improvement of structure index estimation in Euler deconvolution. *Geophysics*, *64*, 48–60.

Barfod, G. H., Vervoort, J. D., Montanez, I. P., & Reibold, S. (2004). *Lu-Hf geochronology of phosphates in ancient sediments*. 5–11.

Bauer, P., Supper, R., Zimmermann, S., & Kinzelbach, W. (2006). Geoelectrical imaging of groundwater salinization in the Okavango Delta, Botswana. *Journal of Applied Geophysics*, *60*(2), 126–141. https://doi.org/10.1016/j.jappgeo.2006.01.003

Baumle, R., & Himmelsbach, T. (2018). Exploration of deep, previously unknown semi-fossil aquifers of the Kalahari Basin (southern Africa). *Grundwasser*. http://dx.doi.org/10.1007/s00767-017-0378-8

Becken, M., & Burkhardt, H. (2004). An ellipticity criterion in magnetotelluric tensor analysis. *Geophysical Journal International*, *159*(1), 69–82. https://doi.org/10.1111/j.1365-246X.2004.02376.x

Beinabaj, H. S. M., Heydariyan, H., Mohammad Aleii, H., & Hosseinzadeh, A. (2023). Concentration of heavy metals in leachate, soil, and plants in Tehran's landfill: Investigation of the effect of landfill age on the intensity of pollution. *Heliyon*, *9*(1), e13017. https://doi.org/10.1016/j.heliyon.2023.e13017

Bellali, A., Jarraya Horriche, F., Gabtni, H., & Bédir, M. (2018). Seismic reflection and structuring characterization of deep aquifer system in the Dakhla syncline (Cap Bon,

North-Eastern Tunisia). *Journal of African Earth Sciences*, *140*, 134–150. https://doi.org/10.1016/j.jafrearsci.2017.12.012

Benson, A. K. (1995). Applications of ground penetrating radar in assessing some geological hazards: Examples of groundwater contamination, faults, cavities. *Journal of Applied Geophysics*, *33*(1), 177–193. https://doi.org/10.1016/0926-9851(95)90040-3

Berdichevskiy, M. N., & Dmitriev, V. I. (1976). DISTORTION OF MAGNETIC AND ELECTRICAL FIELDS BY NEAR-SURFACE LATERAL INHOMOGENEITIES. *Acta Grodaet. Geophys. Et Mantanist. Acad. Sci. Hung.*, *11*, 217–221.

Bernard, J., Lemine, M., Diagana, B., & Ricolvi, M. (2004). Combination of electrical resistivity and magnetic resonance sounding data for mapping an aquifer layer in Mauritania. In *SEG Technical Program Expanded Abstracts 2004* (pp. 1381–1384). Society of Exploration Geophysicists. https://doi.org/10.1190/1.1839667

Bernardo, B., Candeias, C., & Rocha, F. (2022). Characterization of the Dynamics of Leachate Contamination Plumes in the Surroundings of the Hulene-B Waste Dump in Maputo, Mozambique. *Environments*, *9*, 19. https://doi.org/10.3390/environments9020019

Bertoni, C., Lofi, J., Micallef, A., & Moe, H. (2020). Seismic Reflection Methods in Offshore Groundwater Research. *Geosciences*, *10*(8), Article 8. https://doi.org/10.3390/geosciences10080299

Binley, A., Hubbard, S. S., Huisman, J. A., Revil, A., Robinson, D. A., Singha, K., & Slater, L. D. (2015). The emergence of hydrogeophysics for improved understanding of subsurface processes over multiple scales. *Water Resources Research*, *51*(6), 3837–3866. https://doi.org/10.1002/2015WR017016

Binley, A., & Kemna, A. (2005). *DC Resistivity and Induced Polarization Methods* (Vol. 50, pp. 129–156). https://doi.org/10.1007/1-4020-3102-5_5

Blakely, R. J. (1996). *Potential theory in gravity and magnetic application.* Cambridge, University press.

Blakely, R. J., & Simpson, R. W. (1986). Approximating edges of source bodies from magnetic or gravity anomalies. *Geophysics*, *51*, 1494–1498.

Boerner, D. E. (1992). Controlled source electromagnetic deep sounding: Theory, results and correlation with natural source results. *Surveys in Geophysics*, *13*, 435–488. https://doi.org/10.1007/BF01903486

Booker, J. R. (2014). The Magnetotelluric Phase Tensor: A Critical Review. *Surveys in Geophysics*, *35*(1), 7–40. https://doi.org/10.1007/s10712-013-9234-2

Bosum, W., Damaske, D., Roland, N. W., Behrendt, J., & Saltus, R. (1989). The Ganovex IV Victoria Land/Ross Sea aeromagnetic survey: Interpretation of anomalies. *Geologisches Jahrbuch*, *38*, 153–230.

Bourgeois, B., Mathieu, F., Vachette, C., & Vaubourg, P. (1994). AMT measurements compared with gravimetry and magnetometry for structural study of a sedimentary basin: Letlhakeng-Botlhapatlou groundwater project, Botswana. *Journal of Applied Geophysics*, *31*, 7–25. https://doi.org/10.1016/0926-9851(94)90044-2

Boyd, T., & Burnley, P. (2020). *GEOL 452/652—Geophysics* [SEG]. UNLV, Department of Geoscience. https://pburnley.faculty.unlv.edu/GEOL452_652/index.html

Bradford, J. H. (2002). Depth characterization of shallow aquifers with seismic reflection, Part I—The failure of NMO velocity analysis and quantitative error prediction. *GEOPHYSICS*, *67*(1), 89–97. https://doi.org/10.1190/1.1451362

Bravo-Osuna, A. G., Gómez-Treviño, E., Cortés-Arroyo, O. J., Delgadillo-Jauregui, N. F., & Arellano-Castro, R. F. (2021). Reframing the magnetotelluric phase tensor for monitoring applications: Improved accuracy and precision in strike determinations. *Earth, Planets and Space*, *73*(1), 34. https://doi.org/10.1186/s40623-021-01354-y

Bruno, P. P. G., & Vesnaver, A. (2021). Groundwater characterization in arid regions using seismic and gravity attributes: Al Jaww Plain, UAE. *Frontiers in Earth Science*, *8*. https://www.frontiersin.org/articles/10.3389/feart.2020.575019

Buddies, S. (2016). *How Dirt Cleans Water*. Scientific American. https://www.scientificamerican.com/article/how-dirt-cleans-water/

Bugan, R., Tredoux, G., Jovanovic, N., & Israel, S. (2018). Pollution Plume Development in the Primary Aquifer at the Atlantis Historical Solid Waste Disposal Site, South Africa. *Geosciences*, *8*(7), Article 7. https://doi.org/10.3390/geosciences8070231

Cagniard, L. (1953). Basic theory of mag netotelluric method of geophysical prospecting. *Society of Exploration Geophysics*, *18*, 605–635.

Caldwell, T. G., Bibby, H. M., & Brown, C. (2004). The magnetotelluric phase tensor. *Geophysical Journal International*, *158*(2), 457–469. https://doi.org/10.1111/j.1365-246X.2004.02281.x

Carbonell, R., Levander, A., & Kind, R. (2013). The Mohorovičić discontinuity beneath the continental crust: An overview of seismic constraints. *Tectonophysics*, *609*, 353–376. https://doi.org/10.1016/j.tecto.2013.08.037

Carney, J. N., Jordan, C. J., Thomas, C. W., Condon, D. J., Kemp, S. J., & Duodo, J. A. (2010). Lithostratigraphy, sedimentation and evolution of the Volta Basin in Ghana. *Precambrian Research, Volume 183*(Issue 4), 701–724. https://doi.org/10.1016/j.precamres.2010.08.012

Carrier, M. A., Lefebvre, R., Racicot, J., & Asare, E. B. (2008). *Northern Ghana hydrogeological assessment project*. 33rd WEDC International Conference., Accra, Ghana.

Carrier, M.-A., Lefebvre, R., & Asare, E. (2011). *Hydrogeological Assessment Project of the Northern Regions of Ghana (HAP): Final technical report : Water Resources Database Development.* (R1327; Issue R1327). INRS, Centre Eau, Terre et Environnement. https://espace.inrs.ca/id/eprint/1648/

Carrier, R. (2008). *Northern Ghana Hydrogeological Assessment Project*. https://www.academia.edu/20699400/Northern_Ghana_Hydrogeological_Assessment_Project

Carvajal-Flórez, E., & Cardona-Gallo, S.-A. (2019). Technologies applicable to the removal of heavy metals from landfill leachate. *Environmental Science and Pollution Research*, *26*(16), 15725–15753. https://doi.org/10.1007/s11356-019-04888-7

Caselle, C., Bonetto, S., & Comina, C. (2019). Comparison of laboratory and field electrical resistivity measurements of a gypsum rock for mining prospection applications. *International Journal of Mining Science and Technology*, *29*(6), 841–849. https://doi.org/10.1016/j.ijmst.2019.09.002

Castaneda, S. S., Sucgang, R. J., Almoneda, R. V., Mendoza, N. D. S., & David, C. P. C. (2012). Environmetal isotopes and major ions for tracing leachate contamination from a municipal landfillin Metro Manlia, Philippines. *Journal Environmental and Radioactivity*, *110*, 30–37.

Castillo-Widener, M. P. (2013). *Using ground penetrating radar in the investigation of LNAPL contamination within a controlled environment*. https://doi.org/10.13140/RG.2.1.3228.6565

Chandra, S., Ahmed, S., Auken, E., Pedersen, B. J., Singh, A., & Verma, S. (2016). 3D aquifer mapping employing airborne geophysics to meet the india's water future. *CSIR-NGRI.*

Chandra, S., Choudhury, J., Maury, P., Ahmed, S., Auken, E., & Verm, S. (2019). Geological significance of delineating paleochannels with AEM. *Exploration Geophysics*, 1834–7533.

Chandrasekhar, E., Fontes, S. L., Flexor, J. M., Rajaram, M., & Anand, S. P. (2009). Magnetotelluric and aeromagnetic investigations for assessment of groundwater resources in Parnaiba basin in Piaui State of North-East Brazil. *Journal of Applied Geophysics*, *68*(2), 269–281. https://doi.org/10.1016/j.jappgeo.2008.12.001

Chave, A. D., & Jones, A. G. (2012). The Magnetotelluric Method, Theory and Practice. *Cambridge University Press*.

Chave, A. D., & Thompson, D. J. (1989). Some comments on magnetotelluric response function estimation. *Journal of Geophysical Research*, *94*, 14202–14215.

Chegbeleh, L. P., Akudago, J. A., Nishigaki, M., & Edusi, S. N. (2009). ELECTROMAGNETIC GEOPHYSICAL SURVEY FOR GROUNDWATER EXPLORATION IN THE VOLTAIAN OF NORTHERN GHANA. *Journal of Environmental Hydrology*, *17*.

Chen, Y., Chen, Y., Liu, Q., & Liu, X. (2023). Quantifying common major and minor elements in minerals/rocks by economical desktop scanning electron microscopy/silicon drift detector energy-dispersive spectrometer (SEM/SDD-EDS). *Solid Earth Sciences*, *8*(1), 49–67. https://doi.org/10.1016/j.sesci.2022.12.002

Cheunteu Fantah, C. A., Mezoue, C. A., Mouzong, M. P., Tokam Kamga, A. P., Nouayou, R., & Nguiya, S. (2022). Mapping of major tectonic lineaments across Cameroon using potential field data. *Earth, Planets and Space*, *74*(1), 59. https://doi.org/10.1186/s40623-022-01612-7

Christensen, A., & Dransfield, M. (2002). Airborne vector magnetometry over banded iron formation. *In: 72nd Annual International Meeting of SEG.*, 13-16.

Christensen, T. H., Kjeldsen, P., Bjerg, P. L., Jensen, D. L., Christensen, J. B., Baun, A., Albrechtsen, H.-J., & Heron, G. (2001). Biogeochemistry of landfill leachate plumes. *Applied Geochemistry*, *16*(7), 659–718. https://doi.org/10.1016/S0883-2927(00)00082-2

Ciudad, D., Cobos, P., Sanchez, P., & Aroca, C. (2010). *RFID in Metal Environments: An Overview on Low (LF) and Ultra-Low (ULF) Frequency Systemsled*. https://doi.org/10.5772/7978

Clarke, G., & Smout, I. (2018). *Clay, Conductivity, and Rural Water supply: A hydrogeological investigation.* (Dissertation B221637; pp. 2–5). Loughborough Uni.

Connard, G., Couch, R., & Gemperle, M. (1983). Analysis of aeromagnetic measurements from the Cascade Range in central Oregon. *Geophysics*, *48*, 376–390.

Conti, P., Pistis, M., Bernardinetti, S., Barbagli, A., Zirulia, A., Serri, L., T., C., Guastaldi, E., & Ghiglieri, G. (2021). Tectonic Setting of the Kenya Rift in the Nakuru Area, Based on Geophysical Prospecting. *Geosciences*, *11*, 80. https://doi.org/10.3390/geosciences11020080

Cooper, G. (2004). Euler Deconvolution Applied to Potential Field Gradients. *Exploration Geophysics*, *35*. https://doi.org/10.1071/EG04165

Cooper, G., & Cowan, D. R. (2004). Filtering using variable order vertical derivatives. *Computers and Geosciences*, *30*, 455–459. https://doi.org/10.1016/j.cageo.2004.03.001

Cordell, L., & Grauch, V. J. S. (1985). Mapping Basement Magnetization zones from aeromagnetic data in the San Juan Basin, New Mexico, in Hinze, W.J., Ed., the Utility of Regional Gravity and Magnetic Anomaly Maps. *Society of Exploration Geophysics*, 181–197.

Coulibaly, N., Coulibaly, T. J. H., Mpakama, Z., & Savané, I. (2018). The Impact of Climate Change on Water Resource Availability in a Trans-Boundary Basin in West Africa: The Case of Sassandra. *Hydrology*, *5*(1), Article 1. https://doi.org/10.3390/hydrology5010012

Crawford, M. M., Bryson, L. S., Woolery, E. W., & Wang, Z. (2018). Using 2-D electrical resistivity imaging for joint geophysical and geotechnical characterization of shallow landslides. *Journal of Applied Geophysics*, *157*, 37–46. https://doi.org/10.1016/j.jappgeo.2018.06.009

Crowe, W. A., & Jackson-Hicks, S. (2008). Intrabasin deformation of the Volta Basin,. *The Voltaian Basin, Workshop and Excursion*, 31–38.

Dahlin, T. (1996). 2D resisitivity surveying for enviromental and engineering applications. *First Break*, *14*, 275–283.

Dapaah-Siakwa, S., & Gyau-Boakye, P. (2000). Hydrogeological framework and borehole yield in Ghana. *Hydrogeology Journal*, 8: 405-415.

Dawoud, A. M. (2011). Using Airborne Geophysical Survey for Exploring and Assessment of Groundwater Potentiality in Arid Regions. *Journal of King Abdulaziz, 22 (3)*, 207–220.

Day-Lewis, F. D., Slater, L. D., Robinson, J., Johnson, C. D., Terry, N., & Werkema, D. (2017). An overview of geophysical technologies appropriate for characterization and monitoring at fractured-rock sites. *Journal of Environmental Management*, *204*, 709–720. https://doi.org/10.1016/j.jenvman.2017.04.033

de Groot-Hedlin, C., & Constable, S. (1990). Occam's inversion to generate smooth two-dimensional models from magnetolluric data. *Geophysics*, *55*, 1613–1624.

de Jong, S. M., Heijenk, R. A., Nijland, W., & van der Meijde, M. (2020). Monitoring Soil Moisture Dynamics Using Electrical Resistivity Tomography under Homogeneous Field Conditions. *Sensors*, *20*(18), Article 18. https://doi.org/10.3390/s20185313

Demidova, T. A., Yegorov, I. V., & Yanikyan, V. O. (1985). Galvanic distortions of the magnetotelluric field of the lower Caucasus. *Geomagnetic Aeron.*, *25*, 391–396.

Demirci, İ., Gündoğdu, N. Y., Candansayar, M. E., Soupios, P., Vafidis, A., & Arslan, H. (2020). Determination and Evaluation of Saltwater Intrusion on Bafra Plain: Joint Interpretation of Geophysical, Hydrogeological and Hydrochemical Data. *Pure and*

Applied Geophysics, *177*(11), 5621–5640. https://doi.org/10.1007/s00024-020-02573-2

Deng, Y., Byrnes, J. S., & Bezada, M. (2021). New Insights Into the Heterogeneity of the Lithosphere-Asthenosphere System Beneath South China From Teleseismic Body-Wave Attenuation. *Geophysical Research Letters*, *48*(6), e2020GL091654. https://doi.org/10.1029/2020GL091654

Dentith, M., & Mudge, S. T. (2014). *Geophysics for the Mineral Exploration Geoscientist* (First edition). Cambridge University Press.

Dickson, K. B., & Benneh, G. A. (2004). New geography of Ghana. Longmans Group Ltd. *Longman Group Ltd.*

Dunlop, D. J., & Ozdemir, O. (2007). Geomagnetism. In *Sedimentology and structures of the Earth* (Vol. 1).

Dzikunoo, E. A., Vignoli, G., Jorgensen, F., Yidana, S. M., & Banoeng-Yakubo, B. (2020). New regional stratigraphic insights from a 3D geological model of the Nasia sub-basin, Ghana, developed for hydrogeological purposes and based on reprocessed B-field data originally collected for mineral exploration. *Solid Earth*, *11*, 349–361.

Edokpayi, J. N., Rogawski, E. T., Kahler, D. M., Hill, C. L., Reynolds, C., Nyathi, E., Smith, J. A., Odiyo, J. O., Samie, A., Bessong, P., & Dillingham, R. (2018). Challenges to Sustainable Safe Drinking Water: A Case Study of Water Quality and Use across Seasons in Rural Communities in Limpopo Province, South Africa. *Water*, *10*(2), 159. https://doi.org/10.3390/w10020159

Edwards, L. S. (1977). A modified pseudosection for resistivity and IP. *Geophysics*, *42(5)*, 1020–1036.

Egbueri, J. C., Agbasi, J. C., Ayejoto, D. A., Khan, M. I., & Khan, M. Y. A. (2023). Extent of anthropogenic influence on groundwater quality and human health-related risks: An integrated assessment based on selected physicochemical characteristics. *Geocarto International*, *38*(1), 2210100. https://doi.org/10.1080/10106049.2023.2210100

Eke, K. T., & Igboekwe, M. U. (2011). Geoelectric Investigation of Groundwater in Some Villages in Ohafia Locality, Abia State, Nigeria. *Current Journal of Applied Science and Technology*, 190–203. https://doi.org/10.9734/BJAST/2011/600

Elhag, A. B., & Elzien, S. M. (2013). Structures controls on groundwater occurrence and flow in crystalline bedrocks: A case study of the El Obeid area, Western Sudan. *Global Advanced Research Journal*, *2(2)*, 37–46.

Ersoy, A., & Waller, M. D. (1995). Textural characterisation of rocks. *Engineering Geology*, *39*(3), 123–136. https://doi.org/10.1016/0013-7952(95)00005-Z

Evans, R. L., Elsenbeck, J., Zhu, J., Abdelsalam, M. G., Sarafian, E., Mutamina, D., Chilongola, F., Atekwana, E. A., & Jones, A. G. (2019). Structure of the Lithosphere Beneath the Barotse Basin, Western Zambia, From Magnetotelluric Data. *Tectonics*, *38*(2), 666–686. https://doi.org/10.1029/2018TC005246

Ewusi, A., Seidu, J., & Ansah, E. (2020). Efficacy of Geophysical Techniques for Groundwater Exploration in the Volta Basin, Northern Region of Ghana. *Ghana Mining Journal*, *20*, 10–19.

Fairhead, J. D. (2007). Gravity and magnetics in today's oil and mineral industry. *GETECH Group Plc. Kitson House. Elmete Hall Roundhay, Leed. LS821J UK.*

Faleiro, E., Asensio, G., Denche, G., Garcia, D., & Moreno, J. (2019). Wenner Soundings for Apparent Resistivity Measurements at Small Depths Using a Set of Unequal Bare Electrodes: Selected Case Studies. *Energies*, *12*, 695.

Farag, K. S. I., Howari, F. M., & Abdelmalik, K. W. (2019). Imaging of hydrothermal altered zones in Wadi Al-Bana, in southern Yemen, using remote sensing techniques and very low frequency–electromagnetic data. *Arabian Journal of Geosciences*, *12*(18), 554. https://doi.org/10.1007/s12517-019-4702-8

Ferguson, G., Mcintosh, J., Perrone, D., & Jasechko, S. (2018). Competition for shrinking window of low salinity groundwater. *Environmental Research Letters*. https://doi.org/10.1088/1748-9326/aae6d8

Feroci, M., Orlando, L., Balia, R., Bosman, C., Cardarelli, E., & Deidda, G. (1986). Some consideration on shallow seismic reflection survey. *Journal of Applied Geophysics*, *2000*, 127–139. https://doi.org/10.1016/S0926-9851(00)00024-0

Fetter, C. W. (2002). *Applied Hydrogeology*. upper Sadle River.

Fiandaca, G., Doetsch, J., Vignoli, G., & Auken, E. (2015). Generalized focusing of time-lapse changes with applications to direct current and time-domain induced polarization inversions. *Geophysical Journal International*, *203*(2), 1101–1112. https://doi.org/10.1093/gji/ggv350

Filho, J. H., Salazar, F. R. dos S., Capri, M. da R., Neto, C. A., Alcantara, A. K. M., & Peixoto, L. de C. (2012). *State-of-the-Art and Trends in Atomic Absorption Spectrometry*. IntechOpen.com.

Fugro Airborn Survey. (2009b). *Fugro Airborne Surveys Interpretation: Airborne Geophysical Sur vey over the Volta River Basin and Keta Basin Geological Inter pretation Summary Report* (FCR2350/Job 1769). GGSA.

Fugro Airborn Survey. (2009a). *Fugro Airborne Surveys: Logistics and Processing Report, Airborne Magnetic and GEOTEM Survey, Areas 1 to 8* (92). GGSA.

Fugro Airborne Surveys. (2009b). *Airborne Geophysical Survey over the Volta River Basin and Keta Basin Geological Interpretation Summary Report,* (FCR2350/Job No.1769).

Fukushima, K., Kabir, M., Kanda, K., Obara, N., Fukuyama, M., & Otsuki, A. (2022). Simulation of Electrical and Thermal Properties of Granite under the Application of Electrical Pulses Using Equivalent Circuit Models. *Materials*, *15*(3), 1039. https://doi.org/10.3390/ma15031039

Gamble, T. D., Goubau, W. M., & Clarke, J. (1979). Magnetotellurics with a remote magnetic reference. *Geophysics*, *44*(1), 53–68. https://doi.org/10.1190/1.1440923

Ganiyu, S. A., Badmus, B. S., Idowu, O. A., oladunjoye, M. A., & Olurin, T. (2015). 2D Electrical Resistivity Imaging Investigation of Open Dump Site in Basement Complex Formation. *African Review of Physics*.

Garcia, X., Seillé, H., Elsenbeck, J., Evans, R. L., Jegen, M., Hölz, S., Ledo, J., Lovatini, A., Marti, A., Marcuello, A., Queralt, P., Ungarelli, C., & Ranero, C. R. (2015). Structure of the mantle beneath the Alboran Basin from magnetotelluric soundings. *Geochemistry, Geophysics, Geosystems*, *16*(12), 4261–4274. https://doi.org/10.1002/2015GC006100

Genchi, G., Sinicropi, M. S., Lauria, G., Carocci, A., & Catalano, A. (2020). The Effects of Cadmium Toxicity. *International Journal of Environmental Research and Public Health*, *17*(11), 3782. https://doi.org/10.3390/ijerph17113782

George, D. W., Selby, C. M., & Scolnik, R. (1947). Electrical Characteristics of Quartz-Crystal Units and Their Measurement. *Journal of Research of the National Bureau of Standards*, *38*.

Geosoft Inc., O. M. (2021). *Data Processing and Analysis Systems for Earth Science Application.* (2021.2) [English]. Seequent.

Geotomo-Software. (2002). *Geoelectrical Imaging 2D and 3D Geotomo Software Manual*. ABEM Instrument, Bromma, Sweden.

Geris, J., Comte, J.-C., Franchi, F., Petros, A. K., Tirivarombo, S., Selepeng, A. T., & Villholth, K. G. (2022). Surface water-groundwater interactions and local land use control water quality impacts of extreme rainfall and flooding in a vulnerable semi-arid region of Sub-Saharan Africa. *Journal of Hydrology*, *609*, 127834. https://doi.org/10.1016/j.jhydrol.2022.127834

Giroux, B., Chouteau, M., & Descloitres, M. (1997). Use of magnetotellurics methods in the study of deep Maestrichitian aquifer in Senegal. *Journal of Applied Geophysics*, 77-96.

Golshadi, Z., KarbalaeiRamezanali, A., & Kafaei, K. (2016). Interpretation of magnetic data in the Chenar-e Olya area of Asadabad, Hamedan, Iran, using analytic signal, Euler deconvolution, horizontal gradient and tilt derivative methods. *Bollettino Di Geofisica Teorica Ed Applicata*, *57*, 329–342. https://doi.org/10.4430/bgta0182

Grauch, V. J. S., Paul, W. B., & Keith, I. K. (2004). Preliminary interpretation of high resolution aeromagnetic data near Taos New Mexico. *5th Field Conference Geology of the Taos Region*, 244–256.

Greenfield, R. J., & Stoyer, C. H. (1976). Monitoring ground-water contamination with geophysical methods. *Trans. Soc. Min. Eng. AIME; (United States)*, *260:1*. https://www.osti.gov/biblio/7346030

Griffiths, D. H., & Barker, R. D. (1993). Two-dimensional resistivity imaging and modelling in areas of geology. *Journal of Applied Geophysics*, *29*, 211–226.

Grisey, B., & Aleya, L. (2016). Assessing the impact of leachate plumes on groundwater quality in Etueffont landfill (Belfort France). *Environmental Earth Sciences*, *75*, 913.

Groom, R., & Bailey, R. (1989). Decomposition of the Magnetotelluric impedance tensor in the presence of local three-dimensional galvanic distortion. *Journal of Geophysical Research*, *94, B2*, 1913–1925. https://doi.org/10.1029/JB094iB02p01913

Guireli Netto, L., Barbosa, A. M., Galli, V. L., Pereira, J. P. S., Gandolfo, O. C. B., & Birelli, C. A. (2020). Application of invasive and non-invasive methods of geo-environmental investigation for determination of the contamination behavior by organic compounds. *Journal of Applied Geophysics*, *178*, 104049. https://doi.org/10.1016/j.jappgeo.2020.104049

Gunn, D. A., Chambers, J., Uhlemann, S., Wilkinson, P. B., Meldrum, P., Dijkstra, T., Haslam, E., Kirkham, M., Wragg, J., Holyoake, S., Hughes, P., Hen-Jones, R., & Glendinning, S. (2014). Moisture monitoring in clay embankments using electrical resistivity tomography. *Construction and Building Materials*, *92*. https://doi.org/10.1016/j.conbuildmat.2014.06.007

Günther, T., & Müller-Petke, M. (2012). Hydraulic properties at the North Sea island of Borkum derived from joint inversion of magnetic resonance and electrical resistivity soundings. *Hydrology and Earth System Sciences*, *16*(9), 3279–3291. https://doi.org/10.5194/hess-16-3279-2012

Gyau-Boakye, P., & Dapaa-Siakwan, S. (1999). GROUNDWATER: SOLUTION TO GHANA'S RURAL WATER SUPPLY INDUSTRY? *The Ghana Engineer*.

Han, D., Tong, X., Currell, M. J., Cao, G., Jin, M., & Tong, C. (2014). Evaluation of the impact of an uncontrolled landfill on surrounding groundwater quality, Zhoukou, China. *Journal of Geochemical Exploration*, *136*, 24–39. https://doi.org/10.1016/j.gexplo.2013.09.008

Han, K., & Clark, S. M. (2021). Review of calculating the electrical conductivity of mineral aggregates from constituent conductivities. *Solid Earth Sciences*, *6*(2), 111–128. https://doi.org/10.1016/j.sesci.2021.02.003

Hanneson, C., & Unsworth, M. J. (2023). Regional-scale resistivity structure of the middle and lower crust and uppermost mantle beneath the southeastern Canadian Cordillera and insights into its causes. *Geophysical Journal International*, *234*(3), 2032–2052. https://doi.org/10.1093/gji/ggad183

HAP. (2011). *Water resource atlas of the northern regions of Ghana-hydrogeological assessment project (HAP).* [HAP]. Water resource commission.

Harinarayana, T. (2008). Applications of Magnetotelluric Studies in India. *Memoir Geological Society of India*, *68*.

Harris, C. R., Millman, K. J., Van der Walt, S. J., Gommers, R., Virtanen, P., Cournapeau, D., & Oliphat, T. E. (2020). Array programming with NumPy. *Nature*, *585*, 357–362. https://doi.org/10.1038/s41586-020-2649-2

Hasan, M., Shang, Y., & Jin, wj. (2018). Delineation of weathered/fracture zones for aquifer potential using an integrated geophysical approach: A case study from South China. *Journal of Applied Geophysics*, *157*, 47–60. https://doi.org/10.1016/j.jappgeo.2018.06.017

Hautot, S., Single, R. T., Waston, J., Harrop, N., Jerram, D. A., Tarits, P., Whaler, K., & Dawes, G. (2007). 3-D magnetotelluric inversion and model validation with gravity data for the investigation of flood basalts and associated volcanic rifted margins. *Geophysics Journal International*, *170*, 1418–1430.

Hautot, S., & Tarits, P. (2000). Deep structure of the Baringo Rift Basin (central Kenya) from three-dimensional magnetotelluric imaging' Implications for rift evolution. *Journal of Geophysical Research*, *105*, 23493–23518.

Hautot, S., Tarits, P., Perrier, F., Tarits, C., & Trique, M. (2002). Groundwater electromagnetic imaging in complex geological and topographical regions: A case study of a tectonic boundary in the French Alps. *GEOPHYSICS*, *67*(4), 1048–1060. https://doi.org/10.1190/1.1500365

Hayatudeen, M., Rasaq, B., Onaolapo, R. I., & Olummide, A. (2021). FIRST HORIZONTAL AND FIRST VERTICAL DERIVATIVES FROM HIGH RESOLUTION AEROMAGNETIC DATA OVER THE GONGOLA BASIN UPPER BENUE TROUGH NORTHEASTERN NIGERIA. *Global Journal of Pure and Applied Science*, *27, 2021*, 181–192. https://dx.doi.org/10.4314/gjpas.v27i2.10

Hazell, J. R. T., Cratchley, C. R., & Preston, A. M. (1988). The location of aquifers in crystalline rocks and alluvium in Northern Nigeria using combined electromagnetic and resistivity techniques. *Quarterly Journal of Engineering Geology, Vol.*, 159–175.

Heather, L. R.-S., Beth, A. S., Jeffrey, L. L. P. G., & Jeffrey, J. W. (1999). ELECTRICAL IMAGING: A Method for Identifying Potential Collapse and other Karst Features Near Roadways. *Science Application International Corporation*.

Hepburn, E., Madden, C., Szabo, D., Coggan, T. L., Clarke, B., & Currell, M. (2019). Contamination of groundwater with per- and polyfluoroalkyl substances (PFAS) from legacy landfills in an urban re-development precinct. *Environmental Pollution (Barking, Essex: 1987), 248*, 101–113. https://doi.org/10.1016/j.envpol.2019.02.018

Hossain, M. A., Haque, M. I., Parvin, M. A., & Islam, M. N. (2023). Evaluation of iron contamination in groundwater with its associated health risk and potentially suitable depth analysis in Kushtia Sadar Upazila of Bangladesh. *Groundwater for Sustainable Development*, *21*, 100946. https://doi.org/10.1016/j.gsd.2023.100946

Hubbard, S. S., Rubin, Y., & Majer, L. E. (1999). Spatial correlation structure estimation using geophysical and hydrogeological data. *Water Resource Research*, *35*, 1809–1825.

Ibraheem, I. M., Haggag, M., & Tezkan, B. (2019). Edge Detectors as Structural Imaging Tools Using Aeromagnetic Data: A Case Study of Sohag Area, Egypt. *Geosciences*, *9*(5), Article 5. https://doi.org/10.3390/geosciences9050211

Igboekwe, M. U., Agada, I. O., & Amos-Uhegbu, C. (2021). Investigation of Dumpsite Leachate using Electrical Resistivity Tomography at Umueze-Ibeku, Umuahia, South-Eastern Nigeria. *Journal of Scientific and Engineering Research, 8(4)*, 71–80.

Ishizu, K., & Ogawa, Y. (2021). Offshore-onshore resistivity imaging of freshwater using a controlled-source electromagnetic method: A feasibility study. *GEOPHYSICS*. https://doi.org/10.1190/geo2020-0906.1

Iwmi, G., Rao, V., Padalu, G., Dhakate, R., & Sarma, V. S. (2013). Application of electrical resistivity tomography methods for delineation of groundwater contamination and potential zones. *Arabian Journal of Geosciences*, *7*. https://doi.org/10.1007/s12517-013-0835-3

Jiang, Z., Mallants, D., Peeters, L., Gao, L., Soerensen, C., & Mariethoz, G. (2019). High-resolution paleovalley classification from airborne electromagnetic imaging and deep neural network training using digital elevation model data. *Hydrology and Earth System Sciences*, *23*(6), 2561–2580. https://doi.org/10.5194/hess-23-2561-2019

Joel, E. S., Olasehinde, P. I., De, D. K., & Maxwell. (2016). Regional groundwater studies using aeromagnetic technique. *Society of Exploration Geophysics*.

Jones, A. (1988). Static-shift of magnetotelluric data and its removal in a sedimentary environment. *Geophysics*, *53*, 967–978. https://doi.org/10.1190/1.1442533

Jones, A., Ledo, J., & Ferguson, I. (2005). Electromagnetic images of the Trans-Hudson Orogen: The North American Central Plains anomaly revealed. *Canadian Journal of Earth Sciences*, *42*, 457–478. https://doi.org/10.1139/e05-018

Jordan, C. J., Carney, J. N., Thomas, C. W., McDonnell, P., Turner, P., McNanus, K., & McEvoy, F. M. (2009). Ghana Airborne Geophysics Project: BGS Final Report. British Geological Survey Commissioned Report, CR/09/02. 325 pp. *Ghana Geological Survey Department, Accra*.

Jørgensen, F., Sandersen, P. B. E., & Auken, E. (2003). Imaging buried Quaternary valleys using the transient electromagnetic method. *Journal of Applied Geophysics*, *53*(4), 199–213. https://doi.org/10.1016/j.jappgeo.2003.08.016

Kabir, M. (2023). *Impacts of anthropogenic activities & climate change resulting from increasing concentration of Carbon dioxide on environment in 21st Century; A Critical Review*.

Kalmár, D., Hetényi, G., & Bondár, I. (2019). Moho depth analysis of the eastern Pannonian Basin and the Southern Carpathians from receiver functions. *Journal of Seismology*, *23*(5), 967–982. https://doi.org/10.1007/s10950-019-09847-w

Kalsbeek, F., Frei, D., & Affaton, P. (2008). Constraints on provenance, stratigraphic correlation and structural context of the Volta basin, Ghana, from detrital zircon geochronology: An Amazonian connection. *Sedimentary Geology, Volume 212*(Issues 1–4,), 86–95. https://doi.org/10.1016/j.sedgeo.2008.10.005

Kalsbeek, F., & Frei, R. (2010). Geochemistry of Precambrian sedimentary rocks used to solve stratigraphical problems: An example from the Neoproterozoic Volta basin, Ghana. *Precambrian Research*, *176*(1–4), 65–76. https://doi.org/10.1016/j.precamres.2009.10.004

Kamiński, M., Zientara, P., & Krawczyk, M. (2023). Application of airborne laser scanning and electrical resistivity tomography in the study of an active landslide and geology of the cliff, Jastrzębia Góra, Poland. *Bulletin of Engineering Geology and the Environment*, *82*(4), 131. https://doi.org/10.1007/s10064-023-03153-z

Kanthiya, S., Mangkhemthong, N., & Morley, K. C. (2019). Structural interpretation of Mae Suai Basin, Chiang Rai Province, based on gravity data analysis and modelling. *Heliyon*, *5*.

Kearey, P., Brook, M., & Hill, I. (2002). *An Introduction to Geophysical Exploration* (Third Edition). Blackwell Scientific Publications.

Kearey, P., & Brooks, M. (1991). *An Introduction to Geophysical Exploration, 2nd Edition*. Blackwell Scientific Publications.

Keller, G. V., & Frischknecht, F. C. (1966). *Electrical methods in geophysical prospecting.* Pergamon Press Ltd.

Kenworthy, A. (2016, January 10). Top Five Reasons to Use Geophysics in Environmental Projects. *Seequent*. https://www.seequent.com/top-five-reasons-to-use-geophysics-in-environmental-projects/

Kesse, G. O. (1985). *The mineral and rock resources of Ghana.* Balkema.

Khalil, M. H. (2014). Detection of Magnetically Susceptible Dyke Swarms in a Fresh Coastal Aquifer. *Pure and Applied Geophysics*, *171*(8), 1829–1845. https://doi.org/10.1007/s00024-013-0696-4

Khan, A., Connolly, J. A. D., Maclennan, J., & Mosegaardl, K. (2007). Joint inversion of seismic and gravity data for lunar composition and thermal state. *Geophysical Journal International*, *168*, 243–258.

Khoza, T. D., Jones, A. G., Muller, M. R., Evans, R. L., Miensopust, M. P., & Webb, S. J. (2013). Lithospheric structure of an Archean craton and adjacent mobile belt revealed from 2-D and 3-D inversion of magnetotelluric data: Example from southern Congo craton in northern Namibia. *Solid Earth*. https://doi.org/10.1002/jgrb.50258

Kirkby, A. L., Zhang, F., Peacock, J., Hassan, R., & Duan, J. (2019). The MTPy software package for magnetotelluric data analysis and visualisation. *Journal of Open Source Software*, *4*(37), 1358. https://doi.org/10.21105/joss.01358

Kivior, I., & Boyd, D. (1998). Interpretation of the aeromagnetic experimental survey in Euromanga-Cooper basin. *Journal of Canadian ExplorationGeophysics*, *34*, 58–66.

Klitten, K., & Agyekum, W. A. (2021). *Geophysical Wire-line Logging of Boreholes in Nasia River Catchment Basin.* (Danida Project ID 14-P02-GHA; Groundwater Development and Sustainable Agriculture in White Volta Basin of Ghana, pp. 15–45). GEOLOGICAL SURVEY OF DENMARK AND GREENLAND.

Knight, R. (2000). Seeing into the Earth: Noninvasive Characterization of the Shallow Subsurface for Environmental and Engineering Applications. *National Academy Press, Washington, D.C.* http://dx.doi.org/10.17226/5786, 148p

Knight, R., Smith, R., Asch, T., Abraham, J., Cannia, J., Viezzoli, A., & Fogg, G. (2018). Mapping Aquifer Systems with Airborne Electromagnetics in the Central Valley of California. *Ground Water*, *56*(6), 893–908. https://doi.org/10.1111/gwat.12656

Kpiebaya, P., & Abdul-Ganiyu, S. (2020). *Hydrogeological Study of Groundwater for Dry Season Farming in Northern Region of Ghana*. *15*, 187–196.

Kriaa, A., Hajji, M., Jamoussi, F., & Hamzaoui, A. H. (2014). Electrical Conductivity of 1:1 and 2:1 Clay Minerals. *Euro-Mediterranean Journal for Environmental Integration*, 78–88.

Krieger, L., & Peacock, J. R. (2014). MTpy: A Python toolbox for magnetotellurics. *Computers & Geosciences*, *72*, 167–175. https://doi.org/10.1016/j.cageo.2014.07.013

Kumar, A., Fernàndez, M., Vergés, J., Torne, M., & Jiménez-Munt, I. (2021). Opposite Symmetry in the Lithospheric Structure of the Alboran and Algerian Basins and Their Margins (Western Mediterranean): Geodynamic Implications. *Journal of Geophysical Research: Solid Earth*, *126*(7), e2020JB021388. https://doi.org/10.1029/2020JB021388

Kumar, V. P. V., Rao, S. P. B. V., Singh, A. K., Kumar, A., & Rao, R. P. (2021). Dimensionality and directionality analysis of magnetotelluric data by using different techniques: A case study from northern part of Saurashtra region, India. *Journal of Earth System Science*, *130*, 102. https://doi.org/10.1007/s12040-021-01596-0

LANGEO. (2023). *Summary of different array types of electrical method_Langeo Geophysical Instruments*. http://www.langeoinstrument.com/bolg/2016/0824/105.html

Launay, N., Quesnel, Y., Rochette, P., & Demory, F. (2018). Iron Formations as the Source of the West African Magnetic Crustal Anomaly. *Frontiers in Earth Science*, *6*. https://www.frontiersin.org/articles/10.3389/feart.2018.00032

Le Pape, F., Jones, A. G., Jessell, M. W., Hogg, C., Siebenaller, L., Perrouty, S., Touré, A., Ouiya, P., & Boren, G. (2021). The nature of the southern West African craton lithosphere inferred from its electrical resistivity. *Precambrian Research*, *358*, 106190. https://doi.org/10.1016/j.precamres.2021.106190

Le Pape, F., Jones, A. G., Jessell, M. W., Perrouty, S., Gallardo, L. A., Baratoux, L., Hogg, C., Siebenaller, L., Touré, A., Ouiya, P., & Boren, G. (2017). Crustal structure of southern Burkina Faso inferred from magnetotelluric, gravity and magnetic data. *Precambrian Research*, *300*, 261–272. https://doi.org/10.1016/j.precamres.2017.08.013

Lei, J. (2011). Seismic tomographic imaging of the crust and upper mantle under the central and western Tien Shan orogenic belt. *Journal of Geological Research*, *116*, B09305.

Levander, A., & Miller, M. (2012). Evolutionary aspects of lithosphere discontinuity structure in the Western U.S. *Geochemistry Geophysics Geosystems*, *13*. https://doi.org/10.1029/2012GC004056

Li, H., Li, H., Wang, K., & Liu, C. (2018). Effect of rock composition microstructure and pore characteristics on its rock mechanics properties. *International Journal of Mining Science and Technology*, *28*(2), 303–308. https://doi.org/10.1016/j.ijmst.2017.12.008

Lilley, F. E. M., & Weaver, J. T. (2010). Phases greater than 90° in MT data: Analysis using dimensionality tools. *Journal of Applied Geophysics*, *70*(1), 9–16. https://doi.org/10.1016/j.jappgeo.2009.08.007

Lissah, S. Y., Ayanore, M. A., Krugu, J. K., Aberese-Ako, M., & Ruiter, R. A. C. (2021). Managing urban solid waste in Ghana: Perspectives and experiences of municipal waste company managers and supervisors in an urban municipality. *PLOS ONE*, *16*(3), e0248392. https://doi.org/10.1371/journal.pone.0248392

Liu, H., Liang, Y., Zhang, D., Wang, C., Liang, H., & Cai, H. (2010). Impact of MSW landfill on the environmental contamination of phthalate esters. *Waste Management*, *30*(8), 1569–1576. https://doi.org/10.1016/j.wasman.2010.01.040

Liu, Q., Shu, Q., Gao, W., Luo, Y., Li, Z., Yang, J., & Xu, W. (2023). Automatic Interpretation of Potential Field Data Based on Euler Deconvolution with Linear Background. *Applied Sciences*, *13*(9), Article 9. https://doi.org/10.3390/app13095323

Local Gov. Minstry. (2023, July 16). Tamale Metropolitan Assembly. *Ghana District.Com*. http://ghanadistricts.com/Home/District/139

Loke, M. (2001). *Tutorial: 2-D and 3-D Electrical Imaging Surveys*.

Loke, M., & Barker, R. (1996). Rapid least-squares inversion of apparent resistivity pseudo-sections by quasi-Newton method. *Geophysics Prospect.*, *44*, 131–152.

Lubang, J., Liu, H., & Chen, R. (2023). Combined Application of Hydrogeological and Geoelectrical Study in Groundwater Exploration in Karst-Granite Areas, Jiangxi Province. *Water*, *15*, 865.

Luo, Y., Xue, D.-J., & Wang, M. (2010). Reduction to the Pole at the Geomagnetic Equator. *Chinese Journal of Geophysics*, *53*(6), 1082–1089. https://doi.org/10.1002/cjg2.1578

Luparello, C., Sirchia, R., & Longo, A. (2011). Cadmium as a transcriptional modulator in human cells. *Critical Reviews in Toxicology*, *41*(1), 75–82. https://doi.org/10.3109/10408444.2010.529104

MacDonald, A. M., & Davies, J. (2000). *A brief review of groundwater for rural water supply in Sub-saharan Africa*. (BGS Technical Report WC/00/33; Overseas Geology Series). British geological survey.

MacDonald, A. M., Kemp, S. J., & Davies, J. (2005). Transmissivity variations in Mudstones. *Groundwater Journal*, *43*(no.2), 259–269.

Mackie, R. L., Madden, T. R., & Wannamaker, P. E. (1993). Three-dimensional magnetotelluric modelling using difference equations—Theory and com parisons to integral equation solutions. *Geophysics*, *58*, 215–226.

Mainoo, P. A., Manu, E., Yidana, S. M., Agyekum, W. A., Stigter, T., Duah, A. A., & Preko, K. (2019). Application of 2D-Electrical resistivity tomography in delineating

groundwater potential zones: Case study from the voltaian super group of Ghana. *Journal of African Earth Sciences*, *160*, 103618. https://doi.org/10.1016/j.jafrearsci.2019.103618

Maithya, J., & Fujimitsu, Y. (2019). Analysis and interpretation of magnetotelluric data in characterization of geothermal resource in Eburru geothermal field, Kenya. *Geothermics*, *81*, 12–31. https://doi.org/10.1016/j.geothermics.2019.04.003

Malleswari, D., Veeraswamy, K., Abdul-Azeez, K. K., Gupta, A. K., Babu, N., Patro, P. K., & Harinarayana, T. (2019). *Magnetotelluric investigation of lithospheric electrical structure beneath the Dharwar Craton in south India: Evidence for mantle suture and plume-continental interaction | Elsevier Enhanced Reader*. https://doi.org/10.1016/j.gsf.2018.10.011

Manfredi, E. C., Flury, B., Viviano, G., Thakuri, S., Khanal, S. N., Jha, P. K., Maskey, R. K., Kayastha, R. B., Kafle, K. R., Bhochhibhoya, S., Ghimire, N. P., Shrestha, B. B., Chaudhary, G., Giannino, F., Cartenì, F., Mazzoleni, S., & Salerno, F. (2010). Solid Waste and Water Quality Management Models for Sagarmatha National Park and Buffer Zone, Nepal. *Mountain Research and Development*, *30*(2), 127–142. https://doi.org/10.1659/MRD-JOURNAL-D-10-00028.1

Manzella, A., Volpi, G., Zaja, A., & Meju, M. (2004). Combined TEM-MT investigation of shallow-depth resistivity structure of Mt Somma-Vesuvius. *Journal of Volcanology and Geothermal Research*, *131*(1), 19–32. https://doi.org/10.1016/S0377-0273(03)00313-5

Martí, A., Queralt, P., Ledo, J., & Farquharson, C. (2010). Dimensionality imprint of electrical anisotropy in magnetotelluric responses. *Physics of the Earth and Planetary Interiors*, *182*(3), 139–151. https://doi.org/10.1016/j.pepi.2010.07.007

Martinho, E., & Dionísio, A. (2014). Main geophysical techniques used for non-destructive evaluation in cultural built heritage: A review. *Journal of Geophysics and Engineering*, *11*(5), 053001. https://doi.org/10.1088/1742-2132/11/5/053001

Martorana, R., Capizzi, P., Pisciotta, A., Scudero, S., & Bottari, C. (2023). An Overview of Geophysical Techniques and Their Potential Suitability for Archaeological Studies. *Heritage*, *6*(3), Article 3. https://doi.org/10.3390/heritage6030154

Maurice, L., Taylor, R., Tindimugaya, C., Macdonald, A., Johnson, P., Kaponda, A., Owor, M., Sanga, H., Bonsor, H., Darling, W., & Gooddy, D. (2018). Characteristics of high-intensity groundwater abstractions from weathered crystalline bedrock aquifers in East Africa. *Hydrogeology Journal*, *27*. https://doi.org/10.1007/s10040-018-1836-9

McNeice, W. G., & Jones, G. A. (2001). Multisite, multifrequency tensor decomposition of magnetotelluric data. *GEOPHYSICS*, *66*, 158–173.

McNeill, J. D., & Snelgrove, F. B. (1995). Electromagnetic Geophysical Methods applied to to Groundwater Exploration and Evaluation.. *Geonics Limited*.

Meju, M. A., Fontes, S. L., Oliveira, M. F. B., Lima, J. P. R., Ulugergerli, E. U., & Carrasquilla, A. A. (1999). Regional aquifer mapping using combined VES-TEM-AMT/EMAP methods in the semiarid eastern margin of Parnaiba Basin, Brazil. *GEOPHYSICS*, *64*(2), 337–356. https://doi.org/10.1190/1.1444539

Mensah, J. K., Ofosu, E. A., Akpoti, K., Kabo-Bah, A. T., Okyereh, S. A., & Yidana, S. M. (2022). Modeling current and future groundwater demands in the White Volta River

Basin of Ghana under climate change and socio-economic scenarios. *Journal of Hydrology: Regional Studies*, *41*, 101117. https://doi.org/10.1016/j.ejrh.2022.101117

Metronix, G. (1998). Metronix geophysics and magnetotellurics. *Appex*. https://www.metronix.de/metronixweb/en/geophysiks/contact/

Michot, D., Benderitter, Y., Dorigny, A., Nicoullaud, B., King, D., & Tabbagh, A. (2003). Spatial and temporal monitoring of soil water content with an irrigated corn crop cover using surface electrical resistivity tomography. *Water Resources Research*, *39*(5). https://doi.org/10.1029/2002WR001581

Miensopust, M. P., Jones, A. G., Muller, M. R., Garcia, X., & Evans, R. L. (2011). Lithospheric structures and Precambrian terrane boundaries in northeastern Botswana revealed throughmagnetotelluric profiling as part of the Southern African Magnetotelluric Experiment. *Journal of Geophysical Research, 116,* B02401. https://doi.org/10.1029/2010JB007740.

Miller, R., Pullan, S., Waldner, J., & Haeni, F. (1986). Field comparison of shallow seismic sources. *GEOPHYSICS*, *51*, 2067–2092. https://doi.org/10.1190/1.1442061

Min, G., Yuan, H., Wang, X., Wang, K., Li, C., Liu, K., & Hu, S. (2023). Crustal and upper mantle electrical structure and uplift mechanism of the Liupanshan orogenic belt in the NE Tibetan Plateau. *Tectonophysics*, *853*, 229–799.

Mockler, E. M., O'Loughlin, F. E., & Bruen, M. (2016). Understanding hydrological flow paths in conceptual catchment models using uncertainty and sensitivity analysis. *Computers & Geosciences*, *90*, 66–77. https://doi.org/10.1016/j.cageo.2015.08.015

Mohamaden, M. I. I., & Ehab, D. (2017). Application of electrical resistivity for groundwater exploration in Wadi Rahaba, Shalateen, Egypt. *NRIAG Journal of Astronomy and Geophysics*, *6*(1), 201–209. https://doi.org/10.1016/j.nrjag.2017.01.001

Mohamed, A., & Abu El Ella, E. (2021). Magnetic Applications to Subsurface and Groundwater Investigations: A Case Study from Wadi El Assiuti, Egypt. *International Journal of Geosciences*, *12*, 77–101. https://doi.org/10.4236/ijg.2021.122006

Mohamed, A., Al Deep, M., Othman, A., Taha, A. I., Alshehri, F., & Abdelrady, A. (2022). Integrated Geophysical Assessment of Groundwater Potential in Southwestern Saudi Arabia. *Frontiers in Earth Science*, *10*. https://www.frontiersin.org/articles/10.3389/feart.2022.937402

Mohamed, A., & Ella, E. A. (2021). Magnetic application to subsurface and groundwater investigations: A case study from the Wadi El Assiuti, Egypt. *International Journal of Geoscience*, *12*, 77–101.

Mohamed, H. S., Senosy, Mahmoud. M., & Abdel Zaher, M. (2016). Interactive interpretation of airborne gravity, magnetic, and drill-hole data within the crustal framework of the northern Western Desert, Egypt. *Journal of Applied Geophysics*, *134*, 291–302. https://doi.org/10.1016/j.jappgeo.2016.09.002

Mokgatle, T., & Fourie, F. (2017). Groundwater exploration in the Tsineng area using airborne and ground base geophysical methods. *15th Biennial Groundwater Conference*, 14–18.

Moorkamp, M. (2007). Comment on 'The magnetotelluric phase tensor' by T. Grant Caldwell, Hugh M. Bibby and Colin Brown. *Geophysical Journal International*, *171*(2), 565–566. https://doi.org/10.1111/j.1365-246X.2007.03490.x

Morales-Ocaña, C., Bohoyo, F., Escutia, C., Marín-Lechado, C., Rey-Moral, C., Druet, M., Galindo-Zaldívar, J., & Maestro, A. (2023). 3D Geophysical and Geological Modeling of the South Orkney Microcontinent (Antarctica): Tectonic Implications for the Scotia Arc Development. *Tectonics*, *42*(4), e2022TC007602. https://doi.org/10.1029/2022TC007602

Mulwa, J. K., Gaciri, S. J., Barongo, J. O., Opiyo-Akech, N., & Kianji, G. K. (2005). GEOLOGICAL AND STRUCTURAL INFLUENCE ON GROUNDWATER DISTRIBUTION AND FLOW IN NGONG AREA, KENYA. *African Journal of Science and Technology*, *6*, 105–115.

Nagarajan, R., Thirumalaisamy, S., & Lakshumanan, E. (2012). Impact of leachate on groundwater pollution due to non-engineered municipal solid waste landfill sites of erode city, Tamil Nadu, India. *Iranian Journal of Environmental Health Science & Engineering*, *9*(1), 35. https://doi.org/10.1186/1735-2746-9-35

Naif, S., Selway, K., Murphy, S. B., Egbert, G., & Pommier, A. (2021). Electrical conductivity of the lithosphere-asthenosphere system. *Physics of the Earth and Planetary Interiors*, *313*.

Nazari, S., Rochlitz, R., & Günther, T. (2023). Optimizing Semi-Airborne Electromagnetic Survey Design for Mineral Exploration. *Minerals*, *13*(6), Article 6. https://doi.org/10.3390/min13060796

NGA, N. G. A. Inc. (2004). *GM-SYS: Gravity/Magnetic Modeling software User Guide.* Corvallis.

Niwas, S., & Celik, M. (2012). Equation estimation of porosity and hydraulic conductivity of Ruhrtal aquifer in Germany using near surface geophysics. *Journal of Applied Geophysics*, *84*, 77–85. https://doi.org/10.1016/j.jappgeo.2012.06.001

Nurit, T.-G. (2022). Minerals Observed by Scanning Electron Microscopy (SEM), Transmission Electron Microscopy (TEM) and High Resolution Transmission Electron Microscopy (HRTEM). In *Electron Microscopy*. IntechOpen. https://doi.org/10.5772/intechopen.102477

Okpoli, C. (2013). Application of 2D Electrical Resistivity Tomography in Landfill Site: A Case Study of Iku, Ikare Akoko, Southwestern Nigeria. *Journal of Geological Research*, *2013*. https://doi.org/10.1155/2013/895160

Omosuyi, G. O., Adeyemo, A., & Adegoke, A. O. (2007). Investigation of Groundwater Prospect Using Electromagnetic and Geoelectric Sounding at Afunbiowo, near Akure, Southwestern Nigeria. *The Pacific Journal of Science and Technology*, *8*, 172.

Oni, A. G., Eniola, P. J., Olorunfemi, M. O., Okunubi, M. O., & Osotuyi, G. A. (2020). The magnetic method as a tool in groundwater investigation in a basement complex terrain: Modomo Southwest Nigeria as a case study. *Applied Water Science*, *10*(8), 190. https://doi.org/10.1007/s13201-020-01279-z

Oryński, S., Jóźwiak, W., Nowożyński, K., & Klityński, W. (2022). Comparison of 3D, 2D, and 1D Magnetotelluric Inversion Results on the Example of Data from Fore-Sudetic Monocline. *International Journal of Geophysics*, *2022*, e3400950. https://doi.org/10.1155/2022/3400950

Osagie, A. U., Eshanibli, A., & Adepelumi, A. A. (2021). Structural trends and basement depths across Nigeria from analysis of aeromagnetic data. *Journal of African Earth Sciences*, *178*, 104184. https://doi.org/10.1016/j.jafrearsci.2021.104184

Osinowo, O. O., Adabanija, M. A., Adewoye, O. A., Osinowo, O. O., Adabanija, M. A., & Adewoye, O. A. (2019). Structural Interpretation and Depth Estimation from Aeromagnetic Data of Abigi-Ijebu-Waterside area of Eastern Dahomey Basin, Southwestern Nigeria. *Geofísica Internacional*, *58*(4), 259–277.

Osinowo, O. O., Agbaje, M. A., & Ariyo, S. O. (2020). Integrated geophysical investigation techniques for mapping cassava effluent leachate contamination plume, at a dumpsite in Ilero, southwestern Nigeria. *Scientific African*, *8*, e00374. https://doi.org/10.1016/j.sciaf.2020.e00374

Oskooi, B. (2006). 1D interpretation of the Magnetotelluric data from Travale Geothermal Field in Italy. *Journal of the Earth and Space Physics*, *32*, 1–16.

Palacky, G. (1988). Resistivity characteristics of geologic targets in electromagnetic methods in applied geophysics. *Society of Exploration Geophysics*, *1*, 53–129.

Park, S. K. (1985). Distortion of magnetotelluric sounding curves by three-dimensional structures. *GEOPHYSICS*, *50(5)*, 785–797.

Park, S., Shin, S., Lee, D. K., Kim, C. R., & Son, J.-S. (2016). *Relationship between Electrical Resistivity and Physical Properties of Rocks*. https://doi.org/10.3997/2214-4609.201602101

Paterson, N. R., & Bosschart, R. A. (1987). Airborne Geophysical Exploration for Ground Water. *Groundwater*, *25*(1), 41–50. https://doi.org/10.1111/j.1745-6584.1987.tb02114.x

Pedersen, L. B. (1991). Relations between potential field and some equivalent sources. *Geophysics*, *56*, 961–971.

Pellerin, L., & Hohmann, G. (1990). Transient electromagnetic inversion: A remedy for magnetotelluric static shifts. *Geophysics*, *55*. https://doi.org/10.1190/1.1442940

Perozzi, L., Guglielmetti, L., & Moscariello, A. (2021). Quantitative uncertainty analysis of gravity disturbance. The case of the Geneva Basin (Switzerland). *Journal of Applied Geophysics*, *193*, 104431. https://doi.org/10.1016/j.jappgeo.2021.104431

Peter, E. A., Alkali, A., & Udensi, E. E. (2017). *DETERMINATION OF THE DEPTH TO MOHOROVICIC DISCONTINUITY IN THE MINNA AREA IN NIGERIA USING BOUGUER GRAVITY DATA*. http://repository.futminna.edu.ng:8080/jspui/handle/123456789/4616

Pirttijarvi, M., Saartenoja, A., & Korkeakangas, P. (2022). Drone-based electromagnetic survey system ... | Open Research Europe. *Earth and Environmental Science Gateway*. https://open-research-europe.ec.europa.eu/articles/2-3

Porsani, J., Filho, W., Shimeles, F., Dourado, J., & Moura, J. (2004). The use GPR and VES in delineating a contaminating plume in a landfill site: A case study in SE Brazil. *Journal of Applied Geophysics*, *55(3-4)*, 199-209.

Pranata, E., Irawati, S. M., & Niasari, S. W. (2017). Magnetotelluric Data Analysis using Swift Skew, Bahr Skew, Polar Diagram, and Phase Tensor: A Case Study in Yellowstone, US. *Pakistan Academy of Sciences*, *54(3)*, 311–317.

Puopiel, F., & Owusu-Ansah, J. (2014). Solid Waste Management in Ghana: The Case of Tamale Metropolitan Area. *Journal of Environment and Earth Science*, *4*.

Rachie, A. (1998). Modelling the time-domain response of AEM systems. *Exploration Geophysics*, *29*, 103–106.

Raji, W. O., & Adeoye, T. O. (2017). Geophysical mapping of contaminant leachate around a reclaimed open dumpsite. *Journal of King Saud University - Science*, *29*(3), 348–359. https://doi.org/10.1016/j.jksus.2016.09.005

Ramalho, E. C., Francés, A. P., Santos, F. M., & Victorino, A. da M. (2023). 3D electrical structure definition of aquifer systems in the Kalahari basin in Southern Angola based on legacy data reprocessing. *Journal of Applied Geophysics*, *211*, 104968. https://doi.org/10.1016/j.jappgeo.2023.104968

Rapti-Caputo, D., & Vaccaro, C. (2006). Geochemical evidences of landfill leachate in groundwater. *Engineering Geology*, *85*(1), 111–121. https://doi.org/10.1016/j.enggeo.2005.09.032

Rathod, M., Mishra, H., & Karmarkar, S. (2013). Leachate Characterization and Assessment of Water Pollution near Municipal Solid Waste Landfill site. *International Journal of Chemical and Physical Science*, *2*, 186–199.

Rehman, F., Harbi, M. H., Azeem, T., Naseem, A. A., Ullah, M. F., Rehman, S. ur, Riaz, O., Rehman, F., & buelnaga, H. S. O. (2021). Shallow geophysical and hydrological investigations to identify groundwater contamination in Wadi Bani Malik dam area Jeddah, Saudi Arabia. *De Gruyter*, *13*, 272–279. https://doi.org/doi.org/10.1515/geo-2020-0176

Reid, A., Allsop, J., Granser, H., Millet, A., & Somerton, I. (1990). Magnetic interpretation in three dimensions using Euler Deconvolurion. *Geophysics*, *Vol. 55*, 80–91.

Reid, A., Ebbing, J., & Webb, S. (2014). Egregious Euler Errors – The Use and Abuse of Euler Deconvolution Applied to Potential Fields. *Geophysical Prospecting*, *62*. https://doi.org/10.1111/1365-2478.12119

Reynolds, J. M. (2011). *An Introduction to Applied and Environmental Geophysics* (2nd Edition). John Wiley & Sons.

Roch, J. (2007). Airborne Geophysics. *India Geophysical Union*, *11*, 1–28.

Rodriguez, D. B., Deszcz-Pan, M., & Sawyer, A. D. (2001). *Electromagnetic Studies and Subsurface Mapping of Electrical Resistivity in the La Bajada Constriction Area, New Mexico* (1720–F; The Cerrillos Uplift, the La Bajada Constriction, and Hydrogeologic Framework of the Santo Domingo Basin, Rio Grande Rift, New Mexico, p. 27). U.S. Geological Survey.

Romo, J., Flores, C., Vega, R., Vazquez, R., A. Pérez Flores, M., Gómez Treviño, E., J. Esparza, F., E. Quijano, J., & H. García, V. (1997). A closely-spaced magnetotelluric study of the Ahuachapán-Chipilapa geothermal field, El Salvador. *Geothermics*, *26*(5), 627–656. https://doi.org/10.1016/S0375-6505(97)00014-X

Rubin, Y., & Hubbard, S. S. (2005). *Hydrogeophysics.* Springer.

Rung-Arunwan, T., Siripunvaraporn, W., & Utada, H. (2016). On the Berdichevsky average. *Physics of the Earth and Planetary Interiro*, *253*, 1–4.

Saad, R., & Tonnizam, E. (2012). Groundwater Detection in Alluvium Using 2-D Electrical Resistivity Tomography (ERT). *Electronic Journal of Geotechnical Engineering*, *17*.

Saibi, H., Khosravi, S., Cherkose, B. A., Smirnov, M., Kebede, Y., & Fowler, A.-R. (2021). Magnetotelluric data analysis using 2D inversion: A case study from Al-Mubazzarah Geothermal Area (AMGA), Al-Ain, United Arab Emirates. *Heliyon*, *7*(6), e07440. https://doi.org/10.1016/j.heliyon.2021.e07440

Salameh, E. (2021). The Hydrogeological Consequences of the Proposed Extraction of the Deep Groundwater in Jordan. *Journal of Geoscience and Environment Protection*, *9*(8), Article 8. https://doi.org/10.4236/gep.2021.98007

Salem, A., William, S., Fairhead, D., Smith, R., & Ravat, D. (2008). Interpretation of magnetic data using tilt-angle derivatives. *Society of Exploration Geophysics*, *Vol. 7*, 1–10.

Samouëlian, A., Cousin, I., Tabbagh, A., Bruand, A., & Richard, G. (2005). Electrical resistivity survey in soil science: A review. *Soil and Tillage Research*, *83*(2), 173–193. https://doi.org/10.1016/j.still.2004.10.004

Saul, J., Kumar, M. R., & Sarkar, D. (2000). Lithospheric and upper mantle structure of the Indian shield, from teleseismic receiver functions. Geophys. Res. Lett. 27, 2357–2360. *Geophysical Research Letters*, *27*, 2357–2360.

Schulz, B., Sandmann, D., & Gilbricht, S. (2020). SEM-Based Automated Mineralogy and Its Application in Geo- and Material Sciences. *Minerals*, *10*, 1004.

Selway, K. (2014). On the causes of electrical conductivity anomalies in tectonically stable lithosphere. *Survey in Geophysics*, *35*, 219–257.

Sendrós, A., Urruela, A., Himi, M., Alonso, C., Lovera, R., Tapias, J. C., Rivero, L., Garcia Artigas, R., & Casas, A. (2021). Characterization of a Shallow Coastal Aquifer in the Framework of a Subsurface Storage and Soil Aquifer Treatment Project Using Electrical Resistivity Tomography (Port de la Selva, Spain). *Applied Sciences*, *11*, 2448. https://doi.org/10.3390/app11062448

Senos Matias, M., Marques da Silva, M., Ferreira, P., & Ramalho, E. (1994). A geophysical and hydrogeological study of aquifers contamination by a landfill. *Journal of Applied Geophysics*, *32*(2), 155–162. https://doi.org/10.1016/0926-9851(94)90017-5

Severin, P. K. (2004). *Energy Dispersive Spectrometry of Common Rock Forming Minerals*. Kluwer Academic Publishers.

Shahin, M. (2002). Hydrology and Water Resources of Africa. *Kluwer Academic Publishers*.

Shaji, B. (2021). AQUIFER MAPPING USING AEM SKYTEM. *International Journal of Engineering Applied Sciences and Technology*, *6*. https://doi.org/10.33564/IJEAST.2021.v06i03.040

Shao, S., Gao, C., Guo, X., Wang, Y., Zhang, Z., Yu, L., & Tang, H. (2019). Mapping the contaminant plume of an abandoned hydrocarbon disposal site with geophysical and geochemical methods, Jiangsu, China. *Environmental Science and Pollution Research International*, *26*(24), 24645–24657.

Sharma, V. P. (1997). *Environmental and Engineering Geophysics*. Cambridge University Press.

Shawky, H. A., Said, M. M., El-Aassar, A. M., Kotp, Y. H., & Abdel Mottaleb, M. S. A. (2012). *Study the chemical characteristics of groundwater to determine the suitable localities desalination processesin the area between Mersa Alam and Ras Banas, Red sea Coast Eastern Desert, Egypt.*

Siddiqua, A., Hahladakis, J. N., & Al-Attiya, W. A. K. A. (2022). An overview of the environmental pollution and health effects associated with waste landfilling and open dumping. *Environmental Science and Pollution Research*, *29*(39), 58514–58536. https://doi.org/10.1007/s11356-022-21578-z

Siemon, B. (2009). Levelling of helicopter-borne frequency-domain electromagnetic data. *Journal of Applied Geophysics*, *67*(3), 206–218. https://doi.org/10.1016/j.jappgeo.2007.11.001

Siemon, B., Auken, E., & Christiansen, Vest. A. (2009). Laterally constrained inversion of helicopter-borne frequency-domain electromagnetic data. *Journal of Applied Geophysics*, *67*, 259–268.

Siemon, B., Ibs-von Seht, M., Steuer, A., Deus, N., & Wiederhold, H. (2020). Airborne Electromagnetic, Magnetic, and Radiometric Surveys at the German North Sea Coast Applied to Groundwater and Soil Investigations. *Remote Sensing*, *12*(10), Article 10. https://doi.org/10.3390/rs12101629

Silahtar, A., Kanbur, M., & Beyhan, G. (2020). Investigation of a sedimentary basin by using gravity and seismic reflection data in the Isparta basin, southwestern Turkey. *Bulletin of Engineering Geology and the Environment*, *79*. https://doi.org/10.1007/s10064-020-01804-z

Simpson, F., & Bahr, K. (2005). Practical Magnetotellurics. *CambridgeUniversity Press*.

Singh, P. S., Chaubey, S., Dwivedi, D. R., Yadav, R., & Chaurasia, S. K. (2019). Case Study of Solid Waste Management in Gorakhpur city. *Arabian Journal Geoscience*, *7*, 1246–1251.

Slattery, S. R., & Andriashek, L. D. (2012). *Overview of Airborne-Electromagnetic and - Magnetic Geophysical Data Collection Using the GEOTEM® Survey in the Sylvan Lake Area, Central Alberta* (ERCB/AGS Open File Report 2012-08; pp. 18–120).

Smith, J. T. (1995). Understanding telluric distortion matrices. *Gophysics Journal Internation*, *122*, 219–226.

Soussa, H., El Feel, A. A., Alfy, S. Z., & Yousif, M. S. M. (2012). Flood hazard in Wadi Rahbaa area, Egypt . *Arabian Journal Geoscience*, *5*, 45–52.

Spector, A., & Grant, F. S. (1970). Statistical models for interpreting aeromagnetic data. *Geophysics*, *32(2)*, 293–302.

Spratt, J. E., Skulski, T., Craven, J. A., Jones, A. G., Snyder, D. B., & Kiyan, D. (2009). Megnetotelluric investigations of the lithosphere beneath the central Rae craton, mainland Nunavut, Canada. *Journal of Geophysical Research*, *119*, 2415–2439.

Srena, B. F., Gavin, F., Charles, J., & Lemckert, C. (2011). Field and modelling investigations of fresh-water plume behaviour in response to infrequent high-precipitation events, Sydney Estuary, Australia. *Estuarine Coastal and Shelf Science - ESTUAR COAST SHELF SCI*, *92*, 389–402. https://doi.org/10.1016/j.ecss.2011.01.013

St. Johns River Water Management District. (2023). Florida's aquifers. *SJRWMD*. https://www.sjrwmd.com/water-supply/aquifer/

Stagpoole, V. M., Bennie, S. L., Bibby, H. M., Dravitzki, S., & Ingham, M. R. (2009). Deep structure of a major subduction back thrust: Magneto-telluric investigations of the Taranaki Fault, New Zealand. *Tectonophysics*, *463*(1), 77–85. https://doi.org/10.1016/j.tecto.2008.09.035

Stavrev, P., & Reid, A. (2007). Degrees of homogeneity of potential fields and structural indices of Euler deconvolution. *GEOPHYSICS*, *72*(1), L1–L12. https://doi.org/10.1190/1.2400010

Stephen, J., Gokarn, S. G., Manoj, C., & Singh, S. B. (2003). Effects of galvanic distortions on magnetotelluric data: Interpretation and its correction using deep electrical data. *NAtional Geopysical Research Institute*, *112*, 27–36.

Sternberg, B. K., Washburne, J. C., & Pellerin, L. (1988). Correction for the static shift in magnetotellurics using transient electromagnetic soundings | GEOPHYSICS. *GEOPHYSICS*, *53*(11). https://library.seg.org/doi/10.1190/1.1442426

Sumanovac, F. (2012). *Magnetotelluric method in the exploration of deep aquifers.* 3–5.

Swift, C. M. (1967). *A magnetotelluric investigation of an electrical conductivity anomaly in the southwestern United States* [Thesis, Massachusetts Institute of Technology, Dept. of Geology and Geophysics]. http://hdl.handle.net/1721.1/38346

Talwani, M., & Hiertzler, J. R. (1964). Computation of magnetic anomalies caused by two dimensiona bodies of arbitrary shape. *Geological Science*, *9*, 464–480.

Talwani, M., Worzel, J. L., & Landisman, M. (1959). Rapid gravity computations for 2 dimensional bodies with application to the Mendocino submarine fracture zone. *Journal of Geological Research*, *64*, 49–59.

Tarits, P. (1986). Conductivity and fluids in oceanic upper mantle. *Physics of the Earth and Planetary Interiors*, *42*, 215–226.

Telford, W. M., Geldart, L. P., & Sheriff, R. E. (1990, October 26). *Applied Geophysics*. Higher Education from Cambridge University Press; Cambridge University Press. https://doi.org/10.1017/CBO9781139167932

Thaw, M., GebreEgziabher, M., Villafañe-Pagán, J. Y., & Jasechko, S. (2022). Modern groundwater reaches deeper depths in heavily pumped aquifer systems. *Nature Communications*, *13*(1), Article 1. https://doi.org/10.1038/s41467-022-32954-1

Thomas, S., Fountain, D., & Watts, T. (2007). Airborne Geophysics-Evolution and Revolution. *Proceedings of Exploration 07: Fifth Decennial Internation Conference on Mineral Exploration*, 19–37.

Thompson, D. (1982). EULDPH: A new technique for making computer-assisted depth estimated from magnetic data. *Geophysics*, *Vol. 47*, 31–37.

Tian, J., Ye, G., Ding, Z., Wu, Q., Wei, W., Jin, S., & Xie, C. (2019). A study of the deep electrical structure of the northern segment of the Tan Lu fault zone, NE China. *Journal of Asian Earth Sciences*, *170*, 118–127.

Tinivella, U., Giustiniani, M., & Cassiani, G. (2013). Geophysical Methods for Environmental Studies. *International Journal of Geophysics*, *2013*, e950353. https://doi.org/10.1155/2013/950353

Tripathi, K., & Dwivedi, A. K. (2021). Impact of dumping on groundwater: A review. *International Journal of Creative Research Thoughts (IJCRT)*, *9*, 2320–2882.

Tuğrul, A., & Zarif, I. H. (1999). Correlation of mineralogical and textural characteristics with engineering properties of selected granitic rocks from Turkey. *Engineering Geology*, *51*(4), 303–317. https://doi.org/10.1016/S0013-7952(98)00071-4

Twort, A. C., Ratnayaka, D. D., & Brandt, M. J. (Eds.). (2000). 4—Groundwater supplies. In *Water Supply (Fifth Edition)* (pp. 114–II). Butterworth-Heinemann. https://doi.org/10.1016/B978-034072018-9/50006-0

Vadoodi, R., & Rasmussen, T. M. (2022). Joint Interpretation of Magnetotelluric and Potential Field Data From North-Eastern Norrbotten, Sweden. *Pure and Applied Geophysics*, *179*(3), 1069–1088. https://doi.org/10.1007/s00024-022-02959-4

Vanegas-Espinosa, L. I., Vargas-Del-Río, D., Ochoa-Covarrubias, G., & Grindlay, A. L. (2022). Flood Mitigation in Urban Areas through Deep Aquifer Recharge: The Case of the Metropolitan Area of Guadalajara. *International Journal of Environmental Research and Public Health*, *19*(6), 3160. https://doi.org/10.3390/ijerph19063160

Vaudelet, P., Schmutz, M., Pessel, M., Franceschi, M., Guérin, R., Atteia, O., Blondel, A., Ngomseu, C., Galaup, S., Rejiba, F., & Bégassat, P. (2011). Mapping of contaminant plumes with geoelectrical methods. A case study in urban context. *Journal of Applied Geophysics*, *75*(4), 738–751. https://doi.org/10.1016/j.jappgeo.2011.09.023

Veeraswamy, K., Azeez, K. K. A., Patro, P. K., Gupta, A. K., & Babu, N. (2020). Electrical resistivity structure across the Jaisalmer Basin (Rajasthan, NW India) derived from magnetotelluric data: Inferences on basin architecture and basement morphology. *Journal of Applied Geophysics*, *181*, 104147. https://doi.org/10.1016/j.jappgeo.2020.104147

Vest Christiansen, A., & Auken, E. (2012). A global measure for depth of investigation. *GEOPHYSICS*, *77*(4), WB171–WB177. https://doi.org/10.1190/geo2011-0393.1

Viezzoli, A., Tosi, L., Teatini, P., & Silvestri, S. (2010). Surface water–groundwater exchange in transitional coastal environments by airborne electromagnetics: The Venice Lagoon example. *Geophysical Research Letters*, *37*(1). https://doi.org/10.1029/2009GL041572

Vignoli, G., Cassiani, G., Rossi, M., Deiana, R., Boaga, J., & Fabbri, P. (2012). Geophysical characterization of a small pre-Alpine catchment | Elsevier Enhanced Reader. *Journal of Applied Geophysics*, *80*, 32–42. https://doi.org/10.1016/j.jappgeo.2012.01.007

Vignoli, G., Fiandaca, G., Christiansen, A. V., Kirkegaard, C., Auken, E., Vignoli, Fiandaca, Christiansen, A. V., Kirkegaard, & Auken. (2015). Sharp spatially constrained inversion with applications to transient electromagnetic data. *Geophysical Prospecting*, *63*(1), Article 1. https://doi.org/10.1111/1365-2478.12185

Viljanen, A. (2012). 3B. Description of the magnetospheric/ionospheric sources. In A. D. Chave & A. G. Jones (Eds.), *The Magnetotelluric Method: Theory and Practice* (pp. 96–121). Cambridge University Press. https://doi.org/10.1017/CBO9781139020138.005

Vozoff, K. (1972). The magnetotelluric method in the exploration of sedimentary basins. *Geophysics*, *37*, 980–1041.

Vozoff, K. (1990). Magnetotelluric: Principles and practice. *Indian Academy of Science*, *99(4)*, 441–471.

Wagner, F. M., & Uhlemann, S. (2021). Chapter One—An overview of multimethod imaging approaches in environmental geophysics. In C. Schmelzbach (Ed.), *Advances in Geophysics* (Vol. 62, pp. 1–72). Elsevier. https://doi.org/10.1016/bs.agph.2021.06.001

Wahaab, F. A., Lawal, S. K., & Adebayo, L. L. (2017). *Spectral Analysis of Higher Resolution Aeromagnetic Data over Some Part of Kwara State, Nigeria*. *Vol. 6*(Issue 03), 2278–0181.

Waldron, W. F. J., & Snyder, M. (2020). *Geological Structures: A Practical Introduction*. Pressbooks.

Wannamaker, P. E., Hasterok, D. P., Johnston, J. M., Stodt, J. A., Hall, D. B., Sodergren, T. L., Pellerin, L., Maris, V., Doerner, W. M., Groenewold, K. A., & Unsworth, M. J. (2008). Lithospheric dismemberment and magmatic processes of the Great Basin–Colorado Plateau transition, Utah, implied from magnetotellurics. *Geochemistry, Geophysics, Geosystems*, *9*(5). https://doi.org/10.1029/2007GC001886

Wannamaker, P. E., Hohmann, G. W., & Ward, S. H. (1984). Magnetotelluric response of three-dimensional bodies in layered earth. *GEOPHYSICS*, *49(9)*, 1517–1533.

Water Resource Commission, W. (2011). *Final Technical Report: Hydrogeological Assement of the Northern Region of Ghana Project (HAP).* Water resource commission.

Webster, R. J., Kight, P. R., Winburn, S. R., & Cool, A. C. (2003). HEAVY MINERAL ANALYSIS OF SANDSTONES BY RIETVELD ANALYSIS. *International Center for Diffraction Data*, *46*, 198.

WHO, W. H. O. (2022). *Guidelines for drinking-water quality*. (pp. 240–265). World Health Organization.

Wiederhold, H., Kallesøe, A. J., Kirsch, R., Mecking, R., Pechnig, R., & Skowronek, F. (2021). Geophysical methods help to assess potential groundwater extraction sites. *Grundwasser*, *26*(4), 367–378. https://doi.org/10.1007/s00767-021-00495-x

Wijekoon, P., Koliyabandara, P. A., Cooray, A. T., Lam, S. S., Athapattu, B. C. L., & Vithanage, M. (2022). Progress and prospects in mitigation of landfill leachate pollution: Risk, pollution potential, treatment and challenges. *Journal of Hazardous Materials*, *421*, 126627. https://doi.org/10.1016/j.jhazmat.2021.126627

Wilson, M. J. (1994). Clay mineralogy: Spectroscopic and chemical determinative methods. *Chapman and Hall, London, ISBN: 9780412533808*.

Won, I. J., & Bevis, M. (1987). Computing the gravitational and magnetic anomalies due to a polygon: Algorithms and Fortran subroutines. *Geophysics*, *52*, 232–238.

Yadav, K., Shah, M., & Sircar, A. (2020). Application of magnetotelluric (MT) study for the identification of shallow and deep aquifers in Dholera geothermal region. *Groundwater for Sustainable Development*, *11*, 100472. https://doi.org/10.1016/j.gsd.2020.100472

Yan, B., Qiu, S., Xiao, C., & Liang, X. (2019). Characteristics of Mineral Fluids and Geothermal Reservoir in Changbai Mountain, Northeast of China. *Geochemistry International*, *57*, 83–97. https://doi.org/10.1134/S0016702919010038

Yaramanci, U., Lange, G., & Hertrich, M. (2002). Aquifer characterization using surface NMR jointly with other geophysical techniques at the Nauen/Berlin test site. *Journal of Applied Geophysics*, *50*, 47–65. https://doi.org/10.1016/S0926-9851(02)00129-5

Ye, X., Yu, Z., Zhang, Y., Kang, J., Wu, S., Yang, T., & Gao, P. (2022). Mineral Composition Impact on the Thermal Conductivity of Granites Based on Geothermal Field Experiments in the Songliao and Gonghe Basins, China. *Minerals*, *12*(2), Article 2. https://doi.org/10.3390/min12020247

Yidana, S. M., Banoeng-Yakubo, B., Aliou, A.-S., & Akabzaa, T. M. (2012). Groundwater quality in some Voltaian and Birimian aquifers in northern Ghana—Application of mulitvariate statistical methods and geographic information systems. *Hydrological Sciences Journal*, *57*(6), 1168–1183. https://doi.org/10.1080/02626667.2012.693612

Yidana, S. M., Dzikunoo, E. A., Aliou, A. S., Adams, R. M., Chegbeleh, L. P., & Anani, C. (2020). The geological and hydrogeological framework of the Panabako, Kodjari, and Bimbilla Formations of the Voltaian Supergroup—Revelations from groundwater hydrochemical data. *Applied Geochemistry*, *115*, 104533.

Yidana, S., Yiran, G., Sakyi, P., Nude, P., & Banoeng-Yakubo, B. (2011). Groundwater evolution in the Voltaian basin, Ghana-an application of multivariate analyses to hydrochemical data. *Natural Science*, *3*, 837–854.

Yousef, A. F., Salem, A. A., Baraka, A. M., & Aglan, O. sh. (2009). The impact of geological setting on groundwater occurrence in some Wadis in Shalatein—Abu Ramad Area, South Eastern Desert, Egypt. *European Water Resource Association*, *25 (26)*, 53–68.

Yusuf, T. U. (2016). *Overview of Effective Geophysical Methods Used in the Study of Environmental Pollution by Waste Dumpsites.* (41; African Research Review, pp. 123–143). College of Agriculture, Mokwa, Niger state.

Zaru, N., Rossi, M., Vacca, G., & Vignoli, G. (2023). Spreading of Localized Information across an Entire 3D Electrical Resistivity Volume via Constrained EMI Inversion Based on a Realistic Prior Distribution. *Remote Sensing*, *15*(16), Article 16. https://doi.org/10.3390/rs15163993

Zayed, A. M. (2021). Geoeletrical exploration of groundwater by using vertical eletrical sounding technique at Wadi Morra, south Sinai, Egypt. *Austin Publishing Group*, *4*, 1025.

Zhang, W., Sun, Q., Hao, S., Geng, J., & Lv, C. (2016). Experimental study on the variation of physical and mechanical properties of rock after high temperature treatment. *Applied Thermal Engineering*, *98*, 1297–1304. https://doi.org/10.1016/j.applthermaleng.2016.01.010

APPENDICES

APPENDIX 1: Cross sections of Airborne Electromagnetic Data Show on Figure 1.2a (Black lines)

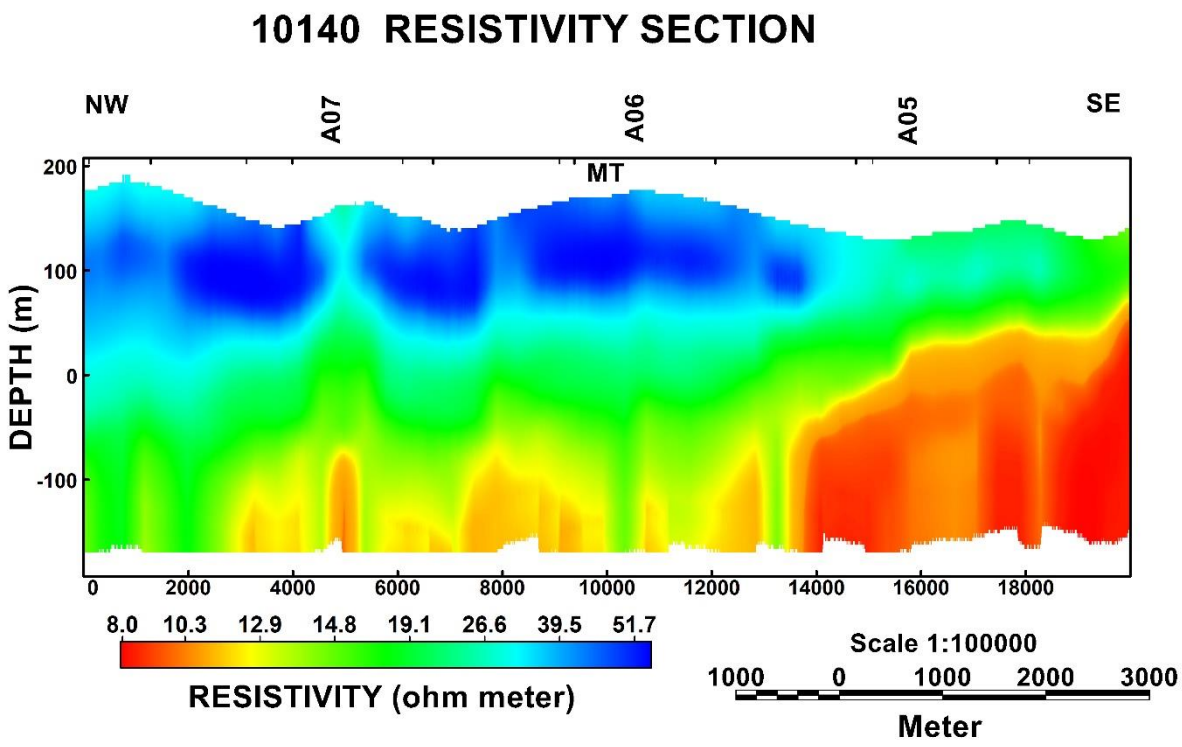

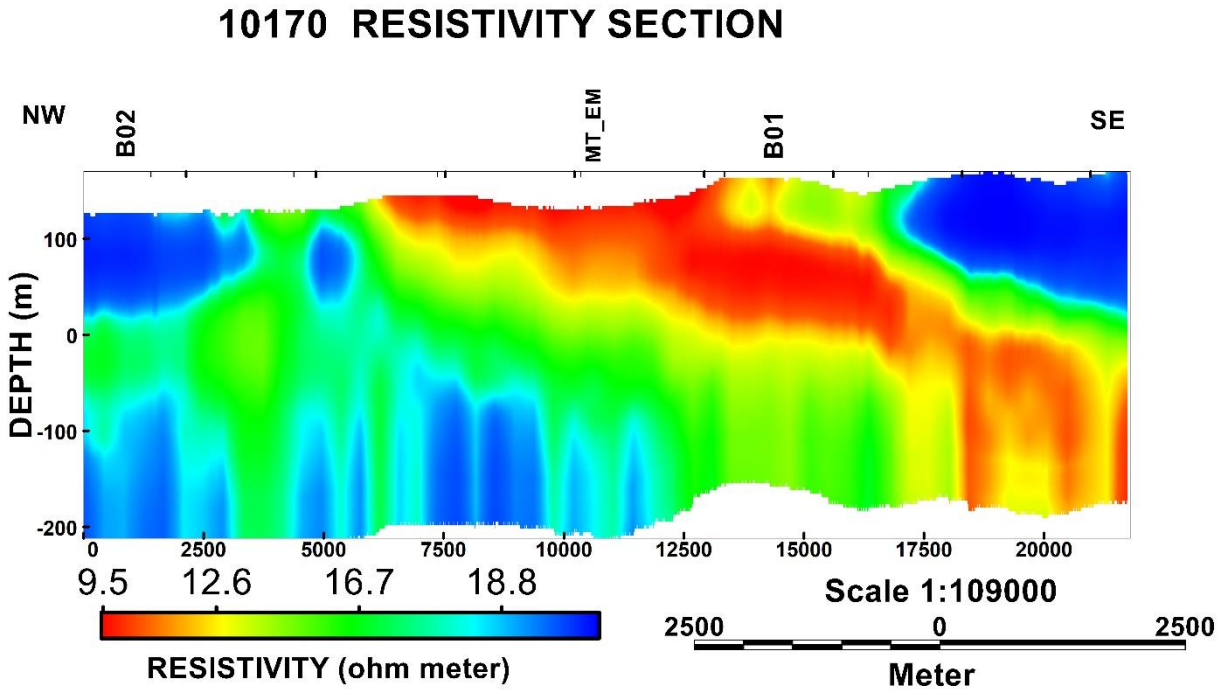

28222 RESISTIVITY SECTION

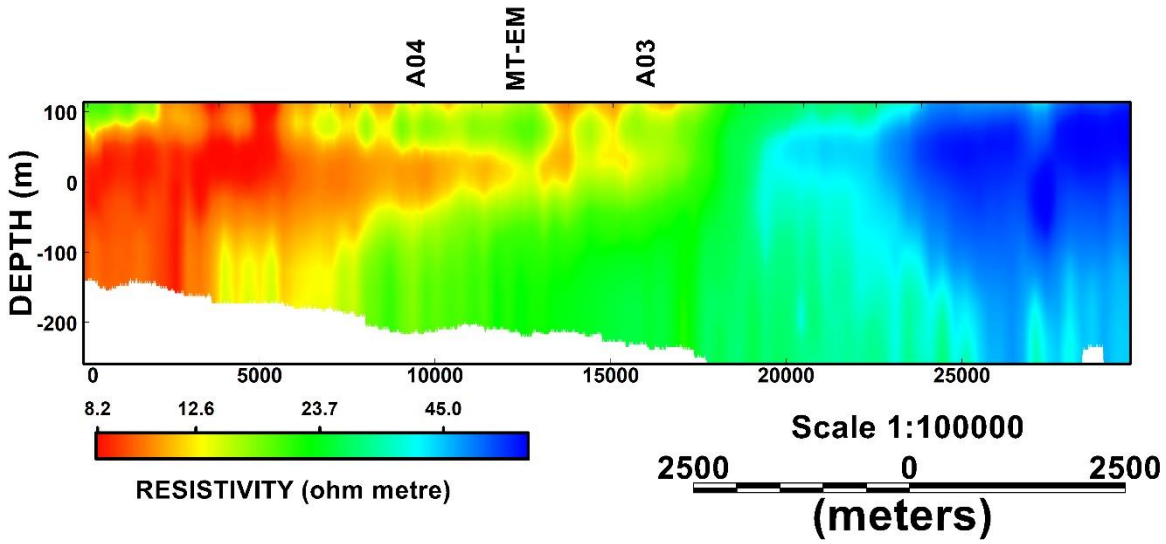

28223 RESISTIVITY SECTION

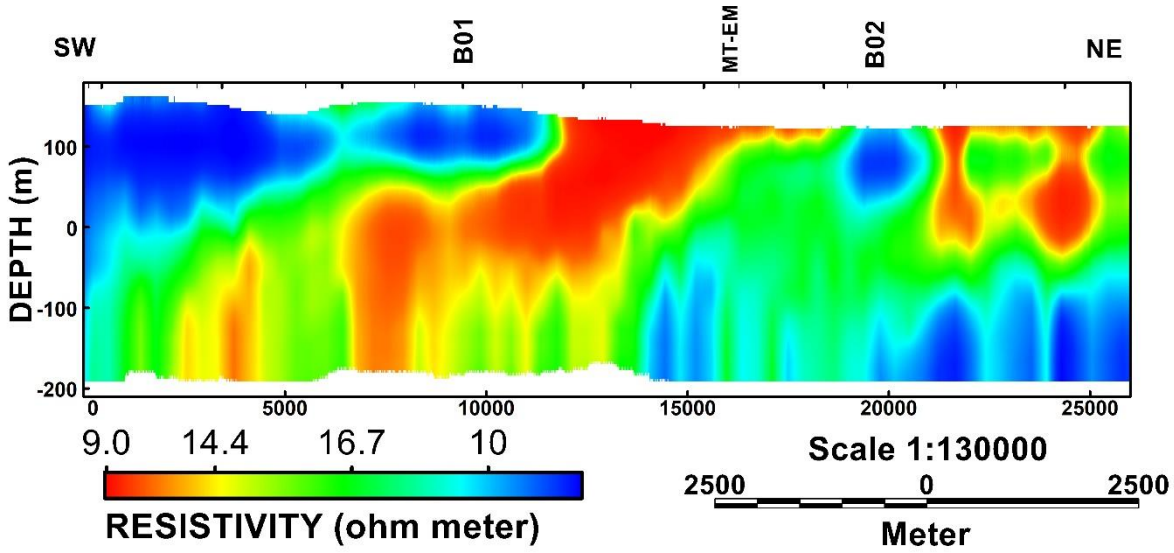

APPENDIX 2: Horizontal slices and Vertical sections from 3-D inversion of first MT survey data

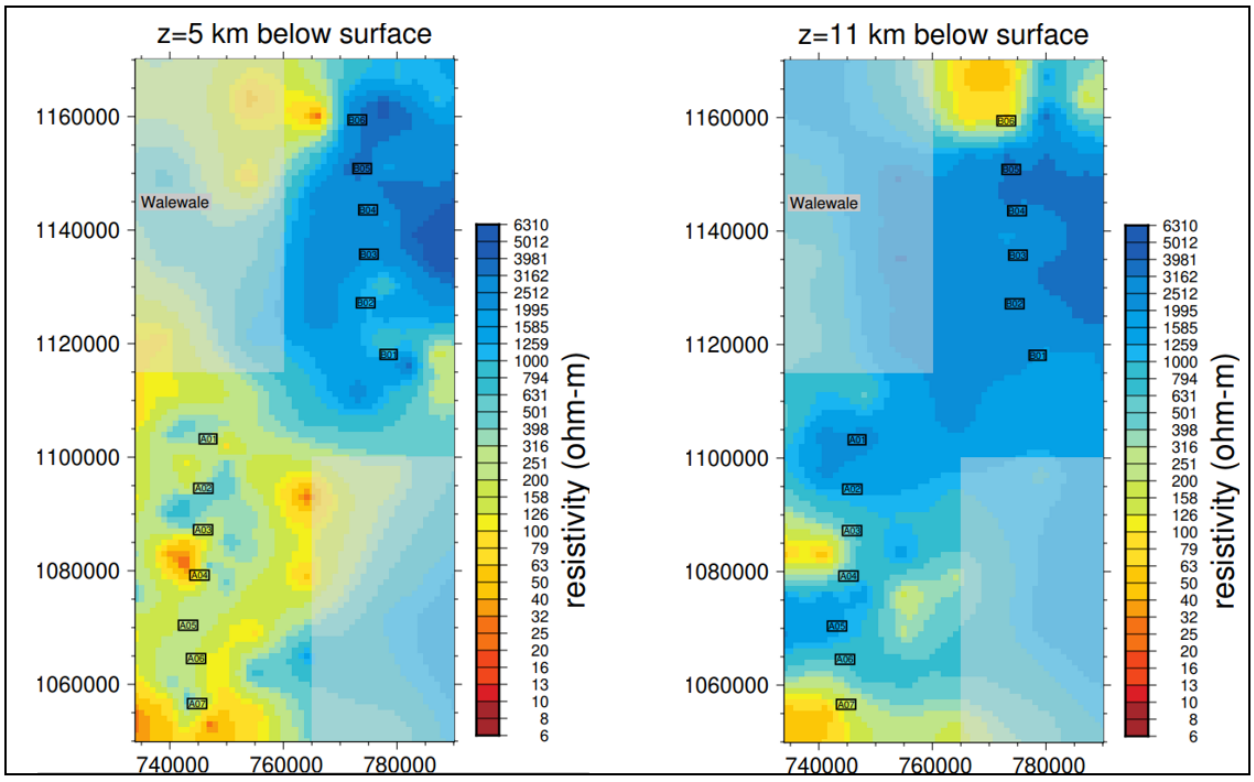

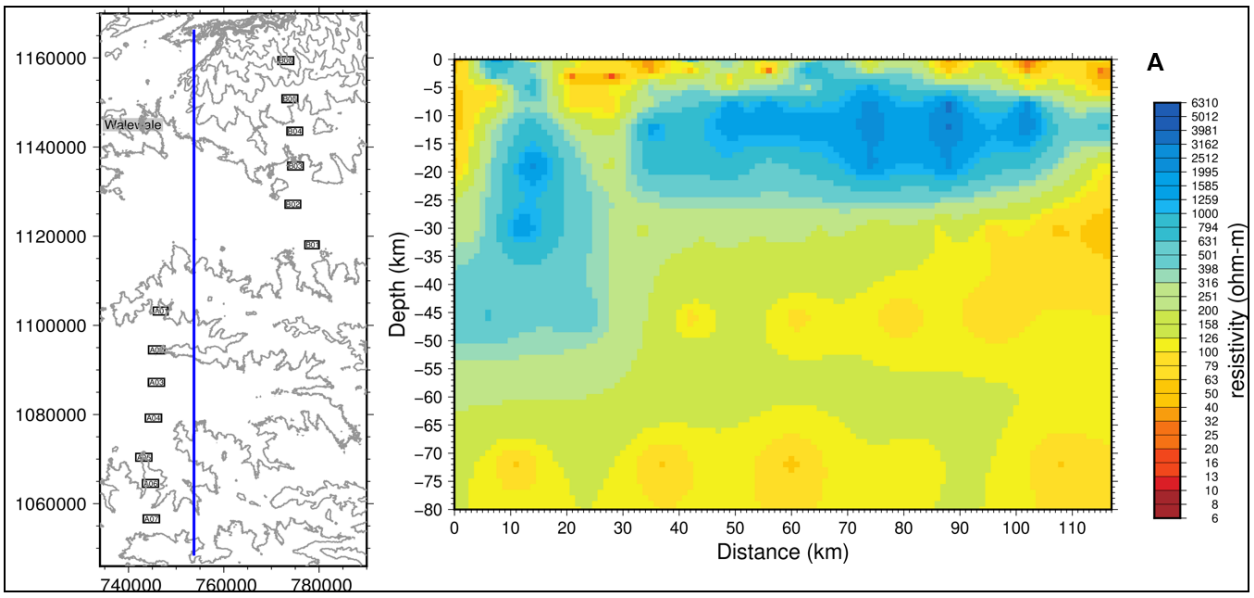

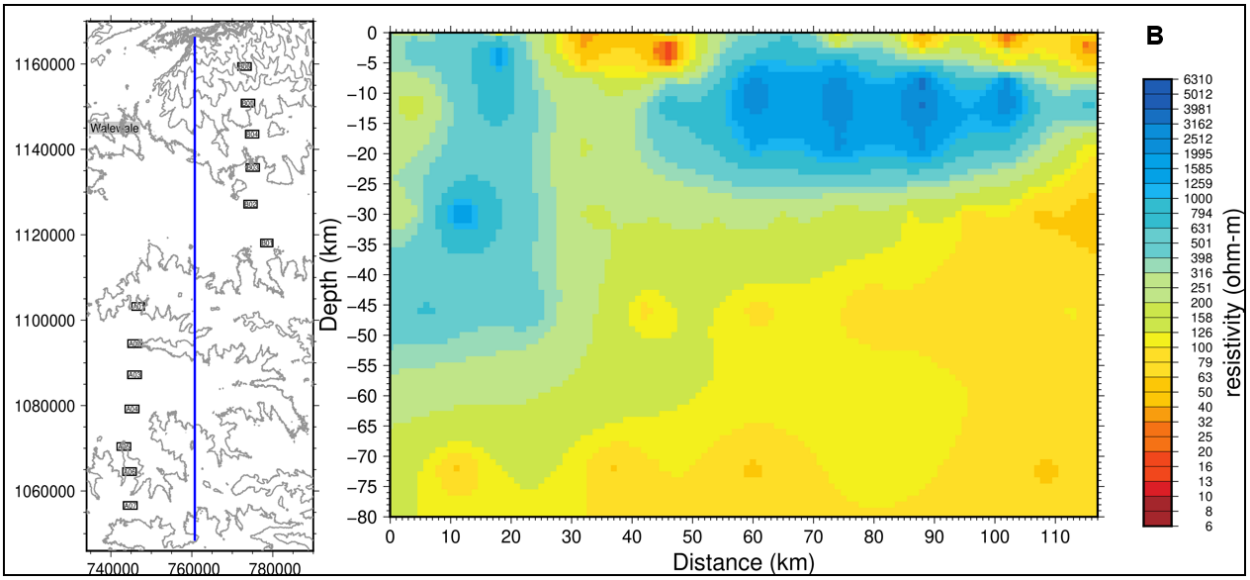
B
Depth (km)
Distance (km)
resistivity (ohm-m)
Walewale
1160000
1140000
1120000
1100000
1080000
1060000
740000
760000
780000
0
10
20
30
40
50
60
70
80
90
100
110
−5
−10
−15
−20
−25
−30
−35
−40
−45
−50
−55
−60
−65
−70
−75
−80
6310
5012
3981
3162
2512
1995
1585
1259
1000
794
631
501
398
316
251
200
158
126
100
79
63
50
40
32
25
20
16
13
10
8
6

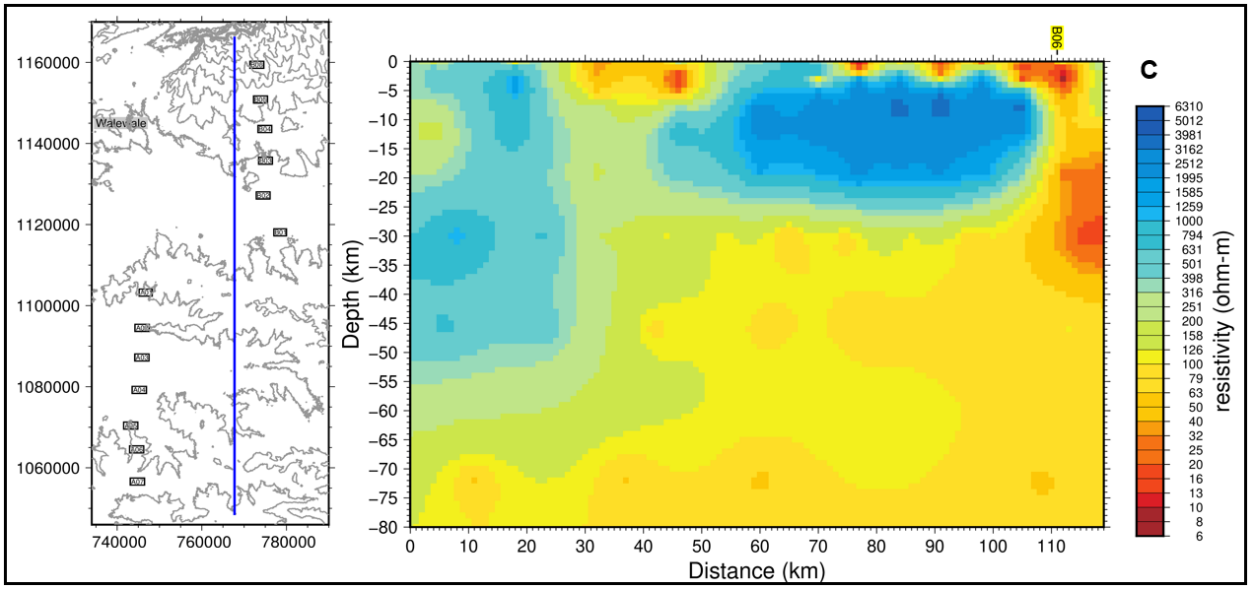
C
B06
Depth (km)
Distance (km)
resistivity (ohm-m)
Walewale
1160000
1140000
1120000
1100000
1080000
1060000
740000
760000
780000
0
10
20
30
40
50
60
70
80
90
100
110
−5
−10
−15
−20
−25
−30
−35
−40
−45
−50
−55
−60
−65
−70
−75
−80
6310
5012
3981
3162
2512
1995
1585
1259
1000
794
631
501
398
316
251
200
158
126
100
79
63
50
40
32
25
20
16
13
10
8
6

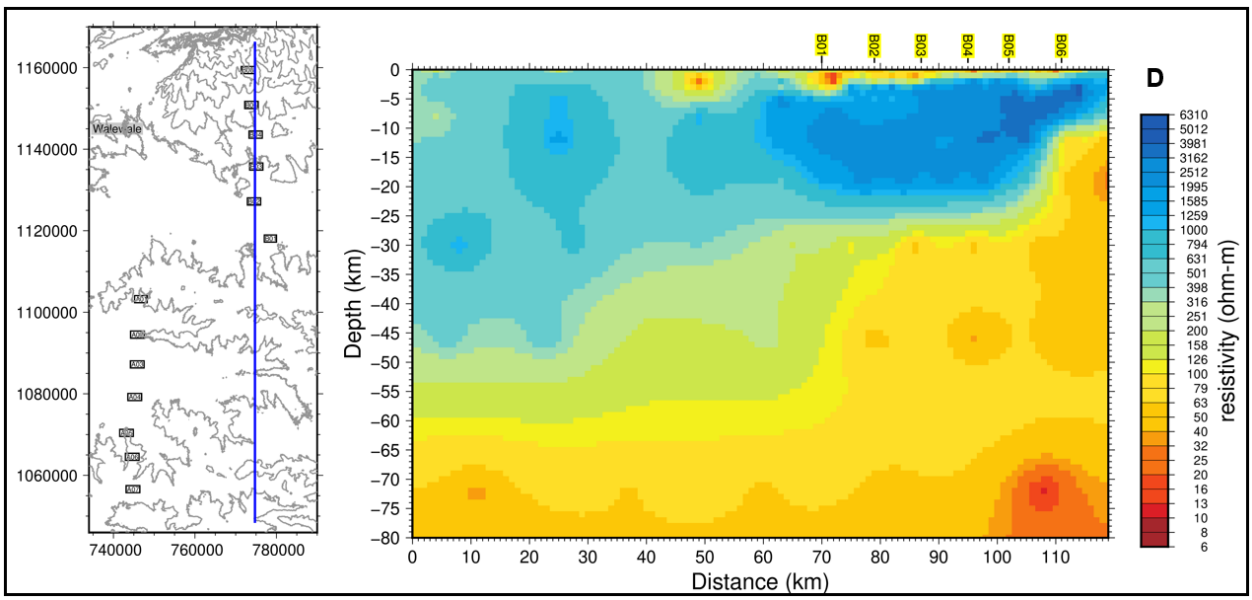
D
B01
B02
B03
B04
B05
B06
Depth (km)
Distance (km)
resistivity (ohm-m)
Walewale
1160000
1140000
1120000
1100000
1080000
1060000
740000
760000
780000
0
10
20
30
40
50
60
70
80
90
100
110
−5
−10
−15
−20
−25
−30
−35
−40
−45
−50
−55
−60
−65
−70
−75
−80
6310
5012
3981
3162
2512
1995
1585
1259
1000
794
631
501
398
316
251
200
158
126
100
79
63
50
40
32
25
20
16
13
10
8
6

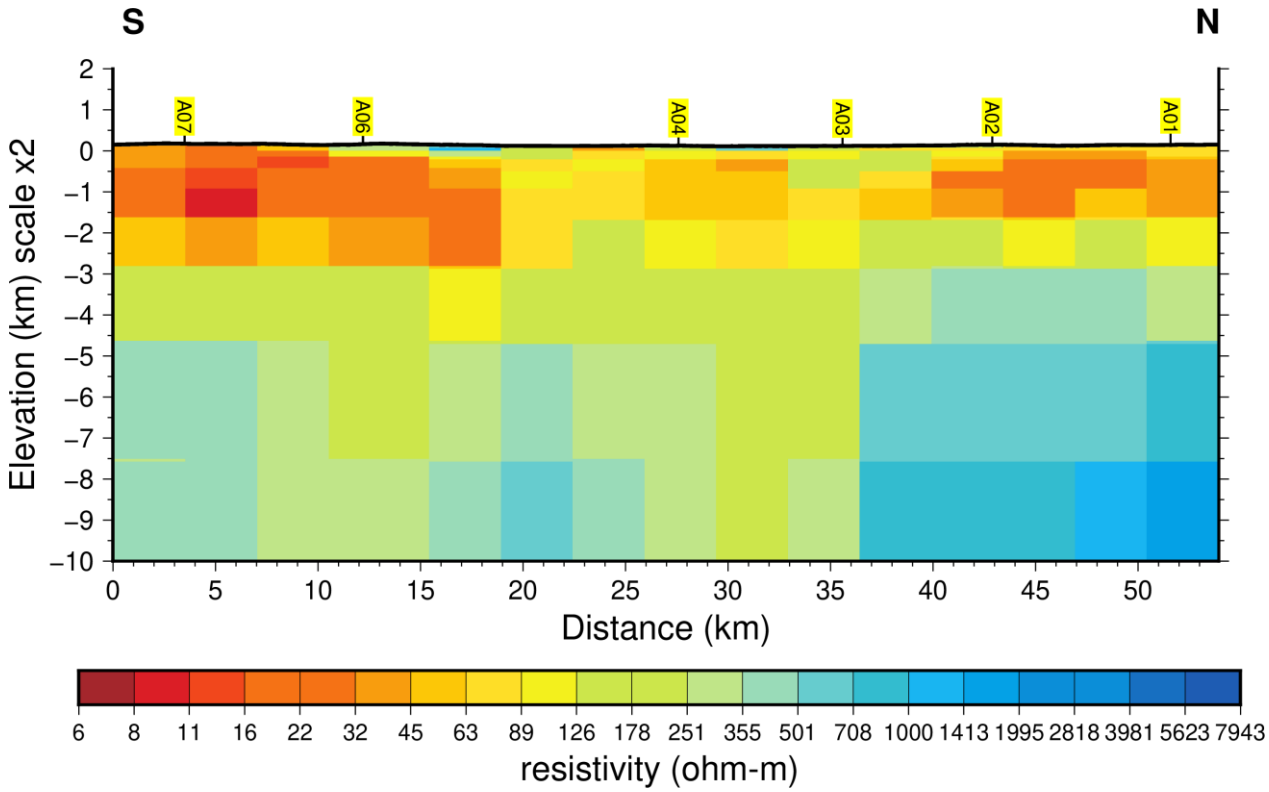
S
N
A07
A06
A04
A03
A02
A01
Elevation (km) scale x2
2
1
0
−1
−2
−3
−4
−5
−6
−7
−8
−9
−10
0
5
10
15
20
25
30
35
40
45
50
Distance (km)
6
8
11
16
22
32
45
63
89
126
178
251
355
501
708
1000
1413
1995
2818
3981
5623
7943
resistivity (ohm-m)

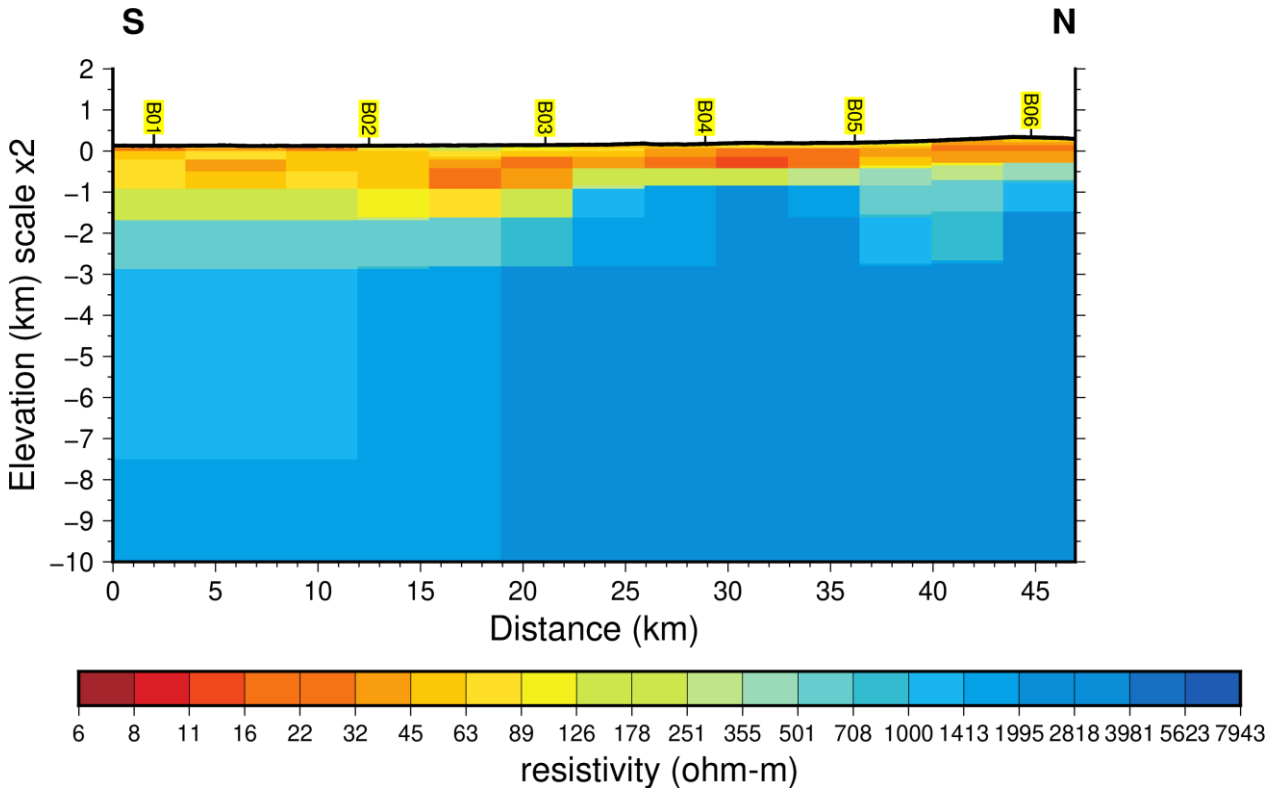
S
N
B01
B02
B03
B04
B05
B06
Elevation (km) scale x2
2
1
0
−1
−2
−3
−4
−5
−6
−7
−8
−9
−10
0
5
10
15
20
25
30
35
40
45
Distance (km)
6
8
11
16
22
32
45
63
89
126
178
251
355
501
708
1000
1413
1995
2818
3981
5623
7943
resistivity (ohm-m)

APPENDIX 3: Horizontal slices and Vertical sections from 3-D inversion of second MT survey data (Localized Survey)

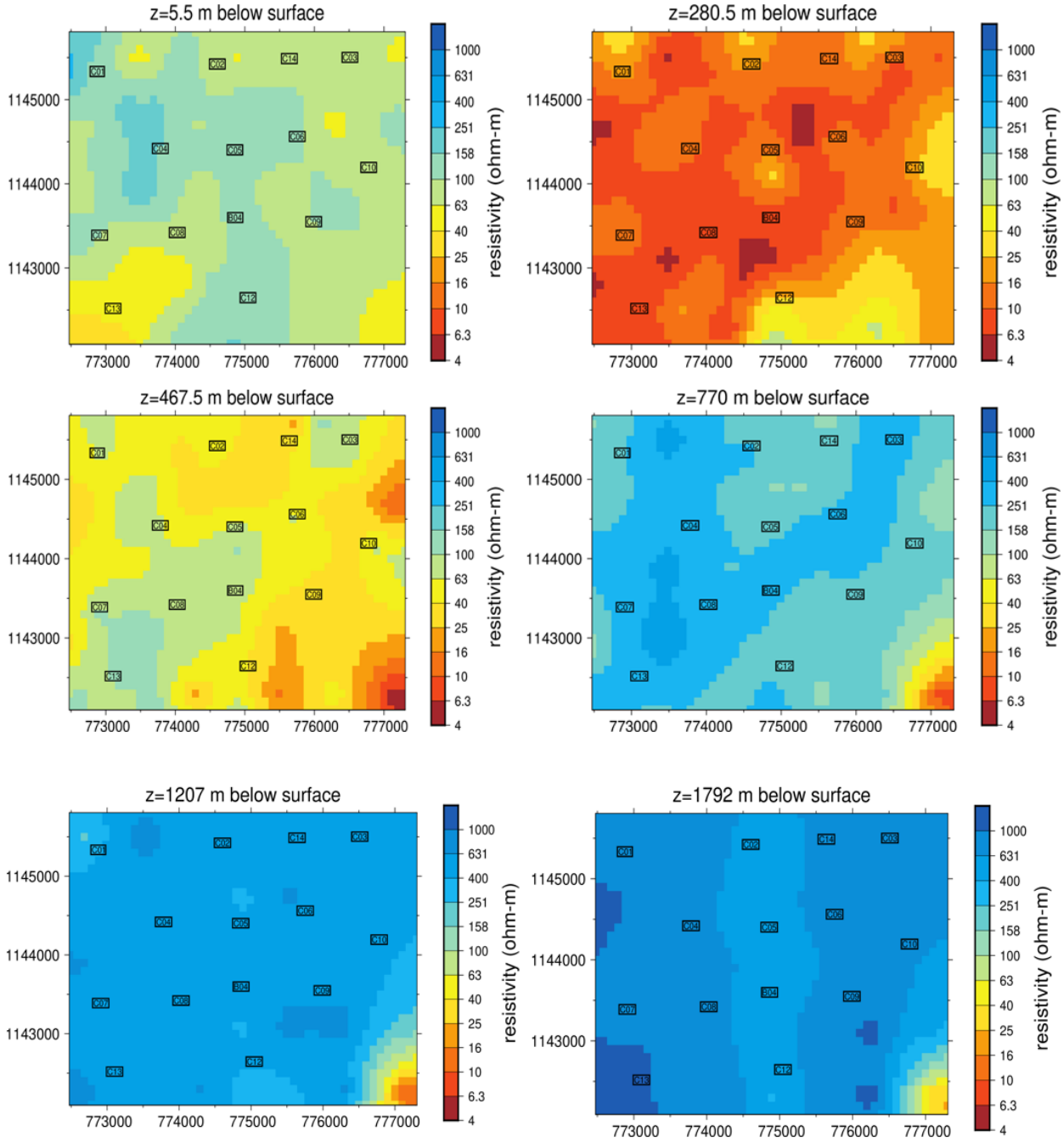

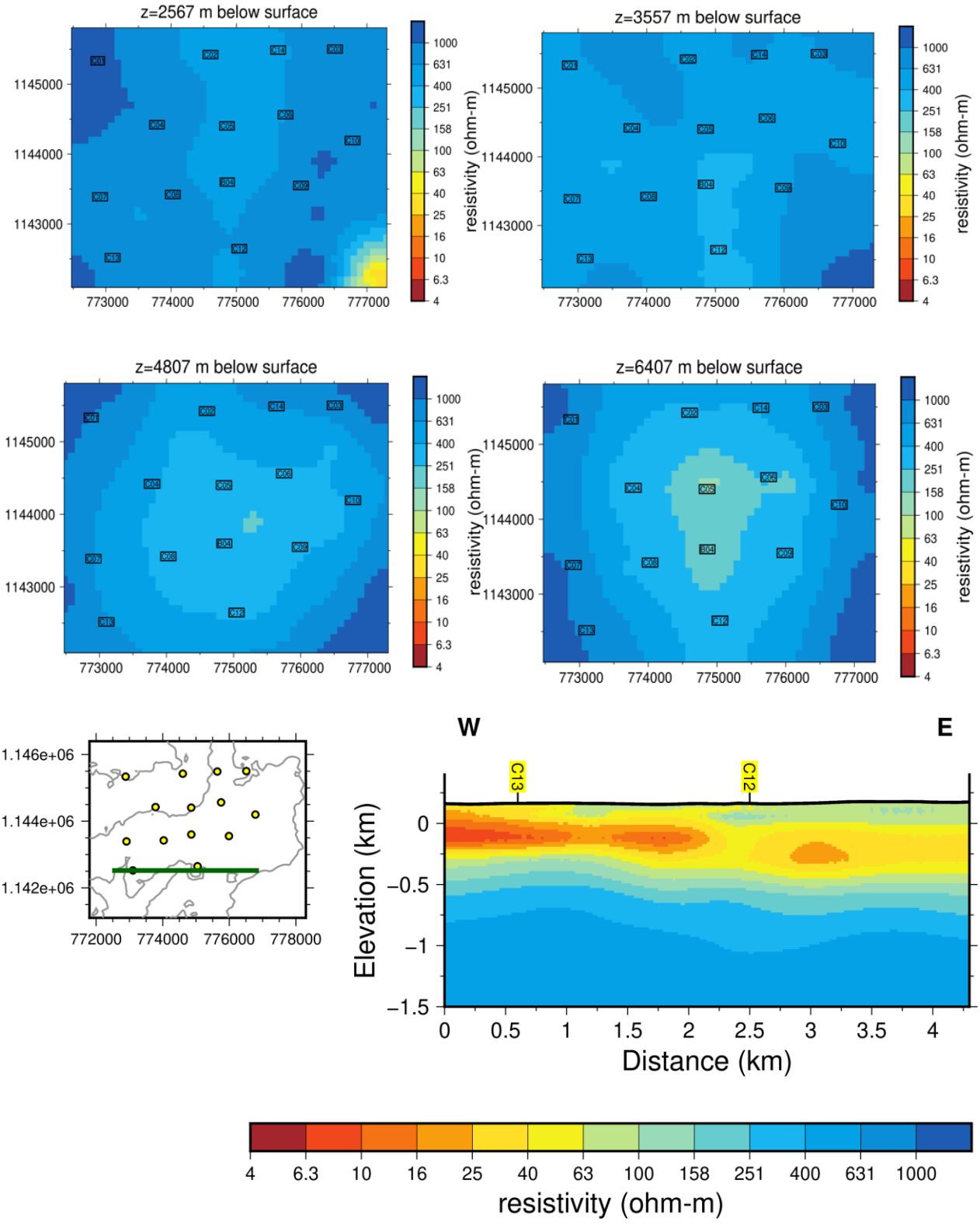
z=2567 m below surface
z=3557 m below surface
z=4807 m below surface
z=6407 m below surface
resistivity (ohm-m)
1000
631
400
251
158
100
63
40
25
16
10
6.3
4
1145000
1144000
1143000
773000
774000
775000
776000
777000
C01
C02
C14
C03
C04
C05
C06
C10
C07
C08
C09
C13
C12
1.146e+06
1.144e+06
1.142e+06
772000
774000
776000
778000
W
E
C13
C12
Elevation (km)
0
−0.5
−1
−1.5
0
0.5
1
1.5
2
2.5
3
3.5
4
Distance (km)
4
6.3
10
16
25
40
63
100
158
251
400
631
1000
resistivity (ohm-m)

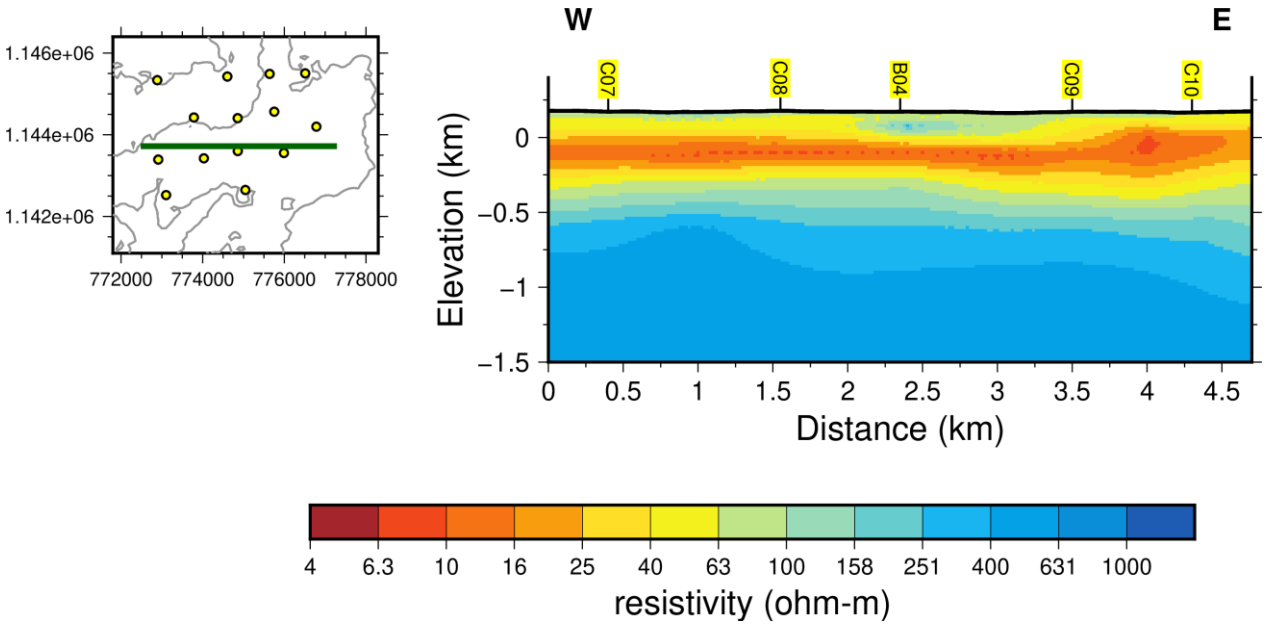
W
E
C07
C08
B04
C09
C10
1.146e+06
1.144e+06
1.142e+06
772000
774000
776000
778000
Elevation (km)
0
−0.5
−1
−1.5
0
0.5
1
1.5
2
2.5
3
3.5
4
4.5
Distance (km)
4
6.3
10
16
25
40
63
100
158
251
400
631
1000
resistivity (ohm-m)

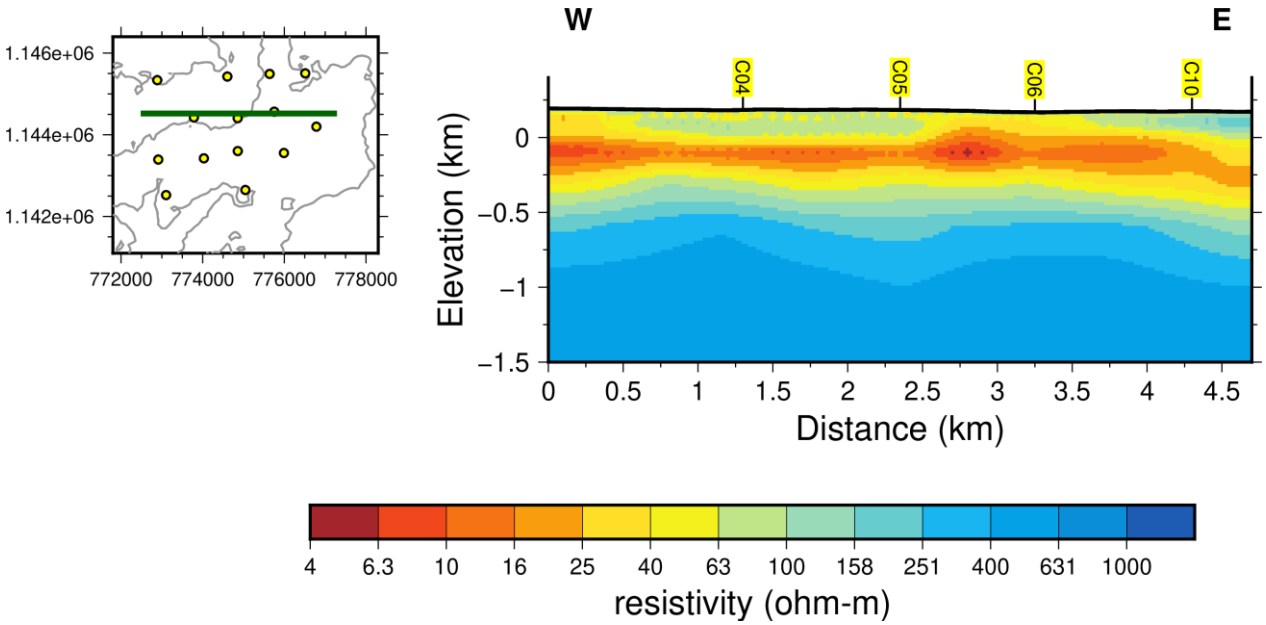
W
E
C04
C05
C06
C10
1.146e+06
1.144e+06
1.142e+06
772000
774000
776000
778000
Elevation (km)
0
−0.5
−1
−1.5
0
0.5
1
1.5
2
2.5
3
3.5
4
4.5
Distance (km)
4
6.3
10
16
25
40
63
100
158
251
400
631
1000
resistivity (ohm-m)

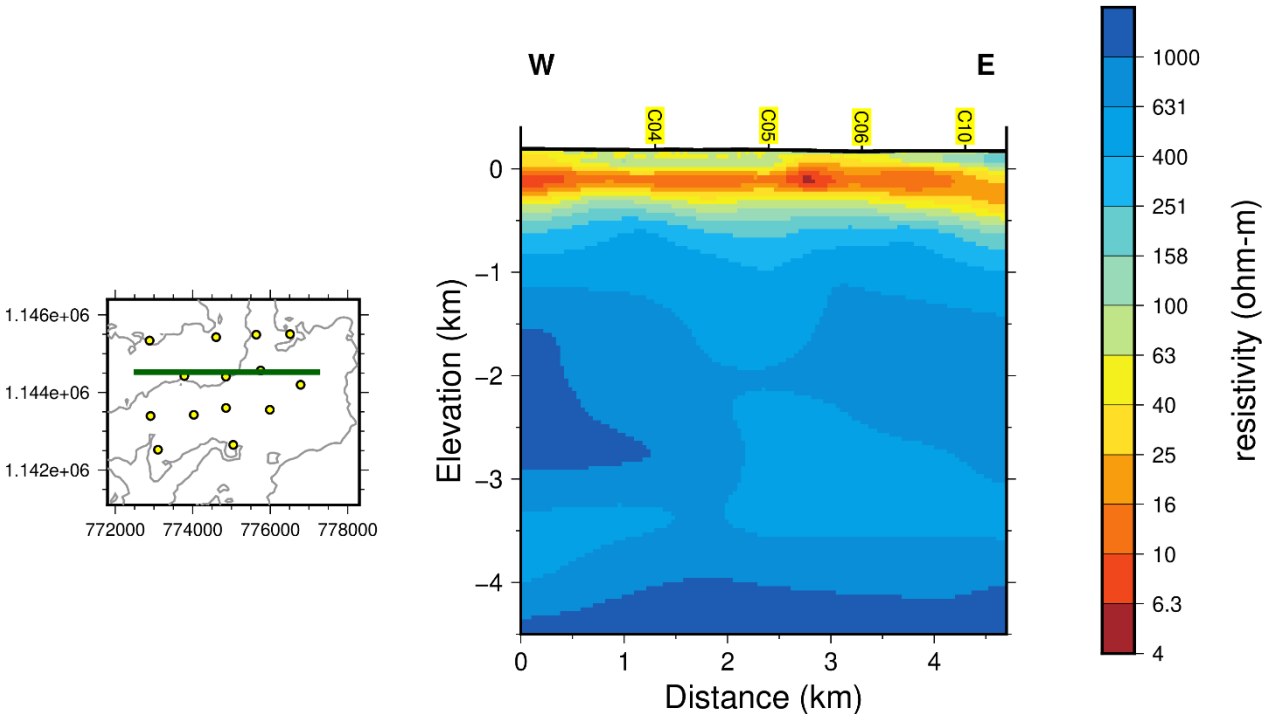
1.146e+06
1.144e+06
1.142e+06
772000
774000
776000
778000
W
E
C04
C05
C06
C10
0
−1
−2
−3
−4
Elevation (km)
0
1
2
3
4
Distance (km)
1000
631
400
251
158
100
63
40
25
16
10
6.3
4
resistivity (ohm-m)

APPENDIX 4: SEM and Spectra images of rock samples from the study area.

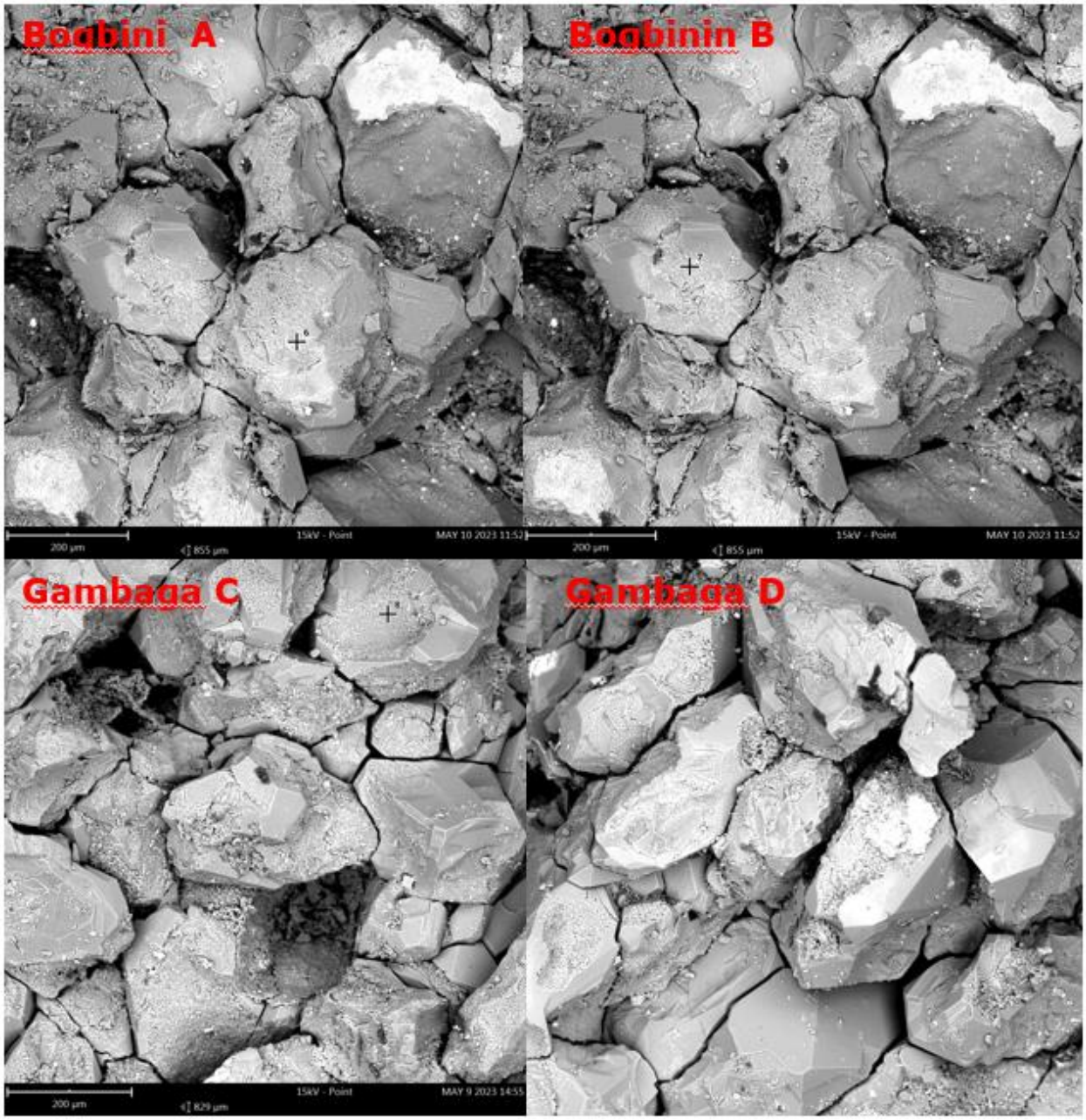

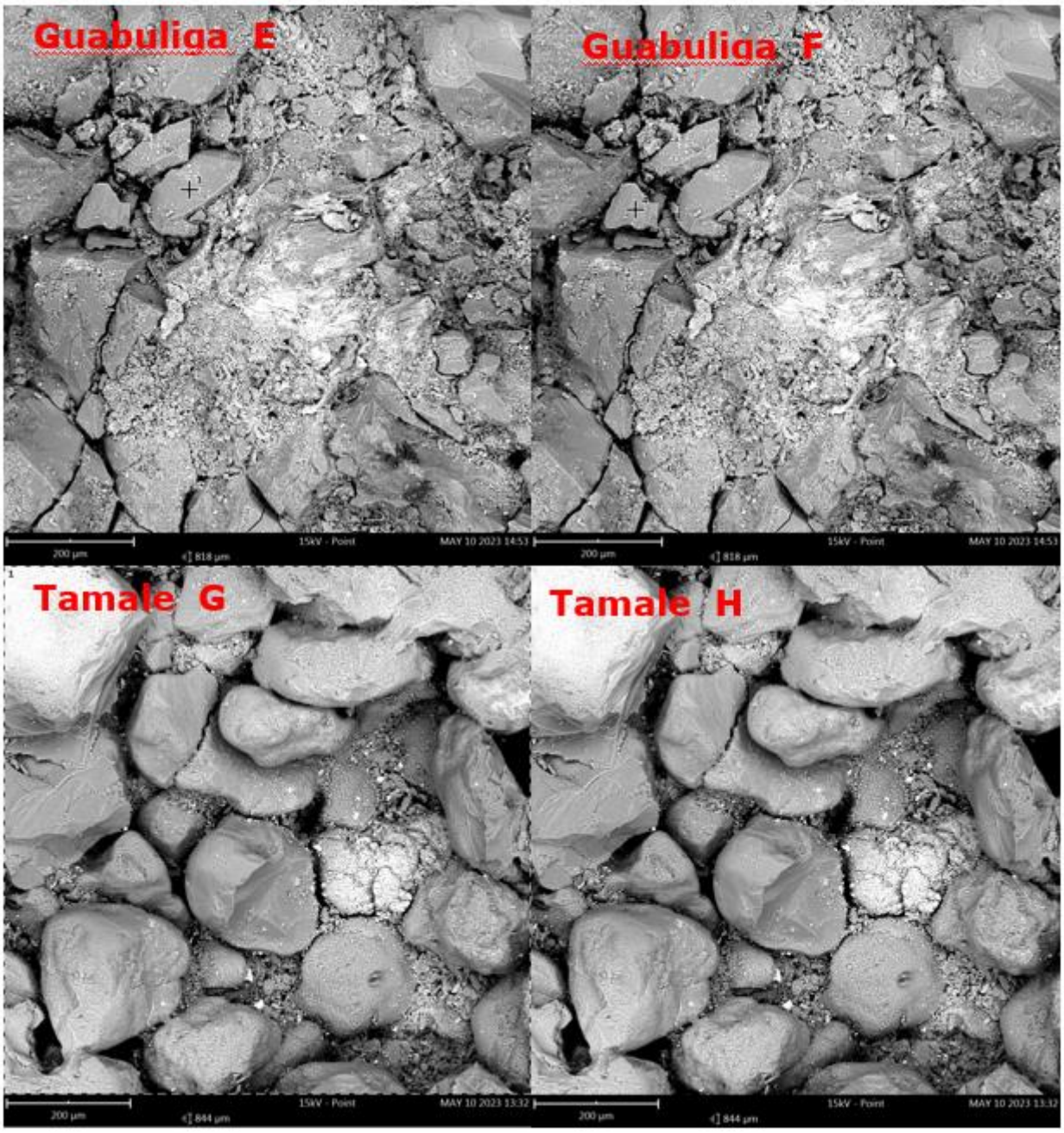
Guabuliga E
Guabuliga F
Tamale G
Tamale H

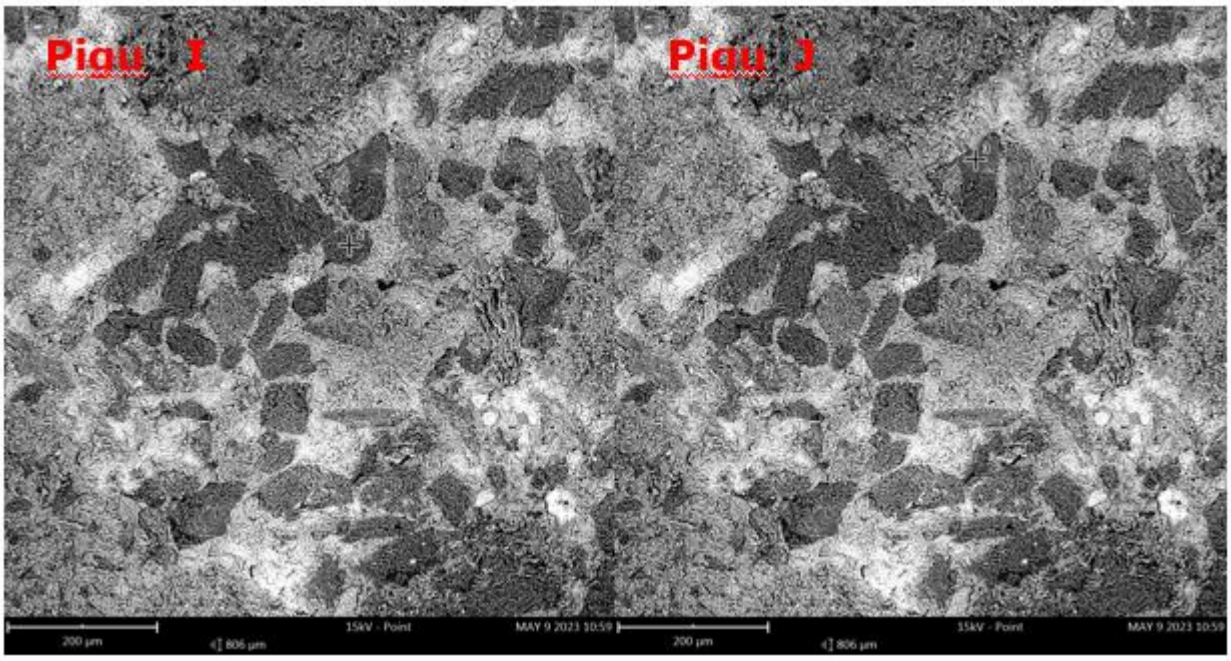
Piau I
200 µm
806 µm
15kV - Point
MAY 9 2023 10:59
Piau J
200 µm
806 µm
15kV - Point
MAY 9 2023 10:59

APPENDIX 5: Spectral energy peak of the different elements identified with SEM-EDX

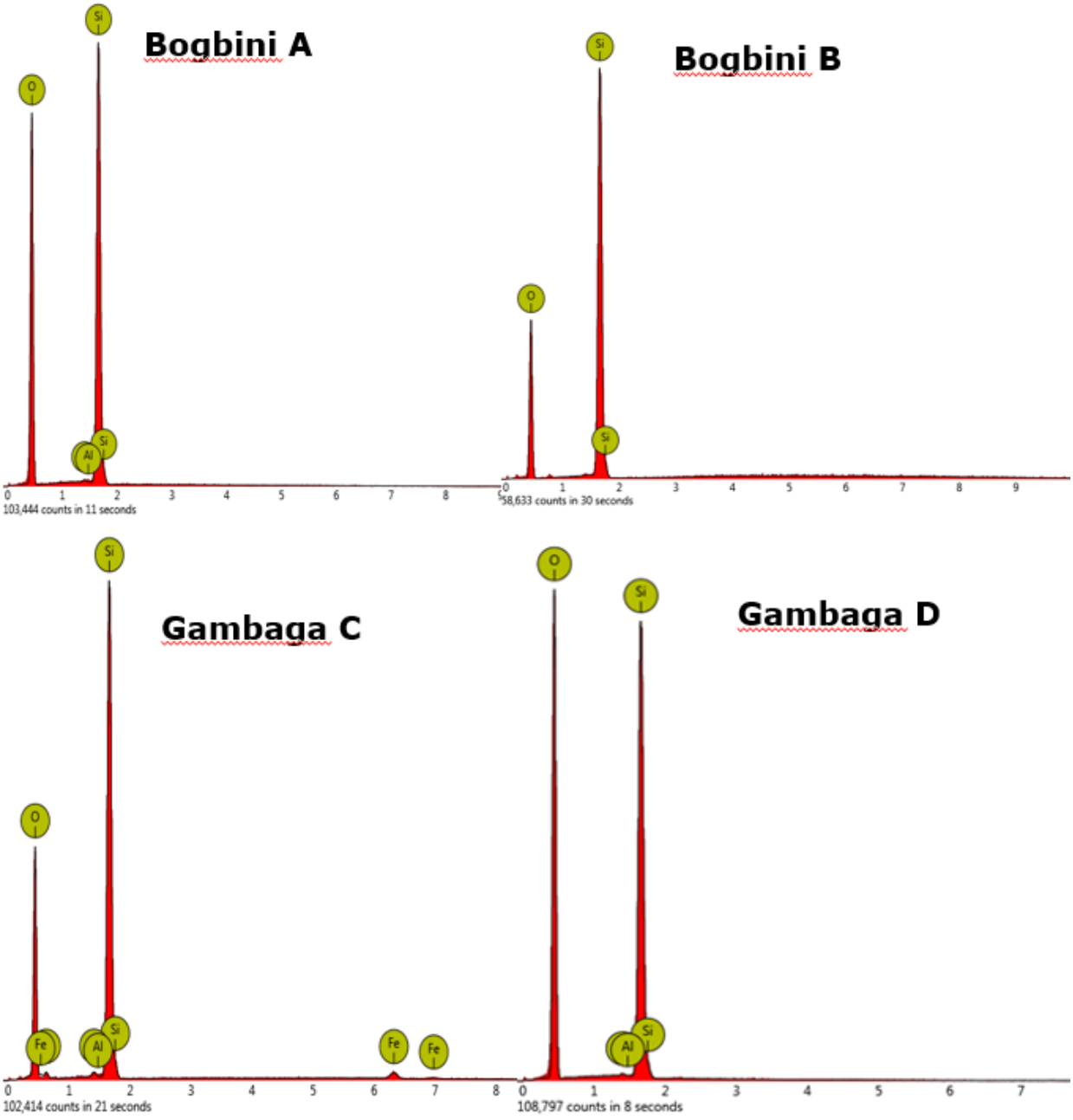

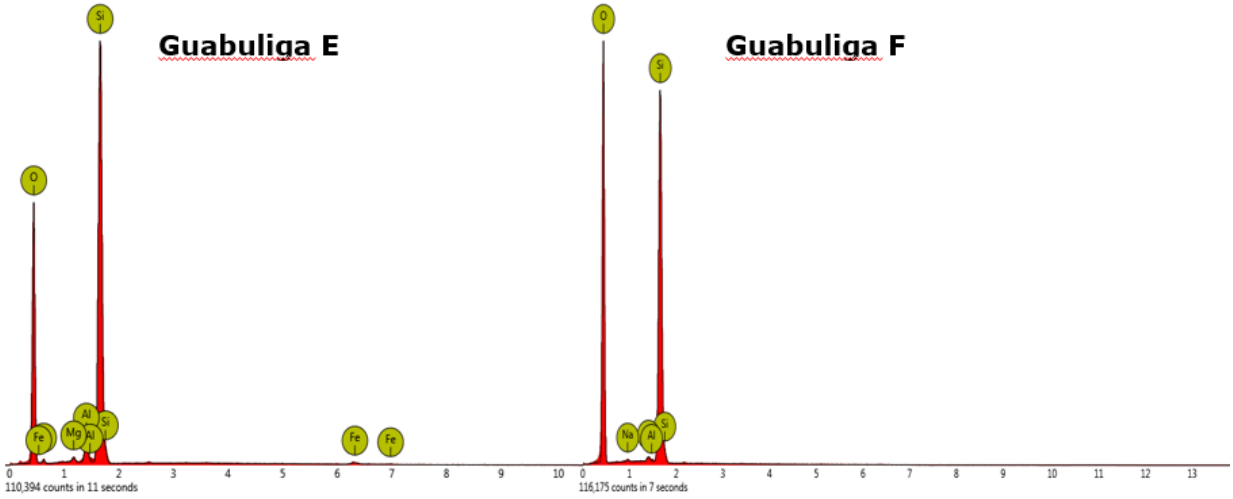
Guabuliga E
Si
O
Fe
Mg
Al
Si
Fe
Fe
0 1 2 3 4 5 6 7 8 9 10
110,394 counts in 11 seconds

Guabuliga F
O
Si
Na
Al
Si
0 1 2 3 4 5 6 7 8 9 10 11 12 13
116,175 counts in 7 seconds

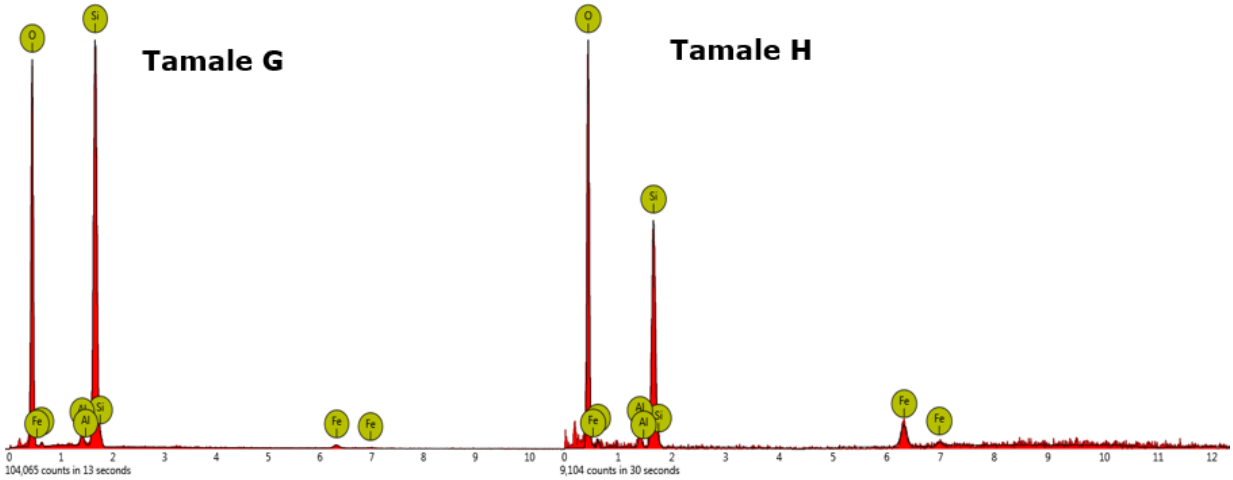
Tamale G
O
Si
Fe
Al
Si
Fe
Fe
0 1 2 3 4 5 6 7 8 9 10
104,065 counts in 13 seconds

Tamale H
O
Si
Fe
Al
Si
Fe
Fe
0 1 2 3 4 5 6 7 8 9 10 11 12
9,104 counts in 30 seconds

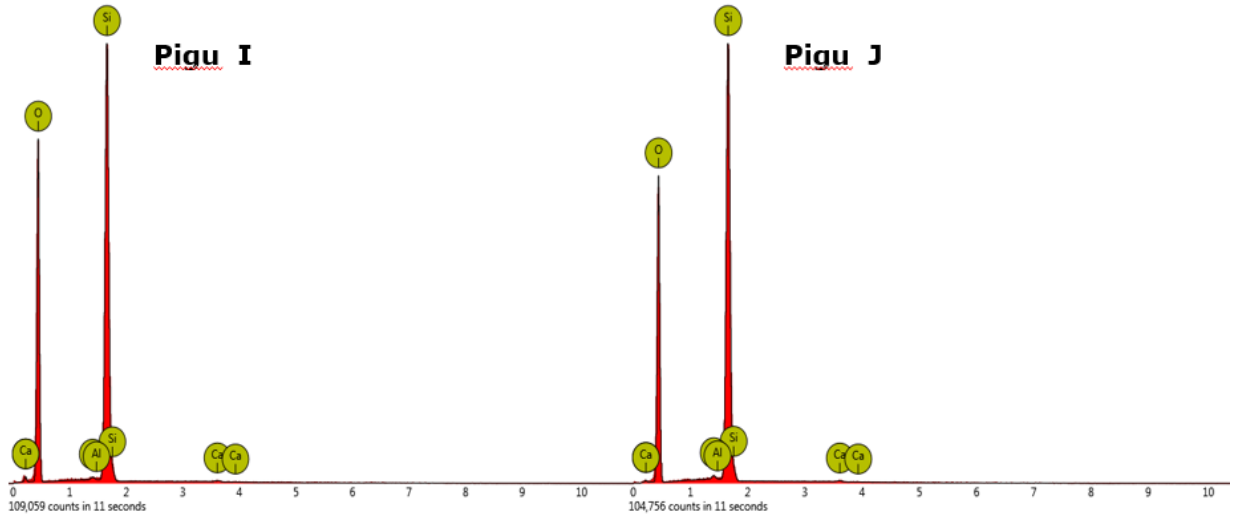
Pigu I
Si
O
Ca
Al
Si
Ca
Ca
0 1 2 3 4 5 6 7 8 9 10
109,059 counts in 11 seconds

Pigu J
Si
O
Ca
Al
Si
Ca
Ca
0 1 2 3 4 5 6 7 8 9 10
104,756 counts in 11 seconds

APPENDIX 6: X-ray diffraction analysis of Pigu sample

Qualitative Analysis Results

Phase name	Chemical formula	FOM	Phase reg. detail	Space Group	DB Card Number
Quartz	Si O2	0.688	S/M:PDF-4 Axiom 2022	154 : P3221	01-075-8320
Clinochlore, Fe+2-bearing, heated, oriented	(Mg , Fe , Al)6 (Si , Al)4 O10 (O H)8	0.780	S/M:PDF-4 Axiom 2022	10 : P12/m1	00-060-0323
Albite, Ca-bearing	Na0.84 Ca0.16 Al1.16 Si2.84 O8	1.143	S/M:PDF-4 Axiom 2022	2 : C-1	04-017-0892
Calcite	Ca (C O3)	0.964	S/M:PDF-4 Axiom 2022	167 : R-3c:H	00-066-0867
Illite (NR)	K0.83 Mg0.05 Ti0.01 Al2.81 Si3.15 O10 (O H) 2	1.935	S/M:PDF-4 Axiom 2022	12 : C12/m1	04-017-0519
Dickite-2M1	Al2 Si2 O5 (O H)4	3.471	S/M:PDF-4 Axiom 2022	9 : C1c1	00-058-2002

Phase Data View

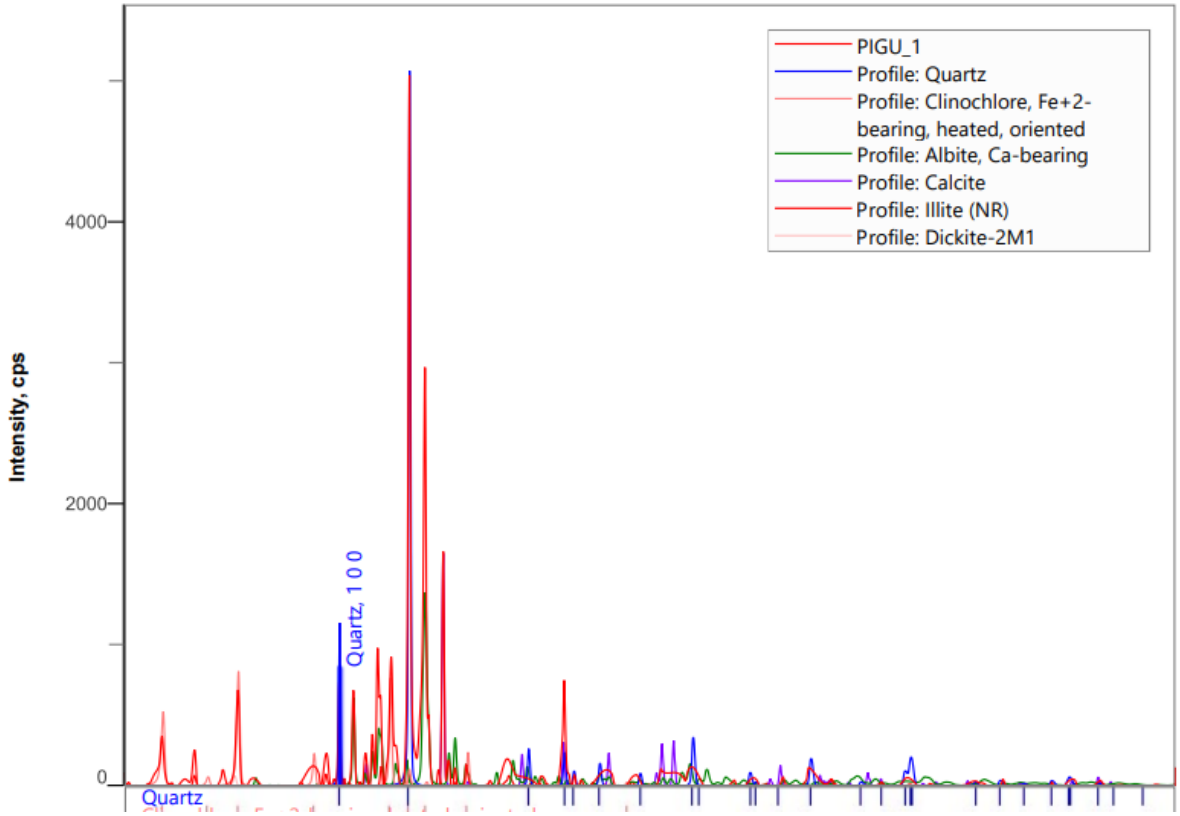

APPENDIX 7

SUPPLEMENTARY FIGURES FOR ARTICLE (CHAPTER FIVE)

In this supplementary section, we present all figures including the full 3-D resistivity models

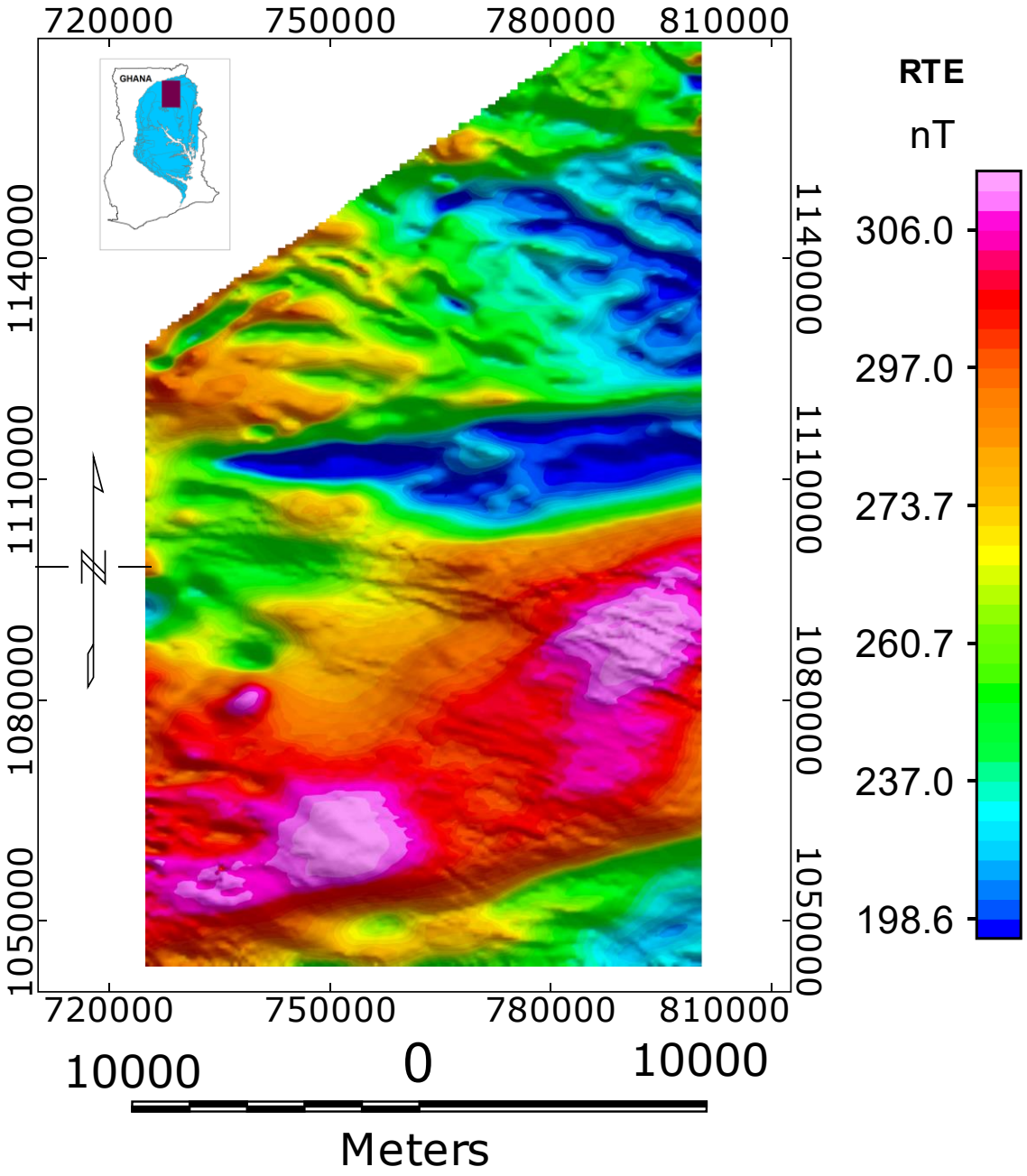

Supplementary Figure 1: Reduced to the Equator showing magnetic anomalies: red represents high magnetic intensity anomaly and blue represents low magnetic anomaly.

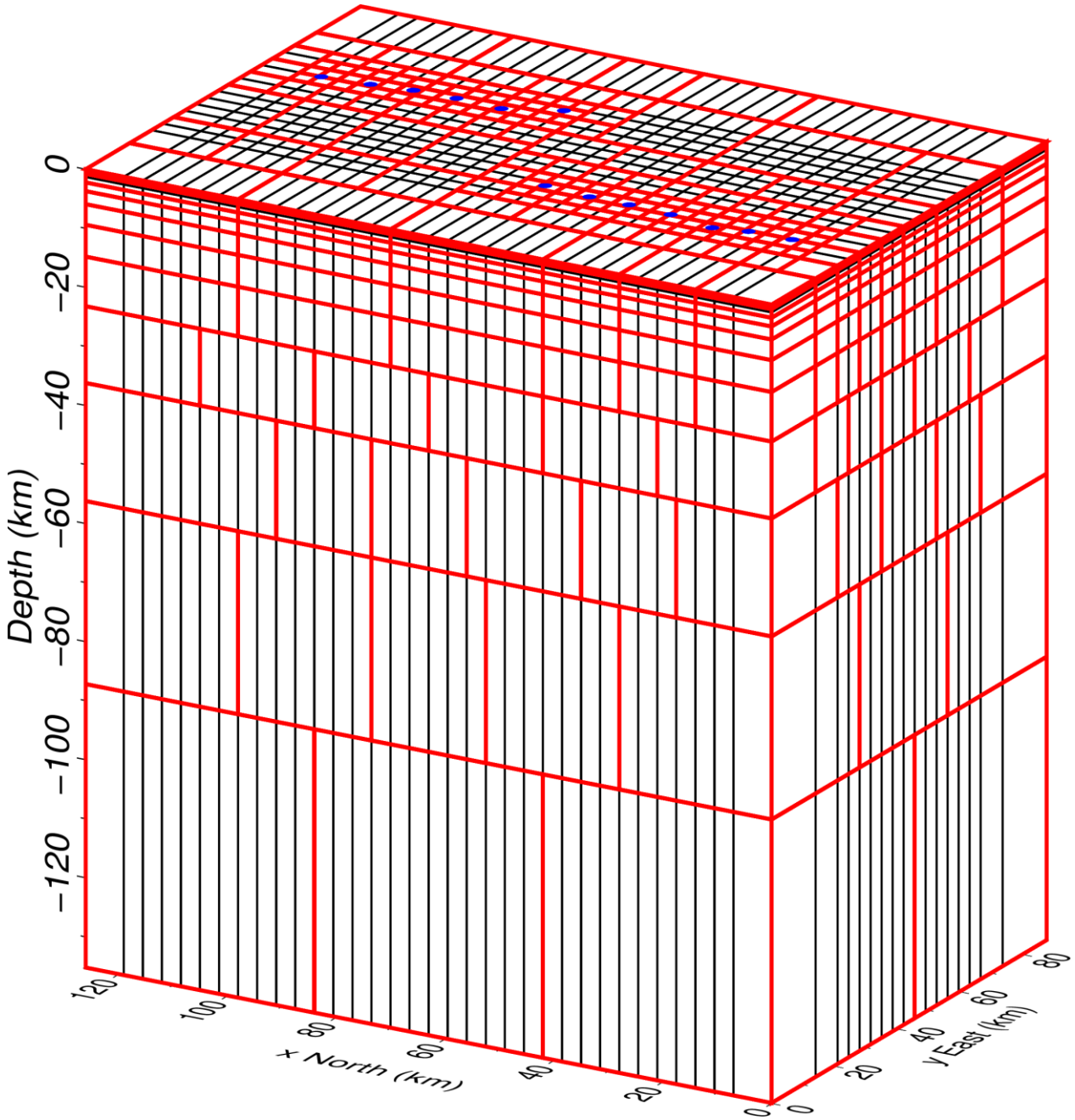

Supplementary Figure 2: 3D model grid. Blue dots on the plan view represent MT stations

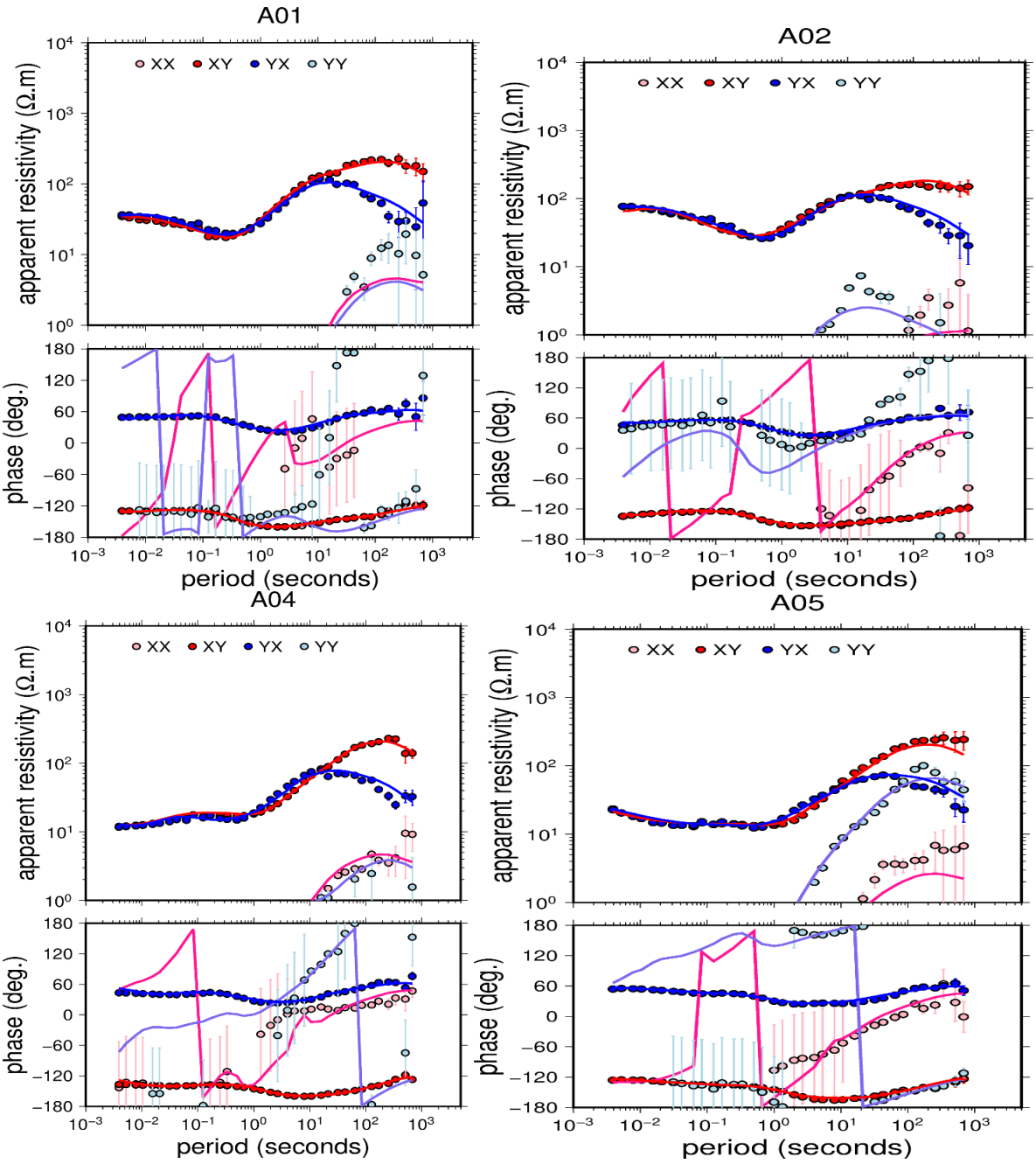
A01
A02
A04
A05
XX
XY
YX
YY
apparent resistivity (Ω.m)
phase (deg.)
period (seconds)

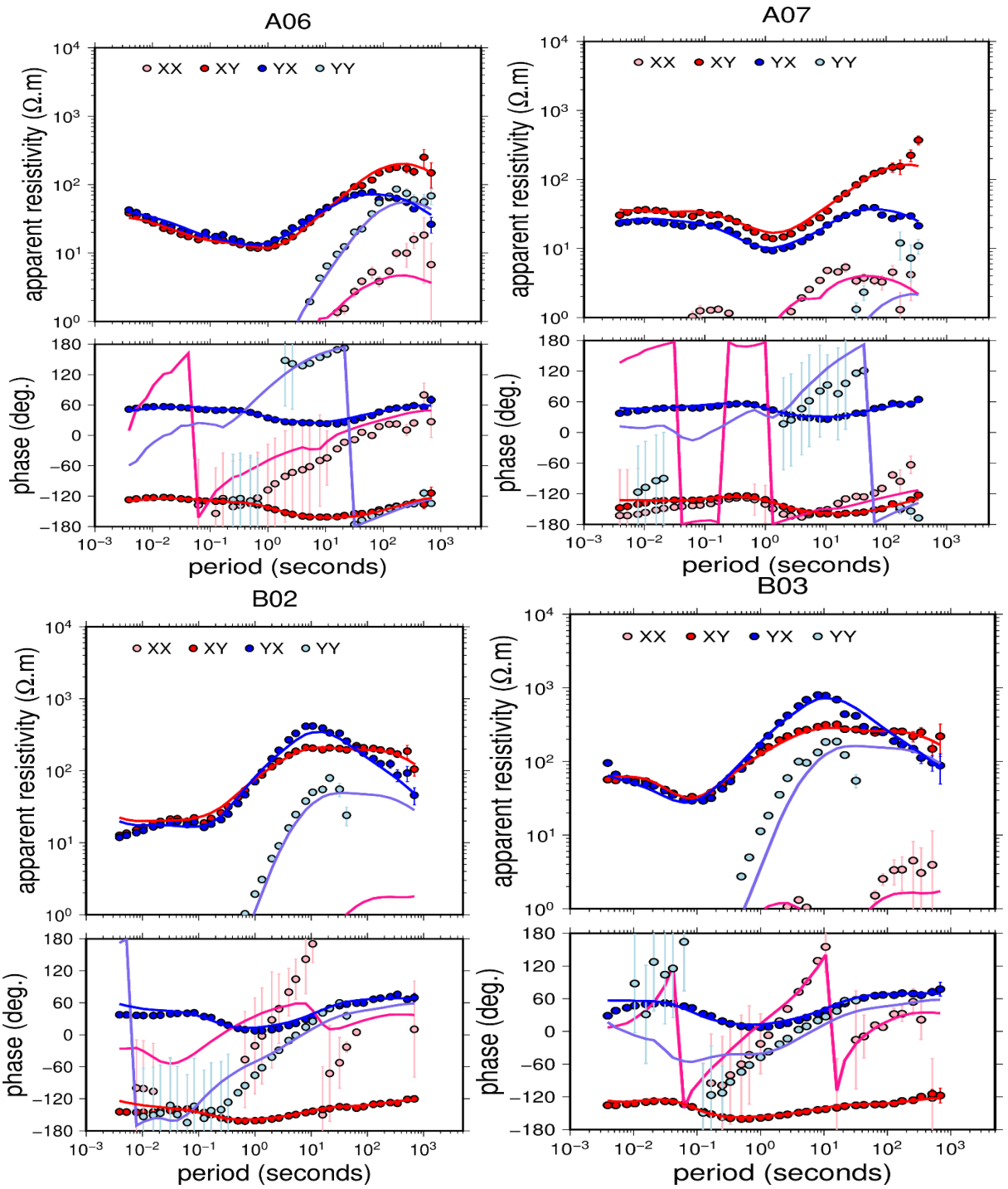
A06
A07
B02
B03
XX
XY
YX
YY
apparent resistivity (Ω.m)
phase (deg.)
period (seconds)

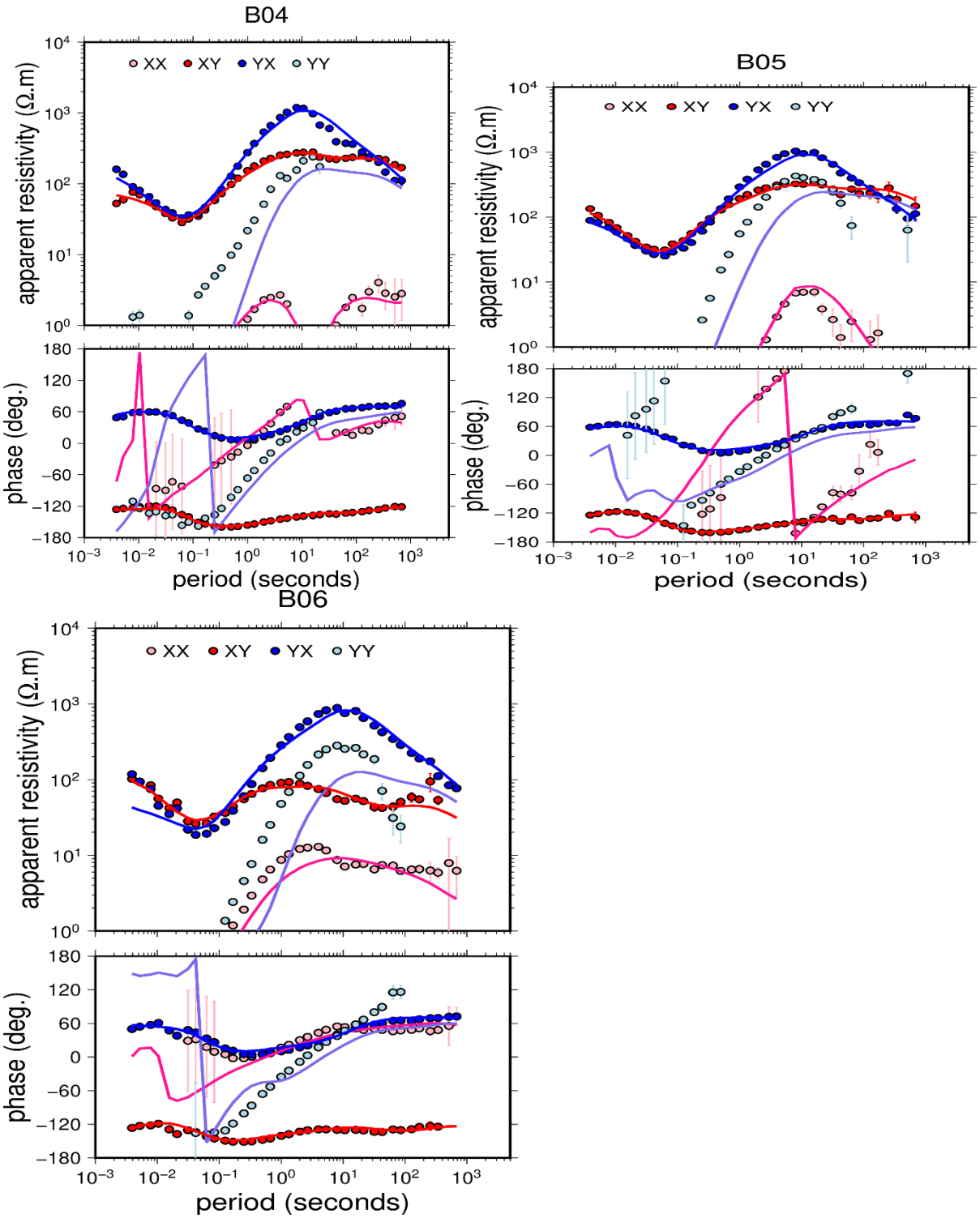

Supplementary Figure 3: Comparison between observed data (dots) and 3-D model response (solid lines) of apparent resistivity and phases for all 4 components of the MT tensor for both profiles.

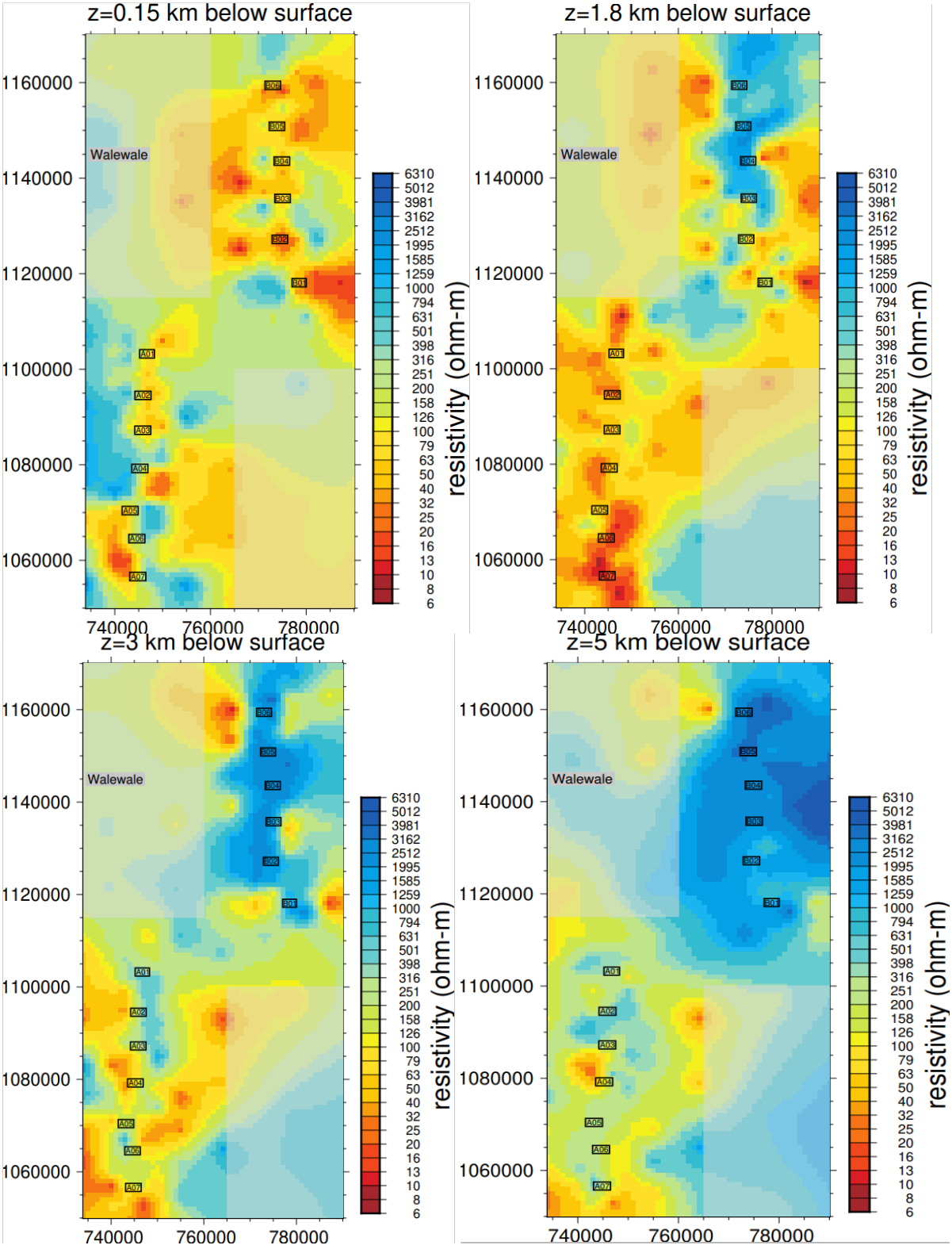
z=0.15 km below surface
z=1.8 km below surface
z=3 km below surface
z=5 km below surface
Walewale
1160000
1140000
1120000
1100000
1080000
1060000
740000
760000
780000
B01
B02
B03
B04
B05
B06
A01
A02
A03
A04
A05
A06
A07
6310
5012
3981
3162
2512
1995
1585
1259
1000
794
631
501
398
316
251
200
158
126
100
79
63
50
40
32
25
20
16
13
10
8
6
resistivity (ohm-m)

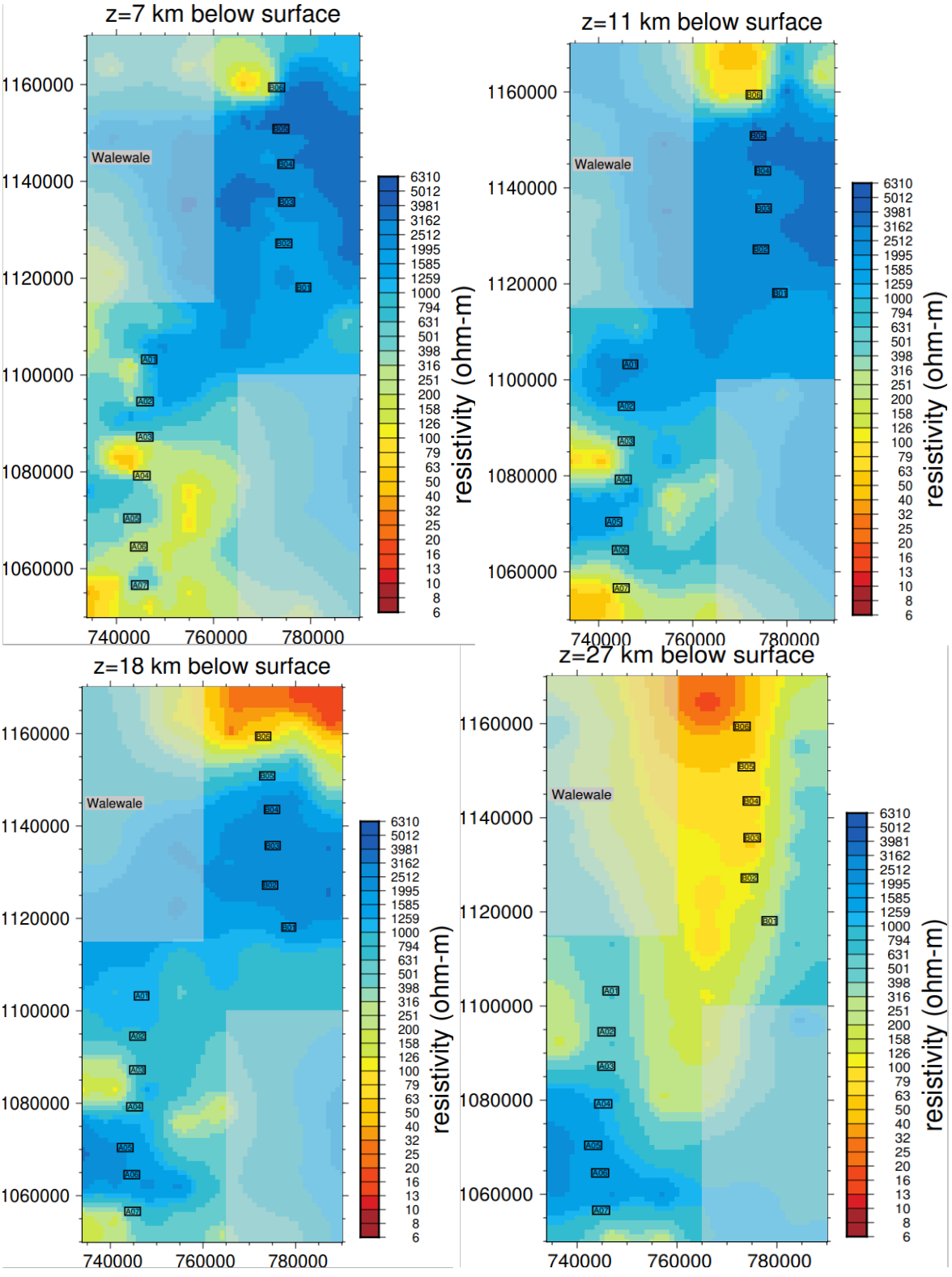
z=7 km below surface
z=11 km below surface
z=18 km below surface
z=27 km below surface
Walewale
resistivity (ohm-m)
6310
5012
3981
3162
2512
1995
1585
1259
1000
794
631
501
398
316
251
200
158
126
100
79
63
50
40
32
25
20
16
13
10
8
6
1160000
1140000
1120000
1100000
1080000
1060000
740000
760000
780000
B01
B02
B03
B04
B05
B06
A01
A02
A03
A04
A05
A06
A07
A08

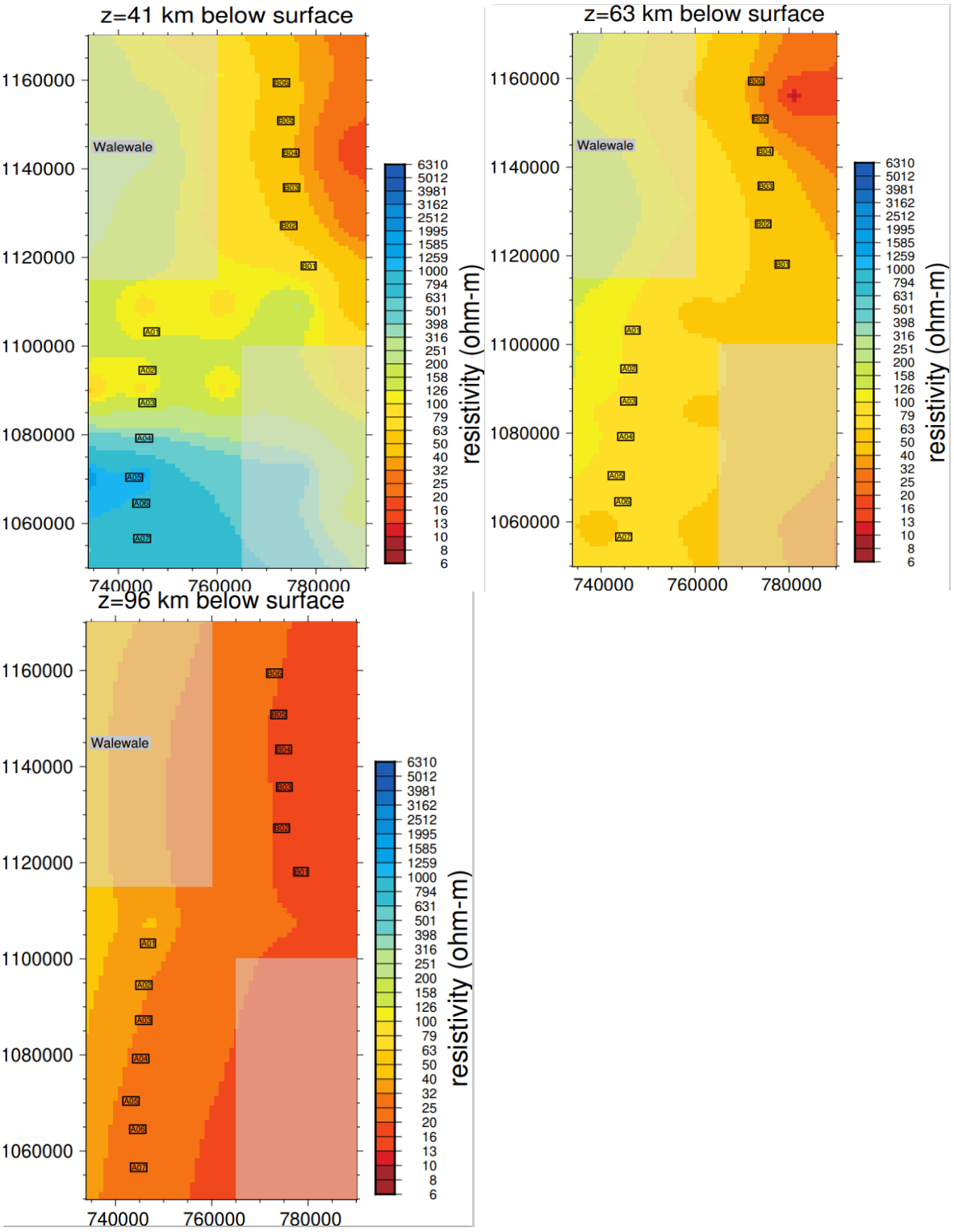

Supplementary Figure 4: 3-D resistivity maps showing variations in resistivity of subsurface conditions at different depths across the study area. A transparent layer was added to areas not well covered by the data.

10140 RESISTIVITY SECTION

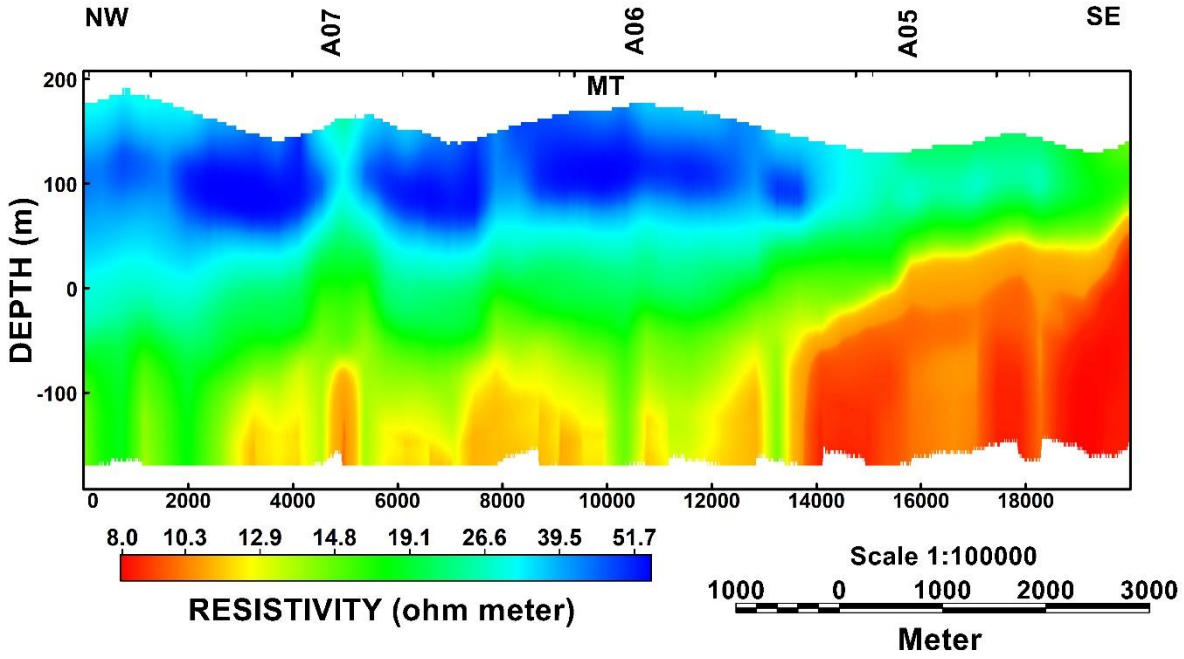

10170 RESISTIVITY SECTION

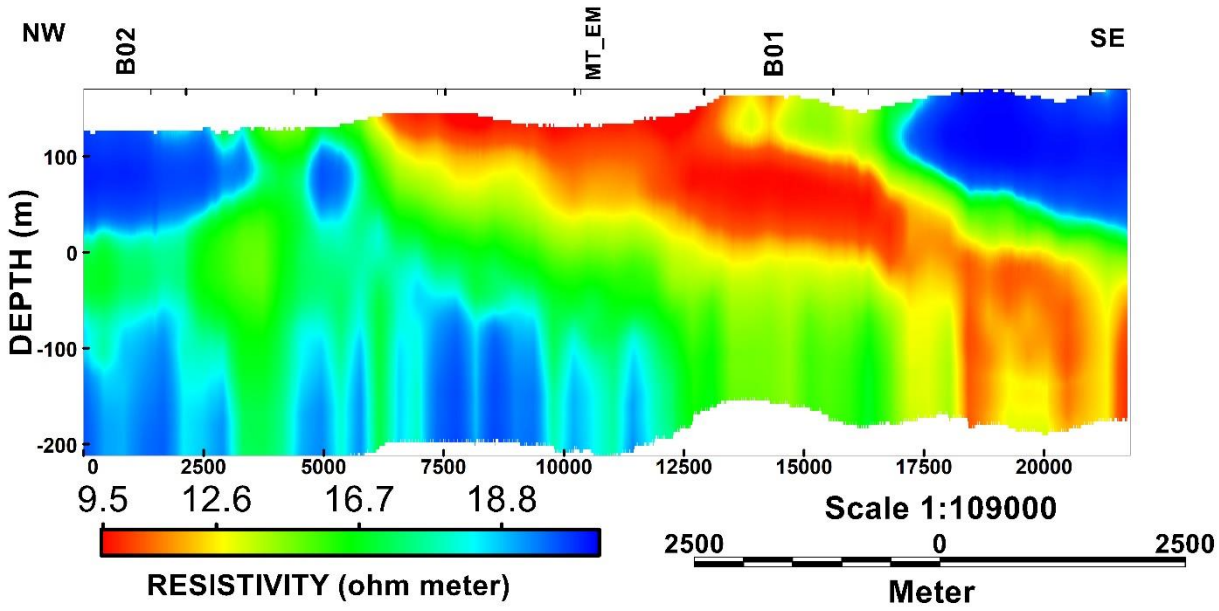

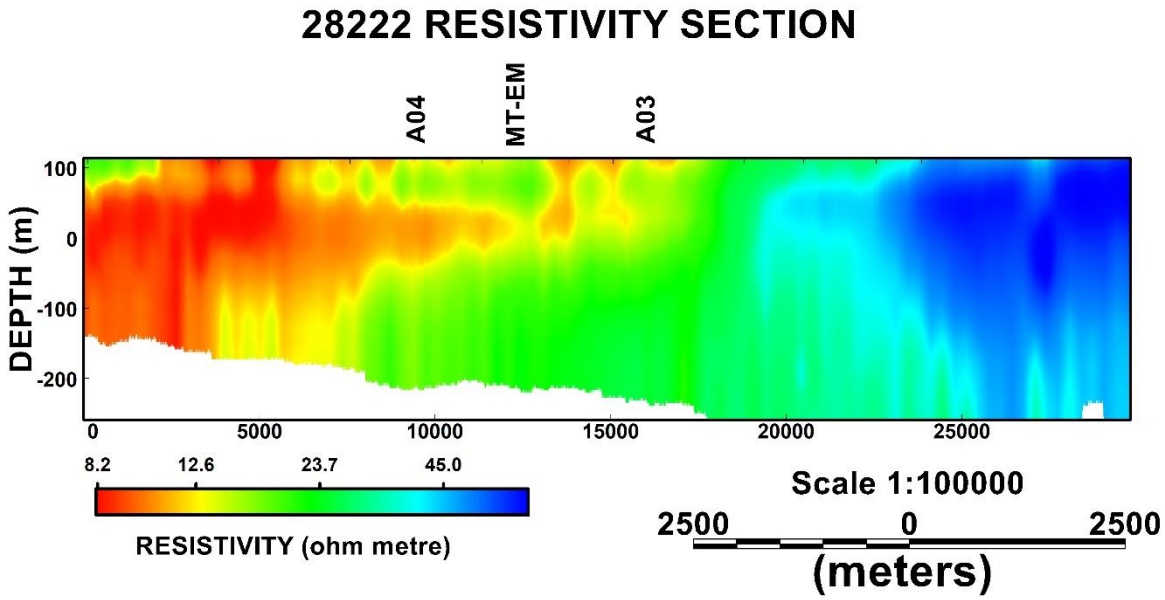

Supplementary Figure 5: 2-D cross-sections along AEM flight lines showing variation in resistivity representing geological variations in the study area. The sections were plotted using the Oasis Montaj program in geosoft.

Titre : Application de techniques géophysiques intégrées pour caractériser les structures souterraines à différentes échelles pour la gestion environnementale dans la partie nord du bassin sédimentaire de la Volta, Ghana.

Mots clés : Volta, Sédimentaire, Bassin, Structures, Magnétotellurique

Résumé : L'insuffisance des informations géologiques et hydrogéologiques a entravé le développement des eaux souterraines dans le bassin nord-Volta. Pour améliorer ces informations, nous évaluons le sous-sol des bassins à différentes échelles de profondeur à l'aide de méthodes géophysiques intégrées. Les données aéroportées et les cartes de résistivité dérivées de l'inversion 3D et 1D des données magnéto-telluriques ont révélé plusieurs zones de faible résistivité avec une signification hydrogéologique probable à différentes profondeurs. Les valeurs de résistivité de ces zones sont similaires à celles d'un forage de recherche de 132 l/min dans la zone. Les couches de faible résistivité sont suggérées comme un possible aquifère de saprock NE-SW et un aquifère potentiel de fracture de contact profond révélé à une profondeur d'environ 250 m. La fracture de contact profond a présenté de nouvelles informations sur les épaisseurs stratigraphiques des deux principales formations géologiques de la région. En outre, les résultats des coupes ERT sur certaines décharges, validées par des échantillons d'eau souterraine, suggèrent une possible migration du lixiviat des décharges vers la nappe phréatique peu profonde, soulignant la nécessité d'une étude des aquifères profonds dans la région. Les interprétations des cartes de résistivité ont été corroborées par la composition minéralogique des roches sous-jacentes révélée par l'analyse pétrographique et SEM-EDx.

Title: Application of integrated geophysical techniques for characterizing subsurface structures at different scales for environmental management in the northern part of the Voltaian sedimentary basin, Ghana.

Keywords: Voltaian, Sedimentary, Basin, Structures, Magnetotelluric

Abstract: The insufficiency of geological and hydrogeological information has impeded groundwater development in the northern Voltaian basin. To improve on this information, we assess the basins subsurface at varying depth scales using integrated geophysical methods. Airborne data and resistivity maps derived from 3D and 1D inversion of magnetotelluric data revealed several low resistivity zones with probable hydrogeological significance at different depths. These zones' resistivity values are similar to a 132 l/min research borehole in the area. The low resistivity layers are suggested as a possible NE-SW saprock aquifer and a potential deep contact fracture aquifer revealed at a depth of about 250m. The deep contact fracture has presented new insights into the stratigraphic thicknesses of the two main geological formations in the area. Also, the results of ERT sections on some dumpsites validated by groundwater samples suggest a possible migration of leachate from the dumpsites into the shallow water table emphasizing the need for deep aquifer investigation in the area. The interpretations of the resistivity maps were corroborated by the mineralogical composition of the underlying rocks revealed by both petrographic and SEM-EDx analysis.